The role of ribosomal protein S6 kinases in cellular senescence, ageing and fatty liver disease

Suchira Upeksha Gallage

A thesis submitted to Imperial College London for the degree of Doctor of Philosophy

MRC London Institute of Medical Sciences
Faculty of Medicine
Imperial College London

Supervised by Professor Jesús Gil and
Professor Dominic Withers

September 2017

Statement of originality.

The work presented in this thesis is my own unless stated otherwise. Please refer to the Methods section for details regarding who aided in specific experiments including *in vivo* experiments and bioinformatics analysis.

Abstract.

The world's elderly population is growing rapidly, and ageing is the largest risk factor for the predominant killer diseases, including cancer, cardiovascular disease and dementia. Ageing and metabolic dysfunction are tightly linked, and there is a need to understand the underlying mechanisms driving these complex processes for therapeutic interventions. Deregulated nutrient sensing, particularly mechanistic target of rapamycin (mTOR) signalling, and cellular senescence are hallmarks of ageing. Previous studies have shown that deletion of ribosomal protein S6 kinase 1 (S6K1), a downstream effector of mTOR, in mice prolongs lifespan and protects from obesity. Given the recent evidence implicating mTOR signalling in cellular senescence and the senescence-associated secretory phenotype (SASP), we hypothesised that a decelerated senescence and SASP response may underlie, at least partially, the health improvements in *S6K1*$^{-/-}$ mice. 600-day-old *S6K1*$^{-/-}$ mice displayed normal levels of senescence in the liver but showed a significant attenuation in age-related induction of SASP markers, inflammation and immune infiltration. Experiments performed in mouse embryonic fibroblasts isolated from S6K1 and/or S6K2 knockout mice or depletion of S6 kinases in human primary fibroblasts confirmed that S6 kinases regulate a proinflammatory SASP subset without affecting the senescence growth arrest. The diminution in age-related inflammation may in part be responsible for the improved healthspan observed in *S6K1*$^{-/-}$ mice. Given the close link between ageing, obesity and cancer, we also studied whether S6 kinases (S6K1 and S6K2) play a causal role in a diet-induced model of non-alcoholic steatohepatitis (NASH). We observed that liver-specific deletion of S6K1 and S6K2 induces a sexually dimorphic phenotype with males showing a beneficial response whilst females showing a worsened outcome, suggesting that gender disparity is an important factor for metabolic and cancer therapy. In summary, we demonstrated that S6 kinases play an important role in the regulation of the proinflammatory SASP and fatty liver disease.

Acknowledgements – *a memoir of a PhD experience.*

I truly feel that I came to know who I really am during my PhD. Although cliché, it has been transformative to say the least. Amidst all the strife, frustrations and difficulties, there were moments of true joy, exhilaration and friendship – some of which transient but some I hope to be long lasting. If I were to go back in time and decide whether to pursue this adventure all over again knowing everything that I know now, I would do so in a heartbeat. This mostly comes down to the amazing people that I have had the privilege to meet and experience these past four and half years with. Of course, there has always been science, which I will forever be passionate about no matter how unforgiving and relentless because in its essence it is so pure and true. Even with all the turbulences and political drivel, I am still enthused and optimistic about the future simply because the excitement and euphoria of solving even a menial problem is like no other. As long as our curiosity remains, there will always be a scientist.

I am forever grateful to my supervisors Jesús Gil and Dominic Withers for their trust and taking me on as their student to go on this journey. I cannot put into words how much I have learnt from you two. I am fortunate to not only have had the privilege of being supervised by two giants in their fields but also to get to know them as human beings.

Jesús, you have always been there for me. No matter how busy, you always made time whether it was meetings or sitting patiently through all my presentations. I am sure you are now well versed with “senescence is a double-edged sword”. I do not know of many supervisors who could have coped with someone so unpredictable that takes random selfies with their supervisors in the most unexpected of times! Not even in my wildest dreams did I imagine that I would literally be with Jesus in Jerusalem! In all seriousness, thank you Jesús for giving me the freedom to pursue my endless hypotheses no matter how much you may have disagreed – I had to learn for myself the importance of specificity, and I can assure you that after disproving my countless ideas it has now been thoroughly ingrained into my cerebrum. In data I trust - you have been instrumental in making me the scientist that I am today.

Dominic, thank you for taking me on as your student, as without your funding none of this would have been possible. Even with your hectic schedule, you took every effort to be there for all my lab meetings. It is truly difficult to co-supervise a student but you did so in such grace; you managed to finely balance giving enough advice and guidance without overbearing me, as no one can be in two labs at the same time – not even me! I will always remember your emphasis on being conservative, particularly when you told my experiment of n=16 was still an n=1 and to repeat it with three independent cohorts for both sexes and genotypes, and there began my journey into sexual dimorphism! Most of all, thank you for all your worldly and scientific wisdom and the importance on looking at the bigger picture, as it was a breath of fresh air at a time when

everyone fixates on the details. I greatly enjoyed these philosophical musings and hope to continue these in the future whenever and in whatever form it may be.

These examples are similar to only a handful of leaves in a forest, and believe me when I say that I could very well write a book. I will, however, stop now for all our sake! Honestly, I could not have asked for better supervisors. Thank you for never losing your faith in me. Most importantly, thank you Dominic for teaching me to ask "why", and thank you Jesús for teaching me to ask "how". I hope that I have not let you down.

Oh Niko (Nikolai), where to begin? This PhD would not have been the same without you! You will forever be my mentor both scientifically and, unfortunately for you, personally too. But our journey did not begin during the PhD now did it? It was during the Masters' and what an experience that was. Your high throughput teaching traumatised me from RT-qPCRs for a year or so, but it has now become my favourite technique. The first year and half was difficult with needing to publish the mTOR story but we got there in the end, and I am sure I can speak for us both that we are very proud of that project.

I know that it was not always easy having me as a student, so thank you for your patience with my countless double and triple checking of every technique, but I hope you also gained something invaluable and am certain you are now ready to supervise any student in the future. It seems odd that three years later our roles switched, and I had to supervise you with the *in vivo* work. I am very fortunate for this because I was lucky enough to repay you, something that very few students get the opportunity to do – to teach the master! Yet, no matter how much time will pass or how experienced I will become, those dilution calculations will haunt me forever, so you will always have ample opportunities to ridicule me, as I know how much you enjoy doing so.

Although science was the heart of the PhD, there was so much more and none more so than my music edification by you, Luca and Steve. You made my daily life in the lab not only more enjoyable but also invigorating. There are so many stories to tell with our countless missteps and failed experiments – I will always remember my "Superman" day when I sucked up all the conditioned media by accident or when doing the polysome profiles you accidently poked a hole in the gradient tube and screamed "help me Suchi!" What could I have done but stare blankly at your face? I cannot reverse time – the hole was already made!

I am genuinely sorry that you had to deal with someone so extreme when I would say one thing in the morning and would do the exact opposite by the afternoon! Only you could have dealt with it daily. Thank you again for your endless advice on all matters whether science or personal, and I am glad that you realised I was not a "robot"! I will never forget that third year summer –

those conversations about “cells” were some of the fondest memories of my PhD. I want to emphasise how grateful I am to meet you, to have been your student and most importantly to be your friend.

To my fellow pea Sath, I am truly grateful to have had the opportunity to meet you, and although you are now in the States, I hope we will remain close friends for the foreseeable future. Our endless discussions about life, philosophy, religion, economy and science were enlightening and taught me many life lessons. This period was a time of tremendous personal growth for us, and we emerged not only much wiser but also more capable of dealing with life’s challenges. We went beyond our limits and learnt how much we can endure. Most importantly, we never stopped questioning whether it was understanding the key to our well-being to how much “I” as an individual can do in this world. I am sure we both look at the world a bit differently now. I cannot appreciate enough how important it was to have a friend like you during one of my darkest hours; it really shone a bright light down a very dark tunnel.

The list continues, and this is simply because I have been blessed to have had tremendous support from all around me. None so much as from my lab mums Silvia Pedroni, Marieke Aarts and Elaine Irvine. Each of you has made such a significant impact on my PhD experience that words cannot fully express my appreciation.

Silvia, none has helped me as tirelessly as you have in my PhD. From the very beginning you have done nothing but your utmost to help pursue my endless hypotheses no matter how tedious. You truly are special as your willingness to help goes beyond any person and to all and everyone in your sight. This would tire anyone, but you are not just anyone. Seeing your resolve over the past four years has shown me what human generosity is capable of. I will do my very best to help others in all the ways that you have done for me, but it is a feat difficult to achieve. But seriousness aside, I am so sorry for almost giving you a heart attack during the Christmas Break when you were doing your genotyping! What would I have done without “mummy” for the final year? I will miss you dearly. Your humour is a special kind and your thoughtfulness is rare, and thank you again for always taking your time to help me and for being ever so protective. I simply had to reiterate this because the amount of time and effort you have dedicated to me is simply unbelievable.

Marieke, I can say the same about you. Your patience is like none other. I have lost count how many times you have reassured me and answered every menial question that I could come up with, and you did this without even a hint of anger or irritation, which is beyond my comprehension. You were composed when I was indignant. You always found the bright side even when I could not. You listened even when nothing could be done. You agreed when no one else

did. You will always be special. I must confess that nearing the end when I could not explain your sudden change in disposition was truly terrifying, as losing you would have been terrible. As you have taught me many times though, only through hindsight would I learn that it was beyond your control, but I cannot emphasise how glad I was to see your recovery to your usual self in no time.

Silvia and Marieke, I wish you both the very best as you embark on your new adventure, and I am sure that it will be the most fulfilling and rewarding experience of your life.

Elaine, I have been lucky to have you over my corner all this time! I cannot appreciate enough how much you have taught me with all the breeding techniques and experimental set ups, as I am fortunate to have learnt these fundamentals from a master of their art, and these will stay with me for my entire scientific career. Most importantly, thank you for always standing up for me even when it was not always easy. I can still remember you losing your mind over Heathrow and my trans-fat diet – thank you so much for your persistence. I could not have done it without you. I really enjoyed our light-hearted conversations about life, shows and technology in our morning dissections with Silvia and Justyna – it made those hours fly by.

Silvia, Marieke and Elaine - your protective roles and enduring patience with my never-ending spouting's about my countless failed experiments, negative data or life are thoroughly appreciated. This clearly shows the importance of having mentors that are both caring and keen listeners for any PhD student. Your willingness to help no matter how busy is second to none. I cannot believe there are people like you, and I am very sorry for my continued pestering about every little thing, but as I said I am very fortunate to have had you all as my watchful guardians.

Justyna, I simply would have faltered in my fibrosis project if not for your help. Although I know you dare not even mention the word "fibrosis"! You truly are one of the kindest, most helpful individuals I have ever known. The world would be a better place if there were more people like you. We only came to know each other unexpectedly when you helped me during the metabolic experiments, but I am glad that I did that project if it was only to meet you. Our conversations made those countless GTTs and ITTs truly enjoyable. Thank you for always believing in me and for your thoughtful and kind messages, which always put a smile on my face.

Oh Luca, I miss you greatly! Thank you for our endless discussions about films, science and the importance of balancing life and work. Most importantly, thank you for teaching me the harsh reality of science – that it is cold and indifferent to hard work or talent, as success is never guaranteed, and sometimes it simply is not meant to be. I have taken your attitude of having low expectations to beyond science and have adapted it to every aspect of my life. I know you may disagree, but being content with little and the realisation that everything is inherently unsatisfactory

can and will help us to appreciate life even more. Once again, thank you for teaching me to take the plunge even if it means accepting the possibility of loss and humility. Although the answer may be both unexpected and undesired, these experiences not only made me stronger but also more capable of dealing with life's struggles and challenges. Life is not worth living if we do not embrace what is truly worthwhile, as trying and failing is better than not trying at all.

Atheeeeena! I have lost count how many times I have said that during these years. Thank you so much for all your help and for being there at testing times. The late evenings in the lab were more enjoyable with you; in fact, they were amongst the fondest moments of my PhD. And I have come to believe that life is just that – a collection of moments since that is all we will remember in the end. Our coffee breaks with Niko were wonderful but now they seem to be a remnant of the past since you both gave up smoking. Is it not curious how one good thing may result in the end of another? Clearly this is another fine example depicting the impermanence of all conditioned phenomena. Nonetheless, I greatly admire and am proud of you both as once addicted it is painful to break free. Athena, I could write endlessly on my thoughts, but all that is worth saying has already been said. Knowing me though, you know I have more to say. This has truly been a special time, and although it is now coming to an end, never lose hope, as the future is ever bright. The world really is our oyster with endless possibilities, and as I have said on many occasions, I have no doubt that you will grab these with both hands. When needed, do take the time to reflect, as time spent contemplating is never wasted time. To end on a high, thank you again for that 25th birthday party, which honestly was one of the best days of my life and much of it was down to you.

Oana! Our time cleaning the developer was enlightening. Some of my most memorable discussions about life, science, books and more were with you while whilst cleaning that horrid room. This brought great joy to hours of being intoxicated with stingy chemicals. Although after two years, I have grown a liking to our beloved developer. Honestly, I am fortunate that I did not have to mop that floor on my own when it flooded, as no PhD can prepare you for that! Then again you did teach me to mop. All jokes aside, selfless devotion is never easy, especially if it means giving up our own ambitions, so thank you for reminding me what is truly important in life. Our bond clearly shows how unlikely events can bring together friendship, and I hope to continue ours for a long time to come. Thank you Dipti for making this difficult task as easy as possible with all your help.

Andreeeeeeeewww! I honestly do not know how to convey my feelings into paper, as you evoke many emotions that it is difficult to pinpoint just a few here; but all of which are good. You kept me sane when I was going insane; you kept me calm when I was being irrational; but you also gave me the nudge when I needed the push. You were my lab dad – tough but caring and ever-present! You honestly made my lab life a lot more enjoyable and knowledgeable, and I am glad

that we had the chance to continue our enlightening discussions when you came back home (Cell Proliferation Group), as it simply was not the same without you.

I want to thank all the members of the Cell Proliferation and Metabolic Signalling groups for your continuous encouragement, support and guidance during the past four and half years. It is because of all of you that I genuinely enjoyed coming to the lab every day. Our varied conversations brought a light to some dark days. I would like to especially thank Sharon for being ever so patient and for always going the extra mile to help clean my lab bench, fridge or office desk even if I did not always want to! You did all this with such finesse that I did not even realise I was doing it, and that is a rare quality and the mark of a great lab manager. Ana and Aimee, thank you for always making time to discuss whatever seemed to be on my mind whether life, science or books. After making you both read my collection, I think our tastes have become one. Sarah, I have always enjoyed our weekly musings after the lab meetings, particularly our philosophical reflections that seem to last forever, and I genuinely am looking forward to graduating together for the second time! Domhnall, I must admit that seeing you bring a sense of déjà vu. You still have some time to go, but you are in good hands. Verena, where did you come from? Although we have only known each other a short while, I feel we connected rather quickly, and this mostly comes down to your carefree nature that allows others to open up so freely. Thank you Joana, for organising all the lab outings and for being the glue that held our lab together. Thank you Selina, Patrizia, Sadaf and Nadine for helping me whenever I needed it and welcoming me to our wonderful lab.

Steeeeeevieee! I am honestly glad to have done my PhD with someone so passionate about science as you. Our conversations whether early in the mornings or late at night were always stimulating and taught me to be rigorous and scrupulous with all my work. At the same time, thank you for adding a bit of spice to lab life with all the music lessons and jokes with Munim. Thanks Munim, for taking your time to make all the orders and for your worldly wisdom.

Paulius, I do not think I have ever met someone so chilled; you are the epitome of cool. It still astounds me that I have never seen you angry and at worst only tired or sad. You are also a fine example to never judge a book by its cover! Dr. Muscle Man, your first impressions do not really show your true character for anyone who takes the time to understand you well will realise that you truly are a thoughtful and caring individual. I am genuinely glad to have shared my PhD experience with you. Stay like this for as long as you can.

Maria, I still cannot believe how effortlessly and quickly we connected, and I am glad that I had the chance to meet someone like you. I cannot remember how many conversations we have had whether it was life's meanings, spirituality or politics. Your worldly knowledge is immense, and

conversing with you is always a pleasure. Thank you for teaching me to be more critical, whilst I hope I taught you to remain optimistic, and whatever happens never lose your sensitivity.

Theresa, I am glad that after all these years I finally managed to get a glimpse into your thoughts, and I was pleasantly surprised. Honestly, I greatly admire how you never incline to make any bold statements, because it takes a lot more courage to say, “I do not know”. Thank you Darran for always being patient and helping me when I needed it the most. I would also like to thank Mark Smith, Maria-Theresa, Loukia Katsouri and Nadia-Tyler Rubinstein for making my lab experience as good as it could be.

You all have seen me grow up literally in front of your eyes. I came to the lab as a baby-faced, eagerly enthusiastic Masters’ student ready to take on the world of science, and you all welcomed me with open arms. Special thanks must go to Selina Raguz and Joana Santos for those coffee breaks during the first week when Niko, who was meant to supervise me, was away recovering from a bad cold – typical! I am so sorry that you all had to endure my numerous phases whether it was growing a beard, rigorous gym routines with excess protein intake, a complete change in my clothing to my initiation into the world of drinking and partying and finally into mindfulness and meditation. I could not have asked for better people to experience all these with, and I cannot put this in another way – you truly have become my second family.

In addition to my lab family, I am also indebted to my peer group, especially Ben (quiet and reserved but full of wisdom until drunk when the beast is unleashed), Ele (one of the bubbliest people that I know), Tim (deeply insightful and a true contemplator), Amalia and Michelle (ever cheery and stupendously easy to talk to) as well as Robin (a cynic at heart but a true gentleman). Thank you for all the chats whether philosophical or scientific and for your never-ending support all the way through. I am also very fond of all the fifth and third floor colleagues from both the past and present who have helped me along the way. I would like to particularly thank Nav for all the helpful comments over the years and for teaching me the importance of being up to date with the literature – I do not know anyone who reads as much as you.

I am also ever thankful to my sensei Rick Bates and all the members of the LMS jujitsu team, particularly my training partner Motasim, for giving me the confidence to defend myself but also teaching when to practice restraint. Although, I do not think I will ever take you on again sensei, especially if I do not want to break my other knee as well! Thanks Ola and Lucien for being so passionate about this art and for encouraging me to keep pursuing it in the future. It has been wonderful to get to know you both and for all our discussions whether about the gym, food and cooking to martial arts.

There were many other members within the LMS that have guided me along the way: Postgraduate Administrator - Mark Ungless, Mentor - Irene-Miguel Aliaga, Bioinformatics – Gopuraja Dharmalingam, Microscopy – Dirk Dormann, CBS Staff, as well as Mahrokh Nohadani and Santiago Vernia for all their help. Santiago, you emerged near the end, but it was truly refreshing to meet someone who is equally passionate about science, as it invoked a burst of energy to begin my new adventure, so thank you again for all your advice and being understanding – I will not forget this!

I am also forever indebted to Imperial College London where I have completed my entire Higher Education (Bachelors, Masters' and now PhD), as well as the Medical Research Council and the Wellcome Trust for the funding.

I would like to also thank my close friends Shahab Haghollahi, Martin Evans and Henry Li, who are all fellow medical/PhD students that I have spent my entire Higher Education with. It has been a long and arduous journey from our A-levels to now finally becoming medics/scientists, but I am glad that I had you during all these years. You all have been a constant source of support, and I am fortunate to have friends like you!

Most importantly, I would like to thank my family – my mum (Champika), dad (Anura) and brother (Chatura). I simply could not have done this without you all – you have taught me almost everything that I know and have made me the man I am today. Thank you mum and dad for picking me up daily, cooking and cleaning, which meant I could literally live in the lab and do all my experiments until ungodly hours.

Dad, I am forever grateful to all the life lessons that you have taught me. All that I know about common sense has its roots in you. I am blessed to have a dad who cares for me as much as you. Your tireless devotion to your family cannot be matched. I could not have asked for a better father. Thanks aiya, for teaching me to always stay true to my word and myself, as that is all we have in the end. You have always watched over me, and I know that I go astray at times, so please be patient and keep me grounded when I cannot find my feet. You will always be my big brother! Mum, you are and will always be everything to me! I will not be here today if it is not for you. It is your word that guides me on my path. Thank you for teaching me about mindfulness and the importance of meditation without for which I could not have faced the harsh challenges of a PhD and life during this period. There are no words to describe my feelings to you all.

I would also like to thank my grandma, aunties, uncles and cousins, whom have all been a source of support and inspiration throughout my life.

All of you that persevered reading this to completion may realise that I am a sentimental being, and this would be true. More importantly, however, what I aimed to convey is how grateful I am for the wonderful people that I have had the pleasure of meeting, learning from and to teach. These bonds should not be taken for granted and unfortunately gratitude is a quality that is lost in our fast-paced, achievement-driven culture. But we should never forget the importance of gratitude, and it should be brought up into our forefronts time and time again because we will not be here without for the help and support of countless people. Some clearly would have made significant impacts on our lives and others although small, accumulate and over time very well could have impacted us more than we ever imagined. Hence, for all those who have helped me throughout my life that I have forgotten to mention whether teachers, friends, family or even my greatest adversaries, you all have taught me much, so please accept my sincere gratitude and thank you very much!

In all my observations, I have only ever found that the ego although crucial for self-confidence is also the root of discord, enmity and conflict whether small or big. There is a subtle but important distinction between reacting and mindfully responding, but we should strive for the latter as the former only ever results in remorse and guilt. We often become fixated in our views and opinions that we are blinded to the truth. Oftentimes we require someone to point and guide us when are lost in this confusion, and I have been fortunate enough to have received such wisdom at these perilous moments. Continuous reflection and improvement is a must for us all. These experiences although difficult to bear have taught me much, and I hope to do better in the future. I am truly sorry if I have offended or hurt anyone, as this was never my intention and not done through any malice but rather heedlessness, so please forgive me if I have done so. I truly believe this long and arduous journey of wise reflection and self-improvement is one of the most noble and worthy pursuits that one can undertake in their lifetimes and one that I will pursue until the very end.

The final but equally important point that I wanted to impart is hope. Believe me when I say that I have lost count the number of times when everything seemed hopeless and in chaos. The sheer number of hypotheses and experiments that went in complete disarray is best not mentioned! But like a phoenix rising from the ashes, slowly at first but then all at once, everything seemed possible. Perseverance and grit are essential for any scientist, and I am still ever more hopeful and optimistic about the future. There is so much cynicism in our world now, and I agree that much of this is justified and can be infuriating; but there is also so much good that we should not overlook. As long as our passion and enthusiasm burns inside us for whatever we do, we should always strive to do better. Aim for perfection whilst having the humility to know that it is beyond our reach. Although, we may never get there it is that hope of one day reaching this goal that at least drives me both in life and science. But what really is perfection and can we ever achieve this? I will question this for a long time to come. It is inevitable that we will all fall countless times, but it is nonetheless important to keep rising each and every time, reflect, accept and move forwards, as it is how we respond to these moments of breaking that defines who we are as individuals.

Dedications.

I would like to dedicate my work to the mice that have been used in biomedical research. Your lives have not only furthered human knowledge but have helped to save countless lives over the years. I know, however, your life is just as important to you as my life is to me. Therefore, we should not take your lives for granted, and I can assure that I do not!

This has been a deep conflict in my education in biomedical research. As a scientist, I fully comprehend the need, as we simply cannot rely solely on the use of cells and mathematical models to understand the complexity of the human body. Yet can taking life no matter the cause be truly good and pure?

This inner conflict that has raged on like an inferno has slowly begun to subside, as I have made my peace and accepted the karmic repercussions for whatever may come; I know that my intentions are good and have always been for the betterment of human lives.

I am the heir to my actions whether wholesome or unwholesome, so please forgive me for any harm that I may have done. I have done my utmost to keep in line not only with the 3Rs (reduce, replace and refine) but also to spread as much goodwill and *metta* as I can when conducting my research.

Table of Contents

List of figures.

List of tables.

Abbreviations.

°C	Degrees centigrade
4EBP	Translation initiation factor 4E binding protein
4OHT	4-hydroxytamoxifen
AAV	Adeno-associated virus
ACK	Ammonium-chloride-potassium
Akt	Akt serine/threonine kinase 1
Alb	Albumin
ALP	Alkaline phosphatase
ALT	Alanine aminotransferase
AMLN	High-trans fat
AMPK	APM-activated protein kinase
ANOVA	Analysis of variance
ARF	Alternative reading frame
AST	Aspartate aminotransferase
ATM	Ataxia telangiectasia mutated
ATP	Adenosine triphosphate
ATPase	Adenosine triphosphatase
ATR	Ataxia telangiectasia and Rad3 related
AU1	AU-binding factor 1
BAD	Bcl-2/Bcl-X_L-antagonist, causing cell death
BMDM	Bone-marrow derived macrophage
BMP	Bone morphogenetic protein
bp	Base pairs
BRAF	B-raf proto-oncogene, serine/threonine kinase
BRD4	Bromodomain containing 4
BrdU	5-bromo-2'-deoxyuridine
BSA	Bovine serum albumin
c-MYC	Cellular homologue of the retroviral v-myc oncogene
C. elegans	Caenorhabditis elegans
C/EBPβ	CCAAT/enhancer binding protein beta
C57BL/6	C57 black 6 inbred mouse strain
CASAVA	Consensus assessment of sequence and variation
CBP	Cap binding protein
CCL	C-C motif chemokine ligand
CCL_4	Carbon tetrachloride
CCN1	Cysteine-rich angiogenic inducer 61
CCT2	Beta subunit of chaperonin containing TCP-1
Cd3e	T-cell antigen receptor complex, epsilon subunit of T3
Cd68	Macrophage antigen CD68
CDK	Cyclin-dependent kinase
cDNA	Complimentary DNA
cGAS	cyclic GMP-AMP synthase
CHK2	Checkpoint kinase 2
CIP1	CDK-interacting protein 1

cm	Centimetre
CM	Conditioned medium
CO_2	Carbon dioxide
COL1A1	Collagen type 1 alpha 1 chain
COL4A1	Collagen type 4 alpha 1 chain
CR	Caloric restriction
Cre	Cre recombinase
CRE-ERT2	Cre-recombinase activated by tamoxifen
CREM	cAMP (cyclic adenosine monophosphate) response-element theta
CXCL	C-X-C motif chemokine ligand
CXCR	C-X-C chemokine receptor
DA	Deoxycholic acid
DAPI	4,6-diamidino-2-phenylindole
DMBA	7,12-dimethylbenz(a)antharacene
DDR	DNA damage response
DEN	Diethylnitrosamine
Dgat2	Diacylglycerol o-acyltransferase 2
DMEM	Dulbecco's Modified Eagle Medium
DMSO	Dimethyl sulfoxide
DNA	Deoxyribonucleic acid
DNase	Deoxyribonuclease
DRI	D-retro inverso isoform
DTT	Dithiothreitol
E2F1	Retinoblastoma-associated protein 1
ECL	Enhanced Chemiluminescence Reagent
EDTA	Ethylenediaminetetraacetic acid
eEF2	Eukaryotic translation elongation factor 2
eEF2K	eEF2 kinase
EGF	Epidermal growth factor
EGR2	Early growth response 2
eIF4E	Eukaryotic translation initiation factor 4E
eMRI	Echo magnetic resonance imaging
EPRS	Glutamyl-prolyl-tRNA synthetase
ERCC1	Excision repair cross-complementation group 1
ERK	Extracellular signal-regulated kinase
Erα	Oestrogen receptor alpha
Fabp4	Fatty acid binding protein 4
FACS	Florescence-activated cell sorting
Fasn	Fatty acid synthase
FBS	Foetal bovine serum
FDG-PET	Fludeoxyglucose F 18 positron emission tomography
FDR	False discovery rate
FGF	Fibroblast growth factor
FITC	Fluorescein isothiocyanate
FOXO4	Forkhead box O4

G1	Gap 1 phase
GAIT	IFN-γ-activated inhibitor of translation
GAPDH	Glyceraldehyde-3-phosphate dehydrogenase
GATA4	GATA binding protein 4
GCK	Glucokinase
GFP	Green fluorescent protein
GLUT2	Glucose transporter 2
GO	Gene ontology
GPR	G-protein coupled receptor
GSEA	Gene set enrichment analysis
GSK3-β	Glycogen synthase kinase 3 beta
GTPase	Guanosine triphosphatase
GTT	Glucose tolerance test
GWAS	Genome-wide association study
H&E	Haematoxylin and eosin
H2B	Histone 2B
H3K27	Histone 3 lysine 27
HCA	High content analysis
HCC	Hepatocellular carcinoma
HEK293T	Human Embryonic Kidney 293 transformed
Het	Heterozygote
HFD	High-fat diet
HMGB1	High mobility group box protein 1
HNF	Hepatocyte nuclear factor
HOMA2	Homeostatic model assessment 2
HRAS	Harvey rat sarcoma viral oncogene homolog
HRT	Hormone replacement therapy
HSC	Hepatic stellate cell
HSP47	Heat shock protein 47
HSV-1	Herpes simplex virus 1
hTERT	Human telomerase reverse transcriptase
HTF	High-trans fat
HWM	Hepatocyte wash medium
ICAM	Intracellular adhesion molecule
IF	Immunofluorescence
IFL	Isolated fatty liver
IGF	Insulin-like growth factor
IGFBP	Insulin-like growth factor binding protein
IL	Interleukin
iMCs	Immature myeloid cells
INK4	Inhibitor of CDK4
IRF3	Interferon regulatory transcription factor 3
IRS	Insulin-like receptor substrate
ITT	Insulin tolerance test
JMJD3	Histone demethylase jumonji domain-containing protein 3

kDa	Kilo dalton
KEGG	Kyoto Encyclopaedia of Genes and Genomes
Klf4	Kruppel like factor 4
Klrd1	Killer cell lectin-like receptor d, member 1
KO	Knockout
L929	L cell, 929, derivative of strain L
LB	Lysogeny broth
LMNB1	Lamin B1
LMS	London Institute of Medical Sciences
LPS	Lipopolysaccharide
LT-HSCs	Long-term haematopoietic stem cells
LUC	Renilla lucufierase
M	Molarity
MACS	Magnetic-activated cell sorting
MAPK	Mitogen-activated protein kinase
MAPKAPK2	Mitogen-activated protein kinase-activated protein kinase 2
MCD	Methionine choline deficient
MDM2	Murine double minute 2
MEF	Mouse embryonic fibroblast
mg	Milligram
mH2A1	macroH2A1
mL	Millilitre
mm	Millimetre
mM	Millimolar
MMP	Matrix metalloproteinase
MRC	Medical research council
mRFP	Monomeric red fluorescent protein
mRNA	Messenger RNA
mTOR	Mechanistic target of rapamycin
mTORC1	mTOR complex 1
mTORC1	mTOR complex 2
N.S	Non-significant
NADH	Nicotinamide adenine dinucleotide reduced
NAFLD	Non-alcoholic fatty liver disease
NASH	Non-alcoholic steatohepatitis
NBS1	Nibrin
NCBP1	Nuclear cap binding protein 1
Ncf	Neutrophil cytosolic factor 2
NDUFS4	NADH: ubiquinone oxidoreductase subunit S4
NES	Normalised enrichment score
NF90	Nuclear factor 90
NFKb	Nuclear factor kappa B
NGS	Next generation sequences
NICE	National Institute for Clinical Excellence
NK	Natural killer cells

NKG2D	Natural-killer group 2, member D
NLRP3	NLR family pyrin domain containing 3
nM	Nanomolar
NRAS	Neuroblastoma rat sarcoma viral oncogene homologue
NT	Non-tumour
O_2	Oxygen
Ob/Ob	Genetically obese mice deficient of leptin
OCT4	Octamer-binding transcription factor 4
OIS	Oncogene-induced senescence
OSKM	Polycistronic cassette containing Oct4, Sox2, Klf4 and c-Myc
P	Passage
PBS	Phosphate buffered saline
PCA	Principal component analysis
Pck1	Phosphoenolpyruvate carboxykinase 1
PCR	Polymerase chain reaction
PD	Population doubling
PDCD4	Programmed cell death 4
PDGFA	Platelet derived growth factor subunit alpha
PDK1	Phosphoinositide-dependent kinase-1
PEI	Polyethylenimine
PFA	Paraformaldehyde
PGC-1α	Peroxisome proliferator-activated receptor gamma, coactivator 1 alpha
PI3K	Phosphoinositide 3-kinase
Pnpla2	Patatin like phospholipase domain containing 2
POLDIP3	S6K1-Aly/REF-like substrate
PPARγ	Peroxisome proliferator-activated receptor gamma
PTEN	Phosphatase and tensin homologue
Ptprc	Protein tyrosine phosphatase, receptor type c
PWAT	Perigonadal white adipose tissue
qPCR	Quantitative polymerase chain reaction
R.B.Cs	Red blood cells
RAPTOR	Regulatory associated protein of TOR
Rb	Retinoblastoma protein
Rheb	small Ras protein enriched in the brain
RICTOR	Rapamycin insensitive companion of TOR
RIN	RNA integrity number
RIPA	Radioimmunoprecipitation assay
RNA	Ribonucleic acid
RNase	Ribonuclease
RORC	RAR (retinoic acid receptor) related orphan receptor gamma
ROS	Reactive oxygen species
RPM	Revolutions per minute
RPS14	Ribosomal protein S14
RPS6	Ribosomal protein S6

RPS6KB1	Ribosomal protein S6 kinase 1 - S6K1
RPS6KB1	Ribosomal protein S6 kinase 2 - S6K2
RSK	p90 ribosomal protein S6 kinase
RT-qPCR	Quantitative reverse transcription-polymerase chain reaction
S	Serine
S6K1	Ribosomal protein S6 kinase 1
S6K2	Ribosomal protein S6 kinase 2
SA-β-Gal	Senescence-associated β galactosidase
SAHF	Senescence-associated heterochromatin foci
SASP	Senescence-associated secretory phenotype
SCAP	SREBP1 cleavage activating protein
SCID	Severe combined immunodeficiency
SD	Standard deviation
SDS	Sodium dodecyl sulphate
SEM	Standard error of mean
shRNA	Short hairpin RNA
siRNA	Small interfering RNA
Sma	Smooth muscle actin
SMS	Senescence messaging system
SOX2	SRY (sex determining region Y)-box 2
SREBP1c	Sterol regulatory element binding transcription factor 1 c
STING	Stimulator of interferon genes
T	Threonine
T	Tumour
TANK1	TANK binding kinase 1
TASCC	TOR-autophagy spatial coupling compartment
TBIL	Total bilirubin
TCA	Tricarboxylic acid
TGFB1	Tumour growth factor beta 1
TGs	Triglycerides
TIMP1	Tissue inhibitor of metalloproteinase 1
TK	Thymidine kinase
TLR	Toll-like receptor
TNFA	Tumour necrosis factor alpha
TP53 or p53	Tumour protein p53
TRAF3IP2	Tumour necrosis factor receptor-associated factor interacting protein 2
TSC	Tuberous sclerosis complex
URI1	Profoldin like chaperone
UTR	Untranslated region
VCAM	Vascular cell adhesion molecule
VEGF	Vascular endothelial growth factor
VSV-G	Vesicular stomatitis virus glycoprotein
WB	Western blot
Wnt	Wingless-Type MMTV integration site family, member

WT	Wild type
X-Gal	5-bromo-4-chloro-3-indolyl β-D-galactopyranoside
Xpd	Excision repair cross-complementation group 2
YY1	Yin-Yang 1
ZFP36L	Zinc finger protein 36, C3H type-like
ZRF1	DnaJ Heat Shock Protein Family Member C2
βTRCP	Beta-transducin E3 ubiquitin protein ligase
γH2AX	Phosphorylated histone H2 variant x
µg	Microgram
µL	Microlitre
µM	Micrometer

“It is very difficult to find a black cat in a dark room, especially when there is no cat”.

The moment that I read this quote from the book “Ignorance: How It Drives Science” by Stuart Firestein, it resonated profoundly within me because not only does it describe much of my PhD experience, but, as Firestein states, “it also illustrates fittingly the daily frustrations of conducting scientific research”. These hindrances are then further intensified when at a given time there is a lack of appropriate tools to conclusively follow our “favourite” hypotheses to the bitter or sweet end. Nevertheless, it is precisely the search for this unknown that enthralls me so very much about science, and why I will continue my pursuit for making the unknown known.

Chapter 1: Introduction.

1.1. Why study the regulation of the basic ageing process?

The world's elderly population is growing at a rapid pace and as people reach late age, they are faced with years of disability characterised by loss of independence and frailty (Campisi, 2013). Ageing affects nearly all biological organisms and can be defined as the gradual deterioration of physiological function in multiple cells and tissues (López-Otín et al., 2013). This ultimately results in reduced fitness, increased susceptibility to pathology and mortality. In addition, ageing is the single largest risk factor for the predominant killer diseases, including cancer, cardiovascular disease and dementia (Tchkonia et al., 2013). Tackling such chronic diseases one at a time, however, will not suffice as mathematical models based on mortality data have predicted that curing a *single* major disease such as cancer, heart disease, type 2 diabetes *etc.,* would only prolong human lifespan by a few years (3-4% of human lifespan); this is primarily due to death by one of the other major diseases such as dementia (Fried et al., 2009; Olshansky et al., 1990, 2001). The alternative would be to target the underlying ageing process such as through dietary restriction, which has been shown to prolong lifespan and improve age-related pathologies in multiple organisms including mice (trend also noted in monkeys) by much larger increments (Fontana et al., 2010). Therefore, by understanding the regulation of the basic ageing process, we would not only be able to increase human lifespan but also healthspan, which is the period of a person's life without debilitating disease to carry out daily functions (Hansen and Kennedy, 2016). Given the rise in the ageing population in the Western world, this underscores the importance of elucidating the common mechanisms underlying ageing, and this remains one of the last bastions for science to conquer. Although we are still in its infancy, the fact that we have now come to accept that the basic ageing process is amenable to therapeutic intervention and the resulting rise in research into ageing, gives hope for this endeavour that was once thought to be insurmountable.

Importantly, ageing is not just associated with degenerative diseases such as dementia but also hyperplastic diseases, *i.e.,* cancer. Although degeneration and cancer may seem as polar opposites since they involve loss and gain of function, respectively, the two share common origins, which is the time-dependent accumulation of cellular damage (Gems and Partridge, 2013). Therefore, the question then is whether there are common processes underlying many of these age-related pathologies that include ageing, degeneration and cancer (Campisi, 2013)?

1.2. Cellular senescence is both a hallmark of ageing and a potent barrier for tumorigenesis.

There is increasing evidence that a stress response termed cellular senescence links many pathologies of ageing, both degenerative and hyperproliferative (Campisi, 2013). Cellular senescence was initially identified by Hayflick and Moorhead when they illustrated that primary human fibroblasts can only divide a finite number of times; however, these cells remain viable and

metabolically active for months to years (Hayflick, 1965; Hayflick and Moorhead, 1961). Nonetheless, like many notable discoveries, the concept of senescence was initially dismissed as an artefact of tissue culture, but the copious amounts of evidence exemplifying the presence of senescent cells in various models of tissue culture, rodents and in humans in recent years have shone light on the validity of this process (Muñoz-Espín and Serrano, 2014).

Even from the early days, it was apparent there was a link between senescence and tumour suppression since senescent cells display a highly stable growth arrest, but the association between senescence and ageing was more complicated (Sager, 1991). Although it was feasible to assume that senescence could recapitulate the loss of regenerative capacity (tissue regeneration and repair) observed with age, the large majority of data were circumstantial in nature*, i.e.,* several markers of senescence increased in multiple tissues with age but nothing was shown that causally implicated senescence in ageing (van Deursen, 2014). Of note, however, was a pivotal study by van Deursen and colleagues, which showed that the onset of multiple age-related pathologies can be delayed by selectively eliminating senescent cells, either from birth or later in life, in a progeroid mouse model, thereby providing the first direct evidence for senescence driving the ageing process (Baker et al., 2011). The question of whether cellular senescence plays a role in chronological ageing, however, still loomed over the field. So, it was reassuring that five years later, van Deursen and colleagues once again published a seminal paper that demonstrated the selectively killing of senescent cells in chronologically aged mice increases both their healthspan as well as median lifespan (Baker et al., 2016). All in all, cellular senescence is now considered both a hallmark of the basic ageing process and also one of the most important barriers against tumorigenesis both *in vitro* and *in vivo* (López-Otín et al., 2013; Pérez-Mancera et al., 2014).

Senescence is not only involved in ageing and tumour suppression as the numerous roles that senescence play in pathophysiology are ever growing and include embryogenesis, wound healing, host immunity, atherosclerosis and more (Muñoz-Espín and Serrano, 2014). The implication of senescence in embryonic development was both surprising and fascinating. Senescent cells were present in different regions of the developing embryo, and disrupting this senescence response resulted in morphological defects of the Wolffian duct and the mesonephros, indicating that senescence does indeed play an essential role during development (Muñoz-Espín et al., 2013; Storer et al., 2013). These studies demonstrated that senescence is not only a pathological response to stress but also part of normal physiology. Therefore, one hypothesis is that senescence presumably evolved from a developmental pathway to later being used as a mechanism to counter tumour growth and ensure tissue homeostasis in response to acute injury in the adult body (Banito and Lowe, 2013).

Overall, it is important to highlight that senescence in physiology is a double-edged sword, whereby it is largely beneficial during early life (in development and in response to acute injury – acute senescence) and detrimental in later life (tissue homeostasis - chronic senescence) (Campisi and d'Adda di Fagagna, 2007). It has been hypothesised that tumour suppressor mechanisms such as cellular senescence have evolved in such a way that they only need to be effective for a relatively short term, *i.e.,* during the reproductive age, since there are very little selective pressures to remove any harmful effects that occur later in life such as the impact of senescence on tissue regeneration (Campisi and d'Adda di Fagagna, 2007). This is termed the antagonistic pleiotropy hypothesis, which is considered a crucial evolutionary theory of ageing (Williams, 1957).

1.3. Deregulated nutrient sensing in ageing and senescence – the link?

Similar to cellular senescence, deregulated nutrient sensing, particularly the insulin and insulin-like growth factor signalling (IIS) pathway, is another hallmark of ageing (López-Otín et al., 2013). Importantly, the IIS pathway is a key activator of the mammalian or mechanistic target of rapamycin (mTOR), a master regulator of cellular growth and metabolism that ensures tissue homeostasis by integrating various internal and external stimuli (Laplante and Sabatini, 2012). It has been suggested that to be a hallmark of ageing a process should ideally fulfil the following criteria: the process should become apparent (either increase or decrease) during normal ageing and the experimental manipulation, either by aggravating or ameliorating, of that process should reduce or prolong lifespan, respectively (López-Otín et al., 2013). Of note, both cellular senescence and deregulated nutrient sensing share these characteristics. In addition to cellular senescence and deregulated nutrient sensing, seven other hallmarks of ageing have been described in a seminal review in the field of ageing and these hallmarks are summarised in Figure 1.1 (López-Otín et al., 2013).

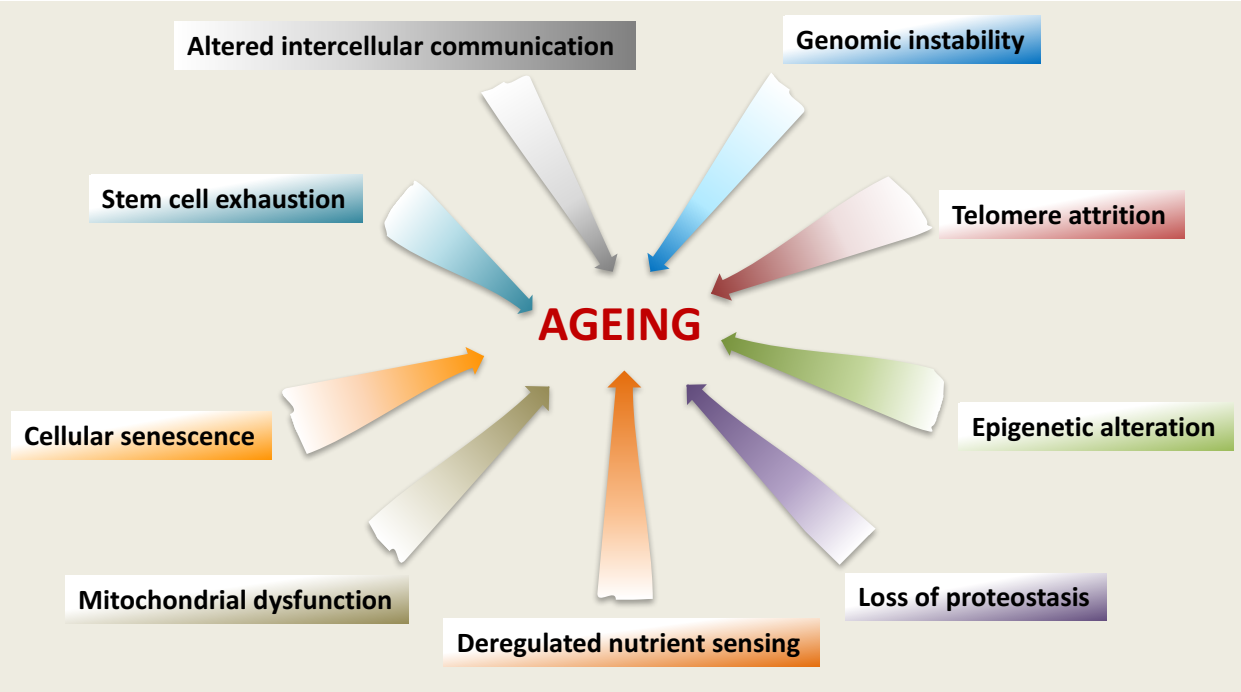

Figure 1.1.Hallmarks of Ageing.
Nine hallmarks of ageing that include cellular senescence and deregulated nutrient sensing. Each hallmark manifests with age and aggravation and amelioration of the process is beneficial and detrimental, respectively, to healthspan. Adapted from (López-Otín et al., 2013).

Interestingly, research into the mechanisms driving ageing has exploded over the past 20 years by the discovery that genetic, dietary or pharmacological approaches can not only drastically prolong lifespan but also improve multiple age-associated pathologies (Gems and Partridge, 2013). Among these, dietary restriction remains the most robust approach to improve healthspan and lifespan in various species. In support of this, the Withers' group have previously shown that knockout (KO) mice for either insulin-receptor substrate 1 (IRS-1) or ribosomal protein S6 kinase 1 (p70 S6K1), two key components of the nutrient sensing IIS pathway that are upstream and downstream of mTOR signalling, respectively, show a marked increase in lifespan and resistance to age-related pathologies (Selman et al., 2008, 2009). Nonetheless, a key limitation in potential therapeutic application lies in our incomplete understanding of the molecular mechanisms driving this lifespan extension. Furthermore, the mTOR pathway, which acts downstream of the IIS pathway, has recently also been implicated in cellular senescence (discussed in length later in the introduction). Therefore, elucidating exactly how these two crucial biological processes (cellular senescence and nutrient sensing) interact and determining whether the increased lifespan in these mice, particularly *S6K1*$^{-/-}$ mice, is due to deregulated senescence is one of the major aims of this project. This is of particular interest because it is not yet known whether cellular senescence plays a role in any of the long-lived mouse models described thus far with the exception of the *INK-ATTAC* mouse (will be described later) that selectively eliminate senescent cells (Figure 1.2).

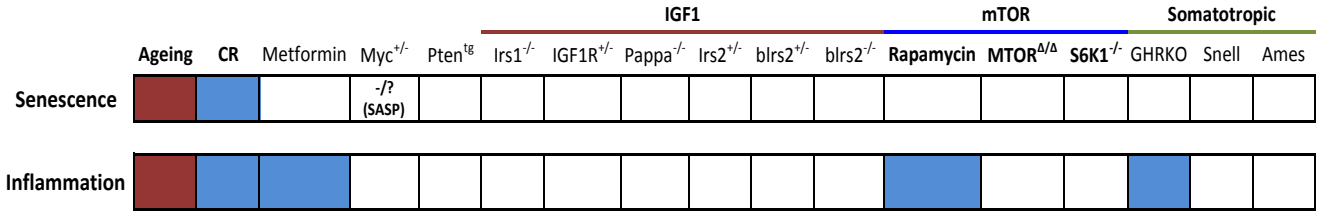

Figure 1.2. What is known about cellular senescence and inflammation in long-lived mouse models?
Cellular senescence and inflammation manifest with age (red colouring) and are attenuated (blue colouring) by caloric restriction (CR). Downregulation of insulin-like growth factor 1 (IGF1) signalling, mechanistic target of rapamycin (mTOR) signalling or somatotropic axis increase lifespan, but it is unknown (white boxes) whether cellular senescence is implicated in this improvement. Adapted from (Hofmann et al., 2015).

1.4. How is senescence induced?

It was originally proposed that senescence was induced solely by telomere shortening due to the "end-replication problem", and this was termed "replicative senescence" (Harley et al., 1990; Olovnikov, 1971; Watson, 1972). Telomere erosion due to repeated cell division is now a well-known phenomenon whereby DNA polymerase fails to completely replicate the lagging strands of a linear piece of DNA (McEachern et al., 2000). These telomeres function as a molecular clock, when critically shortened, results in a DNA damage response (DDR) and activation of the tumour suppressor p53 (Fagagna et al., 2003; Harley et al., 1990; Herbig et al., 2004). It is important to highlight that various other stimuli have now been discovered that can induce senescence irrespective of telomere length, and this is termed "premature senescence" (Kuilman et al., 2010). Some of these include other forms of DNA damage, oxidative stress, reprogramming of somatic cells and cytotoxic drugs (chemotherapeutic agents) (Kuilman et al., 2010).

Paradoxically, it was also discovered that oncogenic activation also stimulates a profound senescence response, termed "oncogene-induced senescence" (OIS) (Serrano et al., 1997). The initial study by *Serrano et al.,* used an $HRAS^{G12V}$ mutant to show this premise, but now more than 50 oncogenes have been reported to induce senescence (Gorgoulis and Halazonetis, 2010). Importantly, the mechanisms orchestrating OIS is independent from replicative senescence induced by telomere shortening since expression of human telomerase (hTERT) failed to bypass the growth arrest driven by HRAS (Wei et al., 1999). OIS instantly garnered widespread acclaim in the senescence field as this provided direct evidence for senescence acting as a barrier during the early stages of tumorigenesis. Nevertheless, there was some initial doubt as to the validity of this process due to the lack of *in vivo* evidence, but this was resolved with the emergence of a series of OIS studies in rodents and humans (Braig et al., 2005; Chen et al., 2005; Collado et al., 2005; Lazzerini Denchi et al., 2005; Michaloglou et al., 2005).

One of the best examples of this was the study by Peeper and colleagues that demonstrated human naevi, which are skin lesions of benign nature, not only express oncogenic markers such as $BRAF^{V600E}$ or NRAS but also stain positive for various senescence markers (discussed below) (Michaloglou et al., 2005). Importantly, these naevi persist for months to years prior to progressing to melanomas by acquiring additional mutations that cancel out the senescence effector systems. For a long time, it was not clear exactly how cells escaped the impact of OIS and progressed to melanomas. A recent paper by Bosenberg and colleagues, however, shed some light on this process (Damsky et al., 2015). They illustrated that reactivation of mTOR signalling in addition to loss of the tumour suppressor $p16^{INK4A}$ is required for the progression of naevi to melanomas as either of these events alone was insufficient for melanoma formation. This also raises rather interesting questions as to the reversibility of the senescent state. For example, is OIS observed in naevi a form of pseudo-senescence that is a temporary growth arrest or did these cells not reach the "deep" or "late" senescence in the first place (Souroullas and Sharpless, 2015)?

1.5. What are the hallmarks and effectors of senescence?

It is imperative to mention that there are no unique markers of senescence and not all senescent cells express all the markers of senescence, thus several of these markers must be present together to define a senescent cell (Figure 1.3) (Salama et al., 2014). It is also important to highlight that it is much easier to detect senescent cells *in vitro* in cell culture models than in mouse models *in vivo.* To overcome this, it is only very recently that specific transgenic mouse models have and/or are been generated to specifically detect and isolate senescent cells from various mouse tissues. *These models will be discussed later on, but unfortunately due to lack of their availability at the onset and the need to age the mice for 600 days, they have not been utilised in this study.*

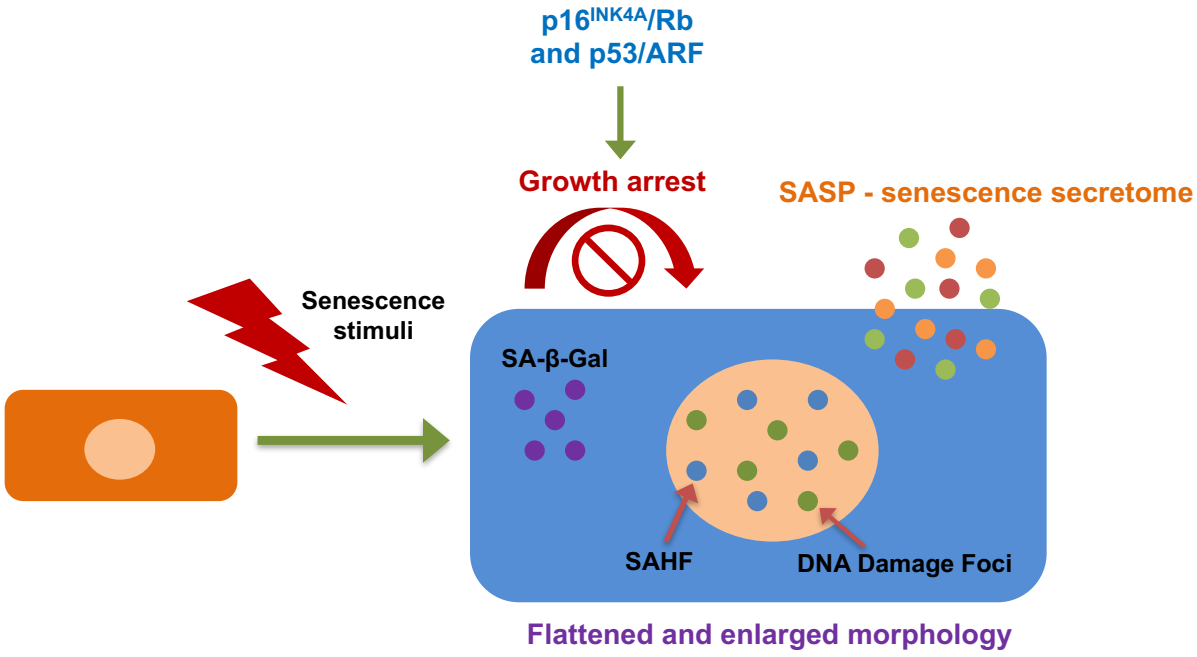

Figure 1.3. Hallmarks of senescence.
Senescence is induced by a variety of stressful stimuli including replicative stress and oncogene activation and the typical senescence phenotype develops over several days. Senescence is characterised by multiple molecular and phenotypic markers including a stable growth arrest caused by $p16^{INK4A}$ and/or p53 activation as well as senescence-associated beta galactosidase (SA-β-Gal) activity. Senescent cells also secrete a myriad of factors ranging from proinflammatory chemokines and cytokines to growth factors and proteases. SASP: senescence-associated secretory phenotype. SAHF: senescence-associated heterochromatic foci. Adapted from (Salama et al., 2014).

The most striking feature of senescent cells is their highly stable G1 phase growth arrest, which differentiates them from the temporary arrest observed in quiescent cells. This is because unlike cells in quiescence, senescent cells are non-responsive to mitogenic or growth factor stimuli (Campisi and d'Adda di Fagagna, 2007). In addition, senescent cells are also distinct from terminally differentiated cells, which for the most part (as some differentiated cells such as hepatocytes are capable of cell division) are also non-dividing. A key distinction between the two is that terminally differentiated cells whether it is an insulin-producing β-cell in the pancreas or a hepatocyte in the liver are generated to perform various biological processes, whereas senescence occurs for the most part (exception being developmental senescence) in response to a stressful stimulus. Of note, however, is that both β-cells and hepatocytes can undergo senescence during ageing or in response to oncogenic activation, respectively, thereby highlighting that it is not only stem cells that undergo senescence (Helman et al., 2016; Kang et al., 2011).

The characteristics of senescent cells include a flattened and enlarged morphology, senescence-associated beta galactosidase (SA-β-Gal) activity, various forms of DNA damage, senescence-associated heterochromatin foci (SAHF) and altered gene transcription (Salama et al., 2014). In addition, senescent cells lose expression of lamin B1 (LMNB1) and high mobility group box protein 1 (HMGB1) from their nucleus. Senescent cells also secrete a complex mixture of factors ranging from extracellular matrix associated proteases, growth factors to inflammatory proteins, and this was termed the senescence-associated secretory phenotype (SASP) or the senescence messaging system (SMS) for their ability to signal and influence their surrounding environment (Coppé et al., 2010a; Kuilman and Peeper, 2009).

In addition to the aforementioned phenotypic characteristics of senescent cells, nearly all types of senescence result in derepression of the INK4/ARF locus, resulting in activation of the $p16^{INK4A}$/retinoblastoma protein (Rb) and/or the ARF/p53/p21 tumour suppressor pathways (Gil and Peters, 2006). It is important to highlight that the regulation of these pathways is quite complex with various upstream and downstream regulators and effectors as well as cross-regulation between the two pathways (Campisi, 2013). Nonetheless, both these pathways act by inducing a potent growth arrest by inhibiting the cyclin-dependent kinases (CDKs), and overexpressing these proteins are sufficient to induce senescence (Beauséjour et al., 2003; McConnell et al., 1998). These two pathways are crucial not only for the induction of cellular senescence but are also considered two of the most important tumour suppressor pathways, thereby highlighting once again the striking similarity between senescence and tumour suppression (Campisi, 2005).

For a long time, it was thought that the senescent state was a cell intrinsic, static state that was an end in itself. It has now become evident, however, that senescent cells possesses a cell extrinsic arm, the SASP, that not only affects tissue homeostasis but is also capable of promoting malignancy (Tchkonia et al., 2013). This diversity of the response depends on the surrounding environment and the genetic context of the cells being exposed to the SASP. In addition, the SASP is a plastic response whereby its constituents depend on the cell type and the senescence stimuli. Of note, however, is that the proinflammatory arm of the SASP is highly conserved among the most widely studied forms of senescence including replicative, irradiation and oncogene-induced senescence (Freund et al., 2010). Even so, there are cases when this proinflammatory SASP is absent such as during mitochondrial dysfunction induced senescence (MiDAS) or when senescence is induced by overexpression of $p16^{INK4A}$ (Coppé et al., 2011; Wiley et al., 2016).

It is important to highlight that one of the most well-known markers of senescence is increased SA-β-Gal activity, which corresponds to the increased lysosomal numbers in senescent cells, but this is also found in macrophages (Bursuker et al., 1982). In addition, T-cells and B-cells also express very high levels of $p16^{INK4A}$ with age, which corresponds to immunosenescence, but

there is a lot of debate as to whether these p16^{INK4A}-expressing lymphocytes are really senescent or whether this is form of "cellular exhaustion" (Liu et al., 2009; Sharpless and Sherr, 2015; Signer et al., 2008). In addition, tumour infiltrating immune cells were also positive for p16^{INKA} expression (Burd et al., 2013). But it is unclear whether the tumours induce p16^{INK4A} expression in these cells in a non-cell autonomous manner or whether p16^{INK4A}-expressing leukocytes are recruited to the site of tumours (Burd et al., 2013). In addition, there is a lot of debate regarding the specificity of anti-mouse antibodies to detect p16^{INK4A} expression in tissues (Demaria et al., 2014). All this should highlight the current difficulty in specifically identifying senescent cells in mouse tissues.

1.6. What are the roles of senescence and the senescence-associated secretory phenotype (SASP) in pathophysiology?

As mentioned earlier, senescent cells have been implicated in numerous pathological responses and diseases, and these are summarised in Figure 1.4. In addition, some of the known SASP factors are shown in Figure 1.5.

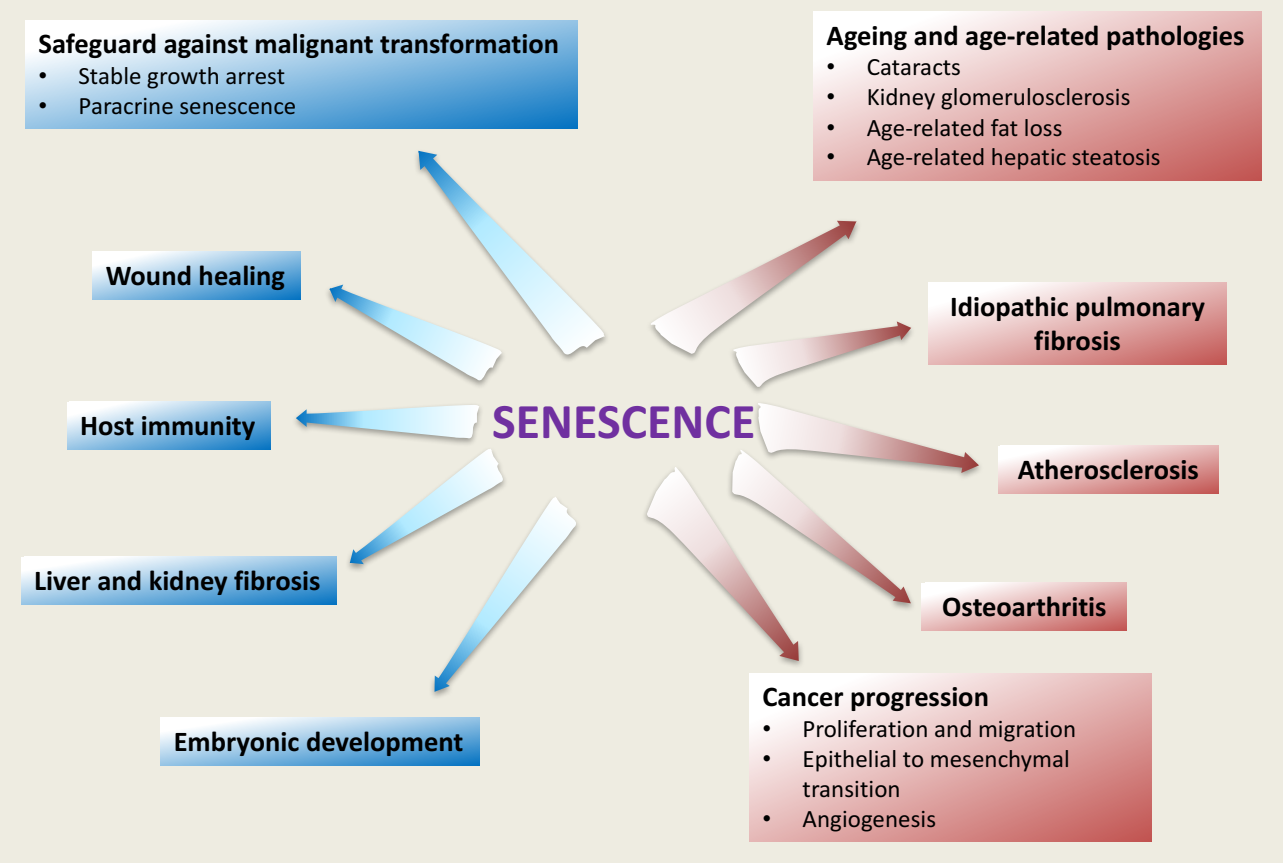

Figure 1.4. Senescence in pathophysiology.
Senescence plays both beneficial and detrimental roles in several adult diseases. Blue colouring – senescence is beneficial. Red colouring – senescence is detrimental. Adapted from (Muñoz-Espín and Serrano, 2014).

IL-1α	IL-1β	IL-6	IL-8	IL-7	IL11
CCL2	CCL3	CCL4	CCL5	CCL13	CCL20
CCL27	CXCL1	CXCL2	CXCL5	CXCL10	GM-CSF
TNFA	PAI2	IGFBP2	IGFBP5	IGFBP6	IGFBP7
MMP1	MMP2	MMP3	MMP9	MMP10	MMP12
MMP13	TIMP1	TIMP2	VEGFA	VEGFC	BMP2
GDF15	TGF-β1	INHBA	ESM1	LOXL2	HMGB1
SERPINA1	LAMNB2	VCAM1			

Figure 1.5. Key SASP factors.
Some of the key SASP factors upregulated during replicative senescence, oncogene-induced senescence and/or irradiation-induced senescence. Adapted from (Acosta et al., 2008, 2013, Coppé et al., 2008, 2010b).

1.6.1. The complex interaction between senescent cells, the SASP and the immune system.

One of the main functions of the SASP is to recruit the immune system to eliminate senescent cells (Kang et al., 2011; Krizhanovsky et al., 2008; Lujambio et al., 2013; Xue et al., 2007). Many of these pioneering studies were first performed in Scott Lowe's lab where they demonstrated this process occur at sites of senescent cell accumulation such as in fibrosis and at the premalignant stage of tumorigenesis. T-helper 1 cells, natural killer (NK) cells, macrophages and neutrophils largely mediated this immune response. The initial study utilised a model whereby the authors co-injected hepatoblasts infected with a doxycycline-inducible short hairpin RNA against the tumour suppressor p53 into athymic nude mice (lacking functional B and T cells but an intact innate immune response). As expected, the tumours continued to grow when p53 was depleted by RNA interference but the restoration of p53 resulted in cellular senescence (not apoptosis) and expression of proinflammatory cytokines, recruitment of immune cells and eventual tumour regression. This clearly depicted a scenario in which cellular senescence acts in concert with the innate immune response to potentially limit tumour growth (Xue et al., 2007). Further work demonstrated that NKG2D+ NK cells play a pivotal role in this immune clearance, and this required secretion of CCL2 (C-C Motif Chemokine Ligand 2) by senescent cells (Iannello et al., 2013).

This highlights the importance of clearing senescent cells within the tissues because although oncogene-induced senescence is a crucial tumour suppressor mechanism, these cells still have the potential to undergo tumorigenesis if the senescence effector systems are bypassed. Therefore, senescent cells help to halt tumorigenesis in a two-step process: first by undergoing a stable cell cycle arrest and then recruiting the immune system via the SASP to eventually eliminate these senescent cells. The best example of this is the follow-up study by Zender and colleagues where they delivered oncogenic $NRAS^{G12V}$ into hepatocytes of C57BL/6 immunocompetent mice through a hydrodynamic tail vein injection of the plasmid. In this model, a small percentage of

hepatocytes (10-20%) become stably transfected with the plasmid and undergo senescence with a secretory phenotype. Importantly, the CD4+ T-cell-mediated adaptive immune response played a pivotal role in mediating the clearance of senescent cells because in either SCID or SCID/beige mice lacking an adaptive immune response, the NRAS+ cells persisted and eventually bypassed senescence and developed hepatocellular carcinoma. This evidently showed the importance of clearing the premalignant senescent cells in preventing liver cancer development, as ablation of this immune response resulted in hepatocellular carcinoma. This process was termed “senescence surveillance” (Kang et al., 2011).

The above studies elucidated which arms of the immune system play a role in this “senescence surveillance” program, but it is equally important to understand which of the SASP factors recruit the immune system for any potential therapeutic interventions. It is highly likely that many of the SASP factors may act in concert to do this. Nevertheless, a recent paper showed that the CCL2-CCR2 axis plays a crucial role clearing senescent hepatocytes in the model of $NRAS^{G12V}$-driven OIS (Eggert et al., 2016). In brief, they showed that senescent hepatocytes via CCL2 recruit CCR2+ immature myeloid cells (iMCs) into the liver, which then differentiate into macrophages that clear the premalignant senescent hepatocytes, as CCR2 deletion promotes hepatocellular carcinoma. Senescent hepatocytes, however, promoted the growth of tumoural cells when tumoural cells were injected following senescence induction. Importantly, they demonstrated this was due to a complex interaction between the senescent hepatocytes, recruited iMCs and natural killer cells. This is because the tumoural cells inhibited the differentiation of the recruited iMCs, which in turn repressed natural killer cell-mediated killing of tumoural cells, thus describing a scenario where senescence-mediated immune cell recruitment can be deleterious (Eggert et al., 2016). In support of this, Alimonti and colleagues also demonstrated a similar situation in the prostate of PTEN (phosphatase and tensin homologue) null (prostate-specific) mice (Di Mitri et al., 2014). Loss of PTEN initially induces senescence in the prostate epithelium, but tumours eventually form and become highly aggressive over time. They showed that CD11b+, Gr-1+ myeloid cells are recruited into the prostate and promote tumour growth by secreting interleukin-1 receptor antagonist (IL-1RA), which prevents a population of premalignant cells from undergoing senescence (Di Mitri and Alimonti, 2016; Di Mitri et al., 2014).

1.6.2. Senescence and the SASP play a dual role in cancer.

Initial studies of the SASP focussed on its protumorigenic properties (Bavik et al., 2006; Coppé et al., 2006, 2008; Krtolica et al., 2001; Parrinello et al., 2005). These studies demonstrated that the SASP from surrounding senescent fibroblasts acts in a non-cell autonomous fashion to promote proliferation and malignant transformation of premalignant epithelial cells as well as modulate the tissue microenvironment in such a way to support this transformation. Many of these studies utilised either *in vitro* functional assays or *in vivo* xenograft models to demonstrate the functional

relevance of the SASP. These experiments were based on co-culturing premalignant or tumoural cells with senescent fibroblasts or co-injecting these cells into mice in different contexts.

Importantly, various SASP factors may act in concert to promote the different stages of malignancy. For example, the proinflammatory growth-regulated oncogene 1 (GROα, also called CXCL1) and amphiregulin (a member of the epidermal growth factor family) promote proliferation and growth of premalignant epithelial cells, while interleukin (IL)-6 and IL-8 induce an epithelial to mesenchymal transition (EMT) (Bavik et al., 2006; Coppé et al., 2008, 2010b; Laberge et al., 2012; Yang et al., 2006). Concurrently, the vascular endothelial growth factor (VEGF) induces angiogenesis to ensure an adequate blood supply is available to support this growth and transition (Coppé et al., 2006). In addition, senescent cells secrete various metalloproteinases including MMP2 and MMP3, which may also aid in degrading the basement membrane to promote subsequent invasion of tumoural cells (Liu and Hornsby, 2007; Parrinello et al., 2005; Qian et al., 2002; Tsai et al., 2005). This underscores the complex interaction that occurs between the senescent fibroblasts, premalignant epithelial cells and the surrounding microenvironment.

It is important to highlight that many of the above studies utilised xenograft models to study the role of the SASP in cancer, but another landmark paper in the field demonstrated that senescent cells also promote tumorigenesis (hepatocellular carcinoma) in a model that better resembles human liver cancer (Yoshimoto et al., 2013). In this study, the authors induced hepatocellular carcinoma by combining the carcinogen DMBA with either a high fat (60% of kcal) diet or in genetically obese mice deficient of leptin (*ob/ob* mice). They first elegantly illustrated that the gut microbiota plays an essential role in hepatocellular carcinoma development through secretion of the metabolite deoxycholic acid (DA), which in turn induces DNA damage and senescence in the hepatic stellate cells (HSCs). The senescent HSCs then secrete a SASP containing proinflammatory factors such as IL-1β, IL-6 and CXCL1 that promotes the proliferation and malignancy of the surrounding hepatocytes. Importantly *Il1β*$^{-/-}$ mice or mice depleted of HSCs through a small interfering RNA (siRNA) against HSP47 showed a significant reduction in their tumour burden. This study was a fine example depicting how senescent cells can affect nearby cells and the microenvironment through the SASP in a paracrine fashion. This is because these mice developed hepatocellular carcinoma, which is of hepatocyte origin, whereas it was the hepatic stellate cells that underwent senescence, suggesting that secreted factors from senescent cells promoted hepatocyte transformation (Yoshimoto et al., 2013). Nevertheless, it is important to mention that this model lacked fibrosis, which is found in 80-90% of human hepatocellular carcinoma patients (Hashimoto et al., 2009).

In addition to promoting malignancy, senescent cells were recently implicated in promoting tumour metastasis and relapse following chemotherapy (Demaria et al., 2017). The study by

Campisi and colleagues first showed that chemotherapeutic agents such as doxorubicin induced senescence in various tissues such as the lung, liver and skin. They then specifically eliminated these senescent cells using the *p16-3MR* genetic mouse model, in which the $p16^{INK4A}$ promoter drives the expression of synthetic Renilla lucufierase (LUC), monomeric red fluorescent protein (mRFP) and truncated herpes simplex virus 1 (HSV-1) thymidine kinase (HSV-TK). Importantly, they illustrated that eliminating senescent cells with ganciclovir (has high affinity for HSV-TK) not only ameliorated various side effects observed with genotoxic drugs such as immunosuppression, cardiac dysfunction and fatigue (physical activity and strength as measured in mice) but also reduced cancer relapse and metastasis when breast tumoural cells were first injected into the mammary pads prior to doxorubicin treatment. This provided the first direct evidence to what was long speculated, which is that senescence cells accumulate following chemotherapy treatment and they contribute to tumour relapse and adverse side effects of these toxic agents (Demaria et al., 2017). Therefore, it is becoming increasingly clear that eliminating senescent cells following chemotherapy may be of benefit for survival and positive outcome.

To further support the concept that senescence-targeted therapy is a viable option for cancer treatment, several phase II and phase III clinical trials are now underway/completed utilising the selective CDK4 and CDK6 inhibitor palbociclib in breast cancer patients (Finn and Slamon, 2015; Finn et al., 2016; Turner et al., 2015). As aforementioned, $p16^{INK4A}$ binds and inhibits CDK4/6 activity to induce senescence, therefore it should not be a surprise that palbociclib also induces senescence in different cancer cell lines including breast tumoural cells (Finn et al., 2009; Michaud et al., 2010). These *in vitro* studies were then followed up by phase II and phase III clinical trials that showed combined treatment of palbociclib with current breast cancer therapies such as letrozole in patients with advanced breast cancer significantly increases median progression-free survival, compared to letrozole alone (Finn and Slamon, 2015; Finn et al., 2016; Turner et al., 2015). Although senescence induced by CDK4/6 inhibition (in both tumoural cells and fibroblasts) display a SASP-like phenotype, it is still unclear whether this SASP recruits the immune system to clear senescent cells and therefore if these senescent cells persist they could potentially become tumorigenic down the line (Goel et al., 2017; Guan et al., 2017). There is, however, a new class of drugs termed “senolytics” that preferentially kills senescent cells as opposed to normal cells, and therefore senolytics could be used following palbociclib treatment to reduce/prevent any potential tumour relapse from occurring. *Senolytics will be discussed in length with regards to ageing below.*

Importantly, it seems that the SASP promotes tumorigenesis of cells that are already primed for malignant transformation or in other words cells that may have already acquired the mutations to cancel out the senescence effector systems. Therefore, an important question is what effects does the SASP exert on normal cells? This leads us to the other spectrum of effects that

the SASP employs. Initial studies focussing on the tumour suppressive roles of the SASP illustrated that certain SASP components such as IL-6 and IL-8 act in a cell-autonomous (autocrine) fashion to reinforce the highly stable growth arrest associated with senescence (Acosta et al., 2008; Kuilman et al., 2008). This hypothesis was strengthened when knockdown of the receptors for these SASP components such as for CXCR2 (receptor for IL-8 and GROα) or IL-6R also bypassed the senescence growth arrest. In addition to the above findings, our group and others also demonstrated that the SASP not only reinforce the growth arrest in an autocrine manner but is also capable of propagating senescence to neighbouring cells in a paracrine manner (paracrine senescence) (Acosta et al., 2013; Hubackova et al., 2012). This was through a complex mechanism involving the inflammasome and its cleavage factors (IL-1α and IL-1β) as well as the transforming growth factor receptor-β superfamily (Acosta et al., 2013; Hubackova et al., 2012).

This concept of paracrine senescence raises rather interesting questions. For example, what is the extent of this paracrine response, and why do senescent cells elicit such a response in the first place as it could be misused to promote malignancy as shown above? The former was clarified through a serial conditioned medium (CM) experiment, which demonstrated that the normal cells being exposed to the SASP (*i.e.,* undergoing paracrine senescence) cannot themselves induce senescence in other cells, thus showing this propagation is restricted (Acosta et al., 2013). To answer the latter, it is possible that the SASP may be used to communicate the damaged state of the cell to the surrounding cells to prepare for tissue repair; alternatively the SASP may communicate to the immune system to effectively clear these damaged cells to ensure tissue homeostasis (Tchkonia et al., 2013). There is evidence for both of these functions.

It is also curious that proinflammatory factors of the SASP are not the sole culprits in mediating this senescence reinforcement, since components within the IIS pathway (insulin-like growth factor binding proteins – IGFBP7) were also shown to be sufficient to induce senescence in both melanocytes and mammary cells (Benatar et al., 2012; Wajapeyee et al., 2008). Therefore, this once again suggests a possible link between nutrient sensing and cellular senescence. This may be explained at least in part by how important it is for cells to maintain a fine balance between nutrient availability and cell damage, stress and proliferation.

1.6.3. The role of senescence and the SASP in wound healing and fibrosis.

In addition to its role in cancer, senescence and the SASP has also been implicated in wound healing and fibrosis (Demaria et al., 2014; Jun and Lau, 2010; Krizhanovsky et al., 2008; Lujambio et al., 2013). In the context of wound healing, it was clearly shown by Lau and colleagues that the matricellular protein CCN1 is expressed at sites of wound repair in the skin and induces myofibroblast senescence, and knock-in mice expressing a defective CCN1 undergoes faster wound closure rates as a result of reduced senescence. Although superficially this may seem

beneficial, it was in fact detrimental because the CCN1 defective mice showed exacerbated fibrosis following wound closure. This is essentially because under conditions of normal wound healing, CCN1-induced senescence in myofibroblasts causes these cells to express various antifibrogenic genes such as the matrix metalloproteinases MMP2, MMP3 and MMP9 that help to degrade the fibrotic scar. In the absence of these proteases, the scar persists and thereby affects tissue structure and homeostasis. Importantly, this work also shows that it is possible to dissociate the wound healing response from the fibrotic phase (Jun and Lau, 2010). Campisi and colleagues followed up this work in wound healing using the p16-3MR transgenic mice where they showed that senescent cells (endothelial and fibroblast in origin) promote wound healing in the skin by inducing myofibroblast differentiation through platelet derived growth factor (PDGF)-AA, because eliminating senescent cells delayed wound healing (Demaria et al., 2014). Overall, it seems that senescence plays a beneficial role during cutaneous wound healing by promoting wound closure and restraining fibrosis.

In addition to wound healing, senescence has been implicated to play a beneficial role in limiting liver fibrosis as well. These pioneering studies by Lowe and colleagues clearly demonstrated that senescence acts as a break in the progression of liver fibrosis in response to acute liver damage (Krizhanovsky et al., 2008; Lujambio et al., 2013). Senescence was shown to do this in a two-step process. This involved degradation of the fibrotic scar through a SASP-like secretome followed by recruitment of the immune system to clear the senescent cells such that the normal tissue architecture is maintained. Lowe and colleagues demonstrated this using the well-defined model of carbon tetrachloride (CCl_4)-induced liver fibrosis. The progression of liver fibrosis is highly complex involving multiple-organ systems and a multitude of different cells within the liver and is explained in detail in the following reviews (Bataller et al., 2005; Friedman, 2008). Thus, the process will be explained in a simplified manner here.

In this model, CCl_4 damages the hepatocytes, and the dying hepatocytes in turn signals via a myriad of factors including reactive oxygen species (ROS), apoptotic bodies and transforming growth factor-β1 (the major pro-fibrogenic cytokine within the liver) to the hepatic stellate cells (HSCs) (Bataller et al., 2005; Friedman, 2008). Kupffer cells, the resident macrophages within the liver, also become activated during this period and secrete among other things platelet-derived growth factor (PDGF), which acts as the major mitogen towards HSCs. The HSCs then in turn proliferate and transdifferentiate into myofibroblasts and secrete fibrogenic compounds including type 1 collagen to form a fibrotic scar that halts the liver injury by providing structure and integrity to the damaged tissue. Under normal circumstances, the HSCs then undergo cellular senescence (accumulated DNA damage from hyperproliferation) and produce a SASP-like secretome containing matrix metalloproteinases that degrade the fibrotic scar. Simultaneously, other SASP factors signal to the immune system (Natural Killer (NK) cells and M1-type macrophages) to clear

the senescent cells. These studies also showed that if the senescence response is ablated in the HSCs by knocking out p53, the fibrosis worsens and eventually results in cirrhosis and HCC (Lujambio et al., 2013; Krizhanovsky et al., 2008). This is an excellent example of acute senescence where senescence acts as a beneficial process triggered in response to an acute injury to halt further damage, followed by resolution of the injury and clearance of any remaining senescent cells. In addition to liver fibrosis, senescence has also been implicated in kidney and lung fibrosis as well but these are beyond the scope of this thesis.

1.6.4. The role of senescence in ageing.

When cellular senescence was initially discovered more than 5 decades ago, Hayflick and Moorhead proposed that it would play a pivotal role in ageing and age-related pathologies given the importance of senescence in cellular lifespan. As alluded to earlier, however, it was only in the past 10 years that cellular senescence was causally implicated in ageing (Baker et al., 2013a, 2008, 2011, 2016). The great length of time it took from the initial discovery to its causal implication were down to many reasons, but it mostly comes down to the difficulty in being able to manipulate senescent cells *in vivo* and identifying senescent cells in whole organisms, particularly in aged tissues where only a small percentage of senescent cells are found (Childs et al., 2015; van Deursen, 2014; Sharpless and Sherr, 2015).

Some of the earliest work on senescence in mammalian ageing were done in the Sharpless lab where they demonstrated that the tumour suppressors $p16^{INK4A}$ and $p19^{ARF}$, but not other cell cycle inhibitors, are highly expressed at the mRNA level ($p16^{INK4A}$ protein expression was observed as well) in multiple tissues in ageing including the liver and kidney (Krishnamurthy et al., 2004). But why do senescent cells accumulate during ageing given that the SASP plays a crucial role in recruiting the immune system? Two possible explanations for this are that there is an increasing number of cells undergoing senescence with age due to accumulated damage and replicative exhaustion and this is worsened with age-related immunosenescence that fails to efficiently clear the senescent cells. In addition, a meta-analysis of genome-wide association studies (GWAS) and age-related pathologies found that the INK4/ARF locus is associated with multiple chronic diseases including various cancers, type 2 diabetes, atherosclerosis and glaucoma (Jeck et al., 2012). In fact, this is in line with a new concept that many developmental pathways including senescence ($p16^{INK4A}$) are reactivated during ageing and contribute to pathology, and this was termed the developmental decay hypothesis (Martin et al., 2014). Further work from the Sharpless group demonstrated using a *$p16^{INK4A}$-luciferase* knockin model that there is an exponential increase in $p16^{INK4A}$ activity throughout the mouse body during ageing. $p16^{INK4A}$ activity, however, did not correlate with mortality but did predict cancer initiation at a specificity exceeding other imaging modalities including FDG-PET (fludeoxyglucose F 18 positron emission tomography) (Burd et al., 2013). Although this clearly depicted that senescence does occur during mammalian ageing, these studies were all correlative, so the question of whether senescence plays a causal

role in ageing remained unclear until very recently. Regarding this, the Van Duersen lab played a crucial part in elucidating the roles that senescent cells play in both progeria and chronological ageing.

The initial studies from the Van Deursen lab studied the role of senescence in a progeroid mouse that undergoes accelerated ageing due to low levels of the mitotic checkpoint protein BubR1 (BubR1 hypomorphic mice – *BubR1*$^{H/H}$) (Baker et al., 2004). In addition, BubR1 expression is markedly reduced during chronological ageing in multiple tissues and moderate overexpression of BubR1 not only extends both healthspan and lifespan during natural ageing but also protects against aneuploidy and cancer; thus strongly implicating BubR1 in ageing (Baker et al., 2004, 2013b). Importantly, the *BubR1*$^{H/H}$ mice show high levels of senescence compared to other progeroid mice such as *Ercc1*$^{\Delta/-}$ mice that show high levels of apoptosis and severe tissue malfunction instead (de Keizer and al., 2017). Although progerias do not fully capture features of chronological ageing, the *BubR1*$^{H/H}$ mouse is nonetheless a good model to study the role of senescence in accelerated ageing in a more cost-effective and timely manner.

Van Deursen and colleagues therefore demonstrated that deleting p16^{INK4A} in *BubR1*$^{H/H}$ mice not only prolongs survival but also attenuates multiple age-related pathologies including sarcopenia (age-related loss of skeletal muscle mass and strength), the incidence of lordokyphosis (curvature of the spine with age) and cataracts. On the other hand, deletion of p19^{ARF} in the *BubR1*$^{H/H}$ mice resulted in an exacerbated senescence response and a further acceleration in ageing due to a compensatory increase in p16^{INK4A} (Baker et al., 2008). In a follow up study, they also showed that the cell cycle inhibitor p21^{CIP1} has a dual role in the ageing response of the *BubR1*$^{H/H}$ mice. Similar to knocking out p19^{ARF}, deleting p21^{CIP1} also resulted in a further increase in senescence due to compensatory p16^{INK4A} activation, which led to poorer survival, reduced skeletal muscle regeneration as well as increased lordokyphosis. Deletion of p21^{CIP1}, however, delayed the onset of cataracts in the *BubR1*$^{H/H}$ mice (Baker et al., 2013a). This highlights the complexity of the situation since many pathways orchestrate cellular senescence and senescence has both beneficial and detrimental roles during an organism's lifespan. In support of this, although deletion of p16^{INK4A} in the BubR1$^{H/H}$ mice reduced senescence and increased survival, these mice showed accelerated lung tumorigenesis (Baker et al., 2008). To further highlight this duality, the Serrano group published a series of studies utilising *p16*^{Ink4a}*/Arf* or *Arf/p53* "super" mice where they marginally but systemically overexpressed these genes in otherwise wild type (WT) mice (Matheu et al., 2007, 2009). Importantly, they showed this mild increase in expression not only reduced the incidence of tumours but also increased chronological lifespan. Interestingly, this increase in lifespan was independent from cancer as this longevity was still preserved even when comparing mice that died without any overt tumours (Matheu et al., 2007, 2009). Thus, although the accumulation of senescent cells may be detrimental to tissue homeostasis, senescence is still

possibly the most crucial mechanism to limit the propagation of damaged cells, so completely deleting this response clearly has detrimental effects.

Therefore, an alternative avenue would be to selectively eliminate accumulated senescent cells in adulthood. This would avoid the possible adverse effects of preventing cells from undergoing senescence in the first place. This is important since senescence has many beneficial roles such as promoting wound healing and restraining oncogenic transformation. To this end, the Van Duersen lab in 2011 published a seminal paper where they demonstrated unequivocally for the first time the causal relationship between cellular senescence and mammalian healthspan (Baker et al., 2011). The authors generated a semi-genetic model to selectively eliminate p16+ cells from a transgenic mouse termed *INK-ATTAC* (p16INK4A-induced apoptosis through targeted activation of caspase). In this model, the caspase 8 enzyme is produced in cells that express $p16^{INK4A}$ and injection of the drug AP20187 activates the caspase enzyme and causes apoptosis of these p16+ cells. The selective killing of p16+ cells from birth in the $BubR1^{H/H}$ progeroid mouse improved various age-associated pathologies including delaying the onset of cataracts and age-associated loss of fat mass, as well as improving skeletal muscle strength. Removal of p16+ cells from later on in life also showed the same benefits on muscle and adipose tissue but failed to improve cataracts that were already formed, thus demonstrating that the selective killing of senescent cells attenuates the progression of age-related decline rather than completely reversing the ageing process in the BubR1 hypomorphic mice (Baker et al., 2011). The importance of this paper cannot be overstated because it has now sparked a rabid interest by both researchers in the field of ageing and by pharmaceutical companies to identify drugs that selectively kill senescent cells for potential use in humans. As alluded to earlier, this class of drugs is termed “senolytics” or “senotherapies”, and this could become a leading candidate for the therapeutic targeting of the basic ageing process.

The emergence of this landmark study conclusively showed that senescence is a causal player, at least, in accelerated ageing, but there was still a lack of evidence for the role of senescence in chronological ageing. Therefore, in 2016 the van Duersen lab published another seminal study where they characterised the effects of specifically removing p16+ cells (from 12 months of age - detectable levels of senescence in their model) in chronological or natural ageing (Baker et al., 2016). They went on to show that accumulation of p16+ cells affects various age-associated pathologies including kidney glomerulosclerosis, heart function, the onset of cancer, loss of activity, exploratory drive and more. Importantly, removal of p16+ cells also increased median lifespan independent of sex or the strain of the mice (Baker et al., 2016). Nevertheless, there were some caveats with the model, so some of the interpretations must be taken with care. For example, the *INK-ATTAC* transgene failed to eliminate senescent cells from the liver and colon, which are two important organs that deteriorate with age. In addition, the drug used to

activate caspase 8 was also given twice weekly to be effective, which can be quite stressful for the mice; consequently, even the mice given the vehicle alone had a reduced lifespan compared to other previously reported studies. Understanding the impact this has is essential because the elimination of p16+ cells failed to ameliorate certain age-associated pathologies such as glucose intolerance, which could either be because of the limitation of the model or that cellular senescence only affects a subset of age-related pathologies (Gil and Withers, 2016). Moreover, senescence is beneficial in limiting fibrosis and promoting wound healing, but the authors did not observe any significant increase in fibrosis in the skin or other organs. Although, wound healing was delayed if senescent cells were eliminated at the onset of the trigger, the *INK-ATTAC* mice otherwise showed normal healing if the treatment was suspended prior to wounding, suggesting that constitutive clearance of senescent cells does not affect acute senescence mechanisms if treatment is stopped (Baker et al., 2016).

In addition, several recent studies have clearly demonstrated that the accumulation of senescent cells is detrimental to other common age-related pathologies such as atherosclerosis and osteoarthritis (Childs et al., 2016; Jeon et al., 2017). Firstly, van Duersen and colleagues clearly showed that in the *Ldlr*$^{-/-}$ (low-density lipoprotein receptor) and high-fat diet model of atherosclerosis there is an accumulation of senescent lipid loaded intimal foam macrophages in the aortic arch and these cells destabilise the atherosclerotic plaque by secreting various matrix metalloproteinases (MMPs), thus causing plaque rupture and complications. Importantly, removing these cells using the *INK-ATTAC* and *p16-3MR* models both reduced the plaque size and stabilised the fibrous cap (Childs et al., 2016). Senescent chondrocytes were also shown to accumulate in the cartilage and synovium of aged mice both during natural osteoarthritis and following ligament transection and the local clearance of these senescent cells reduced post-traumatic osteoarthritis, pain and promoted regeneration in the cartilage (Jeon et al., 2017). Despite the increased knowledge of the role played by senescent cells during ageing, little is known on changes in the SASP and its role during this process.

Following confirmation that clearance of senescent cells using semi-genetic approaches (*INK-ATTAC* or *p16-3MR*) has various beneficial outcomes, the field then moved into identifying drugs that could also preferentially kill senescent cells. Identification of such drugs would have immediate therapeutic benefit, as they could potentially be applied to humans if no adverse effects are found. Senescent cells are not only resistant to apoptosis but they actively suppress the apoptotic program, hence why they persist for extremely long times in cultures (Childs et al., 2014; Wang, 1995). Therefore, senescent cells must rely on certain pro-survival or anti-apoptotic pathways, but senescent cells should also be more sensitive to death if these same pathways are targeted. One of the first studies to illustrate this concept was by Schmitt and colleagues where they showed that therapy-induced senescent cells with a strong SASP response are more

susceptible (but prolonged exposure is toxic to other cells) to inhibition of autophagy or glucose utilisation due to the high proteotoxic stress found in senescent cells (Dörr et al., 2013). The Kirkland lab then identified using transcriptomic approaches that the combined treatment of dasatinib and quercetin, which target a range of pro-survival factors, can selectively eliminate senescent cells both *in vitro* and *in vivo* (Zhu et al., 2015). Although, this study introduced the concept of "senolytics", some have reported that this cocktail has limited efficacy under certain circumstances and is also toxic to proliferating cells (Baar et al., 2017; Chang et al., 2016). Therefore, the search for "true" senolytics ensued.

Two studies, however, shed some light into potential new "senolytics" (Chang et al., 2016; Yosef et al., 2016). These studies demonstrated that the broad-spectrum inhibitors of the BCL family of anti-apoptotic proteins ABT263 and ABT267 show more selectivity towards senescent cells. Importantly, ABT263 treatment of aged mice both cleared senescent cells and rejuvenated haematopoietic and muscle stem cells as well as improved engraftment after bone marrow transplantation (Chang et al., 2016). In addition, ABT267 treatment eliminated senescent epidermal cells and induced stem cell proliferation, thereby increasing tissue regeneration (Yosef et al., 2016). Nevertheless, these drugs have reported side effects including thrombocytopaenia and neutropaenia, thus limiting their feasibility for long-term or repeated treatments in humans (Chang et al., 2016; Yosef et al., 2016). The most promising "senolytic" so far is the recently described FOXO4-DRI (D-retro inverso isoform) cell-penetrating peptide that interferes with the FOXO4 interaction with p53, thus excluding p53 into the cytoplasm and causing mitochondria-induced apoptosis specifically in senescent cells (Baar et al., 2017). Importantly, this peptide had far more selectivity towards senescent cells than any previously described "senolytic" thus far. Treatment with the FOXO4-DRI peptide reduced senescence, liver and kidney damage, age-associated frailty and promoted fur regrowth in response to doxorubicin chemotoxicity, as well as in a model of accelerated ageing (*Xpd*$^{-/-}$ mice) and chronological ageing. Importantly, the observed improvements of the FOXO4-DRi peptide seems to be senescence dependent and not merely an off-target effect of the drug because the improvements in age-related kidney damage were similar when eliminating senescent cells with the *p16-3MR* genetic model (Baar et al., 2017). Nevertheless, only kidney damage was assessed using both approaches, thus follow up studies would need to distinguish between the effects of potential senolytics in a more detailed manner such as whether there is an additive benefit of combining potential senolytics with the semi-genetic approaches if arguing the benefits are solely senescence dependent.

All of this suggests that targeting senescent cells even in the elderly with accumulated damage may have beneficial effects and could restore tissue homeostasis to a great extent. Nevertheless, aged humans would most likely have many chronic diseases including type 2

diabetes, and therefore a better understanding of the role of senescence in physiology is first required before embarking on human senolysis.

Although it is now clear that selectively eliminating senescent cells is beneficial during ageing, there are still important questions that must be answered such as elucidating exactly how senescent cells contribute to age-related pathologies and identifying the precise mechanisms by which tissue rejuvenation occur after senescence clearance. It is important to highlight that senescence has both cell-autonomous and non-cell autonomous effects. It was initially thought, however, that the impact of senescence on ageing was chiefly due to its cell intrinsic (growth arrest) effect on the self-renewal of progenitor and stem cells (Janzen et al., 2006; Molofsky et al., 2006). These tissue-specific stem cells are crucial for organ function as they replace the adult (differentiated) cells as part of normal tissue turnover as well as the ones that have undergone damage (He et al., 2009). There is an age-dependent decline in stem cell function in essentially all adult stem cell niches including the haematopoietic system and forebrain; this was associated with increased $p16^{INK4A}$ and $p19^{ARF}$ expression and deleting $p16^{INK4A}$ improved late-life proliferation of progenitors and functionality of long-term haematopoietic stem cells (Janzen et al., 2006; Molofsky et al., 2006).

One of the best examples of the cell-autonomous effect of senescence in ageing is in the satellite cells of skeletal muscle, which are the resident stem cells in this tissue. It has been robustly demonstrated that there is a decline in the self-renewal of satellite cells and consequently loss of muscle regenerative capacity with age as the satellite cells switch from quiescence to senescence with increasing age. Importantly, they illustrated this switch into senescence is a result of loss of autophagy and that senescence in satellite cells is only evident at geriatric age (García-Prat et al., 2016; Sousa-Victor et al., 2014). It is important to note, however, that senescent cells are not necessarily dysfunctional cells that accumulate due to damage but rather senescence, in certain contexts, can be a compensatory response to age-related decline in functionality of the tissue. For example, the insulin-producing β-cells of the pancreas lose their proliferative capacity with age leading to glucose intolerance. It was recently shown, however, that although p16+ (senescent) β-cells show reduced proliferation with age, these enlarged, senescent cells have higher β-cell mass, glucose uptake and increased glucose-stimulated insulin secretion, compared to young controls (Helman et al., 2016). Therefore, similar to senescence during embryonic development, β-cell senescence may also be an example of a programmed development role as part of the normal maturation of β-cells and this also shows a context whereby senescence enhancing cellular functionality instead of the long-held argument of being non-redundant dysfunctional cells (Helman et al., 2016).

In addition to the cell-autonomous effects of senescent cells, it is now thought that the SASP also plays a key role in in the pathogenesis of ageing (Campisi and d'Adda di Fagagna, 2007). The SASP comprises of many factors but the proinflammatory arm is conserved among many forms of senescence (Campisi, 2013). It is now evident that a major underlying phenomenon of many age-related pathologies is low-level chronic inflammation even in the absence of any noticeable infection that is termed "sterile inflammation" or "inflammaging" (Franceschi et al., 2000, 2007). This sterile inflammation (elevated serum levels of IL-6, TNF-α, C-reactive protein as well as local tissue inflammation) has been associated with numerous age-related diseases, most notably is the age-related frailty syndrome but also others including diabetes, depression and dementias (Ferrucci et al., 1999; Ford et al., 2004; Lanquillon et al., 2000; Leng et al., 2002; Pradhan et al., 2001; Singh-Manoux et al., 2014; Spranger et al., 2003). Furthermore, many high-profile randomised clinical trials have clearly shown that low-dose non-steroidal anti-inflammatory drugs such as aspirin have beneficial effects in cancers such as reducing the incidence of colorectal cancers in patients both with and without a prior history of colorectal cancer, thus providing evidence for cancer protective effects of anti-inflammatory drugs in humans (Baron et al., 2003a, 2003b). One caveat is that aspirin can result in bleeding and therefore impair the early diagnosis of colon cancer, which may bias the results.

Perhaps the best evidence to demonstrate the causal relationship between inflammation and ageing is done by the Dixit lab where they showed that the NLRP3 inflammasome and IL-1 pathway play a prominent role during mammalian healthspan (Youm et al., 2012, 2013). The NLRP3 inflammasome is activated in response to a diverse set of "danger signals" that increase with age including lipotoxic free acids and reactive oxygen species and is crucial for the cleavage and secretion of IL-1β and IL-18. Importantly deleting NLRP3 protected against age-related thymic involution, immunosenescence (loss of naïve T-cells and B-cells), astrogliosis (abnormal increase in astrocytes and their phenotype due to brain injury), as well as improved glucose homeostasis, bone density, distance run and more. In addition, deletion of IL-1R (receptor) improved cognitive function and motor performance in aged mice. Altogether, this provided causal relationship between inflammation and mammalian health (Youm et al., 2012, 2013). It is important to mention, however, that the NLRP3 inflammasome regulates OIS, thus some of the benefits of the global deletion of NLRP3 could be attributed to preventing age-related senescence (Acosta et al., 2013).

Although many systems contribute to this proinflammatory phenotype during ageing such as the abovementioned NLRP3 inflammasome, accumulation of tissue damage and a defective immune response that fails to efficiently clear pathogens and dysfunctional host cells (termed immunosenescence), it is thought that the SASP is an important contributor to this phenotype (Campisi, 2013; Freund et al., 2010). Although there is no direct evidence for senescence affecting systemic (serum) inflammation during ageing, there is conclusive evidence for the SASP

contributing to local inflammation within the tissues. For example, the levels of proinflamamtory cytokines such as *Il6* (both mRNA and protein levels), *Il1a* and *Tnfa* are significantly reduced in the adipose tissue, kidneys and skeletal muscle in aged mice when senescent cells are eliminated (Baar et al., 2017; Baker et al., 2016).

An important question, however, is whether the SASP causally affects any age-related pathologies. Perhaps the best evidence for this is in the aged kidney. Independent groups have demonstrated that glomerulosclerosis (age-related decline in kidney filtration as a result of fibrosis) and plasma urea (occurs due to defective glomerular filtration) are dramatically reduced when eliminating senescent cells. Of note, however, was that senescent cells were not found in the glomerulus but rather in the surrounding tubular cells, thus suggesting that factors secreted by senescent cells (*i.e.,* the SASP) is the most likely culprit that is contributing to this phenotype (Baar et al., 2017; Baker et al., 2016). This may also explain another important question that many in the ageing field has regarding how senescent cells can have such a big impact on ageing when they consist of only 1-5 % of the tissue microenvironment. From everything described thus far, hopefully it should be apparent that senescent cells are very aggressive due to their secretome. Therefore, it is very likely that the SASP influences the tissue milieu to disseminate the damage of senescent cells in ageing. Another recent study supported this concept as the Serrano lab illustrated that *in vivo* reprogramming induced by the expression of the OSKM (Oct4, Sox, Klf4, c-MYC) transcription factors is greatly increased in both progeria and chronological ageing as well as in bleomycin-induced lung injury where there is an abundance of senescent cells. Importantly, it was not the senescent cells that were reprogrammed but rather the surrounding cells and IL-6 secreted by senescent cells enhanced this reprogramming (Mosteiro et al., 2016). The second but equally important point to highlight the improvements with senolysis is that by eliminating the senescent population in aged tissues causes a compensatory proliferative burst in the progenitor compartment, which promotes regeneration and renewal of aged tissues. Although senolysis did not increase cancer risk in aged mice (in fact it delayed the onset of various cancers), it is still important to consider this in humans given the compensatory increase in stem cell proliferation following senolysis. Likewise, excessive stem cell proliferation can cause stem cell exhaustion. Another major concern is that some tissues have a very high proportion of senescent cells such as in the ageing pancreas where up to 50% of pancreatic beta cells are senescent but remain functional, thus what will be the consequences if these cells are also cleared? Therefore, there is still much to learn about the role that senescent cells, and in particularly the SASP, plays in ageing.

1.7. What are the main pathways regulating the senescence-associated secretory phenotype?

Given the important roles that the SASP plays in pathophysiology, it comes as no surprise that the SASP is tightly regulated at almost all the stages of gene expression ranging from transcription, mRNA stability and translation to secretion. The SASP is also subjected to a complex network of autocrine and paracrine feed-forward loops that enhance the phenotype. In the same manner, there are also mechanisms to dampen down the SASP, so that it does not escalate out of control. In addition, the SASP is also temporally regulated, thus further highlighting the complexity of SASP regulation. The following are some of the key mechanisms of SASP regulation.

It was initially shown that a persistent DNA damage response mediated by ATM, NBS1 and CHK2 was crucial for the induction of at least some SASP components that include IL-6 and IL-8 (Rodier et al., 2009). In support of this, $p16^{INK4A}$ and $p21^{CIP1}$-induced senescence that lack a DNA damage response do not express the typical proinflammatory SASP (Coppé et al., 2011; Rodier et al., 2009). Paradoxically, p53, which lies downstream of the DDR, was shown to rather restrain the SASP, as knockdown of p53 increased levels of SASP proteins (Coppé et al., 2008). This led to the hypothesis that p53 acts as a "cell-nonautonomous tumour suppressor", and this was supported by a recent study that illustrated senescent HSCs in response to CCl_4 and DEN secrete a SASP-like secretome that triggers activation of anti-tumoural M1 macrophages. p53 ablation in HSCs, however, caused a switch that resulted in activation of the protumorigenic M2 macrophages instead (Lujambio et al., 2013).

It is now known, however, that it is possible to induce a SASP independent of DNA damage. The first evidence to support this emerged from the Campisi laboratory where they showed that the p38 MAPK (mitogen-activated protein kinase) pathway, which is activated in response to acute cellular stress, regulates the SASP in a DNA damage-independent manner (Freund et al., 2011). Importantly, constitutive activation of p38 MAPK induced a proinflammatory SASP without a DDR and the SASP expression was resistant to knockdown of known SASP regulators in the DNA damage pathway such as ATM (Freund et al., 2011). This argument was further strengthened by a series of *in vivo* studies in developmental senescence (Muñoz-Espín et al., 2013; Storer et al., 2013). As mentioned earlier, these studies showed that senescence plays a crucial role in embryonic development that is mediated through $p21^{CIP1}$ expression (independent of INK4A/ARF or p53), and these senescent cells secreted factors that resembled the SASP such as bone morphogenetic proteins (BMPs) and fibroblast growth factors (FGFs). In addition, developmental senescence bared no signs of DNA damage (γ-H2AX levels), and knockout mice for the DNA damage signalling kinases ATM and ATR still underwent developmental senescence (Muñoz-Espín et al., 2013; Storer et al., 2013). All of this illustrates that although DNA damage is an important mediator of senescence and the SASP, that it is not always necessary for this response.

The master transcriptional regulators nuclear factor kappa B (NF-κB) and CCAAT/enhancer binding protein beta (C/EBPβ) also regulate the SASP, as knockdown of either of these transcription factors abolishes the induction of the SASP at an mRNA level in various models of senescence (Acosta et al., 2008; Chien et al., 2011; Kuilman et al., 2008). In addition, IL-1α has been shown to be an early response gene during senescence that activates NF-κB and C/EBPβ, which in turn induces transcription of proinflammatory SASP factors such as IL-6 and IL-8 (Orjalo et al., 2009). Importantly, both IL-1α and TGF-β (transforming growth factor-beta) can induce paracrine senescence in neighbouring cells by causing DNA damage and/or oxidative stress (Acosta et al., 2013; Hubackova et al., 2012). Various CXCR2 ligands and IL-6 also act in an autocrine feed-forward loop to enhance the activity of NF-κB and C/EBPβ, respectively, thereby reinforcing this phenotype (Acosta et al., 2008; Kuilman et al., 2008). Recently, we have also shown that the inflammasome (a multimolecular innate immune complex) is also a key regulator of the SASP, as several components (caspase 1, ASC and NLRP3) of the inflammasome were upregulated during senescence and knockdown or chemical inhibition of caspase 1 reduced SASP expression (Acosta et al., 2013). The inflammasome cleaves the inactive IL-1β precursor into its mature form, thus allowing IL-1β to be secreted. In contrast to amplifying the senescence and SASP response, the microRNAs miR-146a and miR-146b are induced by IL-1α in senescent cells with a robust SASP to dampen down the SASP response by repressing IRAK1 (interleukin-1 receptor associated kinase 1) and subsequent NF-κB activation (Bhaumik et al., 2009). This could be a mechanism to prevent excessive inflammation (Lujambio, 2016).

In addition to feedback loops, the SASP is also tightly regulated at the epigenetic and mRNA stability levels. Senescent cells undergo dramatic alterations in their chromatin structure and this influences not only the senescence growth arrest but also the induction of the SASP. Specifically, the occupancy of the histone variant macroH2A1 (mH2A1) was enriched in SASP genes during OIS and knockdown of mH2A1 blunted induction of the SASP in cells undergoing both OIS and paracrine senescence (Chen et al., 2015). Recently, it was also reported that during OIS, the chromatin reader BRD4 (bromodomain containing 4) is recruited to sites of senescence-activated super enhancers that are associated with SASP genes regulating immune surveillance, thus promoting their transcription (Tasdemir et al., 2016). Other epigenetic regulators of the SASP include sirtuin 1 (SIRT1) and the histone demethylase jumonji domain-containing protein 3 (JMJD3) (Hayakawa et al., 2015; Tasdemir et al., 2016). There are various mRNA-binding proteins including NF90 (nuclear factor 90), AU1 (AU-binding factor 1) and ZFP36L1 (ZFP36 ring finger protein like 1) that have been implicated in SASP regulation, and ZFP36L1 will be discussed in length later on in relation to mTOR signalling (Alspach et al., 2014; Herranz et al., 2015; Tominaga-Yamanaka et al., 2012).

The SASP is also regulated translationally, which will be discussed later in relation to mTOR, and also by autophagy. Although it is not clear exactly how autophagy impacts senescence, it is now thought that selective autophagy (degradation of specific protein such as GATA4 by p62) and macroautophagy (degradation and recycling of various cellular contents including damaged organelles) play opposing roles during senescence (Kang et al., 2015). For example, in growing cells the autophagy adaptor protein p62 specifically degrades the transcription factor GATA4. Upon senescence induction, however, the DNA damage kinases ATM and ATR inhibit p62-mediated GATA4 degradation, thus stabilising GATA4 protein levels and permitting GATA4-mediated transcription of TRAF3IP2 (tumour necrosis factor receptor-associated factor interacting protein 2) and IL1A, which reinforces SASP expression through NFκB. Importantly, GATA4 is stabilised during both mouse and human ageing. In addition, chemical inhibition of the proteasome via MG132 had no effect on GATA4 stability, whereas general inhibition of autophagy by bafilomycin A1 clearly stabilised GATA4 levels, indicating that is indeed autophagy and not the proteasome regulating GATA4 and SASP levels (Kang et al., 2015). Knockdown of autophagy machinery such as ATG5 or ATG7, however, delayed the production of IL-6 and IL-8 during senescence, suggesting that general autophagy plays a positive role in SASP regulation as opposed to selective autophagy (Young et al., 2009).

Recently, NOTCH signalling was implicated in the temporal regulation of the SASP (Hoare et al., 2016). Narita and colleagues demonstrated that NOTCH-signalling is activated during initiation of senescence in fibroblasts in culture and this is accompanied with a TGF-β-rich secretome, while suppressing the typical proinflammatory secretome. Importantly, TGF-β then contributes to “lateral induction of senescence” in nearby cells. In late senescence, however, NOTCH1 signalling is downregulated and this facilitates upregulation of the proinflammatory secretome and “immune surveillance” (Hoare et al., 2016). Nevertheless, it is imperative to mention that although it is possible to control and study senescence establishment in cell culture systems in a robust manner, it would be extremely difficult to fully dissect this process during *in vivo* senescence, especially for therapeutic targeting. It is also worth mentioning that overexpression of the NOTCH1 intracellular domain induces a senescence state with a permanent growth arrest but with only a modest increase in SA-β-Gal activity due to a reduction in lysosomal markers, thus highlighting that there is no unique marker for senescence (Hoare et al., 2016). To add to the complexity, the high mobility group box protein 1 (HMGB1) is both a senescence marker (HMGB1 nuclear exclusion) and also a SASP factor that promotes IL-6 expression through NF-κB (Davalos et al., 2013).

All in all, a complex hierarchical network ensures SASP regulation and signal amplification. It should also be apparent that there are an increasing number of SASP regulators being identified and another layer of complexity is raised when the composition of the SASP varies during different

senescence contexts, suggesting that perhaps different types of senescence may be dependent on different regulators. Moreover, many of the SASP regulators including NF-κB and CEBP/β also regulate many of these proinflammatory cytokines in non-senescent contexts such as in immune cells during inflammation, thus these regulators may not necessarily always be specific to senescence. Nevertheless, given the plethora of functions that the SASP has been involved in, it is critical that we better understand the mechanisms that drive this heterogeneous phenotype. In particular, it is crucial we dissect exactly which of the SASP factors that is responsible for mediating the different functions of the SASP under different contexts. This would ultimately mean that we could manipulate these factors therapeutically to maximise benefit (tumour suppression, wound healing and healthspan) while minimising any adverse effects (tumorigenesis and tissue degeneration). Alternatively, we could selectively eliminate senescent cells under certain contexts, and the most appealing circumstance seems to be in aged individuals.

1.8. Nutrient sensing is a requisite for life.

Nutrient sensing is an ancient, evolutionary conserved process that is central to survival (Efeyan et al., 2015). The ability to sense and respond to changes in nutrients both in the environment and within an organism has shaped evolution for millennia. All species, whether a simple prokaryote to complex eukaryotes, have evolved countless mechanisms to not only perceive but also to efficiently utilise these nutrients for the generation of cellular energy and the building blocks of cells (Chantranupong et al., 2015). Various nutrient sensing pathways ensure a balance between anabolism during times of excess nutrients and catabolism during times of nutrient scarcity. This is a fine but well-orchestrated process (Efeyan et al., 2015). Therefore, it should not be a surprise that deregulated nutrient sensing affects a multitude of diseases including obesity, cancer, neurodegeneration and even ageing (Laplante and Sabatini, 2012). But what exactly is nutrient sensing, what are the pathways responsible for such a feat, and how do these processes become deregulated in pathophysiology? These are all important questions that have garnered much interest. There is much to say about each of these, but as aforementioned, this thesis will focus primarily on the role of one nutrient sensing pathway named the mammalian or mechanistic target of rapamycin (mTOR) signalling. To be more precise, however, this thesis will focus on one of the major downstream targets of mTOR called the p70 ribosomal protein S6 kinases of which there are two – S6K1 and S6K2.

The major macronutrients that are sensed, taken up and utilised by cells in our body are sugars (namely glucose), lipids and amino acids (Efeyan et al., 2015). In addition, various hormones, growth factors, vitamins, as well as cellular energy (ATP – adenosine triphosphate) among others also activate these nutrient-sensing pathways. There are complex mechanisms to sense each of these nutrients, and some of these pathways converge on one another. For example, in the liver the GLUT2 glucose transporter senses extracellular glucose whereas

intracellular glucose sensing is done by glucokinase (GCK). Lipids, on the other hand, are an extremely diverse set of nutrients that include fatty acids and cholesterol, and these are sensed by various G-protein coupled receptors (GPR40 and GPR120) in the pancreas and cholesterol-sensing protein SREBP1 cleavage activating protein (SCAP), respectively (Brown et al., 2002; Hirasawa et al., 2005; Itoh et al., 2003). This thesis, however, will focus primarily on mTOR signalling, which is activated in response to a diverse range of hormonal and nutrient stimuli, most notably of which is amino acids (Blommaart et al., 1995; Hara et al., 1998). It is important to mention, however, that amino acids are sensed by other mechanisms as well, such as by GCN2 (general control nonderepressible 2) (Wek et al., 1995). All this should highlight the complexity of nutrient sensing, and this is further exemplified in multicellular organisms where nutrient sensing mechanisms are tightly linked to feeding behaviour, but these are beyond the scope of this thesis.

1.9. What is mammalian or mechanistic target of rapamycin (mTOR)?

Before delving deeper into the role of ribosomal protein S6 kinases (S6K1 and S6K2), it is important to first understand, albeit briefly, the larger role that mTOR signalling plays in nutrient sensing, metabolism and disease. This is because although the S6 kinases play crucial roles in various biological processes, they remain only one component of the mTOR signalling pathway.

Many nutrient sensing pathways eventually converge at mTOR, which acts as both a nexus for these stimuli and also prime cells for anabolism and growth (Efeyan et al., 2015; Guertin and Sabatini, 2007; Laplante and Sabatini, 2012; Saxton et al., 2017; Zoncu et al., 2011). mTOR is an important sensor of amino acids, particularly of leucine and arginine, and mTOR is activated in response to growth factors and nutrient stimulation, as well as high ATP: AMP ratios (Blommaart et al., 1995; Hara et al., 1998). Therefore, mTOR serves as an interface between environmental cues (nutrients) and intracellular signals (growth factors and energy levels). Many of these stimuli, however, also converge at AMP-activated protein kinase (AMPK), which acts complementary to mTOR (Hardie et al., 2012). In contrast to mTOR, AMPK is activated under conditions of nutrient deprivation and therefore both inhibits mTOR activity as well as prime cells for catabolism. It is therefore important for the fine balance between anabolism and catabolism for the maintenance of tissue homeostasis (Hardie et al., 2012; Laplante and Sabatini, 2012).

mTOR was initially discovered as a target of the antifungal compound rapamycin in the 1990s, and many of the initial studies focussed on its role in immunosuppression (Brown et al., 1994; Sabatini et al., 1994; Sabers et al., 1995). mTOR's roles in pathophysiology have now grown to include cancer, type 2 diabetes, neurodegeneration and even ageing, and mTOR inhibitors have been clinically approved (in the UK and/or USA) for drug-eluting stents, preventing host-rejection in renal transplantation and for the treatment of renal-cell carcinoma, mantle-cell lymphoma, tuberous sclerosis and pancreatic cancer (Johnson et al., 2013; Laplante and Sabatini, 2012). mTOR is a

large 250 kDa serine/threonine protein kinase that belongs to the family of phosphoinositide-3-kinase-related protein kinases (PIKK) and is found in two distinct protein complexes termed mTOR complex 1 (mTORC1) and mTOR complex 2 (mTORC2) (Loewith et al., 2002). These complexes differ in their sensitivity to rapamycin, subunit composition, regulation, substrate specificity and function (Magnuson et al., 2012). RAPTOR (regulatory associated protein of TOR) and RICTOR (rapamycin insensitive companion of TOR) acts as the major scaffolding proteins for the assembly of mTORC1 and mTORC2, respectively, as well as for binding to regulators and substrates (Hara et al., 2002; Sarbassov et al., 2004). Most studies have focussed on the role of mTORC1, but there is mounting evidence for the role of mTORC2 in pathophysiology as well (Laplante and Sabatini, 2012). *For the purpose of this study, the role of mTORC1 but not of mTORC2 will be discussed in length, as the large body of data have implicated mTORC1 in cellular senescence, ageing and fatty liver disease.*

mTORC1 is activated at the lysosomal surface via highly complex mechanisms involving the vacuolar H^+-ATPase, amino acids, the Ragulator complex, Rag proteins, the recently identified adaptor protein SLC38A9 and others (Ma and Blenis, 2009; Rebsamen et al., 2015; Wang et al., 2015). Nevertheless, the initial signalling pathways that initiate the translocation of mTORC1 to the lysosome for activation are the pro-growth PI3K/Akt (phosphoinositide-3-kinase/Akt serine/threonine kinase 1) and the Ras/MAPK (Harvey rat sarcoma viral oncogene homolog/mitogen activated protein kinase) signalling pathways (Ma & Blenis, 2009). Many of these stimuli in fact converge directly upstream of mTOR on tuberous sclerosis complexes 1 and 2 (TSC1 and TSC2), which inhibit mTOR signalling by activating the intrinsic GTPase (guanosine triphosphatase) activity of the G-protein Rheb (small Ras protein enriched in the brain). TSC1 and TSC2 are crucial tumour suppressor proteins as their loss result in tuberous sclerosis, a rare genetic condition where benign tumours develop in different parts of the body. Therefore, PI3K/Akt and Ras/MAPK pathways activate mTOR by phosphorylating and inhibiting TSC1 and TSC2, which in turn allows active Rheb to physically bind to and activate mTORC1 at the lysosomal surface (Guertin and Sabatini, 2007; Laplante and Sabatini, 2012; Zoncu et al., 2011).

mTOR regulates many crucial processes required for cell growth and proliferation including synthesis of proteins, lipids and nucleotides while suppressing catabolic processes such as autophagy, and this is explained in detail in a recent review by Sabatini and colleagues (Saxton et al., 2017). In particular, mTOR is a master regulator of protein synthesis, as mTOR regulates both translation initiation and elongation and inhibition of mTOR significantly reduces translation rates (Hay and Sonenberg, 2004). Once activated, mTORC1 carries out its functions through an increasing number of targets, but the first and most widely studied mTOR targets are the p70 ribosomal protein S6 kinases 1 and 2 (S6K1 and S6K2) and the translation initiation factor 4E binding proteins (4EBPs) (Brunn et al., 1997; Burnett et al., 1998). The key distinction here is that

mTOR activates the S6 kinases, whereas phosphorylation of 4EBP1 by mTOR causes the dissociation of 4EBP1 from the eukaryotic translation initiation factor 4E (eIF-4E), thus permitting recruitment of eIF4G and eIF4A and initiation of translation (Haghighat et al., 1995; Marcotrigiano et al., 1999). S6K1 also regulates translation initiation and elongation through phosphorylation of several key members of the translational machinery but this will be discussed later on in relation to S6K targets. mTOR has now been implicated in numerous other processes including autophagy, lipid metabolism, lysosome biogenesis, energy metabolism and cell survival (Saxton et al., 2017).

Given that mTOR regulates many aspects of cell growth, it is unsurprising that over 1300 clinical trials of mTOR inhibitors have either been completed or are under way (Johnson et al., 2013). Many of these trials focussed on using rapalogs as a cancer therapeutic. Although rapalogs have now been clinically approved for some cancers, there was limited success in many of the clinical trials and these are summarised in the following reviews (Easton and Houghton, 2006; Faivre et al., 2006; Granville et al., 2006). It is now thought that this is down to several reasons. The first is that S6K1 is known to act in a negative feedback loop once activated by phosphorylating and inhibiting insulin-receptor substrate 1 (IRS-1), thereby inhibiting the PI3K/Akt pathway and consequently mTOR signalling. mTOR inhibition, however, means the loss of this negative feedback of IRS-1 by S6K1 (O'Reilly et al., 2006). The second reason is that rapalogs have been shown to only partially inhibit phosphorylation of 4EBP1 by mTOR, at least under acute treatment; it is now known 4E-BPs are more important for regulating translation initiation and proliferation than the S6Ks (Hsieh et al., 2010). The third is that rapalogs only inhibit mTORC1, whereas the mTORC2-Akt axis remains intact (Saxton et al., 2017). Finally, mTOR inhibition not only induces autophagy, which enables tumoural cells to survive under stressful, nutrient scarce situations, but also only reduces cell growth and proliferation without necessarily inducing apoptosis (Matter et al., 2014; Palm et al., 2015). As a result, second-generation mTOR inhibitors have now been developed such as Torin1 that inhibits both mTORC1 and mTORC2 as well as NVP-BEZ235, which inhibits both mTOR and PI3K, thereby negating the loss of the feedback loop (Engelman et al., 2008; Serra et al., 2008; Thoreen et al., 2009). These inhibitors have shown more promise but are also more toxic, thus the answer may lie downstream mTOR such as the S6 kinases or even further down the pathway. In addition, even after early response to mTOR inhibition, mutations within the kinase or FKBP12-rapamycin-binding domain of mTOR results in acquired resistance. Thus, a third-generation mTOR inhibitor termed RapaLink was made whereby rapamycin is chemically linked to the ATP-competitive mTOR inhibitor, thus allowing inhibition of mTOR even in cases of rapamycin resistance (Rodrik-Outmezguine et al., 2016).

1.20. Ribosomal protein S6 kinases (S6K1 and S6K2) and their substrates.

Now that the wider role of mTOR signalling in pathophysiology has been put into place, it is time to move into understanding precisely which of these functions are carried out by the ribosomal protein S6 kinases.

The p70 ribosomal protein S6 kinase (S6K) family in mammals is composed of two distinct gene products named S6K1 (*RPS6KB1* – *S6Kα* – 17q23.1) and S6K2 (*RPS6KB2* - *S6Kβ* – 11q13.1). It is imperative to mention that the p70 S6K gene family differs from the related but separate p90 ribosomal protein S6 kinase family (*RPS6KA1-4* – *RSK1-4*) because there has been a great deal of confusion in the literature due to their similar nomenclature. This confusion has arisen because all of these kinases were identified based on their ability to phosphorylate a component of the 40S ribosome termed ribosomal protein S6 (RPS6) (Fenton and Gout, 2011; Magnuson et al., 2012; Pardo and Seckl, 2013). Additionally, both S6K1 and S6K2 were initially cloned and characterised in the 1990s, but owing to S6K1 being identified first and the discovery of its importance in various physiological processes, S6K2 was long neglected (Banerjee et al., 1990; Gout et al., 1998; Koh et al., 1999; Kozma et al., 1990; Saitoh et al., 1998; Shima et al., 1998). Therefore, there is still much to learn about the roles that S6K2 play in pathophysiology, but our current understanding of S6K2, however little, was thoroughly summarised in a recent review dedicated to this family member (Pardo and Seckl, 2013).

The S6 kinases are members of the AGC (PKA – cAMP-dependent protein kinase/PKG – cGMP-dependent protein kinase/PKC – protein kinase C) kinase family, and the two kinases share 84% homology in their kinase domain but vary considerably more in their N-terminal (43% homology) and C-terminal (59% homology) domains (Lee-Fruman et al., 1999). Although the family is generally called the p70 S6 kinases, S6K1 and S6K2 differ in their molecular size and the number of known isoforms. Specifically, S6K1 is found as four separate isoforms that are produced due to alternative splicing or alternate start sites – p85 (S6Kα1), p70 (S6Kα2), p60 and p31, but the p70 isoform is the most widely studied isoform (Banerjee et al., 1990; Grove et al., 1991; Karni et al., 2007; Kim et al., 2009; Kozma et al., 1990). In contrast to the p85 isoform, the p70 S6K1 lacks a nuclear localisation domain (NLS) in the N-terminus, thus the p70 isoform is thought to reside in the cytoplasm while the p85 isoform may translocate to the nucleus, but the p70 isoform has been shown to translocate to the nucleus upon growth factor stimulation (Grove et al., 1991; Valovka et al., 2003). The recently identified p60 isoform of S6K1 is thought to be expressed highly in breast cancer cell lines including MCF-7 cells that has known S6K1 amplification (Kim et al., 2009). Not much is known about the p31 isoform, however, which lacks most of the kinase domain, but it was required for transformative properties (colony formation in soft agar) of the splicing factor SF2/ASF in fibroblasts (Karni et al., 2007). S6K2 on the other hand is found as two separate (p56 - S6KβI and p54 - S6KβII) isoforms, and both the p54 and p56 isoforms have an NLS motif in their

C-terminal domain but the p56 isoform has an additional NLS in its N-terminus (Gout et al., 1998). Both S6K2 isoforms reside in the nucleus in quiescent (resting) cells but the p54 isoform, which is the most widely expressed isoform in tissues, can shuttle to the cytoplasm upon growth factor stimulation (Koh et al., 1999; Valovka et al., 2003). *Unless specifically stated, from now on S6K1 and S6K2 will denote p70 S6K1 and p54 S6K2, respectively.*

The S6 kinases are phosphorylated and activated in response to various growth factors, nutrients and mitogens, particularly the insulin/insulin-like growth factor signalling (IIS) pathway (Fenton and Gout, 2011; Magnuson et al., 2012; Pardo and Seckl, 2013). Various upstream signals such as the IIS pathway then converge on mTOR, which phosphorylates p70 S6K1 and p54 S6K2 at threonine-389 (Thr389) and Thr388 residues, respectively, which allows further phosphorylation by phosphoinositide-dependent kinase 1 (PDK1) for full activation (Alessi et al., 1998; Pearson et al., 1995; Pullen et al., 1998). mTOR phosphorylation of S6 kinases is considered essential for full S6K activation and phosphorylation of S6K1 is frequently used as a readout for mTOR activation, as S6K1 activation was shown to be highly sensitive to the mTOR inhibitor rapamycin (Chung et al., 1992; Kuo et al., 1992; Price et al., 1992). Importantly, however, there is evidence to argue that different mTOR pools may regulate S6K1 and S6K2 differently under various contexts, especially because a rapamycin dose (10ng/mL) that efficiently inhibits FGF2 (fibroblast growth factor 2)-mediated S6K1 phosphorylation fails to block S6K2 phosphorylation (Pardo and Seckl, 2013; Pardo et al., 2001).

Considering that the S6 kinases are downstream effectors of mTOR signalling, it should be evident that the S6 kinases regulate many of the same processes as mTOR including cell growth and proliferation, apoptosis, ribosome biogenesis and translation, and these are summarised in the following reviews (Fenton and Gout, 2011; Magnuson et al., 2012; Pardo and Seckl, 2013). Much of the initial work on S6 kinases, however, focussed on regulation of translation because the first identified target of the S6 kinases was the ribosomal protein S6 (RPS6) that is found in the 40S ribosome, but the functional consequence of RPS6 phosphorylation is still not entirely clear. The S6 kinases phosphorylate RPS6 on all the five known phosphorylatable residues (serine 235, 236, 240, 244 and 247) (Ferrari et al., 1991). Importantly, S6K2 was shown to be more important for RPS6 phosphorylation but both the S6 kinases are essential as knockout of either S6K1 or S6K2 fails to completely abolish the S240/S244 phosphorylation, which is only phosphorylated by S6K1 and S6K2, whereas phosphorylation of S235/S236 residues are also carried out by the p90 RSKs (Pende et al., 2004). Furthermore, many of the S6K substrates are also phosphorylated by the p90 RSKs, suggesting that both the mTOR-S6K and the MAPK-RSK pathways converge to regulate various aspects of cell physiology (Magnuson et al., 2012).

It is now known that the 4EBPs are more important for regulation of translation than the S6 kinases, as global translation rates are unaffected in many tested cell types isolated from S6K knockouts including fibroblasts, hepatocytes, skeletal muscle and embryonic stem cells (Chauvin et al., 2014; Hsieh et al., 2010; Mieulet et al., 2007; Pende et al., 2004). Nevertheless, the S6 kinases may sill regulate the translation of specific transcripts and/or enhance the translation efficiency of spliced RNAs through the S6K1-specific interactor SKAR (S6K1-Aly/REF-like substrate – *POLDIP3*) (Ma et al., 2008; Richardson et al., 2004). In line with this, S6K1 may also enhance splicing of mRNA transcripts by phosphorylating cap binding protein 80 (CBP80), which together with CBP20 forms a heterodimeric complex that binds the 5' 7-methyl guanosine cap to promote splicing and nuclear export of mRNAs (Wilson et al., 2000). Furthermore, S6K1 phosphorylates members of the translation machinery that are involved in translation initiation (eIF4B and PDCD4) and elongation (eEF2K). For example, S6K1 promotes translation initiation by phosphorylating eIF4B, which then binds eIF4A in the translation preinitiation complex (Raught et al., 2004). Likewise, S6K1 phosphorylates the eIF4A inhibitor PDCD4 (programmed cell death 4), which causes degradation of PDCD4 by the E3 ubiquitin protein ligase βTRCP (Dorrello et al., 2006). These events collectively increase the helicase activity of eIF4A, which is crucial for unwinding the secondary structures in the 5'UTR (untranslated region) in mRNAs for initiation of translation (Pause and Sonenberg, 1992; Rozen et al., 1990). S6K1 also promotes translation elongation by phosphorylating and inhibiting eukaryotic elongation factor 2 kinase (eEF2K), thus alleviating the inhibition of eEF2 by eEF2K and permitting translation elongation (Wang et al., 2001). The S6 kinases and the downstream target RPS6 have also been shown to regulate the ribosome biogenesis transcriptional program in mouse hepatocytes (Chauvin et al., 2014). Earlier work also demonstrated that the mTORC1-S6K1 axis was required for activation of nucleolar transcription factor UBF (upstream binding factor), which is a key player in the regulation of the 45S ribosomal DNA transcriptional program (Hannan et al., 2003).

In addition to regulating splicing and translation, the S6 kinases through multiple substrates also regulate other stages of gene expression and protein synthesis. For example, S6K1 phosphorylates and activates several transcription factors such as cAMP-response-element modulator τ (CREMτ) and oestrogen receptor α (ERα), and S6K1-mediated phosphorylation of ERα may contribute to progression of breast cancers with S6K1 amplification (de Groot et al., 1994; Yamnik et al., 2009). S6K2 on the other hand, phosphorylates and activates the transcription factor Yin-Yang 1 (YY1). S6 kinases also regulate the transcriptional program during immune (CD4+ T helper 17) cell differentiation by a two-fold mechanism. Firstly, S6K2 promotes the activity of the transcription factor RAR related orphan receptor γ (*RORC*); but S6K2 does this via a non-kinase function, as S6K2 interacts with and translocates RORγ, which lacks a NLS, to the nucleus, thus facilitating RORγ-mediated transcription that is essential for initiation of TH17-cell differentiation (Kurebayashi et al., 2012). S6K1 also promotes TH17-cell differentiation by

increasing the levels of the transcription factor EGR2 (early growth response 2), which in turn inhibits the negative regulator of TH17-cell differentiation GFI1 (Kurebayashi et al., 2012). S6K1 was also recently implicated in host antiviral response through a non-kinase activity by interacting with the signalling adaptor STING, which allows the TANK binding kinase 1 (TBK1) to phosphorylate and activate interferon regulatory transcription factor 3 (IRF3), and disruption of this interaction impaired the induction of T-cell responses and mucosal antiviral immunity (Wang et al., 2016). S6K1 was further implicated in immune cell activation, as S6K1 dampened toll-like receptor (TLR) signalling in macrophages by interfering with the interaction between TAK1 and TAB1 that is required for NFκB and AP-1 activation, thus splenocytes isolated from 6-8 week old *S6K1*$^{-/-}$ mice or depletion of S6K1 in macrophages resulted in enhanced activation of TAK1 and increased production of proinflammatory cytokines in response to lipopolysaccharide (LPS) (Kim et al., 2014). In addition, 6-8 week old S6K1$^{-/-}$ mice underwent early mortality in response to a lethal dose of LPS and this correlated with increased levels of proinflammatory cytokine production (Kim et al., 2014). Finally, S6K1 may also regulate protein folding by phosphorylating CCT-β (*CCT2* – β subunit of chaperonin containing TCP-1) in the multi-subunit complex that interacts with ribosomes and nascent polypeptides to regulate protein folding; but whether this phosphorylation affects protein folding was not assessed (Abe et al., 2009).

S6K1 have also been implicated in regulating other processes such as promoting cell survival by phosphorylating and inhibiting the pro-apoptotic protein BAD (Bcl-2/Bcl-X_L-antagonist, causing cell death). On the other hand, upon genotoxic stress, the p38-MAPK pathway activates S6K1, which phosphorylates MDM2 (murine double minute 2) and prevents it from translocating to the nucleus to target p53 for degradation. As a result, levels of p53 increases, which then induces cell cycle arrest or apoptosis (Lai et al., 2010). All this should highlight that the S6 kinases regulate a diverse range of biological processes including gene expression either directly or indirectly at various stages of protein synthesis. This is further complicated by the fact that S6 kinases take part in several negative feedback loops by phosphorylating and inhibiting IRS-1 (insulin-like receptor substrate-1 that is crucial for PI3K activation), the multifunctional kinase GSK3-β (glycogen synthase kinase 3 beta) and even mTOR itself. Therefore, depending on the context, it can be very difficult to pinpoint exactly how the S6 kinases may be regulating a specific process.

From what has been described thus far, it should be evident that S6K1 and S6K2 share many common targets including RPS6, but the two also have specific targets and functions. Therefore, it is important to note that depending on the context, S6K1 or S6K2 in isolation may be sufficient, but it may also be that both the kinases are required to carry out certain functions (Pardo & Seckl, 2013; Brian, Bilgen & Diane, 2012). It is also important to mention that not all the S6K substrates have the canonical R/KXR/KXXS*/T* (R = arginine, K = lysine, S = serine, T = threonine, * - phosphoacceptor, X = any amino acid) sequence, thus S6Ks can also phosphorylate

substrates with partial or atypical recognition sequences including the recently identified S6K1 target EPRS (glutamyl-prolyl-tRNA synthetase) (Arif et al., 2017; Hsu et al., 2011). The most widely recognised downstream targets of S6 kinases that were mentioned above are summarised in Figure 1.4 below.

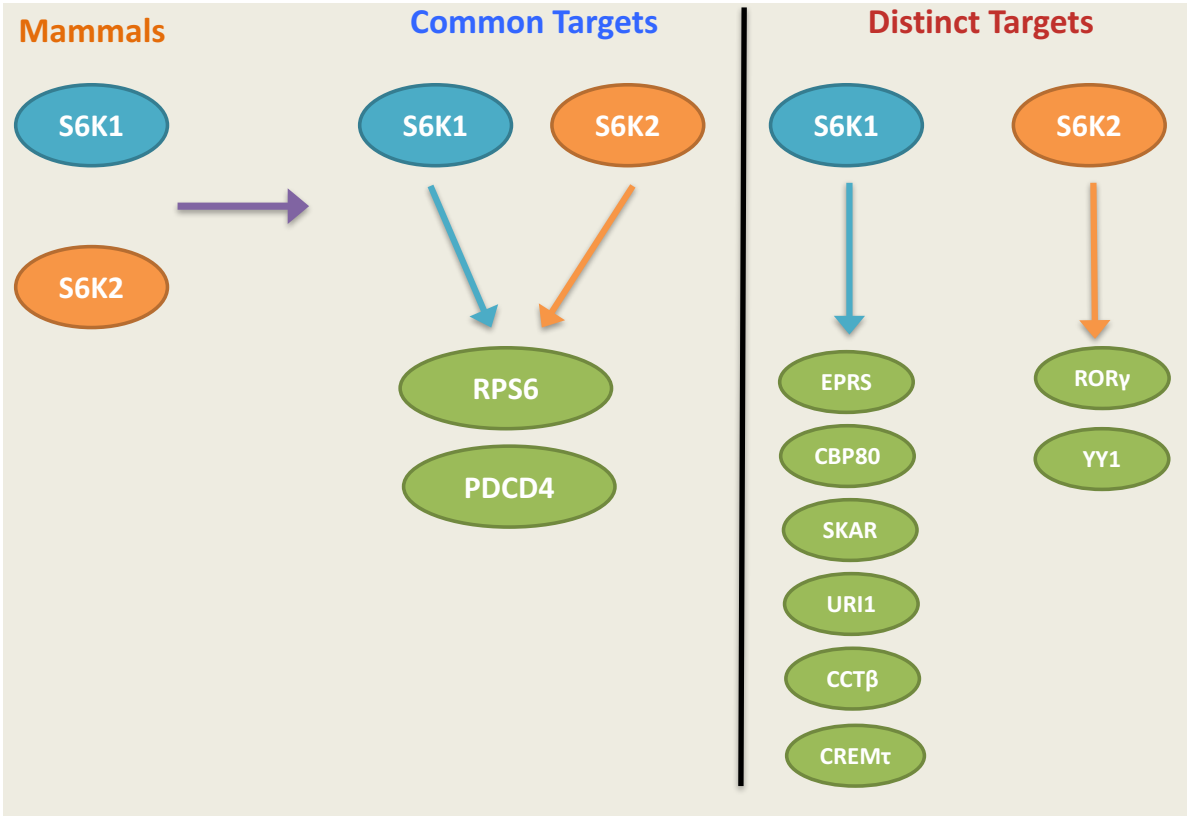

Figure 1.6. Downstream targets of ribosomal protein S6 kinases.
Mammalian cells express two distinct ribosomal protein S6 kinases termed S6K1 and S6K2. The two share common targets but also have specific targets of their own. Some of the key downstream targets of S6 kinases are shown. RPS6: ribosomal protein S6. PDCD4: programmed cell death 4. EPRS: glutamyl-prolyl-tRNA synthetase. SKAR: S6K1 Aly/REF-like target – also called POLDIP3. URI1: profoldin like chaperone. CCTβ: chaperone containing T-complex polypeptide subunit 2. CREMτ: CAMP responsive element modulator τ. RORγ: Retinoid-related orphan receptor γ. YY1: Yin-Yang 1. Adapted from (Magnuson et al., 2012; Pardo and Seckl, 2013).

1.21. The role of S6K1 and S6K2 in pathophysiology, particularly fatty liver disease.

S6K1 and S6K2 are expressed almost ubiquitously throughout mouse and human tissues at the mRNA level, but the expression of the two kinases is often inversely correlated (Gout et al., 1998; Nardella et al., 2011; Shima et al., 1998). There are also differences in expression between organisms. For example, S6K2 was undetectable at the protein level in the mouse kidney, whereas it was abundantly expressed in the human kidney (Nardella et al., 2011). These differences in expression also go in line with sensitivity of S6K inhibition to tumorigenesis, as the same study by Pandolfi and colleagues demonstrated that S6K1 deletion markedly reduces *Pten*$^{+/-}$ mediated

adrenal but not prostate tumorigenesis because S6K2 expression is very low in the adrenal glands in both mice and humans (Nardella et al., 2011). Additionally, both the S6 kinases are often aberrantly activated and/or overexpressed in various cancers, particularly breast cancers, but S6K2 overexpression in cancers is more common than S6K1 (Filonenko et al., 2004; Pardo and Seckl, 2013). Phylogenetic analysis also revealed that S6K1 is the ancestral kinase while S6K2 emerged in mammals, suggesting that it is S6K1 that is required predominantly for normal tissue function, whereas cancers exploit the alternative S6K2 for tumorigenesis (Nardella et al., 2011; Pardo and Seckl, 2013). This theory is strengthened by the *in vivo* phenotypes of the knockout mice. Although both *S6K1*$^{-/-}$ and *S6K2*$^{-/-}$ mice are viable, fertile and born at expected Mendelian ratios, *S6K1*$^{-/-}$ mice are dwarfs, whereas S6K2$^{-/-}$ mice are slightly larger than their wildtype (WT) counterparts due to a compensatory increase in S6K1 levels, but this once again shows the critical nature of S6K1 for cell growth (Pende et al., 2004; Shima et al., 1998). *S6K1*$^{-/-}$*: S6K2*$^{-/-}$ double knockout mice show perinatal lethality and the large majority of mice that survive soon die from cyanosis or hydrocephalus in a pure C57BL/6 strain, but these mice show increased survival when bred in mixed backgrounds (Pende et al., 2004).

As mentioned earlier, the large majority of studies have focussed on the role of S6K1 in pathophysiology, so this will be discussed in detail. From all the *in vivo* studies, it is now evident that S6K1 plays crucial roles in obesity and ageing (Hee Um et al., 2004; Selman et al., 2009). Early work from George Thomas' group clearly demonstrated that the *S6K1*$^{-/-}$ mice are resistant to both age- and diet-induced obesity with increased insulin sensitivity (Hee Um et al., 2004). Further work from their laboratory delineated some of the mechanisms behind this phenotype by showing that S6K1 plays a critical role in the differentiation of embryonic and adipocyte stem cells into preadipocytes without regulating adipocyte hypertrophy in response to a high-fat diet (Carnevalli et al., 2010). Importantly, adipogenic stimuli caused S6K1 to translocate to the nucleus and phosphorylate histone H2B, which resulted in EZH2 (enhancer of zest homologue 2) mediated H3K27 trimethylation of Wnt genes, which then alleviated the inhibition of PPARγ (peroxisome proliferator-activated receptor gamma) and C/EBPα to drive adipogenesis (Yi et al., 2016). The benefits of S6K1 deletion, however, seem to be age- and stimulus-dependent, as young *S6K1*$^{-/-}$ mice were glucose intolerant, hypoinsulinaemic and had reduced β-cell size, which could be due to developmental defects from a dwarf phenotype (Pende et al., 2000). It is imperative to mention that S6K1 is a master regulator of adipogenesis and the observed phenotype is not simply due to their dwarf nature. This is because other dwarfs that are also long-lived such as the hypopituitary Ames dwarf mice (deficient in growth hormone, prolactin and thyroid stimulating hormone) gain considerably more weight (both visceral and subcutaneous adipose mass) compared to their WT controls in response to a high-fat diet, clearly showing that being dwarf does not necessarily protect from weight gain (Brown-Borg et al., 1996).

Given that S6K1 activation is a critical determinant of obesity, it should not be a surprise that the S6 kinases may also be involved in many obesity-related pathologies including fatty liver disease, which is medically referred to as non-alcoholic fatty liver disease (NAFLD) (Hardy et al., 2016). The prevalence of NAFLD (12-38 %) and the more severe non-alcoholic steatohepatitis (NASH - 3-15 %) are rising in the general population (Europe and U.S.A) due to increased numbers of obesity, type-2 diabetes, hypertension and old age (Hardy et al., 2016; Vernon et al., 2011). NAFLD is now the most common cause of liver dysfunction in the Western world, and although it is quite benign in nature, it can progress to liver fibrosis and inflammation that is referred to as NASH and eventually to cirrhosis (irreversible fibrosis of the liver) and hepatocellular carcinoma (HCC) (Bataller and Brenner, 2005; Hardy et al., 2016; Wree et al., 2013). Chronic liver damage owing to alcohol abuse, excessive intake of fatty foods and/or hepatitis virus infection is required for the progression of NAFLD to liver fibrosis and cancer but as mentioned earlier the exact mechanisms driving this response are both complex and are still being elucidated (Bataller and Brenner, 2005). Nevertheless, there is still an undying need to understand the pathogenesis of fatty liver disease, particularly because HCC is the sixth most common malignancy and the second leading cause of cancer mortality in the world, and patients with advanced form of the disease only have an expected lifespan of 4-6 months from diagnosis, as there is no effective treatment for end-stage disease except for transplantation (El-Serag, 2011). Sorafenib remains the only drug treatment for liver cancer, but resistance to therapy is a common problem and the National Institute for Clinical Excellence (NICE), which is the U.K equivalent to the Food and Drug Administration (FDA), does not recommend sorafenib due to lack of benefit to patients to justify the high cost. Therefore, given the limited supply of livers for transplantation and the high cost and morbidity of the surgery itself, it is increasingly important to find alternate treatments for this debilitating disease (Llovet et al., 2016).

NAFLD is characterised by accumulation of hepatic triglycerides (TGs), which is termed hepatic steatosis. Although NAFLD is damaging, this morbidity and mortality are not drastically affected in people with steatosis from NAFLD alone that is termed isolated fatty liver (IFL) (Dam-Larsen et al., 2009; Ekstedt et al., 2006). On the other hand, NASH diagnosis increases the risk of mortality, and this is worsened if fibrosis is present, especially as advanced fibrosis was found in 88% of patients with HCC, and cirrhosis remains the single largest risk factor for HCC development (Dam-Larsen et al., 2009; Ekstedt et al., 2006; Hashimoto et al., 2009). The primary reason why steatosis alone is somewhat harmless is because storing lipids in tissues that were evolutionarily adapted to handle this feat such as in perigondal (epididymal) white adipose tissue or as relatively stable, inert lipid droplets in the liver is more beneficial than having highly reactive free fatty acids (FFAs) roaming in the blood that can cause both systemic and local tissue damage (Hardy et al., 2016). One of the finest examples to illustrate this point was done by depleting the enzyme DGAT2 (diacylglycerol acyltransferase 2), which catalyses the final step of hepatic FFA

conversion into triacylglycerols (TAGs), in obese mice that were also fed a methionine-choline deficient diet (MCD) to induce liver damage, inflammation and fibrosis. As expected, depletion of DGAT2 reduced steatosis but these mice, however, showed exacerbated hepatic inflammation, fibrosis, oxidative stress and apoptosis, suggesting that hepatic steatosis is a protective, adaptive response to prevent progressive liver damage (Yamaguchi et al., 2007).

The epidemiology of fatty liver disease is further complicated by sexual differences, as both the prevalence and severity of NAFLD, NASH and HCC are higher in men than women (Nordenstedt et al., 2010). Importantly, however, this trend seems to be the case only until menopause, as the prevalence of NAFLD in postmenopausal women even extended above men and the fibrosis severity was no different between the genders at this stage, thus strongly implying a hormonal (*i.e.,* oestrogen) influence in the pathogenesis of fatty liver disease (Kojima et al., 2003; Yang et al., 2014). Even by the early noughties, there was accumulating evidence to support the protective effects of oestrogen against various aspects of liver disease including oestrogen's antioxidant properties, as reviewed by (Shimizu, 2003). Strong causal evidence is found in both rodents and humans to support this. For example, oestrogen treatment in both male and female rats reduced liver damage and fibrosis induced by CCL_4 treatment, whereas female rats that underwent ovariectomies showed increased liver damage and fibrosis, thus highlighting oestrogen's protective roles in liver fibrosis (Xu et al., 2002). In addition, postmenopausal women with type 2 diabetes mellitus given hormone replacement therapy (HRT) had significantly reduced levels of liver enzymes that are indicative of liver damage (McKenzie et al., 2006).

As aforementioned, *S6K1*$^{-/-}$ mice are protected from both age-and diet induced obesity. In line with this, it was demonstrated that adeno-associated virus (AAV) mediated depletion of S6K1 and S6K2 specifically in the liver of adult (8 weeks old) mice improved both glucose tolerance and insulin sensitivity without affecting body weight or food intake in response to 8-weeks of a high-fat diet (HFD) (Bae et al., 2012). In addition, they found increased mTOR signalling ($pS6^{2S240/S244}$ and $pS6^{S235/S236}$) in the liver, perigonadal white adipose tissue (PWAT – also called epididymal fat) and muscle in WT mice given an HFD compared to chow controls, and S6K depletion increased insulin signalling ($pAkt^{S473}$) compared to their WT counterparts on the HFD. Importantly, they also showed that hepatic steatosis and *de novo* lipogenesis were reduced in the livers of S6K1/2 depleted mice, and this coincided with reduced expression of SREBP1c (sterol regulatory element binding transcription factor 1 c), which is required for cholesterol synthesis (Bae et al., 2012). Not much is known, however, about the combined contribution of both S6K1 and S6K2 in obesity and metabolic disease, but it was shown from an independent group that dietary lipids (*e.g.,* oleic acid) activate (phosphorylation of T389) S6K1 in muscle, and global S6K1/2 double knockout mice are also protected from HFD-induced weight gain as well as glucose and insulin intolerance (Castañeda et al., 2012).

From the above studies, it is clear that depletion of S6 kinases is protective against excess intake of dietary lipids and glucose intolerance, but what is unknown is the impact of S6 kinases in liver pathology such as the progression of fatty liver disease (NAFLD) into liver fibrosis and inflammation (NASH) and eventually into HCC development. This is of importance because development of hepatocellular carcinoma is generally slow, taking years as a result of accumulated damage; but this also means the mechanisms driving the transformation of hepatocytes to malignancy are highly complex and are influenced by the surrounding stroma, immune cells, inter-organ communication including gut microbiota and others. In addition, there is a scarcity of *in vivo* evidence for the contribution of the combined effects of the S6 kinases (S6K1 and S6K2), especially regarding tissue specific effects. This is of particular interest, because although the data on mTOR signalling on liver damage and cancer have been largely positive, some were rather controversial (discussed below), thus raising important questions whether to target downstream pathways instead such as the S6 kinases.

There is mounting evidence from large-scale resource studies utilising multiomics to point that mTOR and PI3K/Akt signalling are significantly correlated in many cancers and also frequently hyperactivated in HCC; and mTOR activation ($pS6K1^{T389}$, $pS6^{S240/S244}$) is often clearly detected by immunohistochemistry in up to 40-50% of HCC patients (Sahin et al., 2004; Sieghart et al., 2007; Villanueva et al., 2008; Zhang et al., 2017). Upregulation of mTOR signalling was also observed in cholangiocarcinoma, which is a highly lethal liver cancer of biliary origin (Andersen et al., 2012). It is important to note, however, that mutations in mTOR or related signalling pathways are rare in HCC with only RPS6KA3 (p90 RSK-1 that activates PI3K/RAS signalling) with a 9.6% mutation rate; but mTOR signalling in HCC closely associated with deregulated EGF, IGF and PTEN pathways, thus suggesting that upregulation of mTOR signalling is a consequence of activation of nutrient sensing pathways that lie upstream (Cleary et al., 2013; Guichard et al., 2012; Kan et al., 2013; Villanueva et al., 2008). No matter the means of mTOR activation, it should be unsurprising that it is indicative of poorer outcome given its role in cell growth and proliferation. This is because high mTOR signalling was associated with poorly differentiated tumours, worsened prognosis and earlier recurrence independent of the aetiology of HCC (Baba et al., 2009; Villanueva et al., 2008; Zhou et al., 2010). First and second-generation mTOR inhibitors are being tested in phases I, II and III clinical trials for HCC as well as the combined use of mTOR inhibitors with sorafenib, and these are summarised in this detailed review (Matter et al., 2014). More importantly, there is a general consensus that mTOR activation is key both for the initiation of HCC and for the progression of malignant hepatocytes to liver cancer, thus further highlighting the importance of studying the role of mTOR signalling in the progression from fatty liver disease into HCC (Calvisi et al., 2011; Matter et al., 2014).

Nevertheless, a recent article from the Karin group showed that persistent mTOR inhibition increased liver damage, inflammation and incidence of HCC in a widely used model of liver cancer (Umemura et al., 2014). The Karin group utilised their previously described HCC model of combining a HFD with diethylnitrosamine (DEN), which was one of the first studies to provide causal evidence to show that genetic or dietary obesity greatly enhanced liver cancer induced by a chemical carcinogen, and this was due to low-level chronic inflammation (elevated levels of IL-6 and TNF-α) (Park et al., 2010). Although mTOR downregulation either with chronic rapamycin treatment or by specifically deleting RAPTOR, which is crucial for mTORC1 assembly, in hepatocytes reduced hepatic steatosis, they observed enhanced liver damage and fibrosis, inflammation and development of hepatocellular carcinoma. Therefore, they argue that persistent mTOR inhibition may not be suitable for treatment of obesity-promoted liver cancer (Umemura et al., 2014). mTOR, however, has numerous targets and there are many preclinical and clinical studies demonstrating the benefits of mTOR inhibition for liver cancer therapy, therefore elucidating whether the downstream targets of mTOR such as the S6 kinases may play a role in NASH and HCC is still clinically relevant.

1.22. How is mTOR signalling linked to organismal ageing?

Out of the diverse roles that mTOR has been implicated in, its involvement in organismal ageing is one of great interest to many. There have been numerous studies from yeast to mice showing that inhibiting mTOR signalling prolongs lifespan and improves age-related pathologies, as reviewed in (Johnson et al., 2013; Lamming et al., 2013). Of note, however, are two studies from 2009 that clearly demonstrated that downregulation of mTOR signalling by either rapamycin treatment or S6K1 deletion causes a significant extension in lifespan (Harrison et al., 2009; Selman et al., 2009). Firstly, the use of rapamycin showed that it is possible to prolong mammalian lifespan by a chemical intervention (Harrison et al., 2009). What was of even more interest was that rapamycin was started from day 600 in mice, which is equivalent to roughly 60 years in humans. Although it is difficult to directly extrapolate from mice to humans, this was still a remarkable finding, as it illustrated that it may be possible to extend human lifespan even if treatment was started from middle-to-late age (Johnson et al., 2013). To further support this, the Kaeberlein group published a recent study showing that 3 months of low-dose rapamycin treatment in middle-aged male and female mice (20-21 months old) is sufficient to increase median post-treatment life expectancy by 42% and also to improve various health parameters (Bitto et al., 2016). Nevertheless, females given the high-dose (roughly 27 times greater than the original study) intermittent rapamycin treatment failed to increase lifespan, whereas it did in males, and instead shifted cancer prevalence towards a highly aggressive form of haematopoietic malignancy from other cancer types, thus further highlighting sexual dimorphisms in mTOR signalling (Bitto et al., 2016). In support, rapamycin treatment was shown to differentially regulate lifespan of male and female mice, as female mice showed increased sensitivity to rapamycin with a lower dose required to

capture the longevity phenotype (Miller et al., 2014). There are numerous studies that have emerged through the years demonstrating mTOR inhibition to improve various aspects of health including ameliorating age-related cardiac dysfunction, abolishing cognitive defects in a mouse model of Alzheimer's disease and rejuvenating ageing haematopoietic and epithelial stem cells (Chen et al., 2009; Flynn et al., 2013; Iglesias-Bartolome et al., 2012; Yilmaz et al., 2012). In addition, the mTOR inhibitor RAD001 was shown to improve immune function in the elderly, as they were more responsive (higher serum antibody titres) to an influenza vaccine, thus underscoring that rapamycin treatment, at least for short-term, may be beneficial in aged individuals (Mannick et al., 2014). Genetic evidence of mTOR depletion increasing lifespan also exists, as mTOR hypomorphic mice displayed longevity in both male and female mice (Wu et al., 2013).

It is important to mention, however, that long-term rapamycin treatment has deleterious side effects, which is not surprising considering that rapamycin was initially approved by the FDA for its immunosuppressive properties (Johnson and Kaeberlein, 2016). Some of the side effects of rapamycin treatment include impaired glucose homeostasis, increased rates of cataracts and testicular degeneration in mice at the same doses that increased longevity (Lamming et al., 2012; Wilkinson et al., 2012). Short-term rapamycin treatment may be beneficial, however, as showed in the Kaeberlein study, but it is important to find a suitable dose and treatment regime, as high-doses still had deleterious effects in female mice (Bitto et al., 2016). In line with this, deletion of RICTOR, which is crucial for assembly of mTORC2, showed a significant reduction in lifespan of male mice, indicating that the increased longevity is primarily due to inhibition of mTORC1 (Lamming et al., 2014).

It is reasonable that inhibiting a multifunctional kinase such as mTOR will yield some undesirable side effects. Therefore, it is crucial that we try to dissociate the lifespan extending effects of rapamycin from its more serious side effects, and all this requires a more thorough understanding of the downstream signalling of mTOR. To this end, the Withers group and others have demonstrated that knocking out S6K1 in mice, which lies directly downstream of mTOR, also shows a significant lifespan extension as well as improvements in age-related pathologies (Arif et al., 2017; Selman et al., 2009). For example, these mice showed improved insulin sensitivity (assessed by HOMA2), improved motor function (assessed by the rotarod test), improved ratios of naïve to memory T-cells (for both $CD4^+$ and $CD8^+$ T-cells), as well as improved bone density, compared to age-matched controls (Selman et al., 2009). It was also recently shown that haematopoietic stem cell function is preserved in old *S6K1*$^{-/-}$ mice, as donor engraftment of long-term haematopoietic stem cells (LT-HSCs) was improved when cells were isolated from *S6K1*$^{-/-}$ mice compared to controls (Selman et al., 2016). Therefore, targeting S6K1 or even further down the pathway may be an alternative approach, as it may yield fewer side effects.

In support of this, a recent paper published showed that the multifunctional tRNA synthetase EPRS is a downstream target of S6K1 that regulates lifespan and adipogenesis (Arif et al., 2017). In particular, EPRS has a non-canonical function in the GAIT (IFN-γ-activated inhibitor of translation) complex, which requires phosphorylation at S999 position by S6K1. The authors demonstrated first using a loss of function (S999A) mouse mutant of EPRS that it recapitulates the lifespan extension observed in the *S6K1*$^{-/-}$ mice. In addition, they independently confirmed that S6K1 deletion increases mice lifespan. Even more, using a gain of function (S999D) mouse mutant crossed into the *S6K1*$^{-/-}$ mouse, they went on to demonstrate that this partially restores the body weight loss observed in the *S6K1*$^{-/-}$ mice (Arif et al., 2017). What was rather surprising was how a single phosphorylation event recapitulated the extension in lifespan observed in the *S6K1*$^{-/-}$ mice. Nevertheless, S6K1 has numerous targets with both beneficial and detrimental effects during ageing. Therefore, although the global deletion of S6K1 has an overall beneficial outcome, it is possible that the extension in lifespan observed in the EPRS S999A is capturing one of the positive arms of the loss of S6K1 (Selman and Withers, 2017).

Nevertheless, it is imperative to mention that the EPRS S999A mutant did not recapitulate all of the phenotypes observed in the *S6K1*$^{-/-}$ mice (Arif et al., 2017; Selman and Withers, 2017). Therefore, it is very likely that additional S6K1 effectors mediate at least some of the other beneficial aspects during ageing. For example, it was surprising to see how inflammation was unaffected in the EPRS S999A loss of function mutant considering the role of EPRS in the GAIT complex, and this is of considerable interest given the mounting evidence implicating sterile inflammation or inflammaging in ageing and age-related pathologies. It is still unknown whether *S6K1*$^{-/-}$ mice display an attenuation in age-related inflammation and whether this contributes to any age-related pathologies. Again, any therapeutic application would mean we first need to better understand exactly what is mediating this lifespan extension in these mice, and we hypothesise that a decreased senescence and SASP response (chronic senescence) is, at least in part, responsible for this phenotype.

1.23. What is known about mTOR and S6 kinases in cellular senescence?

Although not much is known about the S6 kinases and senescence, there is now mounting evidence for the role of mTOR in various aspects of cellular senescence (Xu et al., 2014). For example, it was initially shown by Demidenko and colleagues that rapamycin treatment reinitiates proliferation of growth-arrested cells in a model of chemical-induced senescence (IPTG-induced p21-expression and growth arrest) only once IPTG was removed (Demidenko et al., 2009). It was then demonstrated that depletion of RAPTOR (mTORC1) but not RICTOR (mTORC2) bypassed replicative and oncogene-induced senescence, suggesting that it is mTORC1 that is responsible for mTOR-mediated senescence (Kolesnichenko et al., 2012). Furthermore, both mTOR and

auto(lysosomes) were shown to accumulate at a region located at the trans side of the Golgi apparatus in cells undergoing OIS (Narita et al., 2011). Interestingly, they demonstrated this region was a site that allowed the spatial coupling of protein synthesis with autophagy; hence this region was termed the TOR-autophagy spatial coupling compartment (TASCC). Even more, disrupting localisation of mTOR to the TASCC diminished synthesis of IL-6 and IL-8 (Narita et al., 2011). Rapamycin treatment was also shown to inhibit the SASP in models of irradiation-induced senescence as well as in therapy-induced senescence (Dörr et al., 2013; Iglesias-Bartolome et al., 2012), but it was not known precisely how mTOR regulates the SASP, exactly what components of the SASP are regulated by mTOR and what are the functional consequences of this.

We and others recently reported, however, that mTOR through 4EBP1 directly regulates the SASP by coupling translation with mRNA stability (Herranz et al., 2015; Laberge et al., 2015). Importantly, mTOR regulated the SASP in replicative, oncogene and irradiation-induced senescence in five different types of fibroblasts (IMR-90, HFFZ, BJ, WI-38 and TIG3). In addition the same results were observed using shRNA-mediated knockdown of mTOR, three different mTOR inhibitors (rapamycin, Torin1 and NVP-BEZ235), as well as by overexpressing a dominant negative form of 4EBP1, thereby illustrating that this is a conserved, robust feature of mTOR-4EBP1 signalling. Secretome analysis by mass spectrometry showed that mTOR does not regulate the SASP at a global level but regulates specific components within the SASP (roughly half of detected SASP components), and this included IL-6, IL-8 and other key proinflammatory factors that are necessary for mediating SASP functions. Importantly, using an analogue to radiolabelled-methionine assays (Click-iT AHA assay), we showed that this SASP downregulation was specific as a global translation inhibitor (cyclohexamide) was not only toxic to cells (at doses that decreased translational to a similar level to that of Torin1) but also abolished the translation of all tested components. In brief, by a combination of polysome profiling and phosphoproteomic analyses, we showed that mTOR does not primarily regulate the SASP at a translation level (only to some extent – 20%) but rather by specifically regulating the translation of the kinase MAPKAPK2, which is a kinase downstream of p38 MAPK (a known regulator of the SASP). MAPKAPK2 in turn phosphorylates and inhibits the RNA-binding protein ZFP36L1 and the closely related family member ZFP36L2, thereby preventing the degradation of the SASP. ZFP36L1 and ZFP36L2 are zinc-finger proteins, which are known to degrade mRNAs by directly binding to AU-rich elements within the 3'UTR. Importantly, mTOR inhibition did not rescue the senescence-associated growth arrest, which we showed was due to inhibition of cyclin D3, thereby demonstrating that it is possible to dissociate the cell intrinsic growth arrest that persisted from the SASP induction that was abolished. SASP inhibition by mTOR and ZFP36L1 also had functional consequences in both *in vitro* and *in vivo* models of OIS and cancer. Overall, we illustrated how the coordinated regulation of protein synthesis with mRNA stability occurs in senescence, which may be of interest to other biological processes as well (Herranz et al., 2015). Campisi and colleagues

also demonstrated that mTOR regulates the SASP in irradiation-induced senescence, but this was primarily by regulating the translation of IL-1α (Laberge et al., 2015).

There is also some evidence that suggests S6K1 also regulates cellular senescence and the SASP. For example, the above study from Campisi and colleagues showed that knockdown of S6 kinases (did not specify whether S6K1, S6K2 or both) reduced IL-6 secretion as well as the protein expression of other SASP components in irradiation-induced senescence in fibroblasts (Laberge et al., 2015). A recent study also showed that S6K1 and S6K2 in concert regulate the senescence growth arrest through the nuclear epigenetic factor ZRF1 (DnaJ Heat Shock Protein Family Member C2) in a model of TSC1 loss induced senescence in mouse embryonic fibroblasts (MEFs) (Barilari et al., 2017). Although it was interesting to identify ZRF1 as a novel downstream target of the S6 kinases, they studied this in a very specific senescence context, i.e., in a model where hyperactivation of mTOR causes senescence in roughly 30% of MEFs. One major caveat was that this did not induce a pronounced senescence response, and they did not show if this form of senescence elicits a SASP response and whether the S6 kinases regulate it. Importantly, it should be apparent that deleting S6 kinases in a model of mTOR-induced senescence would bypass this growth arrest. Therefore, it is still unclear whether S6 kinases regulate the senescence growth arrest in widely studied forms of senescence such as replicative or oncogene-induced senescence. In line with this, it was shown that S6 kinases play a key role in endothelial cell senescence as overexpression of a constitutively active form of S6K1 increased SA-β-Gal activity, p53 and $p21^{CIP1}$ levels as well as ICAM and VCAM1 expression in human umbilical vein endothelial cells (HUVECs); and shRNA mediated depletion of S6K1 reduced SA-β-Gal activity in L-arginine-induced senescence in these endothelial cells (Xiong et al., 2014; Yepuri et al., 2012). Nevertheless, it is still not entirely clear whether the S6 kinases are required for regulation of cellular senescence, especially in replicative senescence of fibroblasts, which is a model of cellular lifespan and whether the long-lived S6K1 knockout mice have a decelerated senescence and SASP response during mammalian ageing.

1.24. The rationale and aims of the 1st project – the role of ribosomal protein S6 kinases in cellular senescence and ageing.

Given that ageing is a risk factor for a panoply of diseases and that it is malleable to pharmacological intervention, there is great interest to target human ageing, specifically to improve diseases of ageing with the aim of increasing healthspan. Doing so would require that we better understand the regulation of the basic ageing process. In addition, a complex, stress response termed cellular senescence links many pathologies of ageing, both degenerative and hyperplastic. Even more, there is mounting evidence that nutrient sensing pathways that include insulin and insulin-like growth factor signalling and mTOR are some of the most evolutionary conserved pathways in ageing. Importantly, mTOR signalling has now been implicated in senescence, thereby suggesting a possible link between these two biologically crucial processes. The p70 ribosomal protein S6 kinases (S6K1 and S6K2) that are directly downstream of mTOR are of particular interest to us, as the Withers' group has shown that *S6K1*$^{-/-}$ mice are long-lived and resistant to certain age-associated pathologies. Therefore, we hypothesised that a decelerated senescence response (chronic senescence) may be one mechanism for this lifespan extension, and we aim to characterise the senescence response both in mammalian ageing and in a wide range of cellular models that are depleted of S6K1 and/or S6K2.

- To investigate whether the S6 kinases (S6K1/2) regulate senescence and the SASP.

- To determine whether this has a role in the context of ageing.

1.25. The rationale and aims of the 2nd project – the role of ribosomal protein S6 kinases in fatty liver disease.

Nutrient sensing is a requisite for life and it is deregulated during ageing, obesity and related diseases including fatty liver disease and hepatocellular carcinoma. The prevalence of fatty liver disease and liver cancer are rising in the Western world and there is still no approved treatment in the U.K for end-stage disease except liver transplantation. In addition, there is a scarcity of available livers and the surgery is both expensive and risky. Therefore, it is essential to better understand the molecular pathways and pathogenesis of fatty liver disease with the ultimate aim of identifying drug targets both for hepatocellular carcinoma and for preventing the progression of non-alcoholic steatohepatitis (NASH – liver fibrosis and inflammation) to liver cancer. To this end, the p70 ribosomal protein S6 kinases (S6K1 and S6K2) are members of the nutrient sensing mTOR signalling pathway, and deletion of S6K1 prolongs mammalian lifespan and protects from age and diet-induced obesity. Therefore, there is much therapeutic potential for targeting the S6 kinases for obesity-associated pathologies. In support, AAV-mediated knockdown of S6K1 and S6K2 in the liver blunted development of hepatic steatosis, but it is still unknown whether the S6 kinases are also important for progression to liver fibrosis and liver cancer. Therefore, we hypothesised that the liver-specific deletion of S6 kinases will also protect from liver fibrosis and liver cancer and aimed to characterise this in a diet-induced model of liver fibrosis.

- To generate mice with liver-specific deletion of S6K1 and S6K2.

- To determine whether these mice are protected from development of non-alcoholic steatohepatitis and hepatocellular carcinoma.

Chapter 2: Methods.

2.1. Ethics statement for animal work.

All procedures conformed to the UK Animals (Scientific Procedures) Act 1986 and were approved by Imperial College's animal welfare and ethical review body under either PPL "Mechanisms regulating energy homeostasis" 70/7438 or "The Mechanisms of Aging and Age-related Disease" 70/8700.

2.2. Animal care and diets.

Mice were housed in groups of two to five same-sex littermates on a 12-hour light/dark cycle under specific pathogen-free barrier conditions within individually ventilated cages with *ad libitum* access to water and chow. Breeding was done in heterozygote pairs (one male and female) or trios (one male and two females). Mice were weaned at 21 days or delayed a few days to reach an appropriate size for self-sufficiency. Mouse chow (RM3 expanded; Special Diets Services) or high-trans fat (40% kcal fat – mostly primex, 20% kcal fructose and 2% cholesterol, D09100301; Research Diets) was used. The HTF diet was given for 30 weeks (please see below for details).

Dr. Silvia Pedroni and Dr. Elaine Irvine aided during dissections. Mr. Darran Hardy aided with ear notching/weaning at times of barrier restrictions (breeding and animal experiment facilities have a 48-hour barrier rule) and ran the blood count. Ms. Justyna Glegola aided with dissections, weighing, changing of diets and in some of the metabolic tests (glucose and insulin tolerance tests and echoMRI).

2.3. DNA extraction for genotyping.

DNA from ear biopsies was extracted by an alkaline-heat hydrolysis approach. The ear notch was placed into a 1.5 mL Eppendorf tube (Germany) and 300 µL of NaOH (0.06M) was added. Samples were placed inside a heat block (100^{o}C for 10-15 minutes) followed by cooling at room temperature (RT) for 10 minutes before addition of 100 µL Tris-HCL (1M, pH8) to neutralise the solution. Samples were inverted for mixing prior to taking 1 µL for the PCR reaction. PCR reactions were performed in a DNA Engine Dyad Peltier Thermal Cycler (Bio-Rad, USA) using the ThermoPrime 2x ReddyMix PCR Master Mix (Gibco, USA).

For genotyping of embryo heads, 600 µL of NaOH and 200 µL Tris-HCL was used instead. A 1:25 dilution in distilled water was done before taking 1 µL for the following PCR reaction.

2.4. Agarose gel electrophoresis.

The PCR products for genotyping were separated by agarose gel (2-3%) electrophoresis in TAE buffer (40 mM Tris, 20 mM acetate and 1 mM EDTA – pH 8.0) with 10 µL of ethidium bromide at

150V for 45-60 minutes. The bands were then visualised relative to a 1kb plus DNA ladder (Invitrogen, USA) by exposure to ultraviolet light (Bio-Rad Gel Doc™ XR+ and Image lab software).

2.5. Global *S6K1*$^{-/-}$ mice.

Breeding colonies of *S6K1*$^{-/-}$ mice in a C57BL/6 inbred strain were established in Professor Withers' laboratory (Selman et al., 2009). Female *S6K1*$^{-/-}$ and wild type controls were generated from heterozygous breeding pairs or trios and maintained on a C57BL/6 background after 10 backcrosses. Mice were overnight fasted (16 hours – *ad libitum* access to water) and culled by cervical dislocation at 600 days for the old cohort and at 90 days for the young cohort for organ harvesting. Body weight was measured 16 hours following fasting (fasted body weight). Fasted blood glucose levels were recorded with an Elite glucometer (Bayer, Germany) from the carotid artery of a decapitated mouse.

S6K1$^{-/-}$ genotypes were identified using the 9580 (forward) 5'-CAT-CTT-TAC-TGA-AGG-AGC-TAC-TGG-3', 9957 (reverse) 5'-AGC-AGG-CTG-GAC-TCA-AAC-TCA-TAG-3' and Neomycin (Reverse) 5'-TTC-GCA-GCG-CAT-CGC-CTT-CTA-TC-3' primers. The WT allele corresponds to a band at 375 base pairs, whereas the S6K1 deletion corresponds to a band at 175 base pairs. PCR reactions were run using the following cycling conditions: 94^{o}C for 3 minutes, followed by 4 cycles of 94^{o}C for 30 seconds, 63^{o}C for 30 seconds and 72^{o}C for 1 minute. This was followed by 34 cycles of 94^{o}C for 30 seconds, 60^{o}C for 30 seconds and 72^{o}C for 1 minute. A final extension at 72^{o}C for 5 minutes was done followed by 18^{o}C for 10 minutes.

2.6. Global *S6K2*$^{-/-}$ mice.

Breeding colonies of *S6K2*$^{-/-}$ mice in a C57BL/6 inbred strain were established in Professor Withers' laboratory. Heterozygous breeding pairs were used and mice maintained on a C57BL/6 background after 10 backcrosses.

S6K2$^{-/-}$ genotypes were identified using the 14902 (forward) 5'-GCA-CAC-CAG-GGG-CTA-CATA-ATG-3', 22572 (reverse) 5'-GCA-CTG-CAT-ACA-ATC-TTG-GCC-TAG-3' and 15254 (Lar3) 5'-CAC-AAC-GGG-TTC-TGT-TAG-TCC-3' primers. The WT allele corresponds to a band at 600 base pairs, whereas the S6K2 deletion corresponds to a band at 350 base pairs. PCRs were run using the following cycling conditions: 94^{o}C for 3 minutes, followed by 4 cycles of 94^{o}C for 30 seconds, 64^{o}C for 30 seconds and 72^{o}C for 1 minute. This was followed by 30 cycles of 94^{o}C for 30 seconds, 62^{o}C for 30 seconds and 72^{o}C for 1 minutes. A final extension at 72^{o}C for 5 minutes was done followed by 18^{o}C for 10 minutes.

2.7. Liver-specific *S6K1$^{-/-}$: S6K2$^{-/-}$* mice.

Breeding colonies of *S6K1$^{fl/fl}$: S6K2$^{-fl/fl}$* mice and *albumin-cre* heterozygotes in a C57BL/6 inbred strain were established in Professor Withers' laboratory (Smith et al., 2015). *S6K1$^{fl/fl}$: S6K2$^{-fl/fl}$* mice were then bred with albumin-cre heterozygotes to obtain control (*albumin-cre$^{-/-}$/S6K1$^{fl/fl}$: S6K2$^{fl/fl}$*) and knockout (*albumin-cre$^{+/-}$/S6K1$^{fl/fl}$: S6K2$^{fl/fl}$*) mice. Importantly, expression of cre-recombinase was maintained in heterozygosity. At 16 weeks of age, mice were kept in a chow diet or fed an HTF diet (composition described above) for 30 weeks. At 46 weeks of age, mice were overnight fasted (16 hours – *ad libitum* access to water) and culled by cervical dislocation. Whole liver photos were acquired at the time of cull.

Cre-recombinase was identified using the forward 5'-AGC-GAT-GGA-TTT-CCG-TCT-CT-3' and reverse 5'- CAC-CAG-CTT-GCA-TGA-TCT-CC-3' primers and corresponds to a band at 300 base pairs. PCRs were run using the following cycling conditions: 95^{o}C for 3 minutes, followed by 34 cycles of 95^{o}C for 35 seconds, 55^{o}C for 1 minute and 72^{o}C for 1 minute. A final extension at 72^{o}C for 2 minutes was done followed by 16^{o}C for 5 minutes.

S6K1 floxed allele was identified using the 1859_25 (forward) 5'-TCC-ACC-CAC-CAG-TAA-AGA-GC-3' and 1859_26 (reverse) 5'-CCT-CAG-TCT-CCT-GAG-TGT-TAA-GG-3' primers. The WT allele corresponds to a band at 250 base pairs, whereas the S6K1 floxed allele corresponds to a band at 500 base pairs. PCRs were run using the following cycling conditions: 94^{o}C for 5 minutes, followed by 4 cycles of 94^{o}C for 30 seconds, 62^{o}C for 30 seconds and 72^{o}C for 1 minute. This was followed by 34 cycles of 94^{o}C for 30 seconds, 59^{o}C for 30 seconds and 72^{o}C for 2 minutes. A final extension at 72^{o}C for 10 minutes was done followed by 16^{o}C for 5 minutes.

S6K2 floxed allele was identified using the 14902 (forward) 5'-GCA-CAC-CAG-GGG-CTA-CATA-ATG-3', 22572 (reverse) 5'-GCA-CTG-CAT-ACA-ATC-TTG-GCC-TAG-3' and 15254 (Lar3) 5'-CAC-AAC-GGG-TTC-TGT-TAG-TCC-3' primers. The WT allele corresponds to a band at 600 base pairs, whereas the S6K2 floxed allele corresponds to a band at 650 base pairs. PCRs were run using the following cycling conditions: 94^{o}C for 3 minutes, followed by 4 cycles of 94^{o}C for 30 seconds, 64^{o}C for 30 seconds and 72^{o}C for 1 minute. This was followed by 30 cycles of 94^{o}C for 30 seconds, 62^{o}C for 30 seconds and 72^{o}C for 1 minutes. A final extension at 72^{o}C for 5 minutes was done followed by 18^{o}C for 10 minutes.

2.8. Metabolic testing and weighing of mice.

For the NASH study, bodyweights from group-housed mice were measured weekly at 2-3 pm from weaning until completion of the study. Glucose and insulin tolerance tests as well as EchoMRI analysis were done at 8-10 weeks of age and again at 36-38 weeks of age. Fed and fasted measurements were done at 9 and 11 weeks of age and again at 44 and 45 weeks of age.

Metabolic phenotyping was done in all chow-fed mice prior to giving the HTF diet. HTF diet was given for 20 weeks (16 to 36 weeks of age) prior to metabolic phenotyping again.

Fed mice were weighed prior to EchoMRI analysis of body composition, which provided lean and fat mass in grams. Percentage fat or lean mass was calculated by taking into account of the body weight.

Glucose (1g/kg) and insulin (0.75 U/kg, Actrapid) were given by intraperitoneal (I.P) injection. Glucose levels from tail vein whole blood was measured with an Elite glucometer (Bayer) prior to I.P injection and at 15, 30, 45, 60, 90 and 120 minutes post IP injection. For glucose tolerance tests (GTTs), mice were fasted overnight for 16 hours and experiments were done in the morning (started at 9-10 am). For insulin tolerance tests (ITTs), mice were fasted in the morning for 4 hours prior to starting the experiment between 1-2 pm.

2.9. Vetscan VS2 for analysis of blood parameters.

Whole blood was collected into lithium-heparin coated tubes (Abaxis, UK) from the carotid artery following cervical dislocation of mice. 120-140 µL of whole blood was then added into either the mammalian liver profile rotor (Abaxis, UK) or the comprehensive diagnostic profile rotor for geriatric testing (Abaxis, UK) and ran on the VetScan VS2 Chemistry Analyzer (Abaxis, UK).

Serum aspartate aminotransferase (AST) was measured using the AST Activity Assay Kit from 36-week-old chow-fed and HTF-fed mice (Sigma-Aldrich, USA), according to manufacturer's protocol. Serum was obtained from tail-vein whole blood collected into EDTA-free, sterile blood tubes (Sarstedt, Germany). Blood from individual mice was kept in the fridge while blood collection was done. Blood was then left at RT for 5 minutes to allow coagulation and then centrifuged at *6000 rpm* for 5 minutes. Serum (top, clear phase) was transferred into new tubes and stored at -80^{o}C.

2.10. Peripheral whole blood analysis of immune cell composition.

Blood was collected using citrate as anticoagulant from tail vein whole blood and diluted using saline to a volume of at least 200 µl. Complete blood counts were obtained using the Sysmex XE2100 automated cell counter (Sysmex Corporation, Japan).

2.11. Chemical compounds and treatments.

4-hydroxytamoxifen (4OHT) was obtained from Sigma-Aldrich, USA. 4OHT (125 nM) was dissolved in dimethylsulfoxide (DMSO). LY2584702 (2 µM, Key Organics, UK) and Torin1 (25 nM, Tocris, UK) were also dissolved in DMSO. Cells were treated with the indicated drugs the day after seeding. 4OHT was replenished every four days and LY2584702 and Torin1 were replenished

every two days. Lipopolysaccharide (100 ng/mL, Sigma-Aldrich, USA) and ATP (adenosine 5'-triphosphate disodium salt hydrate) (5mM, Sigma-Aldrich, USA) were dissolved in sterile water.

2.12. Plasmids and vectors.

IMR-90 lung fibroblasts expressing the ER: RAS^{G12V} chimaeric fusion protein that activates upon 4OHT (125 nM) treatment was created by stably transducing pLNC-ER: RAS retroviral vector held at the Cell Proliferation group (described in detail below). Upon addition of 4OHT, these cells undergo a growth arrest and display senescence characteristics, thus representing a model of oncogene-induced senescence. Cells treated with DMSO were used as controls. pBABEpuro empty vector (EV) or expressing $HRAS^{G12V}$ (RAS) was used to transduce mouse embryonic fibroblasts (plasmids held at the Cell Proliferation Group). pGIPZ (mir30-based) lentiviral shRNA vectors were obtained from the library held at the MRC LMS Genomics core facility. Please see Table 1 for shRNA sequences.

2.13. Bacterial transformation and purification of plasmid DNA.

Chemically competent *E. coli* DH5α^{TM} cells were thawed on ice before gentle mixing of 50 µL of cells with 1 µL (~ 100 ng) of plasmid DNA. Cells were incubated on ice for 30 minutes followed by a heat-shock at 42^{o}C for 45 seconds before cooling on ice for 2 minutes. Bacteria were then grown in 200 µL of LB broth at 400 rpm for 1 hour at 37^{o}C. 50 µL of the mixture was then spread on LB agar plates with the antibiotics (ampicillin 100 µg/mL) and cultured overnight for 16-18 hours. Single colonies were then picked and inoculated in either 30-80 mL of LB broth in antibiotics for 16-18 hours at 37^{o}C shaking (220 rpm). Bacteria transformed with pGIPZ plasmids were grown in low salt LB with both ampicillin (100 µg/mL) and zeocin (25 µg/mL). Plasmids were purified using the HiSpeed® Plasmid Midi kit (Qiagen, Germany) according to manufacturer's instructions. Plasmid DNA was eluted in 200 µL of distilled water.

2.14. Cell Culture.

Human foetal lung (IMR-90) fibroblasts, human embryonic kidney 293 transformed (HEK293T) cells and L929 fibroblasts were obtained from the American Type Culture Collection (ATCC). For proliferation and maintenance of IMR90 and HEK293T, cells were grown in Dulbecco's Modified Eagle Medium (DMEM) supplemented with 10% foetal bovine serum (FBS, Sigma-Aldrich, USA), 1x Antibiotic-Antimycotic (Gibco, USA) and kept incubated at 37^{o}C and 5% CO_2. Mouse embryonic fibroblasts were maintained in DMEM supplemented with EmbryoMax® FBS (Millipore, USA) and 1x Antibiotic-Antimycotic at 37^{o}C and 5% CO_2. L929 fibroblasts were maintained in DMEM-F12 Ham (Gibco, USA) supplemented with heat-inactivated HyClone FBS (GE Healthcare, USA) and 1x Antibiotic-Antimycotic at 37^{o}C and 5% CO_2. Cells were cultured in the indicated medium during experiments unless otherwise stated. Differentiation of bone-marrow derived macrophages is explained in detail below.

Cell number and viability measurements were determined using the Guava Viacount reagent (Millipore, USA) and the Guava Cytometer (Millipore, USA). Cells were routinely assessed for mycoplasma as done as part of a service at the MRC LMS.

2.15. Preparation and passaging of mouse embryonic fibroblasts (MEFs).

Mouse embryonic fibroblasts were prepared from 13.5-day embryos of mice bred in heterozygosity for S6K1 or S6K2. Therefore, both wild type and knockout MEFs were prepared from the same mother and MEFs from at least 3 independent mothers were used for experiments. *S6K1$^{-/-}$: S6K2$^{-/-}$* MEFs were prepared by breeding *S6K1$^{+/-}$: S6K2$^{-/-}$* mice together (*i.e.,* S6K1 heterozygous and S6K2 homozygous). Wild type MEFs used as controls for *S6K1$^{-/-}$: S6K2$^{-/-}$* MEFs were prepared from embryos of wild type mothers that were obtained at earlier stages of breeding for generation of double deletion. *Dr. Silvia Pedroni aided in the breeding and preparation of S6K2$^{-/-}$ and S6K1$^{-/-}$; S6K2$^{-/-}$ MEFs.*

MEFs were prepared by first removal of the embryo from the uterus and yolk sac and then the head and viscera from the embryo. Remaining tissue was minced and triturated in trypsin-EDTA (0.05%, Gibco, USA) using a scalpel and gentle pipetting (P1000 Gilson) and then incubated at 37^{o}C and 5% CO_2 for 15 minutes with periodic (every 5 minutes) resuspension. A single-cell suspension was obtained by passing cells through a 100 µm sterile nylon cell strainer (Falcon, USA). Cells were cultured for 3-5 days until confluency. MEFs were frozen at this point in complete DMEM (as above) with 10% DMSO.

2.16. Cumulative population doublings of MEFs.

Passage 1 MEFs of the indicated genotypes were seeded at a density of $2x10^6$ cells in 10 cm dishes, and cell counts were done every 4 days (1 passage) until wild type cells reached replicative exhaustion. Medium was replaced every 2 days and experiments were done in 21% O_2. Cell counts were made after trypsinisation and resuspension in complete medium. For counting, cells were diluted in 1 in 4 in Guava Viacount reagent (Millipore, USA) and quantified on the Guava Cytometer (Millipore, USA) by selectively eliminating any debris and dead cells, thus providing an accurate representative of viable cell number. Cumulative population doublings per passage was calculated as $\log_2$ (number of cells at time of subculture/ number of cells plated) and plotted against the total time in culture (passage 2 until 8).

RNA was extracted from cells at passages 2 and 8. Cells were also seeded for 5-bromo-2'-deoxyuridine incorporation and senescence-associated beta galactosidase activity at passages 2 and 8. These methods are described in detail below.

2.17. Preparation and activation of bone-marrow derived macrophages (BMDMs).

Collection of conditioned medium from L929 cells that secrete macrophage-colony stimulating factor (M-CSF).

L929 fibroblasts were seeded in T175 dishes and at 80% confluency, fresh DMEM-F12 Ham (complete with HyClone FBS and antibiotics) was added. Medium was collected and pooled 7 days later, filtered through a 0.45 µm pore and frozen at -80^{o}C for the use of BMDM differentiation.

Preparation of BMDMs from 10-week old mice.

Tibia and femurs from 10-week-old mice of the indicated genotypes were flushed with PBS + 2% FBS using a 25-gauge needle (0.5 x 16 mm) to collect the bone-marrow. Cells were spun down (1200 rpm for 5 minutes) and resuspended in 20% L929 conditioned medium diluted in DMEM-F12 Ham supplemented with heat-inactivated HyClone FBS (GE Healthcare, USA) and 1x Antibiotic-Antimycotic. Cells were then passed through a 0.70 µm pore cell strainer, counted and plated in 5 x 10 cm dishes. BMDMs were differentiated using 20% L929 conditioned medium and DMEM-F12 Ham as described above for 7 days. Specifically, 10 mL of medium was added to sides of dishes without tilting on day 4. On day 5, 5mL of medium was removed from dishes and replaced with 10 mL of fresh medium. On day 6, 10 mL of medium was removed from dishes and replaced with 10 mL of fresh medium. Medium was never completely removed, as essential cytokines secreted from macrophages are required for differentiation. BMDMs were counted and seeded on day 7 for stimulation. *Dr. Silvia Pedroni aided in isolation of bone marrow and differentiation into BMDMs.*

Stimulation of BMDMs with lipopolysaccharide (LPS) and ATP.

Following differentiation, BMDMs were seeded at a density of 5x10^{5} in 6 cm dishes in 5 mL of 20% L929 with DMEM-F12 Ham as described above. On the following day, medium was replaced and cells were stimulated with ultrapure 100 ng/mL LPS (Sigma-Aldrich, USA) alone for 6 hours or in combination with 5 mM ATP (Sigma-Aldrich, USA) for the final hour.

2.18. Reverse transfection of small interfering RNAs (siRNAs).

Lyophilized siRNAs were obtained from Qiagen either in Flexitubes® or in 96-well format Flexiplates® for the S6 kinase target screen. siRNAs were first reconstituted in RNase-free water to a concentration of 1 µM and aliquoted. Please see Table 2 for siRNA sequences.

For RNA analysis, 1.2x10^{5} (for growing cells) or 2.4x10^{5} IMR-90 ER: RAS fibroblasts in suspension (DMEM with 10% FBS but without antibiotic) were reverse-transfected with the indicated siRNAs in a 6 cm dish to a final volume of 4 mL. A transfection mix consisting of 4 µL of DharmaFECT1™ (GE Healthcare, UK), 144 µL of 1 µM siRNA (35 nM final concentration) and 700 µL plain DMEM for each sample was briefly vortexed and incubated at RT for 30 minutes prior to

cell seeding. The transfection medium was replaced with fresh complete medium with or without 4OHT 16 hours later once cells had adhered. Allstars scrambled siRNA served as a negative control.

For immunofluorescence analysis in 96-well format, $1.75x10^3$ (for day 5 analysis) or 1.25-$1.5x10^3$ (for day 8 analysis) IMR90 ER: RAS fibroblasts in suspension (DMEM with 10% FBS but without antibiotic) were reverse transfected with the indicated siRNAs in a final volume of 100 µL. A transfection mix consisting of 0.1 µL of DharmaFECT1™ (GE Healthcare, UK), 3.6 µL of 1 µM siRNA (35 nM final concentration) and 17.5 µL plain DMEM for each sample was briefly vortexed and incubated at RT for 30 minutes prior to cell seeding. The transfection medium was replaced with fresh complete medium with or without 4OHT 16 hours later once cells had adhered. Allstars scrambled siRNA served as a negative control.

2.19. Production and transduction of retrovirus and lentivirus into target cells.

HEK293T cells were used for packaging of retrovirus or lentivirus. HEK293T cells were plated in 10 cm dishes the day prior to the day of transfection (day 0) to achieve a predicted confluence of 70-80%.

For generating IMR90 ER: RAS^{G12V} fibroblasts, HEK293T cells with GagPol expression (held at the Cell Proliferation lab) were used for transfection. On the day of transfection, a mix of 20 µg of the retroviral plasmid, 2.5 µg of pVSV-G (vesicular stomatitis virus glycoprotein, Clontech), 75 µL of linear 25 kDa PEI (1 mg/mL polyethylenimine (w/v), Polysciences) and 1 mL of plain DMEM was made. The mix was briefly vortexed, incubated for 30-60 minutes at RT and added in a drop-wise manner onto the HEK293T GagPol cells. 24 hours later, medium was replaced with fresh 6 mL (to concentrate the virus) complete DMEM and transfection efficiency was monitored by checking for expression of mCherry using the Olympus CKX41 inverted light microscope. On the same day, IMR90 fibroblasts were seeded at a density of 10^6 per 10 cm dish. On the following day (24 hours later), the viral supernatant was harvested and passed through a 0.45 µm cellulose acetate filter (VWR International, USA). The supernatant was then supplemented with 4 µL of 8 mg/mL of polybrene to increase the infection efficiency. Medium was removed in IMR90 fibroblasts and replaced with the virus supernatant for 3 hours. 2 additional rounds of transduction were carried out before replacing with fresh complete DMEM. 48-72 hours following transduction, cells were split and selected with Geneticin® (400 µg/mL).

For generating MEFs expressing either empty vector (EV) or constitutively expressing $HRAS^{G12V}$, the above procedure with slight modifications was carried out. Specifically, transfection was performed using HEK293T cells with 10 µg of EcoHelper (pCL-Eco, Addgene) instead of GagPol and VSV-G. In addition, $1.5x10^6$ MEFs were seeded for transduction. Transduction was

carried out by first pooling all the empty vector or $HRAS^{G12V}$ supernatant together and adding an equal amount of virus titre (6 mL) to each 10 cm MEF dish. In addition, a single 8-hour round of transduction was performed to reduce stress to cells. 48-72 hours following transduction, MEFs were selected in 3 µg/mL of puromycin and transduction efficiency for mCherry was assessed by flow cytometry using Guava EasyCyte™ (Millipore, USA). A transduction efficiency of 95% or greater was achieved.

For lentiviral transduction of shRNAs into IMR90 ER: RAS^{G12V} fibroblasts, a modified approach was used. Transfection was carried out using HEK293T cells with 10 µg of the indicated pGIPZ (2.5 µg each for pool of 4 shRNAs) lentiviral shRNA vector, 8 µg of psPax2 (Addgene), 2 µg of VSV-G, 75 µL of PEI and 1 mL of plain DMEM. A single 3-hour transduction was done by diluting the virus supernatant at a 1:3 ratio to reduce stress to cells. Lentiviruses infect at greater efficiency than retroviruses since lentiviruses can infect both dividing and non-dividing cells, whereas retroviruses can only infect dividing cells. 48-72 hours following transduction, cells were selected in 0.75 µg/mL of puromycin.

2.20. Analysis of gene expression.

Total RNA extraction.

TRIzol® reagent (Ambion) and the RNeasy Mini Kit (Qiagen, Germany) were used to extract total RNA from cells and tissues. Cells were washed once with PBS before lysis in 800 µL of TRIzol. Cells were then scraped off the dishes, vortexed to homogenise lysate and stored at -80^{o}C to further facilitate homogenisation. Livers were snap frozen and stored at -80^{o}C. Snap frozen liver tissues were cut (30 mg for ageing study or 75-150 mg for HTF study) with a chilled scalpel on dry ice and then lysed and homogenised in 800 µL TRIzol using the IKA® T10 basic ULTRA-TURRAX homogeniser (IKA, Germany). 200 µL of chloroform (Sigma-Aldrich, USA) was added to samples, vortexed for 15 seconds and incubated at room temperature for 3 minutes before centrifugation at 12, 000 rpm at 4^{o}C for 15 minutes for phase separation. The clear aqueous phase (upper layer) was carefully transferred to a separate tube and mixed with an equal volume of 70% RNase-free ethanol before purification with RNeasy Mini Kit (Qiagen, Germany). RNA was eluted in 30-50 µL of RNase-free water and the concentration measured using a NanoDrop® ND-1000 spectrophotometer at an absorbance of 260 nM (A_{260}) ultraviolet light. RNA purity was determined by measuring the 260/280 ratio (~ 2 to ensure no protein and phenol contamination). RNA was either used directly or stored at -80^{o}C.

Complementary DNA (cDNA) synthesis.

SuperScript® II reverse transcriptase (Invitrogen, USA) kit was used to generate cDNA. 1-5 µg of RNA (an equal amount for all samples in a given experiment) was mixed with RNase-free water to

a final volume of 11 µL. 1 µL of Random Hexamers (50 ng/mL, Invitrogen - USA) and 1 µL of deoxynucleotide mix (10 mM dNTPs, Bioline - UK) were added to each sample. The mix was briefly vortexed, heated at 65^{o}C for 5 minutes to melt secondary RNA structures and then rapidly cooled to 4^{o}C. 4 µL of first-strand buffer (5X), 2 µL of dithiothreitol (100 mM DTT) and 1 µL of SuperScript II reverse transcriptase (200 U/µL) were added to the mix, vortexed and run in a DNA Engine Dyad Peltier Thermal Cycler (Bio-Rad, USA) with the following cycling conditions: 25^{o}C for 10 minutes, 42^{o}C for 50 minutes and 70^{o}C for 15 minutes. Samples were diluted with distilled water to a maximum of 16.7 ng/µL depending on how much cDNA was reverse transcribed (equal amount for all samples in a given experiment).

Quantitative reverse transcription-polymerase chain reaction (RT-qPCR).

RT-qPCRs were performed in a CFX96 Real-Time PCR system (Bio-Rad, USA). 50-150 ng of cDNA (an equal amount for all samples in a given experiment) was used. A mix of 9 µL of cDNA/water, 0.5 µL each of forward and reverse primer (0.25 µM final concentration) and 10 µL of SYBR Green (2X) or Taqman (2X) PCR Master Mix (Applied Biosystems, USA) was made in a final volume of 20 µL.

RT-qPCRs for SYBR Green were run using the following cycling conditions: 52^{o}C for 2 minutes, 95^{o}C for 5 minutes, followed by 40 cycles of 60^{o}C for 30 seconds, 72^{o}C for 15 seconds and fluorescence measurement. RT-qPCRs for TaqMan were run using the following cycling conditions: 50^{o}C for 2 minutes, 95^{o}C for 10 minutes, followed by 40 cycles of 95^{o}C for 15 seconds, 60^{o}C for 1 minute and fluorescence measurement.

Gene expression was normalised to either ribosomal protein S14 (RPS14) or the indicated housekeeping genes and analysed by the comparative Ct method. Primers were designed using Primer-BLAST (NCBI) to generate a PCR product no longer than 200 base pairs and to span an exon-exon junction to avoid amplification of genomic DNA. Please refer to Table 3 for the list of primers used in RT-qPCR.

2.21. RNA-sequencing of ageing and NASH samples.

RNA sequencing was performed by taking liver RNA from both the ageing and NASH study. For the ageing study, an n = 5 female mice per genotype (WT or KO) per age (young or old) with a total of 20 samples were used. For the NASH study, an n = 3-4 mice for both sexes (males and females) per genotype (Control or KO) per treatment (chow or high-trans fat diet) were used.

Assessment of RNA purity and integrity.

RNA purity and integrity were first assessed prior to cDNA library preparation and deep sequencing using the Agilent 2100 Bioanalyser and the RNA 6000 Nano Kit with the 2100 Expert software, according to manufacturer's protocol. RNA integrity was assessed by measuring the peaks corresponding to the 18S and 28S ribosomal RNA with an RNA integrity score (RIN) above 7 for tissue samples being acceptable. All samples had an RIN above 7 (Figure 2.1)

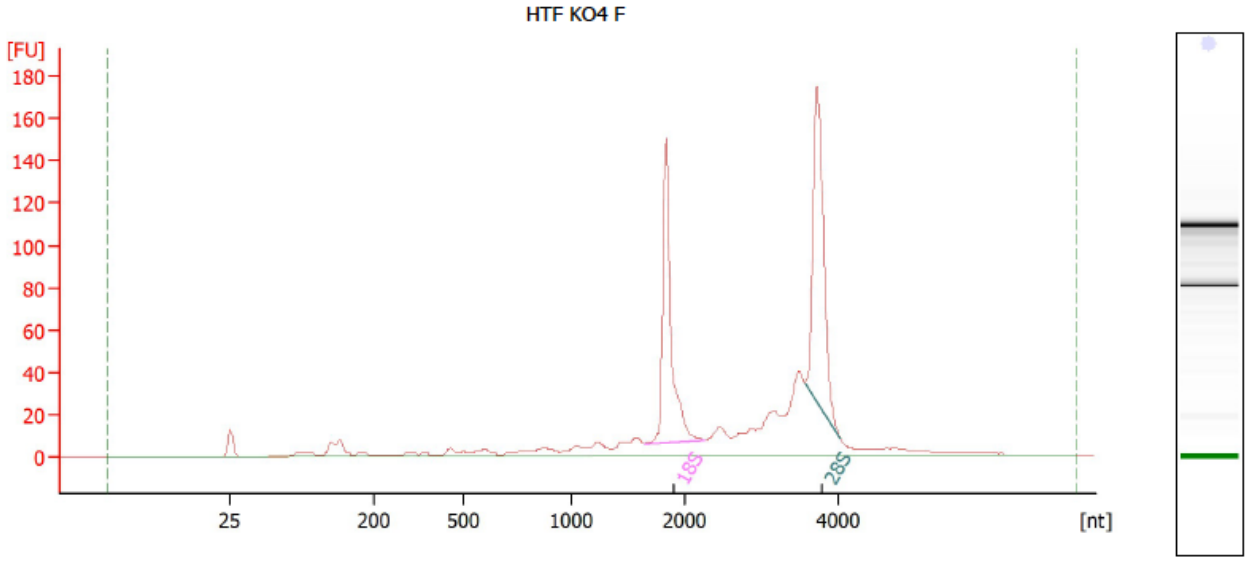

Overall Results for sample 8 : HTF KO4 F

RNA Area:	742.7	RNA Integrity Number (RIN):	8.7 (B.02.08)
RNA Concentration:	487 ng/µl	Result Flagging Color:	
rRNA Ratio [28s / 18s]:	1.2	Result Flagging Label:	RIN: 8.70

Fragment table for sample 8 : HTF KO4 F

Name	Start Size [nt]	End Size [nt]	Area	% of total Area
18S	1,639	2,252	143.2	19.3
28S	3,571	4,032	169.6	22.8

Figure 2.1. Representative Bioanalyser profile prior to RNA-sequencing.
RNA was assessed using the Agilent 2100 Bioanalyser and the RNA 6000 Nano kit with the 2100 Expert software. The representative Bioanalyser trace depicts two well-defined peaks for the 18S and 28S ribosomal RNA and an RNA integrity score of 8.70. This trace represents RNA isolated from the liver of a mouse fed a high-trans fat diet.

cDNA library preparation, RNA sequencing and bioinformatics analyses.

The MRC LMS Core Facility prepared and sequenced the cDNA library. cDNA libraries were prepared from 500 ng of total RNA per sample using the TruSeq stranded mRNA library prep kit, according to manufacturer's protocol (Illumina, USA). Once the cDNA library was prepared, quality was checked on the Agilent 2100 Bioanalyser using the HS DNA chip and concentration measured using the Qubit (Life Technologies, USA). The cDNA library was then sequenced on the HiSeq 2500 (Illumina, USA) following hybridisation to the flowcell. The cDNA library for the ageing study was run on 4 lanes, whereas the cDNA library for the NASH study was run on 8 lanes using single-

end, 50-base pair reads to achieve a minimum of 40 million reads per sample. The Real Time Analysis (RTA version 1.18.64) with default filter and quality settings on the HiSeq 2500 was used to process the sequencing data.

CASAVA software (version 1.8.4) was used to demultiplex library reads by sample according to the indexing. *The bioinformatics analysis for generation of read counts, principal component and clustering analysis, as well as gene ontology and gene set enrichment analysis was carried out primarily by Mr. Gopuraja Dharmalingam and some analysis was also done by Dr. Thomas Carroll, who are both part of the MRC LMS Bioinformatics Core Facility.* Raw reads were mapped to *mm9* genome using top hat aligner. Gene based counts were then obtained using 'HTseq counts module'. Differential expression analysis was then performed using 'DESeq2' Bioconductor package. Principal component analysis was done by analysing the top 1000 most variable genes between the groups. Hierarchical clustering of samples was done by comparing the expression of all genes in a given sample to genes in all samples. The '*dist'* function in 'DESeq2' was used to get the sample-to-sample distances. Distances were visualised by *'pheatmap'* function available in 'pheatmap R package'.

Gene ontology was performed using 'GoSeq' by taking the differentially expressed genes between groups, and the data are represented as the -log10 fold change of the p value. Gene ontology terms included biological processes, cellular component or molecular functions. Gene set enrichment analysis (GSEA) was carried out using the Broad institute GSEA application. The genes were ranked based on Wald statistics available from 'DESeq2' comparisons. Genes with very few read counts were excluded from analysis.

2.22. Crystal violet staining.

Cells were seeded at a density of 1.5-2x10^4 in 6-well dishes and maintained in culture until control (growing) cells reached confluence (usually 14 days). Medium was replenished every 2-4 days with the appropriate drug treatments. Cells were then fixed with 0.5% glutaraldehyde (v/v) (Sigm-Aldrich, USA) in phosphate buffered saline (PBS) for 1 hour and washed twice with water and left to air-dry over-night. Cells were then stained with 0.2% crystal violet (w/v) (Sigma-Aldrich, USA) and washed twice in water before acquisition of images by scanning the plates. *Any image correction (brightness) was applied to the entire image and in the same manner to all images for a given experiment.*

2.23. Senescence-associated beta galactosidase (SA-β-Gal) staining.

Cytochemistry.

Passage 2 and 8 MEFs were seeded at a density of $8x10^4$ in 6-well dishes and fixed the following day with 0.5% glutaraldehyde (v/v) (Sigm-Aldrich, USA) in PBS for 15 minutes. Cells were then washed twice in 1 mM magnesium chloride ($MgCl_2$) in PBS (pH 5.5) and incubated in X-gal staining solution (1mg/mL X-Gal – Thermo Scientific, 5 mM $K_3[Fe(CN)_6]$ and 5 mM $K_4[Fe(CN)_6*3H_2O]$) for 8 hours at 37°C. Cells were washed twice in water and images were acquired using the Olympus CKX41 inverted light microscope and the attached Olympus DP20 digital camera at X100 magnification. The percentage of SA-β-Gal positive (blue staining) cells was estimated by counting at least 150 cells per well.

Frozen liver sections (16 µm) were washed briefly in ice-cold PBS and then fixed in 0.5% glutaraldehyde (v/v) (Sigm-Aldrich, USA) in PBS for 15 minutes. Slides were then washed twice in 1 mM magnesium chloride ($MgCl_2$) in PBS (pH 5.5) and then incubated in X-gal staining solution (1mg/mL X-Gal – Thermo Scientific, 5 mM $K_3[Fe(CN)_6]$ and 5 mM $K_4[Fe(CN)_6*3H_2O]$) for 8 hours at 37°C. Slides were washed twice in water before dehydration (75% ethanol for 2 minutes, 100% ethanol for 3 minutes – Fisher Chemical, Histo-Clear for 5 minutes – National Diagnostics) and mounting using VectaMount (Vectorlabs, UK).

Any image correction (brightness) was applied to the entire image and in the same manner to all images for a given experiment.

Fluorescence.

$1.5\text{-}2.5x10^3$ IMR90 ER: RAS cells were seeded in 96-well plates and treated with or without 4OHT, LY2584702 (2 µM) or Torin1 (25 nM) on the following day. 8 days later, cells were incubated with fresh DMEM containing DDAO galactoside (9*H*-(1,3-dichloro-9,9-dimethylacridin-2-one-7-yl) β-D-Galactopyranoside) (Molecular Probes™) for 2 hours. Cells were then fixed in 4% formaldehyde solution (v/v) (Sigma-Aldrich, USA), washed three times with PBS and then stained with 4', 6-diamidino-2-phenylindole (1 µg/mL DAPI) for 15 minutes to stain the nuclei. Fluorescent images were acquired and analysed by high-content analysis microscopy using the InCell Analyzer 2000 (GE Healthcare, UK) and the InCell Investigator software. The percentage of SA-β-Gal positive (blue staining) cells was estimated by counting at least 1000 cells per well.

2.24. 5-bromo-2'-deoxyuridine (BrdU) incorporation.

Cell proliferation was assessed by measuring BrdU incorporation on the indicated day. IMR90 ER: RAS fibroblasts were seeded at a density of $1\text{-}3x10^3$ in 96-well plates in triplicate, allowed to adhere over-night and treated with or without 4OHT on the following day. Cells were then pulsed

overnight (17 hours) in BrdU (50 μM) before fixation in 4% formaldehyde solution (v/v) for 1 hour. Cells were washed 2-3 times in PBS, permeabilised with 0.2% Triton X-100 (v/v) (Sigma-Aldrich, USA) for 15 minutes and blocked (0.5% BSA (w/v) and 0.2% fish skin gelatin (v/v) in PBS) for 1 hour at room temperature (RT) with gentle shaking. Fixed cells were then incubated with mouse anti-BrdU primary antibody, DNAse (0.5 U/μL – Sigma-Aldrich, USA) in the presence of 1 mM $MgCl_2$ in blocking solution and incubated for 30 minutes at RT. Cells were then washed three times in PBS before incubation with goat anti-mouse Alexa Fluor 594® secondary antibody in blocking solution for 30 minutes. Cells were washed twice in PBS before incubation with 1 μg/mL DAPI for 15 minutes to stain the nuclei. Cells were then washed three times in PBS and kept at 4°C for analysis by high-content analysis microscopy (described in detail below).

Passage 2 and 8 MEFs from the population doubling experiment were seeded at a density of $8x10^3$ in 96-well plates in triplicate and allowed to adhere over-night. Whereas, passage 2 MEFs for the time course were seeded at a density of $3x10^3$ in 96-well plates in triplicate and allowed to adhere-overnight. Cells were pulsed for 8 hours with BrdU (50 μM) and processed as above.

2.25. Immunofluorescence with high content analysis.

Immunofluorescence (IF) and high content analysis (HCA) were performed as previously described (Acosta et al., 2013). Please refer to Table 4 for the list of antibodies and dilutions used in IF. For IF based HCA, cells were seeded in 96-well plates (Nunc – Thermo Fisher Scientific, USA), allowed to adhere overnight, treated with the indicated drugs on the following day and then fixed on the desired day of analysis. Medium was replaced every 2-4 days. Cells were fixed in 4% formaldehyde solution (v/v) for 1 hour, permeabilised with 0.2% Triton X-100 (v/v) for 15 minutes and blocked (0.5% BSA (w/v) and 0.2% fish skin gelatin (v/v) in PBS) for 1 hour at RT with gentle shaking. Cells were then incubated with primary antibody for 1 hour at RT, washed three times with PBS followed by incubation with the appropriate secondary antibody (Alexa Fluor 488® and/or 594® - 1:750 dilution) for 30 minutes at RT. Cells were then washed twice in PBS before incubation with 1 μg/mL DAPI for 15 minutes to stain the nuclei. Cells were then washed three times in PBS and kept at 4°C

For SASP (IL-8, IL-1β *etc*) and RPS6 staining, a modified approach was taken. Cells were permeabilised in 0.3% Triton X-100 and blocked in a solution containing 5% donkey serum, 0.3% Triton X-100 and 0.1% bovine serum albumin (BSA) for 1 hour. Cells were then incubated with primary antibody for 1.5 hours at RT followed by incubation with secondary antibody for 30 minutes at RT. Both primary and secondary antibodies were prepared in this blocking solution.

An automated-high-throughput microscope (InCell Analyzer 2000, GE Healthcare, UK) was used for image acquisition at either X200 or X400 (γ-H2AX only) magnification. The image

acquisition was set up to scan an appropriate number of fields so that at least 1000 cells/well were detected. The InCell Analyzer 2000 acquired up to 4 different wavelengths (DAPI, FITC – 488, Texas Red – 594 and PE-Cy5 – DDAOG). Experiments were performed in either duplicate or triplicate wells.

The InCell Investigator software (GE Healthcare, UK) was used for image processing and quantification. DAPI staining was used to segment the nuclei and for the identification of cells. A top hat segmentation was used to segment the nuclei (a minimum area of 120 μm^2). The cell area was defined by a collar segmentation approach that placed a border of 2 μm around the DAPI staining. Alternatively, cytoplasmic intensity was measured by a multiscale top-hat approach. The cellular expression of the analysed protein was determined by measuring the mean intensity of pixels in the reference channel (FITC 488 or Texas Red 594) within the specified nuclear or cytoplasmic region. A threshold filter defining the positively and negatively expressing cells for a certain protein or signal was set up by assigning a nuclear/cytoplasmic intensity value to each cell that correlates to the specific expression. Consequently, the software generates a percentage of the positive and negative cell populations per well by classifying each cell as either positive or negative for the expression of the analysed protein or signal (Figure 2.2). Alternatively, normalised intensity values for a given staining was obtained by subtracting the intensity of the background intensity (secondary antibody alone) to raw intensity values. Normalised intensity values were used to calculate fold changes to a specified condition (cells treated with 4OHT). Specificity of antibodies was first confirmed by robust controls (shRNAs/siRNAs, overexpression or drug inhibition). *Any image correction (brightness) was applied to the entire image and in the same manner to all images for a given experiment.*

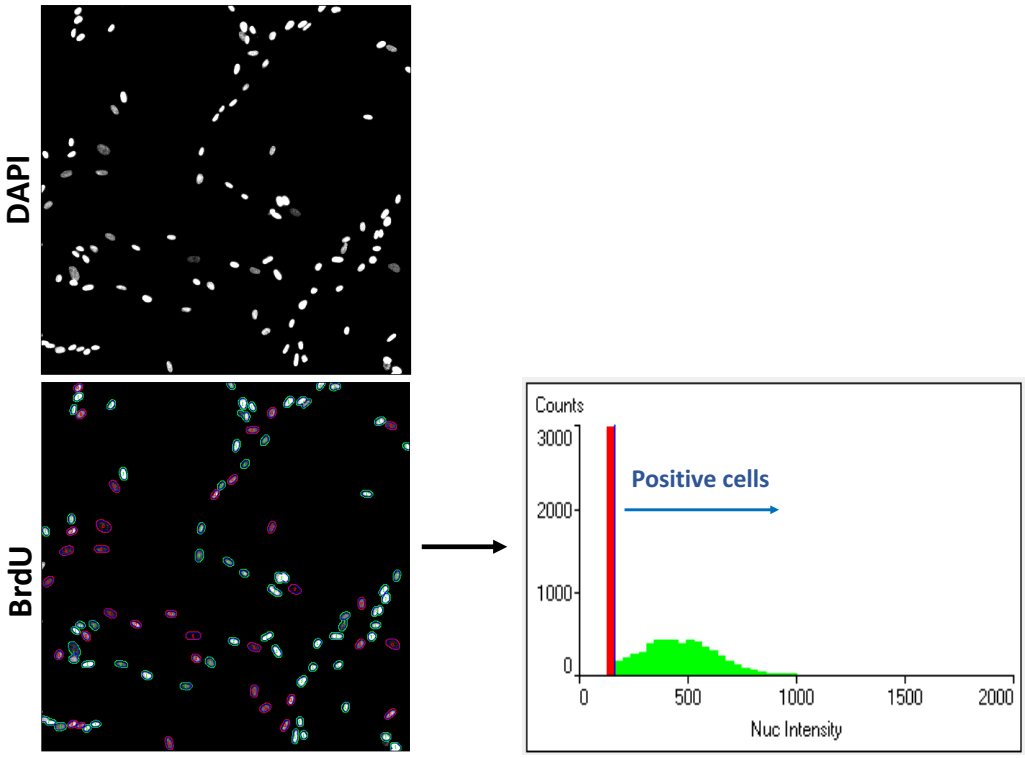

Figure 2.2. Representative high content analysis for BrdU staining.
Illustration depicts analysis of BrdU positive cells but the analysis can be altered depending on the type of staining pattern and whether it is a nuclear or cytoplasmic stain. Top image: DAPI staining was used to identify cells. Bottom image: BrdU positive and negative cells are shown in green and red, respectively. Bottom right: in this scenario, nuclear intensity levels were used to determine whether the cell has incorporated BrdU. A threshold filter in the histogram clearly shows two distinct populations for BrdU.

2.26. Immunohistochemistry.

Liver lobes were placed into 4% paraformaldehyde solution (Santa Cruz Biotechnology, USA) and fixed overnight at 4°C. On the following day, livers were washed briefly in PBS before transfer onto 70% ethanol and kept at 4°C prior to paraffin embedding. *Ms. Mahrokh Nohadani* then embedded livers in paraffin, cut 4 µm sections and carried out haematoxylin and eosin (H&E) staining. Images were acquired at X100 magnification using the Zeiss Axiophot inverted light microscope and the attached Canon DS126171 digital camera.

For Ki67 immunofluorescence staining, paraffin-embedded liver sections (4 µm) were first deparaffinised and rehydrated as follows: 2 rounds of Histoclear for 10 minutes each, 100% ethanol for 2 minutes, 75% ethanol for 2 minutes, 25% ethanol for 2 minutes and water for 5 minutes. Antigen retrieval was then performed to unravel crosslinked epitopes by boiling sections in a steamer for 20 minutes in 10 mM sodium citrate buffer (pH 6). 100 mM stock buffer was made by dissolving 29.4 grams of sodium citrate trisodium salt dihydrate (Sigma-Adlrich, USA) in 1 litre of distilled water with 5 mL of Tween-20 (Sigma-Aldrich, USA). The stock was then diluted to 10

mM in distilled water and pH adjusted to 6. Sections were allowed to cool for 20 minutes at RT following antigen retrieval. Sections were then permeabilised in 0.1% TBST (0.1% Triton-X 100 in TBS (v/v)), washed in TBS and then blocked for 10 minutes in Protein Block Serum-Free (Dako, USA) prior to overnight incubation in rabbit anti-Ki67 antibody (Abcam, UK) diluted in Antibody Diluent with Background Reducing Components (Dako, USA) at 4^{o}C in a humidified chamber. On the following day, sections were washed three times in TBS with gentle shaking and incubated with Alexa Fluor 594® secondary antibody (1:500 dilution) for 1 hour at RT. Sections were then washed three times in TBS and incubated in 1 μg/mL DAPI (Sigma-Aldrich, USA) for 15 minutes to stain the nuclei. Sections were washed three times in TBS and twice in water and mounted in Fluoromount-G aqueous mounting medium (Southern Biotech, USA). Image acquisition and analysis was done by high-content analysis microscopy (InCell Analyzer 2000). *Any image correction (brightness) was applied to the entire image and in the same manner to all images for a given experiment.*

2.27. Sirius red staining and quantification by circularly polarised light microscopy.

Paraffin-embedded liver sections (4 μm) were first deparaffinised and rehydrated as follows: 2 rounds of Histoclear for 5 minutes each, 2 rounds of 100% ethanol for 2 minutes each, 70% ethanol for 2 minutes, and water for 5 minutes. Sections were then incubated in Mayer's Haematoxylin (Sigma-Aldrich, USA) for 10 minutes at RT with gentle shaking. Sections were washed in slightly warm (alkaline) running tap water for 10 minutes and then stained with Picro Sirius Red Stain Kit (Abcam, UK) for 1 hour at RT with gentle shaking. Sections were washed three times in acidified water (0.5% acetic acid (v/v)) and dehydrated as follows: 70% ethanol for 2 minutes, 2 rounds of 100% ethanol for 2 minutes each and Histolcear for 2 minutes. Sections were then mounted in VectaMount (Vectorlabs, UK).

Images were acquired at X40 magnification using the Olympus IX70 inverted microscope with the circularly polarised light filter and the attached Canon DSLR 126291 camera. Images (original magnification X40) were stitched in ImageJ software to produce a complete liver section and the collagen (orange) was quantified as a percentage of total liver section area (pixels) using Image J software (Figure 2.3). Liver blood vessels for chow-fed mice were manually removed to avoid any bias in collagen staining**.** *Dr. Dirk Dormann in the MRC LMS Microscopy Facility wrote the script for fibrosis quantification for use in Image J software. Any image correction (brightness) was applied to the entire image and in the same manner to all images for a given experiment.*

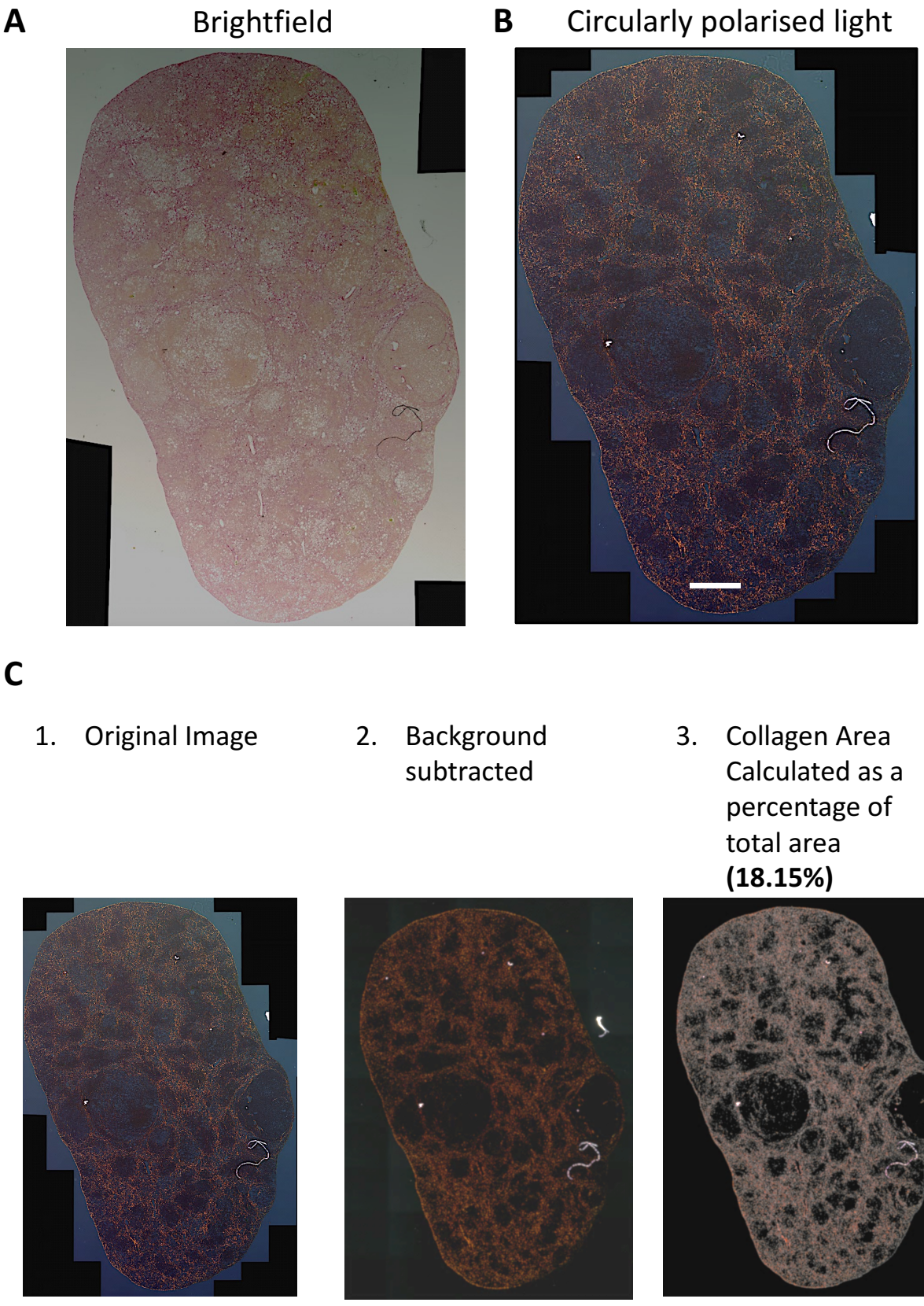

Figure 2.3. Quantification of collagen deposition by circularly polarised light microscopy. **A.** Bright field image of Picro Sirius Red for collagen fibres**. B.** Circularly polarised light image of Picro Sirius Red for collagen fibres. **C.** Images (original magnification X40) were stitched in ImageJ software to produce a complete liver section and the collagen (orange) was quantified as a percentage of total liver section area (pixels). Scale bar, 1 mm.

2.28. Western blot analysis.

The indicated cells were seeded in 6 cm dishes. Cells were washed twice in ice-cold PBS, and then scraped in RIPA lysis and extraction buffer (50 mM Tris pH8, 150 mM NaCl, 1% Triton-X 100, 0.5% Na-Doc, 0.1% SDS and 1 mM EDTA) containing cOmplete, Mini, EDTA-free protease and phosphatase inhibitors (Roche, Switzerland). Livers were snap frozen and stored at -80^{o}C. Snap frozen liver tissues were cut (30 mg for ageing study or 75-150 mg for HTF study) with a chilled scalpel on dry ice and then lysed and homogenised in a 1:8 ratio of tissue to RIPA buffer using the IKA® T10 basic ULTRA-TURRAX homogeniser (IKA, Germany). Lysates were incubated on ice for 10 minutes and then spun at *16,000 g* (4^{o}C) for 10 minutes. Supernatant was transferred to a fresh 1.5 mL Eppendorf tube (Germany). Protein concentration was then measured using the BioRad *DC*® Protein Assay (BioRad, UK) at an absorbance of 595 nm according to manufacturer's protocol. Protein concentrations were estimated by extrapolation from a BSA standard curve (0, 0.25, 0.5, 1, 2 and 4 µg/µL) prepared in the RIPA lysis buffer. Protein samples (15-30 µg – equal amount for all samples) were then denatured in 5X Laemmli sample buffer for 10 minutes at 94^{o}C. The composition for 10 mL of 5X Laemmli buffer: 875 µL from 1M Tris-HCL pH 6.8, 4.5 mL Glycerol, 2.5 mL of 20% SDS, 1.25 mL β-mercaptoethanol, 1 mL of 0.25% Bromophenol Blue and distilled water.

Samples were then loaded into a 4-15% Mini-PROTEAN TGX Precast Gel (BioRad, UK). Electrophoresis was conducted at 140V for 1 hour until clear band separation was achieved with the Precision Plus Protein Ladder (BioRad, UK) in Tris-Glycine Running buffer (25 mM Tris, 192 mM Glycine, 0.1% SDS (v/v)). Electrotransfer of protein samples onto a 0.2 µm nitrocellulose membrane (BioRad, UK) was conducted at 100V for 1 hour in Transfer buffer (25 mM Tris, 192 mM Glycine 20% (v/v) methanol). Ponceau S (Sigma-Aldrich, USA) was used to visualise efficient transfer of proteins onto membrane. The membrane was then blocked in 5% skimmed milk (w/v) (Sigma-Aldrich, USA) made in PBS-T (0.1% Tween-20 (v/v), Sigma-Aldrich) for 1 hour at RT with gentle agitation. The membrane was incubated overnight in primary antibody diluted in either 5% skimmed milk (w/v) or 5% BSA (w/v) (Sigma-Aldrich, USA) in PBS-T at 4^{o}C with gentle shaking. Please refer to Table 4 for the list of antibodies and dilutions used. The following day, the membrane was washed in PBS-T and incubated in secondary antibody conjugated to horseradish-peroxidase (1:5000 dilution) for 1 hour at RT. The membrane was washed in PBS-T and then covered in Amersham™ Enhanced Chemiluminescence Reagent (ECL) Western Blotting Detection Reagent (GE Healthcare, USA) and developed by exposure to a high performance chemiluminescence Hyperfilm™ (GE Healthcare, USA).

2.29. Statistical analysis.

Results are given as either mean ± standard error of mean (SEM) or as mean ± standard deviation (SD). SEM was used primarily for *in vivo* experiments to assess how well the sample mean represents the population mean. SD was used primarily for *in vitro* experiments to determine the deviation of individual values to the mean. Statistical analysis for comparison of two groups was done using unpaired student's t-test. Comparison of three or more groups with one variable was done using one-way analysis of variance (one-way ANOVA) with Tukey's multiple comparison test. Comparison of four groups with two variables (*e.g.,* age and genotype) was done using two-way analysis of variance (two-way ANOVA) with Tukey's multiple comparison test. Repeated-measures two-way ANOVA with Sidak's multiple comparison test was done for experiments with multiple time points - glucose and insulin tolerance tests as well as for the cumulative population doublings. Linear regression was performed for correlation. All statistical analysis was done in Graph Pad Prism 6 unless stated otherwise. A p-value of < 0.05 was considered statistically significant. * $P < 0.05$, ** $P < 0.01$, *** $P < 0.001$.

Chapter 3: S6K1 regulates age-related inflammation in the liver.

3.1. Introduction.

S6K1$^{-/-}$ mice, in particular females, are long-lived and resistant to a variety of age-related pathologies, yet the exact mechanisms for this lifespan extension are unclear. It is very likely that many processes contribute to this improvement in healthspan, and in fact a compensatory increase in AMPK activity and lack of EPRS phosphorylation may mediate some of these benefits in *S6K1*$^{-/-}$ mice (Arif et al., 2017; Selman et al., 2009). Since cellular senescence is a hallmark of ageing, we were interested in understanding whether a decelerated senescence response contributes to this improved healthspan (López-Otín et al., 2013). mTOR signalling plays an important role in cellular senescence, and we and others have recently shown that the mTOR-4EBP1 axis regulates the senescence secretome (SASP) (Herranz et al., 2015; Laberge et al., 2015). Nevertheless, it is unknown whether the mTOR-S6K1 axis regulates cellular senescence during mammalian ageing and whether this plays a role in healthspan. Therefore, the primary aim of this project was to understand whether *S6K1*$^{-/-}$ mice have a reduced senescence and SASP response during ageing.

3.2. Characterisation of global S6*K1*$^{-/-}$ mice.

To investigate whether aged *S6K1*$^{-/-}$ mice have a reduced senescence response during ageing, we examined aged cohorts of WT and *S6K1*$^{-/-}$ female mice (600 days old) and their younger counterparts (90 days old) for comparison (Figure 3.1). Female mice were chosen for this study because it was previously shown that female *S6K1*$^{-/-}$ mice display a more pronounced improvement in lifespan and healthspan compared to their male counterparts (Selman et al., 2009). In addition, 600 days was chosen as the endpoint because we were interested in studying healthy ageing*, i.e.,* the mechanisms that drive the ageing process before the onset of dominant pathologies (*e.g.,* cancer). Leaving the mice to age for longer will result in both unexpected deaths and increased incidences of age-related pathologies such as cancer, cataracts, dermatitis and rectal prolapses.

S6K1 deletion was confirmed by genotyping and immunoblotting (Figure 3.2 A and B). As previously described, *S6K1*$^{-/-}$ mice showed a significant reduction in their body weight gain, and this was more pronounced with increasing age (Figure 3.3 A and B). Importantly, this was not merely due to their dwarf nature but a specific effect on age-related fat gain because there was a significant reduction in perigonadal white adipose tissue (PWAT – also called epididymal fat) mass even once correcting for their body weight (Figure 3.3 C and D). On the contrary, although *S6K1*$^{-/-}$ mice showed a significant reduction in the absolute liver weight, the % weight was even greater when correcting for their body weight (Figure 3.3 E and F). As reported before, there was no

difference in fasted glucose levels (Figure 3.3 G). *S6K1*$^{-/-}$ mice also showed a visible reduction in age-related hepatic lipid accumulation in the liver, which is termed steatosis (Figure 3.3 H).

To better understand the health of the aged mice, biochemical analysis of key blood parameters was performed using the VetScan VS2 comprehensive diagnostic profile for geriatric and wellness testing (Figure 3.4). Except for a few parameters, no drastic alterations were observed between young and old WT mice. Plasma albumin, which is a marker of liver and kidney health, significantly declined with age, and there was a trend towards improvement in *S6K1*$^{-/-}$ mice although this was not statistically significant. (Figure 3.4 A). Plasma amylase, which is a marker of pancreatic damage and inflammation, significantly increased with age and was lower in *S6K1*$^{-/-}$ mice (Figure 3.4 B). Various kidney damage markers such as blood urea nitrogen, creatinine and potassium levels were mildly affected by age, but there was not a significant effect of deleting S6K1 on these parameters. This suggests that more severe disease states must be present to observe noticeable differences between age and genotype or that more detailed examination of histology and other functional tests must be used to delineate any differences at this age (600 days).

In summary, the phenotype of *S6K1*$^{-/-}$ mice showed several age-related improvements and resembled what has been described previously (Selman et al., 2009).

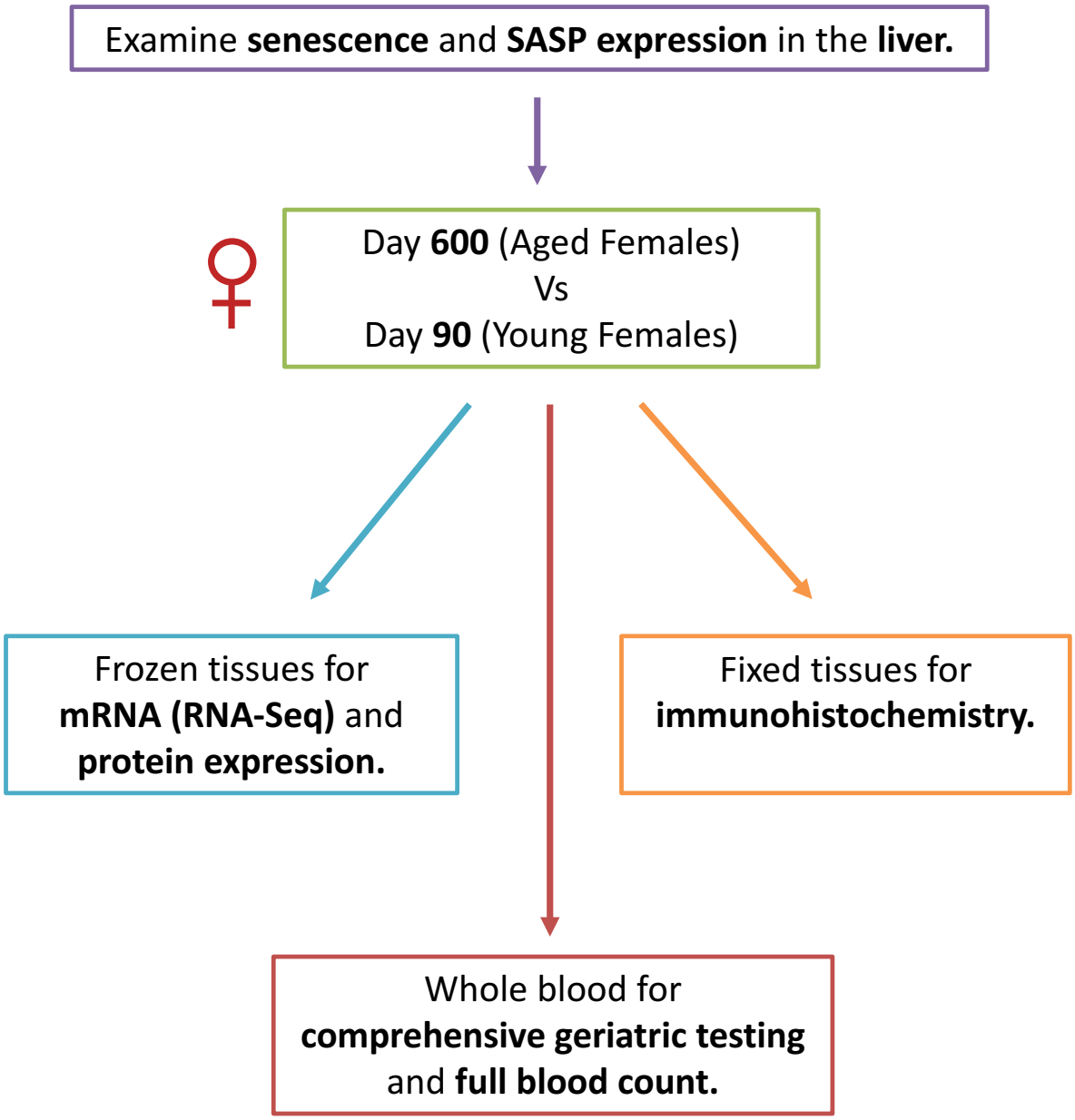

Figure 3.1. Schematic depicting the workflow for the ageing cohort.
90-day and 600-day-old female S6K1 wild type and knockout mice were dissected and assessed for various parameters including mRNA expression, immunohistochemistry and whole blood analyses. SASP: senescence-associated secretory phenotype. RNA-Seq: RNA-sequencing.

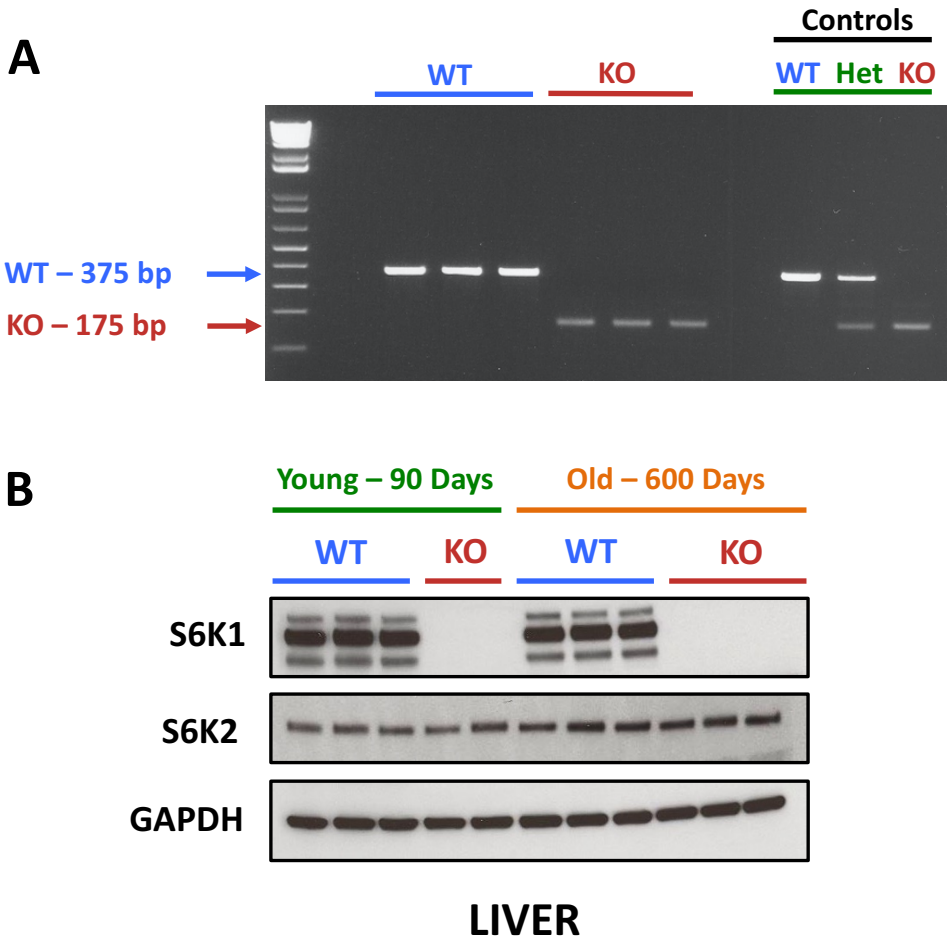

Figure 3.2. Confirmation of S6K1 deletion.
A. Representative PCR analysis from a tail tip for the S6K1 wild type (top band) and S6K1 deletion (bottom band) in *S6K1*$^{-/-}$ mice. **B.** Representative immunoblot analysis of S6K1, S6K2 and GAPDH protein expression in whole liver lysates of young (90 days) and old (600 days) S6K1 wild type and knockout mice.

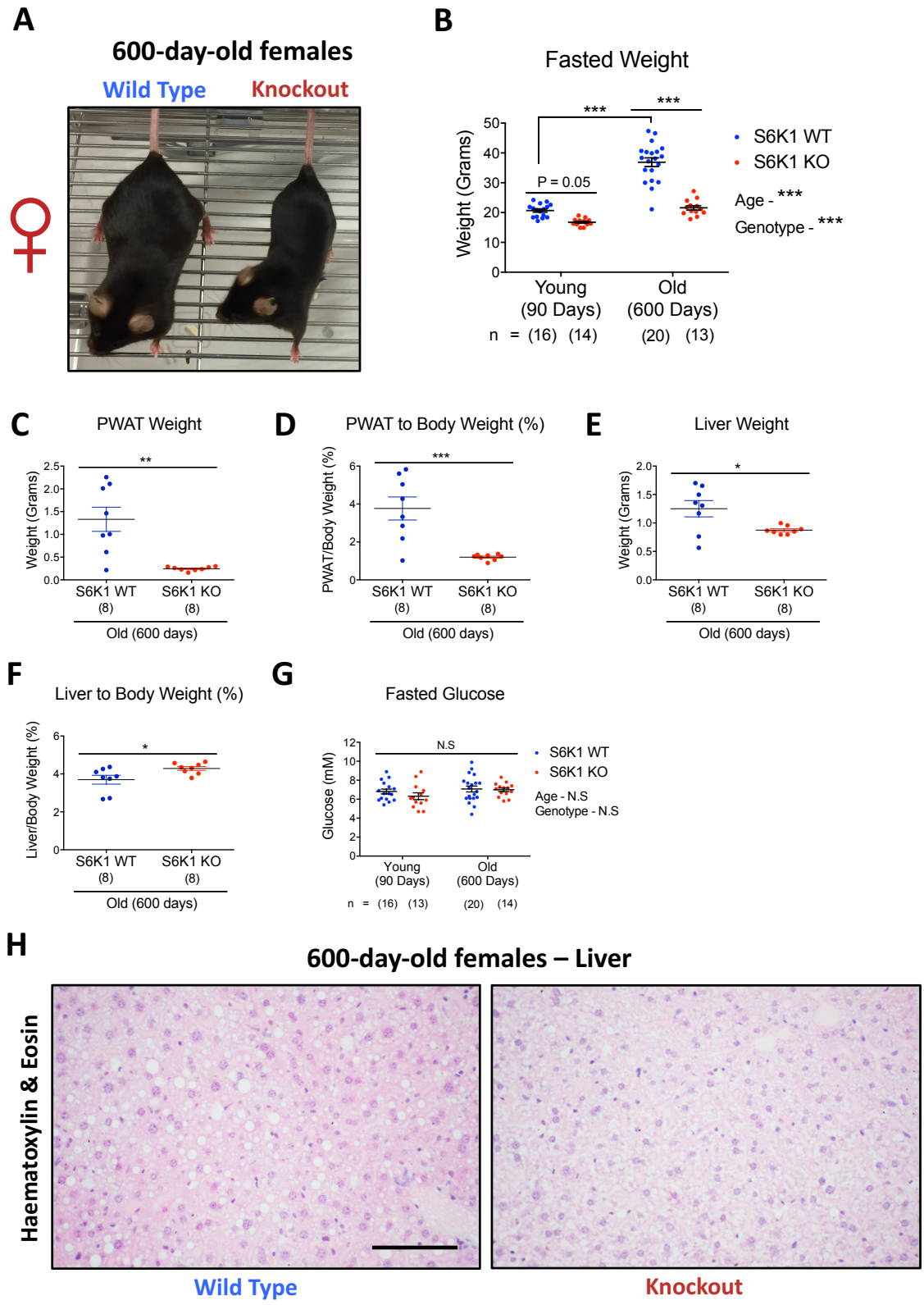

Figure 3.3. Characterisation of *S6K1*$^{-/-}$ mice.
A. Representative photograph of 600-day-old wild type (left) and *S6K1*$^{-/-}$ (right) female mice. **B.** Fasted body weight (grams) in 90-day and 600-day-old wild type and *S6K1*$^{-/-}$ female mice. **C.** Perigonadal white adipose tissue (PWAT) weight (grams). **D.** PWAT weight corrected for the body weight as a %. **E.** Liver weight (grams). **F.** Liver weight corrected for the body weight as a %. **G.** Fasted blood glucose levels (mM) in 90-day and 600-day-old wild type and *S6K1*$^{-/-}$ female mice. **H.** Representative microphotographs of haematoxylin and eosin staining of the liver. Data are expressed as means ± SEM and number of mice used is indicated directly on all graphs. Statistical significance was calculated using two-way analysis of variance with Tukey's multiple comparison test (B and G) or using unpaired student's t-test (C-F) (* P < 0.05, ** P < 0.01, *** P < 0.001). N.S: non-significant. Scale bar, 100 µm.

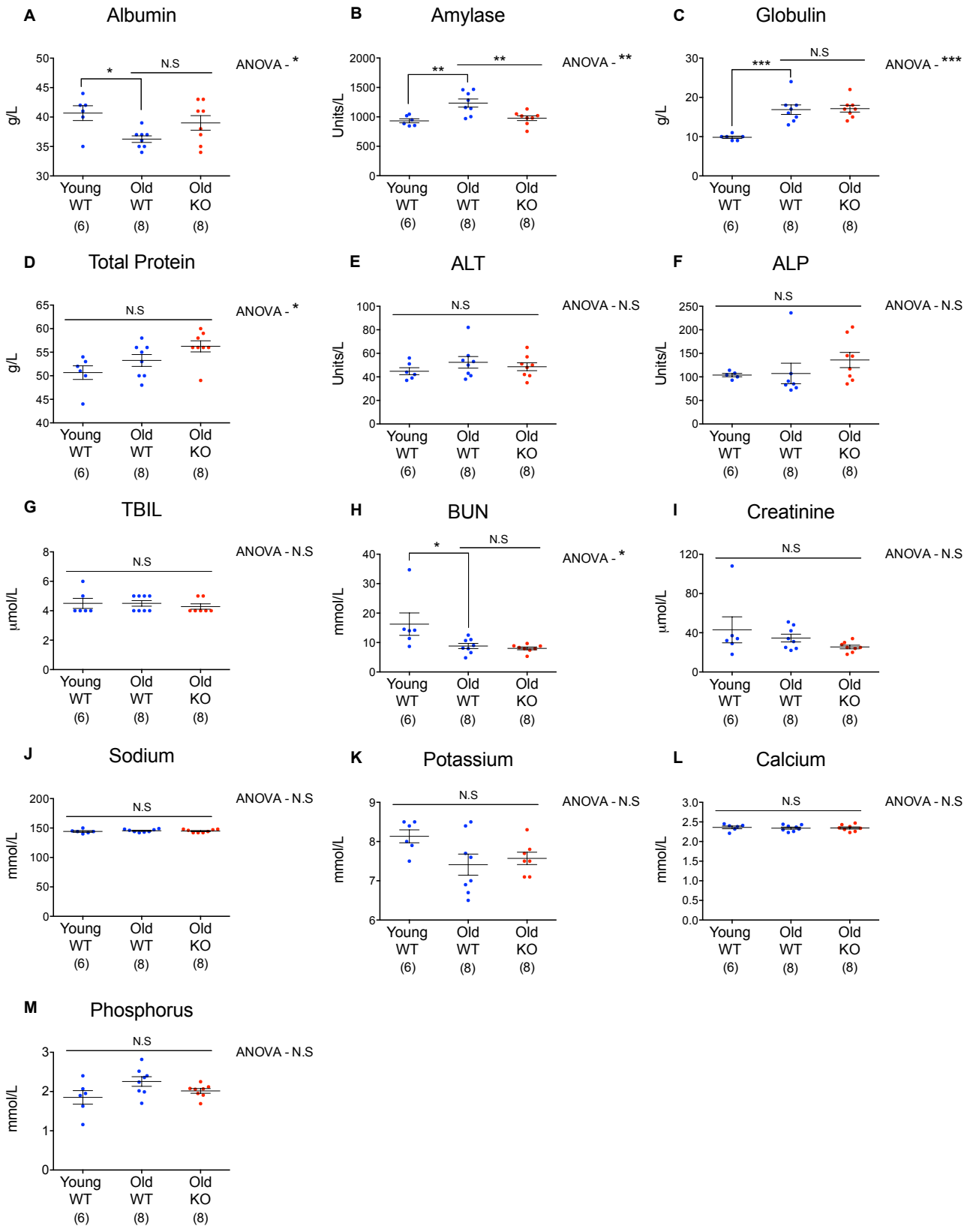

Figure 3.4. Analysis of various blood parameters of *S6K1*$^{-/-}$ *mice.*
Whole blood was used to analyse the concentration of various blood parameters. **A.** Albumin (g/L). **B.** Amylase (Units/L). **C.** Globulin (g/L). **D.** Total protein (g/L). **E.** Alanine aminotransferase (Units/L). **F.** Alkaline phosphatase (Units/L). **G.** Total bilirubin (µmol/L). **H.** Blood urea nitrogen (mmol/L). **I.** Creatinine (µmol/L). **J.** Sodium (mmol/L). **K.** Potassium (mmol/L). **L.** Calcium (mmol/L). **M.** Phosphorus (mmol/L). Data are expressed as means ± SEM and number of mice used is indicated directly on all graphs. Statistical significance was calculated using one-way analysis of variance with Tukey's multiple comparison test (* $P < 0.05$, ** $P < 0.01$, *** $P < 0.001$). N.S: non-significant.

3.3. S6K1 deletion does not prevent senescence in the ageing liver.

Following metabolic characterisation of *S6K1*$^{-/-}$ mice, we then looked at age-related senescence. We specifically looked at the aged liver because not only is the liver a key metabolic organ, but senescence has been implicated in liver pathology including fatty liver disease, liver fibrosis and acting as a safeguard against hepatocellular carcinoma (Kang et al., 2011; Krizhanovsky et al., 2008; Ogrodnik et al., 2017). Importantly, both hepatocytes and hepatic stellate cells can undergo cellular senescence. As expected, an increase in mRNA expression for several markers of senescence (*p16*^{Ink4a} and *p19*^{Arf}) was observed in WT old mice compared to WT young mice (Figure. 3.5 A). The mRNA expression of these senescence markers, however, did not significantly alter in *S6K1*$^{-/-}$ mice, suggesting that deletion of S6K1 does not prevent senescence in the aged liver (Figure 3.5 A). In addition, there was a visible increase in senescence-associated beta galactosidase (SA-β-Gal) positive areas in the liver of WT old mice compared to WT young mice, and this was even more apparent in mice that were of ill-health (dermatitis) (Figure 3.5 B and C). A statistically significant increase in SA-β-Gal in WT old mice compared to WT young mice was not observed by quantification, but this is likely due to the technical difficultly in detecting senescent cells in tissues. Surprisingly, old *S6K1*$^{-/-}$ mice did show a significant increase in SA-β-Gal in the liver compared to WT old mice, suggesting an accumulation of senescent cells or an exacerbated senescence response in *S6K1*$^{-/-}$ mice (Figure 3.5 C). We then examined whether S6K1 might be affecting the senescence secretome (SASP) and/or age-related inflammation, as both are also thought to contribute to age-related pathology.

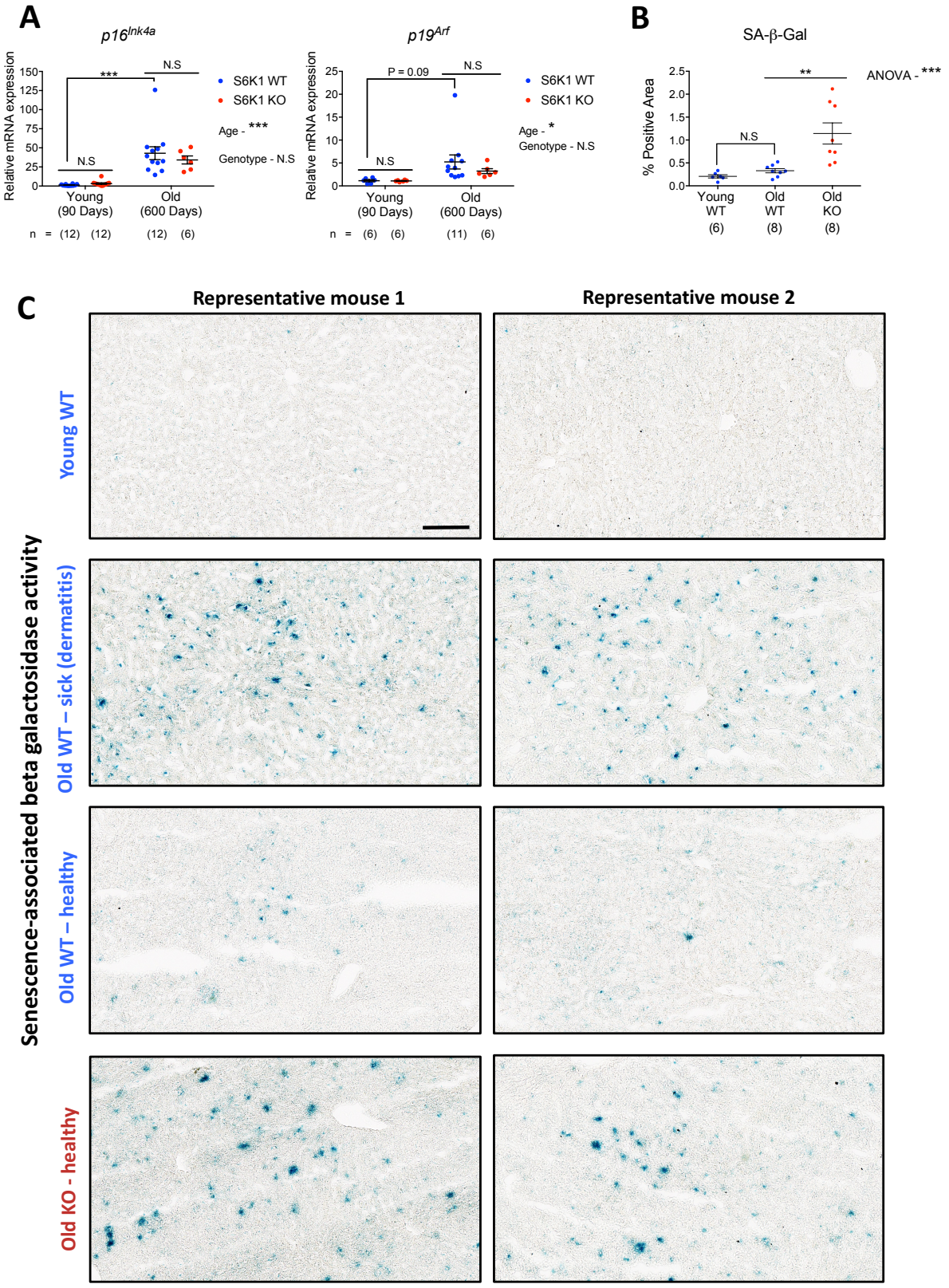

Figure 3.5. S6K1 deletion does not prevent senescence in the ageing liver.
A. Relative mRNA expression of *p16*^{Ink4a} and *p19*^{Arf}, respectively, assessed by RT-qPCR from whole liver lysates of young (90 days) and old (600 days) wild type and *S6K1*$^{-/-}$ mice. mRNA expression was normalized to *Rps14* housekeeping gene. **B.** Percentage positive area for senescence-associated beta galactosidase (SA-βGal) staining of the liver. **C.** Representative microphotographs of senescence-associated beta galactosidase staining of the liver of young (90 days) and old (600 days) wild type and *S6K1*$^{-/-}$ mice. Data are expressed as means ± SEM and number of mice used is indicated directly on all graphs. Statistical significance was calculated using two-way analysis of variance with Tukey's multiple comparison test (* $P < 0.05$, ** $P < 0.01$, *** $P < 0.001$). N.S: non-significant. Scale bar, 100 μm.

3.4. RNA sequencing analysis of wild type and *S6K1*$^{-/-}$ mice.

We then aimed to investigate the effects of S6K1 deletion on age-related SASP expression in the liver. The SASP in mammalian ageing, however, has not been fully characterised. Others have shown that the mRNA expression of certain SASP factors such as *Il6, Il1a* and *Tnfa* increases with age and decreases upon senescence elimination in the kidney or adipose tissue, but this has not been systematically carried out (Baar et al., 2017; Baker et al., 2016). Therefore, to do this in an unbiased manner, we performed global gene expression analysis of the liver (all cell types) in young and old mice for both the genotypes (Figure 3.6 A). *The MRC LMS Core Facility prepared and sequenced the cDNA library. The bioinformatics analysis was carried out primarily by Mr. Gopuraja Dharmalingam.* A total of 3098 genes were differentially expressed (adjusted $P < 0.05$) in old WT mice compared to young WT mice and 328 genes were significantly altered (adjusted $P < 0.05$) in old KO mice compared to old WT mice. In line with this, principal component analysis showed that the largest difference among the groups was caused by age (47.04% of the variation) followed by genotype (23.74% of the variation) (Figure 3.6 B and C). Unbiased hierarchical clustering analyses separated the young and old mice into two distinct groups (Figure 3.6 D).

We then compared SASP signature from IMR-90 foetal lung fibroblasts undergoing HRAS^{G12V}-induced senescence to the differentially expressed genes in old WT mice compared to young WT mice (Figure 3.7 A). Although the SASP signature was significantly enriched by gene-set enrichment analysis (GSEA) in the ageing liver of old WT mice, only 39/94 (41%) of the factors contributed to the core enrichment, suggesting that the SASP in the ageing liver is likely to be different. Furthermore, this analysis was performed from whole liver lysates, thus many different cell types including Kupffer cells will likely contribute to this signature. There were still some conserved SASP factors such as various interleukins and chemokines that contributed to the core enrichment. Therefore, we looked at some of these factors by RT-qPCR. As expected, expression of several secreted factors such as *Il1b* increased with age, and this induction was significantly blunted in old *S6K1*$^{-/-}$ mice (Figure 3.7 B). Nevertheless, we wanted to define what the SASP in ageing is and to understand whether S6K1 regulates it.

To define the SASP in the ageing liver, we first filtered the gene expression data for secreted factors and then considered the differentially expressed genes with a log2 fold change (Log_2FC) of greater than 0.75 in WT old mice compared to young mice, which was classified as the secreted factors that increase with age. We then compared this list to the differentially expressed genes between the two genotypes of old mice (Figure 3.8 A). Surprisingly, many of the highly expressed secreted factors in ageing were also downregulated in *S6K1*$^{-/-}$ mice (Figure 3.8 B). Conversely, others have reported through heterochronic parabiosis experiments that young blood contains secreted factors deemed to be beneficial for health and that these factors decline with age (Conboy et al., 2005; Loffredo et al., 2013; Villeda et al., 2011). Therefore, we next sought to

examine whether S6K1 deletion reverses this change. Nevertheless, *S6K1*$^{-/-}$ mice did not affect the expression of secreted factors that decreased with age (Figure 3.9). It is important to mention, however, that some believe it is not necessarily that young blood is beneficial but rather old blood is detrimental; although it is likely a combination of both (Rebo et al., 2016).

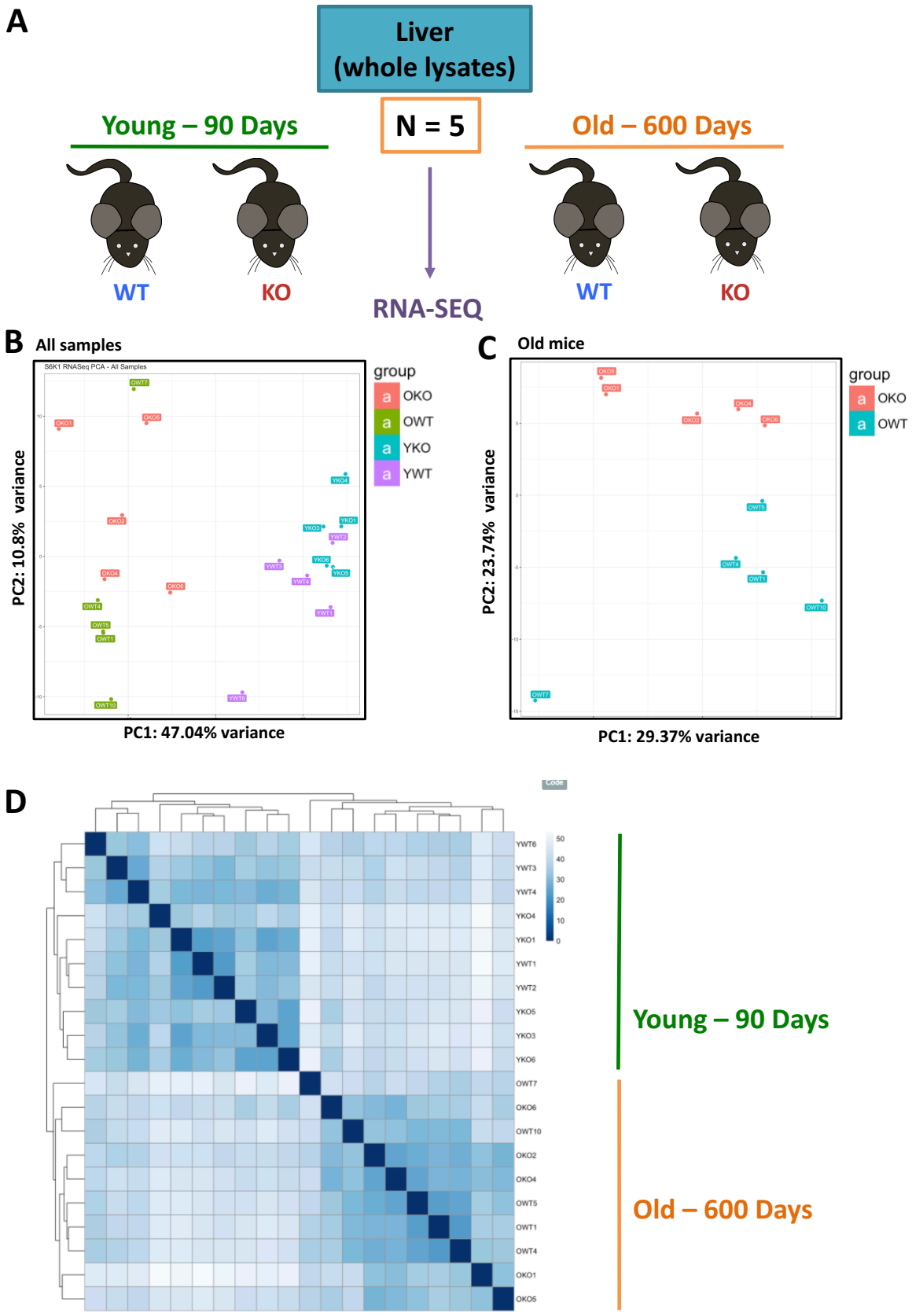

Figure 3.6. RNA-sequencing of the liver from young and old mice.
A. Schematic illustrating the workflow for the RNA sequencing. **B.** Principal component analysis of the top 1000 most variable genes between 90 and 600-day-old female S6K1 wild type and knockout mice. **C.** Principal component analysis of the top 1000 most variable genes between 600-day-old female S6K1 wild type and knockout mice. **D.** Clustering analysis by gene expression between 90 and 600-day-old female S6K1 wild type and knockout mice. 5 mice per genotype with a total of 20 mice were used for the RNA sequencing and analysis.

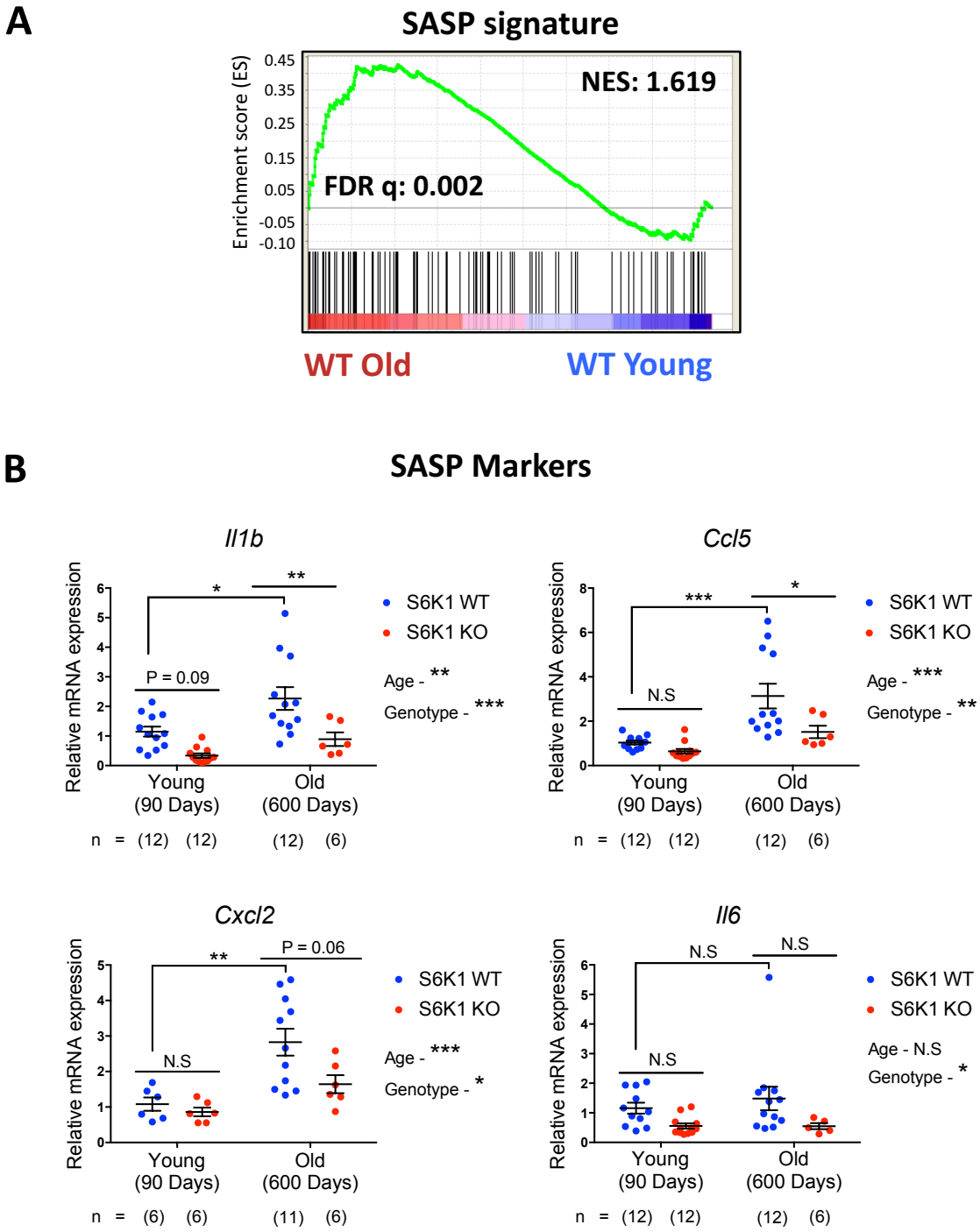

Figure 3.7. *S6K1*$^{-/-}$ mice show an attenuation in SASP induction in the liver.
A. The SASP signature from IMR-90 foetal lung fibroblasts undergoing HRAS^{G12V}-induced senescence was compared with the differentially expressed genes obtained by RNA sequencing of whole liver lysates between WT old (600 days) mice compared to WT young (90 days) mice. **B.** Relative mRNA expression of *Il1b, Ccl5, Cxcl2* and *Il6* assessed by RT-qPCR of young (90 days) and old (600 days) wild type and *S6K1*$^{-/-}$ mice. mRNA expression was normalized to *Rps14* housekeeping gene. Data are expressed as means ± SEM and number of mice used is indicated directly on all graphs. Statistical significance was calculated using two-way analysis of variance with Tukey's multiple comparison test (* P < 0.05, ** P < 0.01, *** P < 0.001). N.S: non-significant. SASP: senescence-associated secretory phenotype. NES: normalised enrichment score. FDR: false discovery rate.

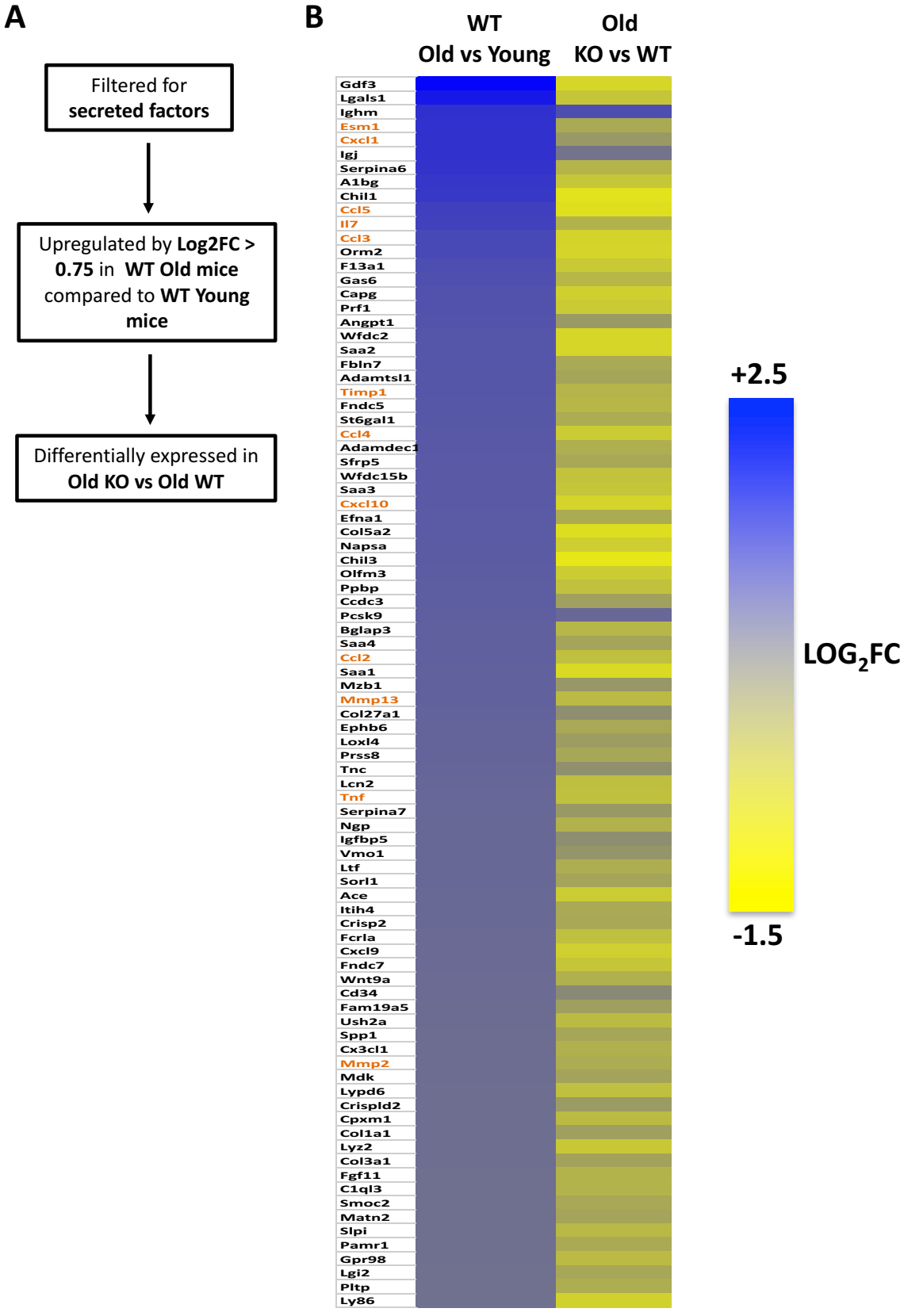

Figure 3.8. *S6K1*$^{-/-}$ mice display lower expression of age-related secreted factors.
A. Schematic illustrating the workflow for identifying secreted factors that increase at an mRNA level during ageing in the liver. **B.** Heatmap illustrating the secreted factors that differ by age and genotype. Gene expression data obtained by RNA sequencing was first filtered for secreted factors. The genes that increased by at least a log2 fold change (Log2FC) of greater than 0.75 in WT old mice compared to WT young mice was classified as the secreted factors that increase with age. This list was then compared to the differentially expressed genes between the two genotypes of old mice. Known SASP factors are labelled in orange.

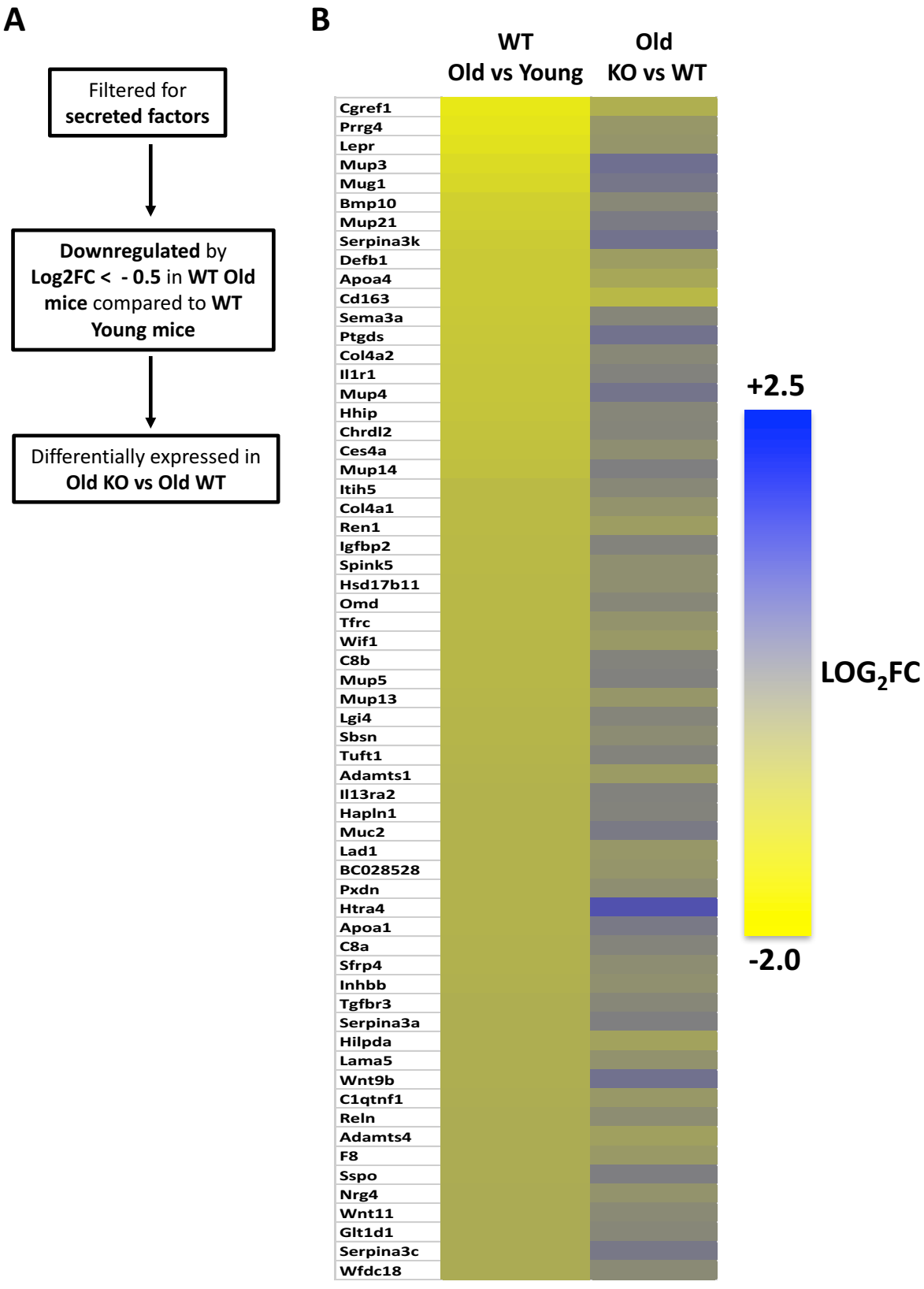

Figure 3.9. S6K1 deletion does not affect expression of secreted factors that decreased with age.
A. Schematic illustrating the workflow for identifying secreted factors that decrease at an mRNA level during ageing in the liver. **B.** Heatmap illustrating the secreted factors that differ by age and genotype. Gene expression data obtained by RNA sequencing was first filtered for secreted factors. The genes that decreased by at least a log2 fold change (Log2FC) of less than 0.5 in WT old mice compared to WT young mice was classified as the secreted factors that decrease with age. This list was then compared to the differentially expressed genes between the two genotypes of old mice.

3.5. *S6K1*$^{-/-}$ mice show an attenuation in inflammation and immune cell markers in the ageing liver.

It is believed that chronic, low-grade inflammation in the absence of any noticeable infection, termed sterile inflammation or inflammaging, is associated with many pathologies. The SASP is thought to contribute to this phenotype. In line with this, GSEA revealed that multiple inflammatory pathways including chemokine signalling, immune and defense response were significantly enriched in old WT mice compared to young WT mice (Figure 3.10 A). More importantly, these pathways were significantly downregulated in old *S6K1*$^{-/-}$ mice compared to old WT mice (Figure 3.10 A). We then aimed to understand whether S6K1 regulates inflammatory factors that increases with age. Interestingly, 82% of the factors (chemokine signalling) that were downregulated in *S6K1*$^{-/-}$ mice also increased during ageing, suggesting S6K1 regulates age-related inflammation in the liver (Figure 3.10 B). In addition, other pathways known to regulate inflammation including TNF signalling via NFκB, toll-like receptor (TLR) and caspase-1 signalling as well as inflammatory response to lipopolysaccharide (LPS) were significantly enriched with age and downregulated in *S6K1*$^{-/-}$ mice (Figure 3.11 A). Although it is likely that S6K1 regulates many of these inflammatory pathways indirectly and that there might be overlap between different signatures, it is, however, clear that *S6K1*$^{-/-}$ mice show a reduction in inflammatory pathways in the ageing liver.

The SASP plays an important role in the recruitment of immune cells, which may contribute to age-related inflammation in the liver (Figure 3.12 A). As expected, there was an increase in mRNA expression of the macrophage marker *Cd68* in WT old mice compared to WT young mice, and this induction was prevented in old *S6K1*$^{-/-}$ mice (Figure 3.12 B). A similar trend was also observed for transcripts that could be used as surrogate markers for T-cells *(Cd3e),* B-cells *(Ptprc)* and neutrophils *(Klrd1)* (Figure 3.12 B). Overall, *S6K1*$^{-/-}$ mice showed an attenuation in age-related inflammation and immune infiltration in the liver.

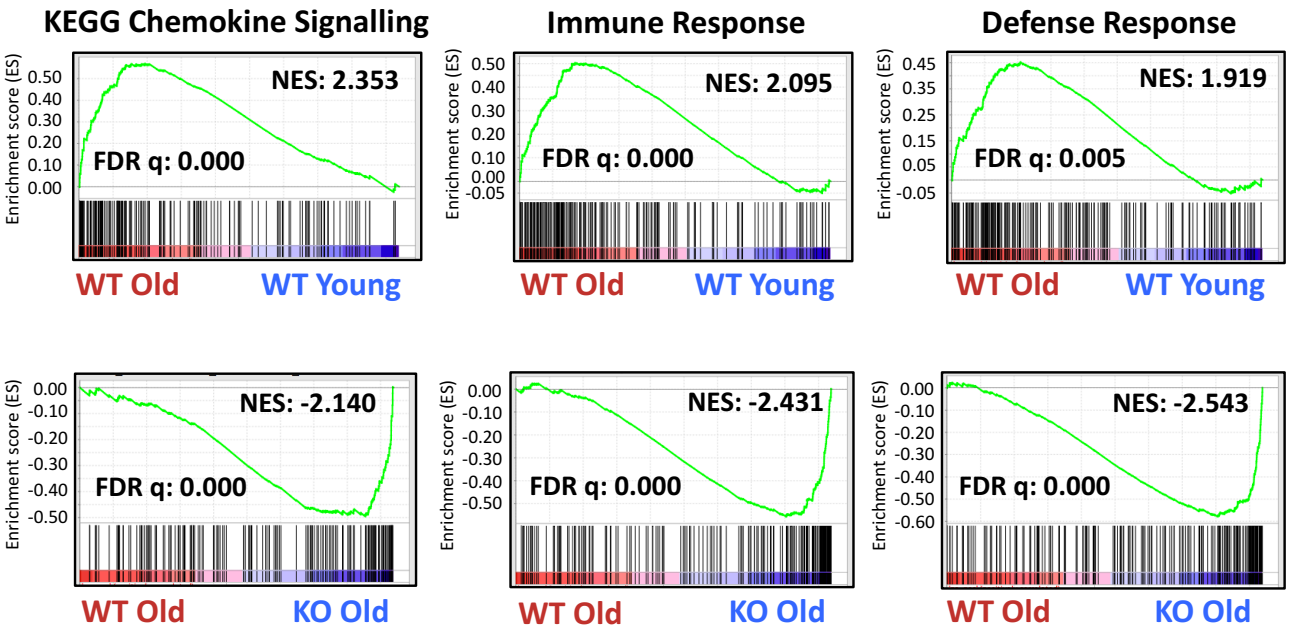

B

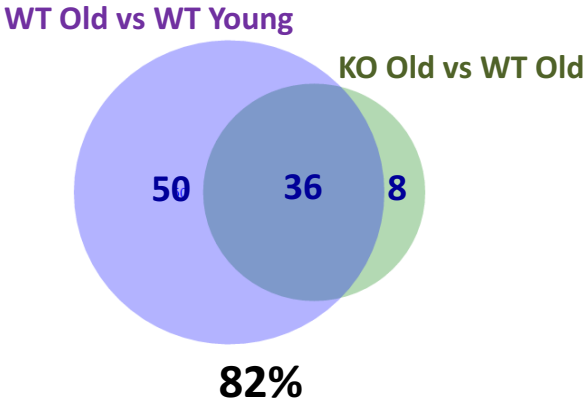

Figure 3.10. S6K1 regulates age-related inflammation in the liver.
A. Gene-set enrichment analysis (GSEA) depicting the indicated inflammatory signatures that increase with age and decline in the liver of *S6K1*$^{-/-}$ mice. **B.** A Venn diagram displaying the overlapping genes that significantly contributed to the core enrichment for the chemokine signalling gene set in WT old vs young mice and old KO vs WT mice. NES: normalised enrichment score. FDR: false discovery rate.

A

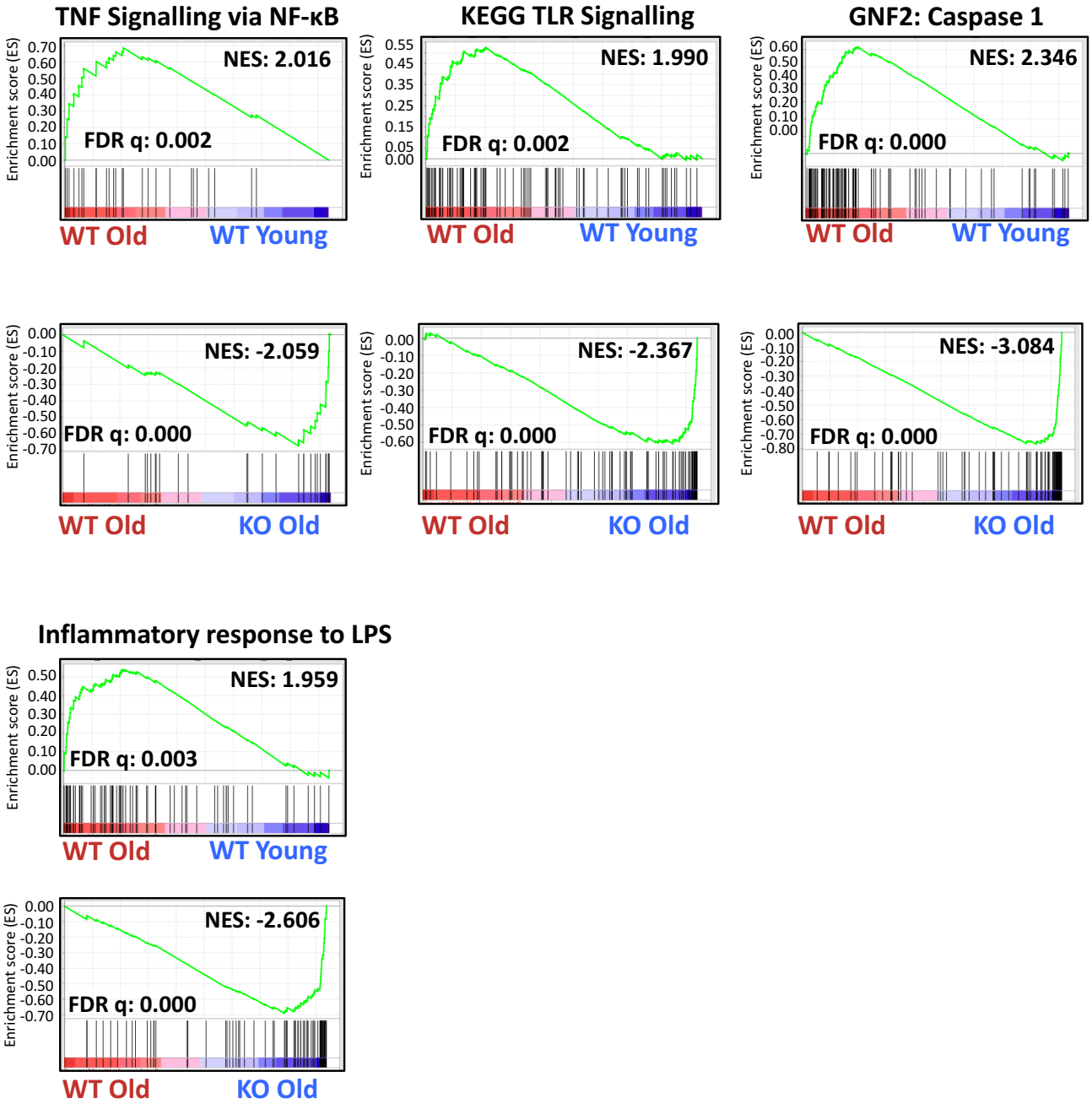

Figure 3.11. S6K1 regulates multiple inflammatory pathways during ageing.
A. Gene-set enrichment analysis (GSEA) depicting the indicated inflammatory signatures that increase with age and decline in the *S6K1*$^{-/-}$ mice. NES: normalised enrichment score. FDR: false discovery rate.

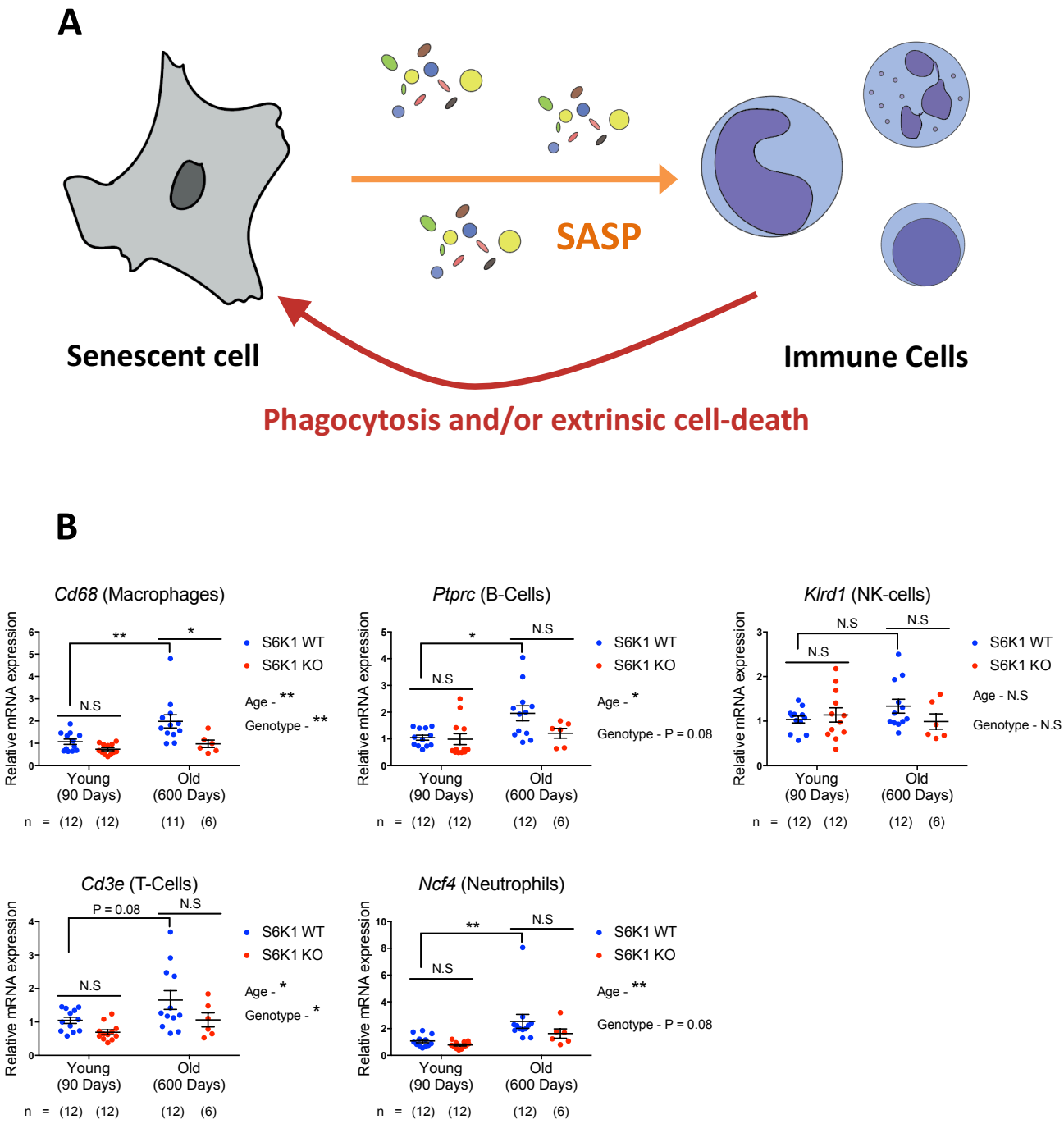

Figure 3.12. Age-related immune cell infiltration.
A. Schematic showing senescent cells recruiting the immune system via the senescence secretome. **B.** Relative mRNA expression of *Cd68, Ptprc, Klrd1, Cd3e* and *Ncf4* assessed by RT-qPCR of young (90 days) and old (600 days) wild type and *S6K1*$^{-/-}$ mice. mRNA expression was normalized to *Rps14* housekeeping gene. Data are expressed as means ± SEM and number of mice used is indicated directly on all graphs. Statistical significance was calculated using two-way analysis of variance with Tukey's multiple comparison test (* $P < 0.05$, ** $P < 0.01$, *** $P < 0.001$). N.S: non-significant.

3.6. *S6K1*$^{-/-}$ mice do not display decreased numbers of immune cells in the blood.

The reduced immune infiltration in *S6K1*$^{-/-}$ mice could be due to a systemic effect on immune cells such as a defect in the development and activation of macrophages or *S6K1*$^{-/-}$ mice may have a reduced senescence secretome and as a result less recruitment of immune cells into the liver (Figure 3.13). To answer the former, we performed a full blood count in young and old mice. We observed a reduction in the total white blood cell count, particularly in lymphocytes, in WT old mice compared to WT young mice, but there was not a significant difference in the absolute number of white blood cells or lymphocytes between old WT and *S6K1*$^{-/-}$ mice (Figure 3.14). When looking at the composition (% of a particular immune cell in the peripheral blood) of the blood, there was a shift in the ratio of neutrophils to lymphocytes with age and this was exacerbated in old *S6K1*$^{-/-}$ mice (Figure 3.15). Overall, there was a reduction in the number of blood lymphocytes relative to other immune cells in old *S6K1*$^{-/-}$ mice, but this may reflect an increase in functionality because it was previously reported that aged *S6K1*$^{-/-}$ mice have an improved ratio of both CD4 and CD8 naïve to memory T-cells (Selman et al., 2009). This suggests that old *S6K1*$^{-/-}$ mice require less peripheral lymphocytes to carry out their functions. It has also been reported that there is an age-related skewing towards the myeloid lineage (neutrophils and monocytes) and the data suggest that this also occurs in our cohort and this phenomenon is slightly exacerbated in *S6K1*$^{-/-}$ mice (Geiger et al., 2013).

Next, we isolated bone marrow-derived macrophages (BMDMs) from young mice of the two genotypes and examined their activation ability. Similar to what has been reported before with *S6K1* knockdown in the macrophage cell line THP-1 (Kim et al., 2014), BMDMs from 10-week old *S6K1*$^{-/-}$ mice showed a trend towards a more inflammatory phenotype in response to 6 hours of lipopolysaccharide (LPS) treatment with or without ATP (signals 1 and 2 to fully activate macrophages), thus indicating that *S6K1*$^{-/-}$ mice do not have a defect in immune-cell activation, at least at young age (Figure 3.16).

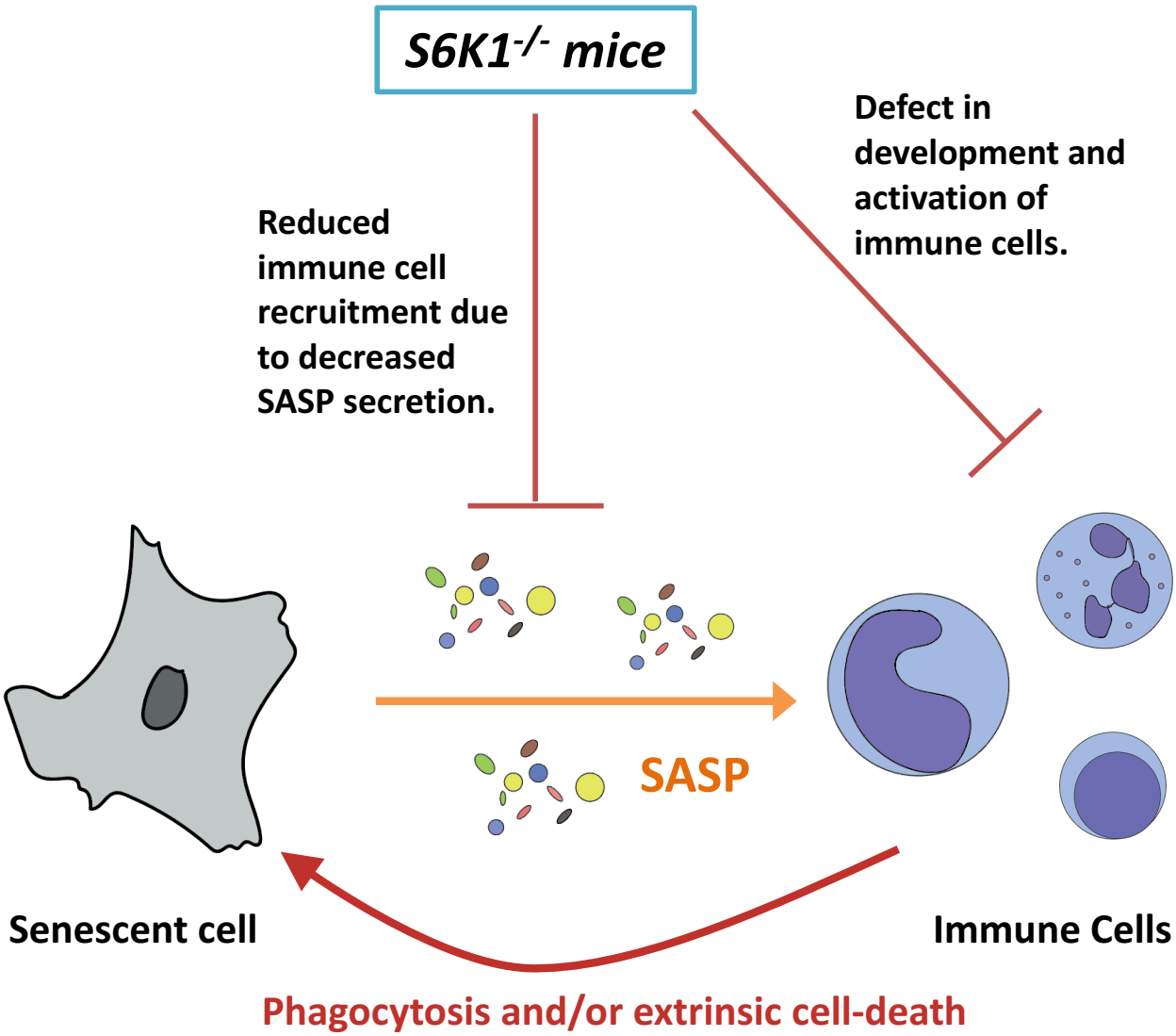

Figure 3.13. Why is there reduced immune cell infiltration in old *S6K1*$^{-/-}$ mice?
A. Schematic explaining possible scenarios for the observed reduction in immune cell markers in old *S6K1*$^{-/-}$ mice.

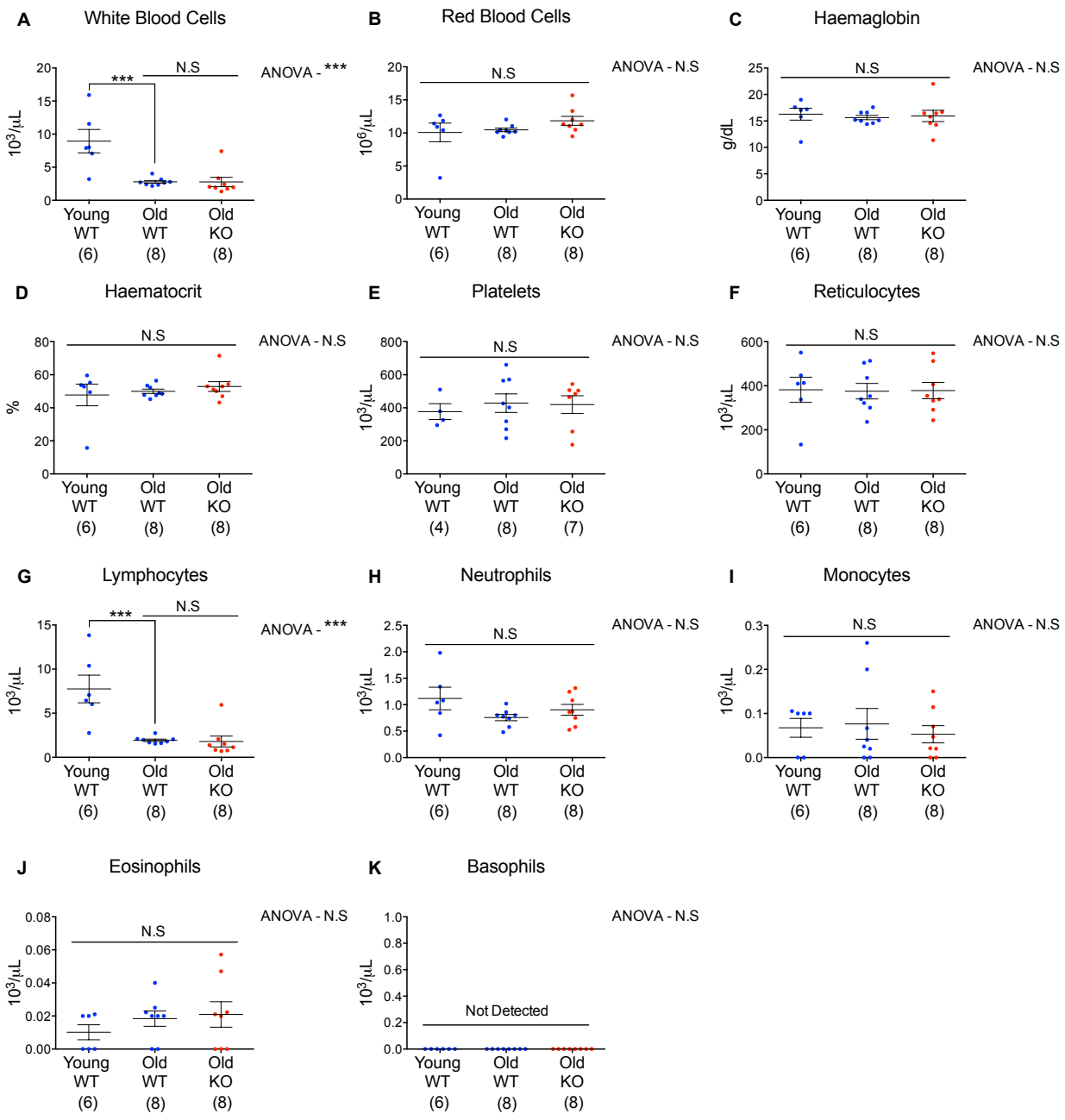

Figure 3.14. *S6K1*$^{-/-}$ mice do not have any significant alterations in their full blood count profile.

Whole blood was used to assess the full blood count. **A.** White blood cell count (10^3/µL). **B.** Red blood cell count (10^6/µL). **C.** Haemaglobin (g/dL). **D.** Haematocrit (%). **E.** Platelet count (10^3/µL). **F.** Reticulocytes (10^3/µL). **G.** Lymphocytes (10^3/µL). **H.** Neutrophils (10^3/µL). **I.** Monocytes (10^3/µL). **J.** Eosinophils (10^3/µL). **K.** Basophils (10^3/µL). Data are expressed as means ± SEM and number of mice used is indicated directly on all graphs. Statistical significance was calculated using one-way analysis of variance with Tukey's multiple comparison test (* $P < 0.05$, ** $P < 0.01$, *** $P < 0.001$). N.S: non-significant.

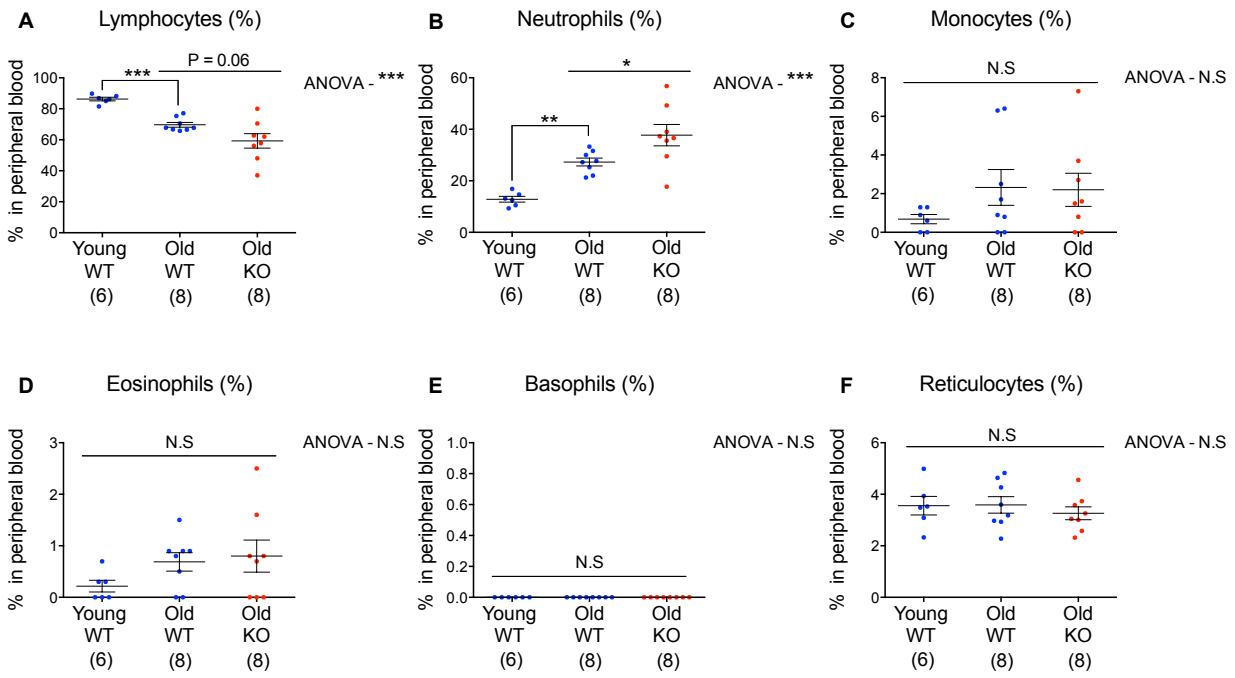

Figure 3.15. *S6K1*$^{-/-}$ mice display a skewing towards the myeloid lineage in their peripheral blood profile.
Whole blood was used to assess the full blood count. **A.** Percentage of peripheral lymphocytes. **B.** Percentage of peripheral neutrophils. **C.** Percentage of peripheral monocytes. **D.** Percentage of peripheral eosinophils. **E.** Percentage of peripheral basophils. **F.** Percentage of peripheral reticulocytes. Data are expressed as means ± SEM and number of mice used is indicated directly on all graphs. Statistical significance was calculated using one-way analysis of variance with Tukey's multiple comparison test (* $P < 0.05$, ** $P < 0.01$, *** $P < 0.001$). N.S: non-significant.

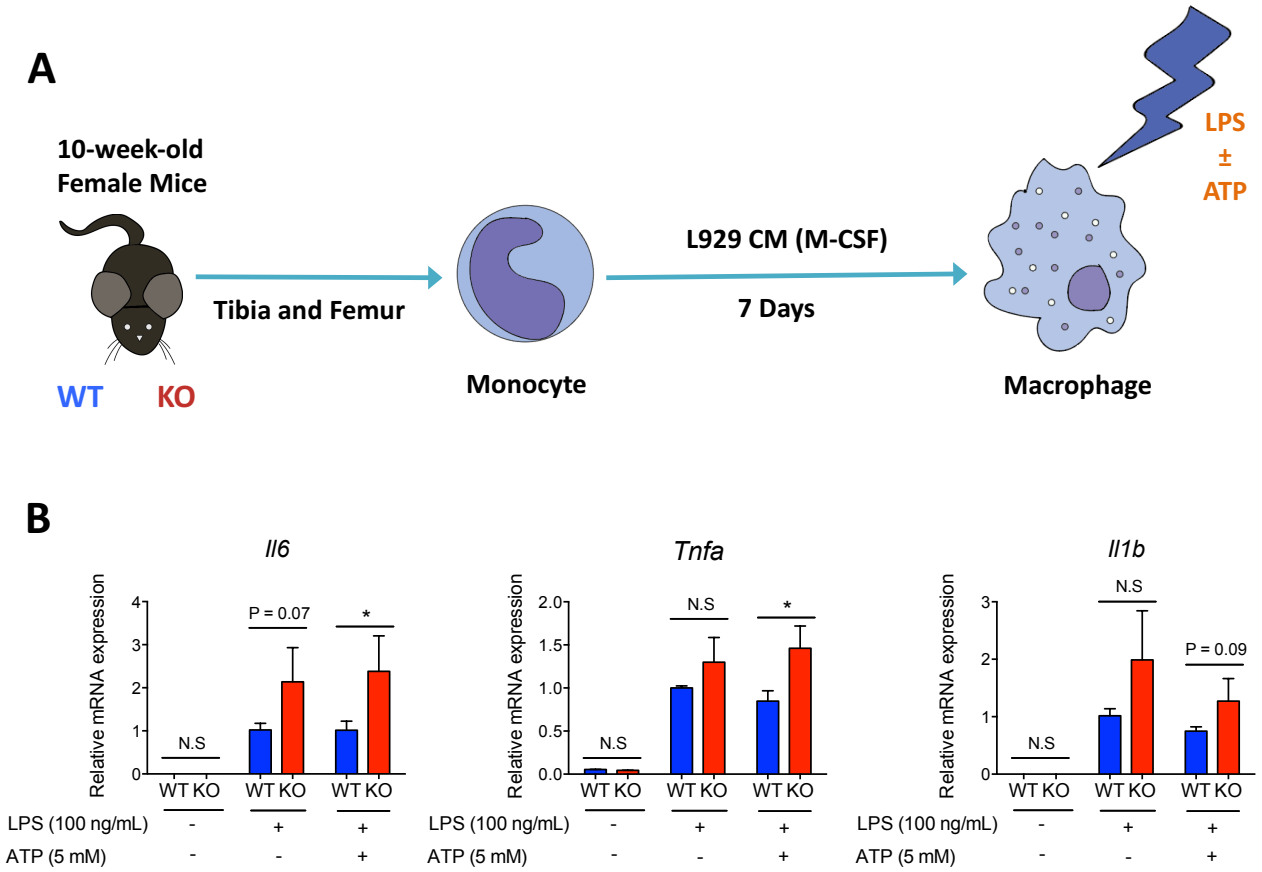

Figure 3.16. *S6K1*$^{-/-}$ bone marrow-derived macrophages (BMDMs) illicit a more pronounced response when treated with lipopolysaccharide (LPS) and ATP.
A. Schematic illustrating the workflow for the BMDM differentiation process. BMDMs were differentiated from 10-week-old female S6K1 wild type and knockout mice and treated with 100 ng/mL LPS alone or in combination with 5 mM ATP. BMDMs were treated with LPS for 6 hours and ATP was added in the final hour. **B.** Relative mRNA expression of *Il6, Tnfa* and *Il1b* assessed by RT-qPCR of 10-week-old wild type and *S6K1*$^{-/-}$ mice. mRNA expression was normalized to *Rps14* housekeeping gene. Data are expressed as means ± SEM and 4 mice per genotype were used. Statistical significance was calculated using unpaired student's t-test (* $P < 0.05$, ** $P < 0.01$, *** $P < 0.001$). L929 CM: L929 conditioned medium. N.S: non-significant.

3.7. Summary.

Overall, *S6K1*$^{-/-}$ mice showed a significant reduction in their body weight gain, which was primarily due to a reduction in adipose tissue weight, as well as resistance to age-related hepatic steatosis and several improvements in blood parameters. S6K1 deletion did not prevent senescence in the ageing liver but downregulated multiple inflammatory pathways, immune infiltration and expression of age-related secreted factors. Importantly, there was not a significant effect on the absolute white blood cell count in the peripheral blood and BMDMs isolated from young *S6K1*$^{-/-}$ mice activated in response to LPS treatment, suggesting that the attenuation in inflammation is not due to a systemic defect in the immune system.

There are several crucial experiments that still remain to be done to conclusively show that *S6K1*$^{-/-}$ mice have decreased SASP in the ageing liver without affecting the senescence growth arrest. These are discussed in length in the main Discussion chapter, hence they will be discussed in brief here. Importantly, we first aim to carry out immunohistochemistry stainings of additional senescence markers such as p16^{INK4A} and γ-H2AX given that preliminary SA-β-Gal staining suggested that *S6K1*$^{-/-}$ mice may have increased numbers of senescent cells. This could be due to diminished senescent cell clearance in *S6K1*$^{-/-}$ mice as a result of a decreased SASP response. Therefore, immunohistochemistry staining for SASP markers such as IL-1β or CCL2 would be ideal as well, but this has proven to be difficult given their secretory nature. Therefore, we have isolated various cell fractions (piece of whole liver, hepatocytes, immune cells and the stromal component) from the mouse liver and intend to carry out RT-qPCR analysis. We have, in collaboration, also done single-cell RNA sequencing of the whole liver in both young and old mice for the two genotypes. By doing this, we aim to answer exactly which cell type(s) is undergoing senescence in the ageing liver, what is the percentage of senescence and whether *S6K1*$^{-/-}$ mice truly have senescent cells that no longer express the proinflammatory SASP. In addition, we should also be able to identify the composition of the SASP in senescent cells in the ageing liver, as this will likely differ from the SASP found in fibroblasts undergoing senescence in cell culture experiments.

The above experiments are essential to understand whether the reduction in inflammation that was observed in old *S6K1*$^{-/-}$ mice is due to reduced SASP or due to decreased immune cell infiltration? To answer the latter, we aim to carryout immunohistochemistry stainings for various immune cells such as macrophages (F4/80), T-cells (CD3e) and B-cells (B220) to determine whether immune infiltration is indeed increased with age in old WT mice and whether this is prevented in old *S6K1*$^{-/-}$ mice. This is important given that we have only shown this by RT-qPCR analysis and it is crucial if we are to propose that the underlying reason for the increased number of senescent cells in *S6K1*$^{-/-}$ mice is due to decreased immune cell recruitment. In addition, we have also prepared BMDMs from 600-day-old WT and *S6K1*$^{-/-}$ mice and stimulated the cells with

either LPS or IL4 to induce M1 and M2 polarisation, respectively. This will enable us to understand whether there is an age-dependent effect on macrophage activation and whether S6K1 deletion impacts this since the observed reduction in inflammation may partly be due to a systemic effect.

Finally, it is imperative to understand whether the regulation of the SASP we have observed by S6K1 is specific to the liver or whether it is also preserved in other tissues because the increased lifespan and healthspan observed in *S6K1*$^{-/-}$ mice is likely due to cumulative beneficial outcomes from multiple tissues. Therefore, we aim to characterise senescence and SASP in other tissues where senescence has been shown to play a pivotal role such as the kidneys, adipose tissue, muscle and heart.

Chapter 4: S6 kinases regulate the SASP.

4.1. Introduction.

Once we found that S6K1 regulates age-related inflammation and potentially the senescence secretome in the liver, we aimed to confirm this in established, cellular models of replicative and oncogene-induced senescence. The advantage of cell culture models is that they provide a solid basis to elucidate the potential mechanisms by which S6 kinases regulate the senescence-associated secretory phenotype (SASP), as this is difficult to dissect in old mice.

4.2. S6K1 and/or S6K2 deletion does not prevent replicative senescence.

As mentioned previously, there are two closely related members of p70 ribosomal protein S6 kinases (S6K1 and S6K2) that share many functions including phosphorylation of the ribosomal protein S6 (RPS6), as well as functions that are unique to each kinase. Therefore, to obtain a comprehensive analysis of the role of ribosomal protein S6 kinases in cellular senescence, we isolated mouse embryonic fibroblasts (MEFs) from *S6K1*$^{-/-}$, *S6K2*$^{-/-}$ and *S6K1*$^{-/-}$*: S6K2*$^{-/-}$ embryos at 13:5 days gestation (Figure 4.1). We aimed to understand whether S6K1 and S6K2 regulate senescence.

Similar to what was observed in the ageing liver, S6K1 deletion did not prevent replicative senescence; and surprisingly, *S6K1*$^{-/-}$ MEFs underwent senescence slightly earlier (Figure 4.2 A). Whereas, *S6K2*$^{-/-}$ MEFs reached replicative exhaustion at the same rate as wild type (WT) MEFs (Figure 4.2 B). *S6K1*$^{-/-}$*: S6K2*$^{-/-}$ MEFs underwent replicative senescence at a significantly earlier rate than the WT counterparts (Figure 4.2 C). Deleting either S6K1 or S6K2 or both did not slow down cell proliferation when assessed by DAPI (4'-6;-diamidino-2-phenylindole) staining for cell count and by BrdU (5-bromo-2'-deoxyuridine) incorporation (Figure 4.3). This was done utilising quantitative immunofluorescence (IF) by high-throughput microscopy and high-content analysis (InCell Analyzer 2000). Complete ablation of phosphorylation of ribosomal protein S6 (S240/S244) was observed only in cells with combined deletion of S6K1 and S6K2 (Figure 4.3).

We then focussed on characterising *S6K1*$^{-/-}$*: S6K2*$^{-/-}$ MEFs in greater detail because the combined deletion of S6K1 and S6K2 had a bigger impact on replicative senescence than deleting either S6K1 or S6K2 in isolation. As expected, there was a noticeable reduction in BrdU incorporation and an increase in senescence-associated beta galactosidase (SA-β-Gal) activity in WT MEFs at late passage (P8) compared to early passage (P2), whereas *S6K1*$^{-/-}$*: S6K2*$^{-/-}$ MEFs showed a stronger arrest with no significant alteration in SA-β-Gal activity, indicating that deletion of S6K1 and S6K2 does not prevent replicative senescence (Figure 4.4).

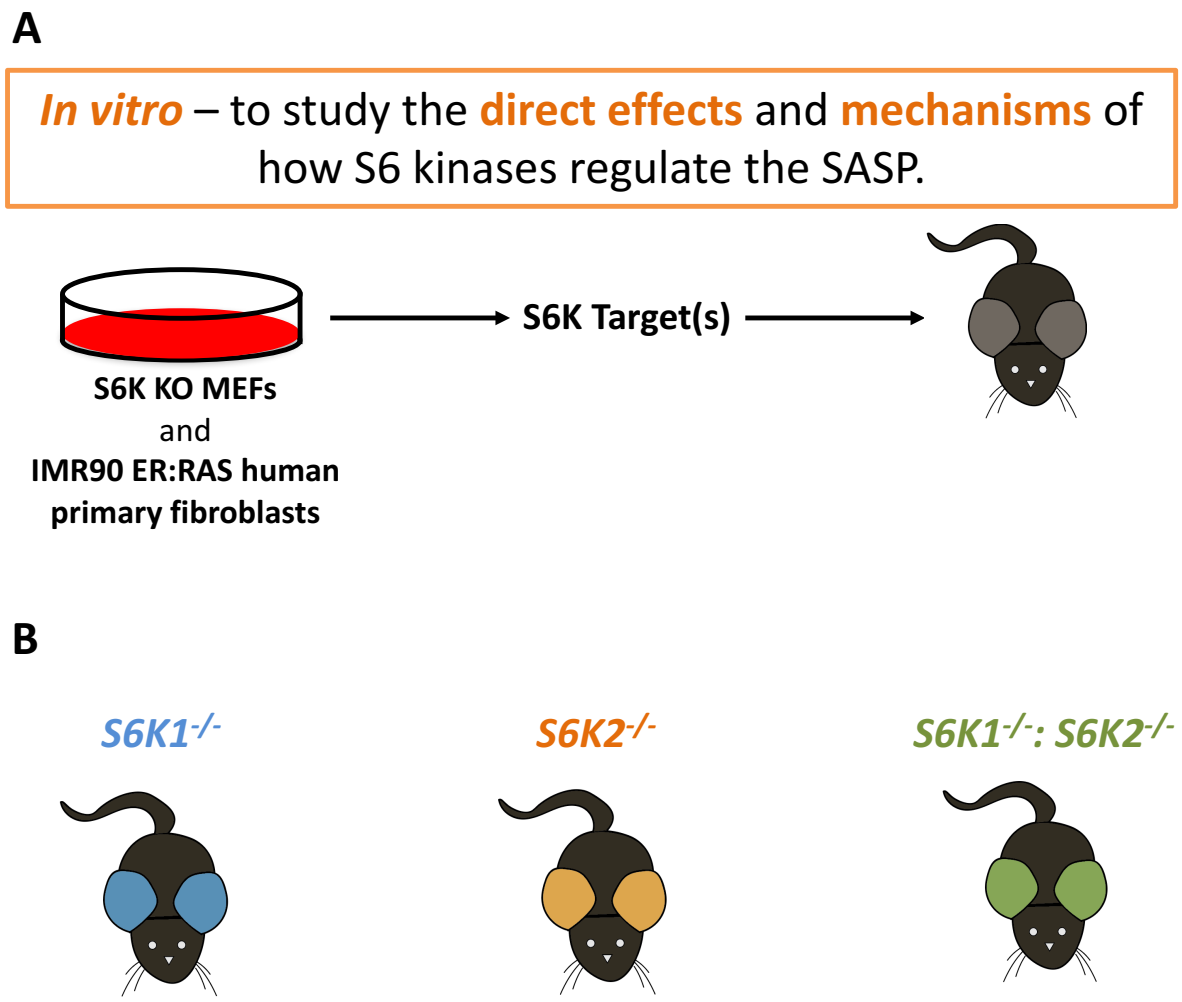

Figure 4.1. Schematic depicting the workflow for the *in vitro* senescence experiments.
A. Cellular models of senescence (replicative senescence and oncogene-induced senescence) to study whether S6 kinases directly regulate the senescence secretome and to elucidate the mechanisms by which S6 kinases regulate the SASP. IMR90 human primary fibroblasts stably infected with the ER: RAS chimaeric fusion protein (oestrogen receptor bound to $HRAS^{G12V}$) to study oncogene-induced senescence. RAS is activated upon treatment with 4-hydroxytamoxifen (4OHT – 125 nM). **B.** Mouse embryonic fibroblasts (MEFs) were derived from *S6K1*$^{-/-}$, *S6K2*$^{-/-}$ and *S6K1*$^{-/-}$*: S6K2*$^{-/-}$ embryos at 13.5 gestation days.

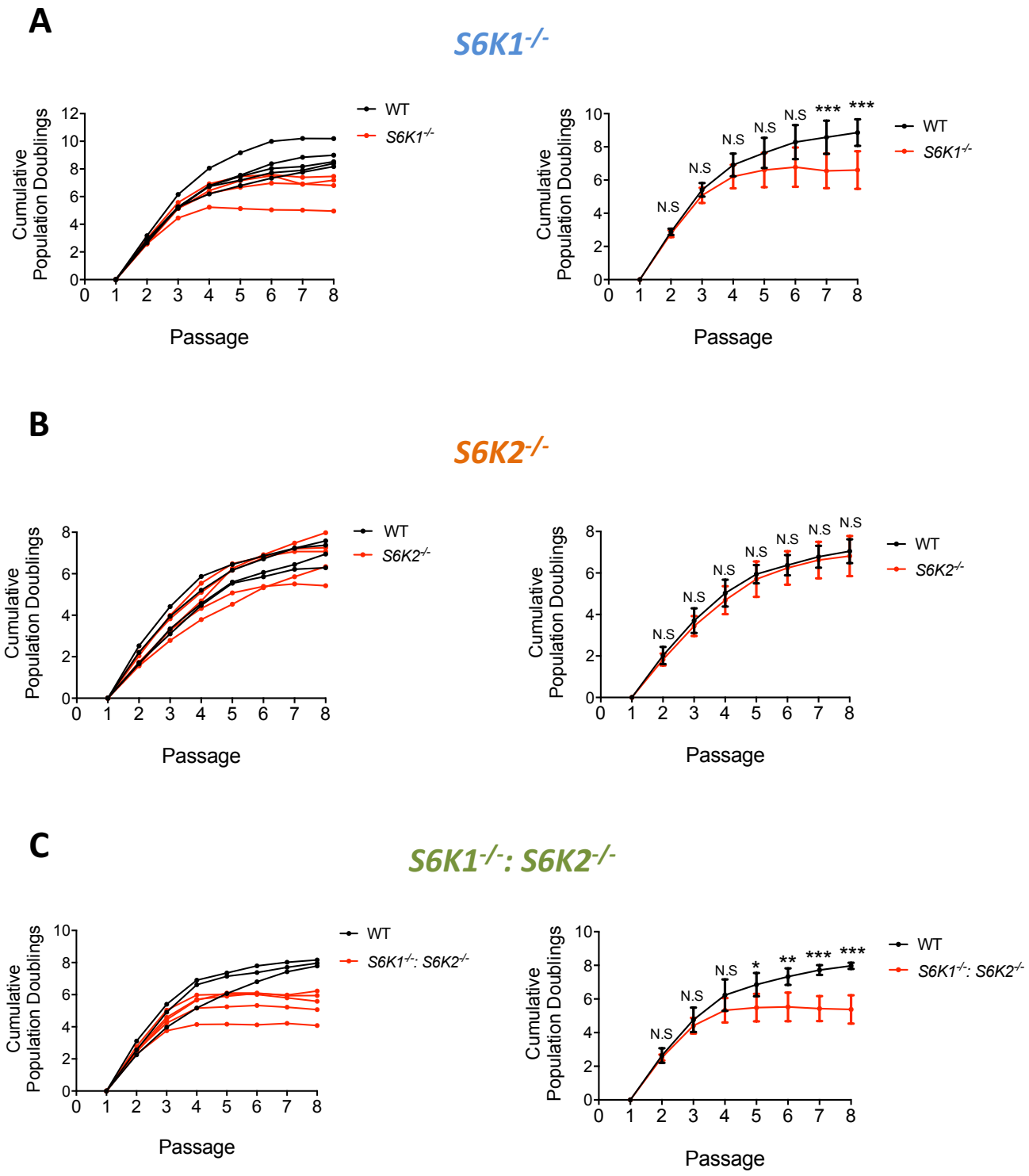

Figure 4.2. Deletion of S6K1 and/or S6K2 does not prevent replicative senescence. Cumulative population doublings (PDs) were performed by passaging fibroblasts every 4 days for 8 passages. **Left:** PDs of each individual MEF-line derived from a single embryo. **Right:** Average PDs for the indicated genotype. **A.** Cumulative PDs of *S6K1* wild type (WT) and knockout (KO) MEFs. **B.** Cumulative PDs of *S6K2* WT and KO MEFs. **C.** Cumulative PDs of *S6K1: S6K2* WT and double knockout MEFs. Data are expressed as mean ± SD. MEFs isolated from 3-5 independent pairs of embryos from at least 3 different mothers were used. Statistical significance was calculated using repeated two-way analysis of variance with Sidak's multiple comparison test (* $P < 0.05$, ** $P < 0.01$, *** $P < 0.001$). N.S: non-significant.

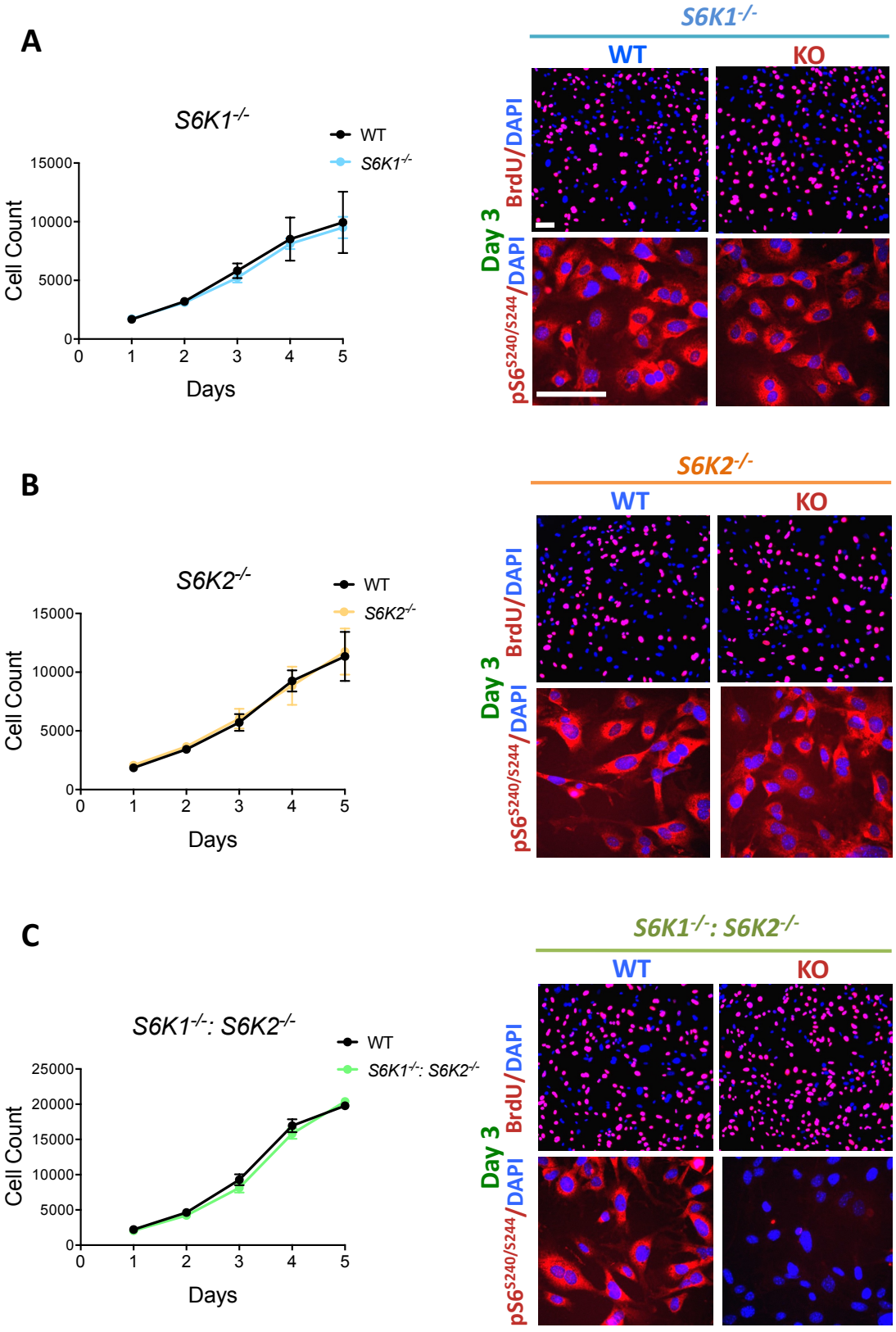

Figure 4.3. Deletion of S6K1 and/or S6K2 does not slow down proliferation at early passage. Passage 2 (P2) MEFs were assessed for cell count and cell proliferation. **Left:** time course of cell count assessed by high-throughput microscopy of DAPI staining between days 1 and 5. **Right:** Representative immunofluorescence images of BrdU incorporation and phosphorylated ribosomal protein S6 (S240/S244) staining on day 3. **A.** *S6K1* wild type (WT) and knockout (KO) MEFs. **B.** *S6K2* WT and KO MEFs. **C.** *S6K1: S6K2* WT and KO MEFs. Data are expressed as mean ± SD. MEFs isolated from 2 independent pairs of embryos performed in triplicate wells of a single experiment. Scale bar, 100 µm.

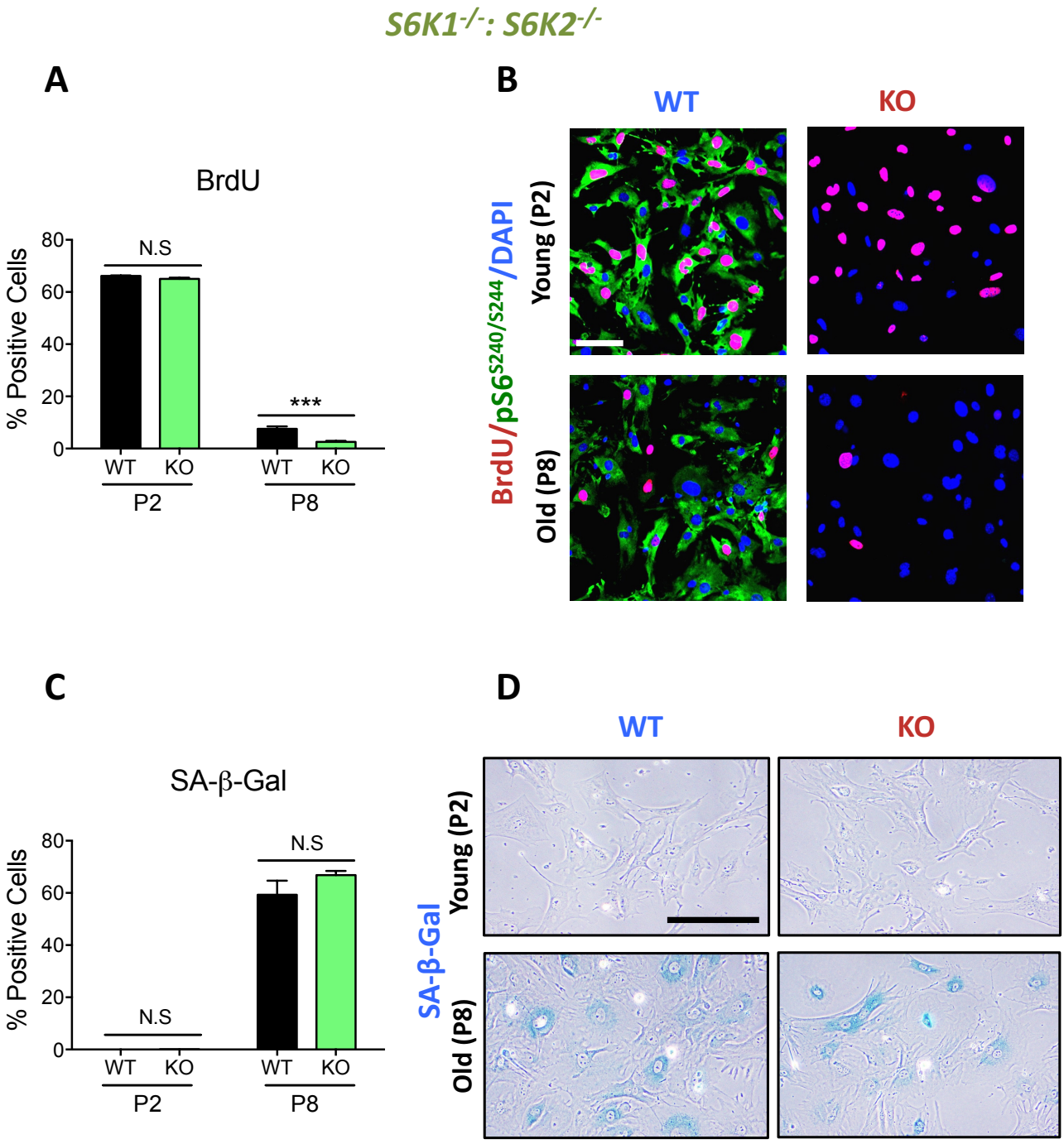

Figure 4.4. Deletion of S6K1 and S6K2 does not affect BrdU incorporation and senescence-associated beta galactosidase (SA-β-Gal) activity.
A. Percentage of BrdU positive cells at passage 2 (P2) and P8 MEFs quantified by high-throughput microscopy. **B.** Representative immunofluorescent images for BrdU incorporation and phosphorylated ribosomal protein S6 (S240/S244) staining. **C.** Percentage of SA-β-Gal positive cells at passage 2 (P2) and P8 MEFs. **D.** Representative microphotographs for SA-β-Gal staining. Data are expressed as mean ± SD. MEFs isolated from 3-5 independent pairs of embryos from at least 3 different mothers were used. Statistical significance was calculated using two-way analysis of variance with Tukey's multiple comparison test (*** $P < 0.001$). N.S: non-significant. Scale bar, 100 µm.

4.3. S6K deletion results in a reduced SASP.

Once we confirmed that deleting S6K1 and/or S6K2 does not prevent replicative senescence, we next assessed the mRNA expression of senescence and SASP components to understand whether the S6 kinases regulate the SASP. As expected, there was an increase in mRNA expression of the cell cycle inhibitor *p16*^{Ink4a} in WT MEFs at late passage (P8) compared to early passage (P3), and S6K deletion did not prevent this upregulation, thus further confirming that they are not affecting the senescence growth arrest (Figure 4.5). Interestingly, however, the mRNA expression of interleukin 1 beta and alpha (*Il1b* and *Il1a*) was significantly lower in both *S6K1*$^{-/-}$ and *S6K1*$^{-/-}$*: S6K2*$^{-/-}$ MEFs at late passage (P8), and the effect was once again stronger with double S6K1/2 deletion (Figure 4.5). Deletion of S6K2, however, did not significantly affect *Il1b* and *Il1a* expression in replicative senescence (Figure 4.5). We focussed on *Il1b* and *Il1a* because they play an important role in the SASP feedback loop and interleukin 1 receptor knockout (*Il1r*$^{-/-}$) mice show improvements in age-related parameters (Acosta et al., 2013; Youm et al., 2013).

To investigate whether S6 kinases also regulate the SASP during oncogene-induced senescence (OIS), we overexpressed (retroviral vector) a constitutively active form of HRAS (G12V) and assessed *p16*^{Ink4a} as well as *Il1b* and *Il1a* expression at day 10 following selection and plating (Figure 4.6 A). Western blotting confirmed HRAS^{G12V} overexpression, S6K deletion and ablation of RPS6 phosphorylation (S240/S244) in the *S6K1*$^{-/-}$*: S6K2*$^{-/-}$ MEFs (Figure 4.6 B). Consistent with previous results, S6K deletion significantly blunted the mRNA expression of *Il1b* and *Il1a* without affecting the cell cycle inhibitor *p16*^{Ink4a}*.* The effect on *Il1b* and *Il1a* expression was again greater with combined deletion of S6K1 and S6K2 (Figure 4.6 C-E).

Altogether, the data indicate that the S6 kinases regulate the SASP without preventing the senescence growth arrest.

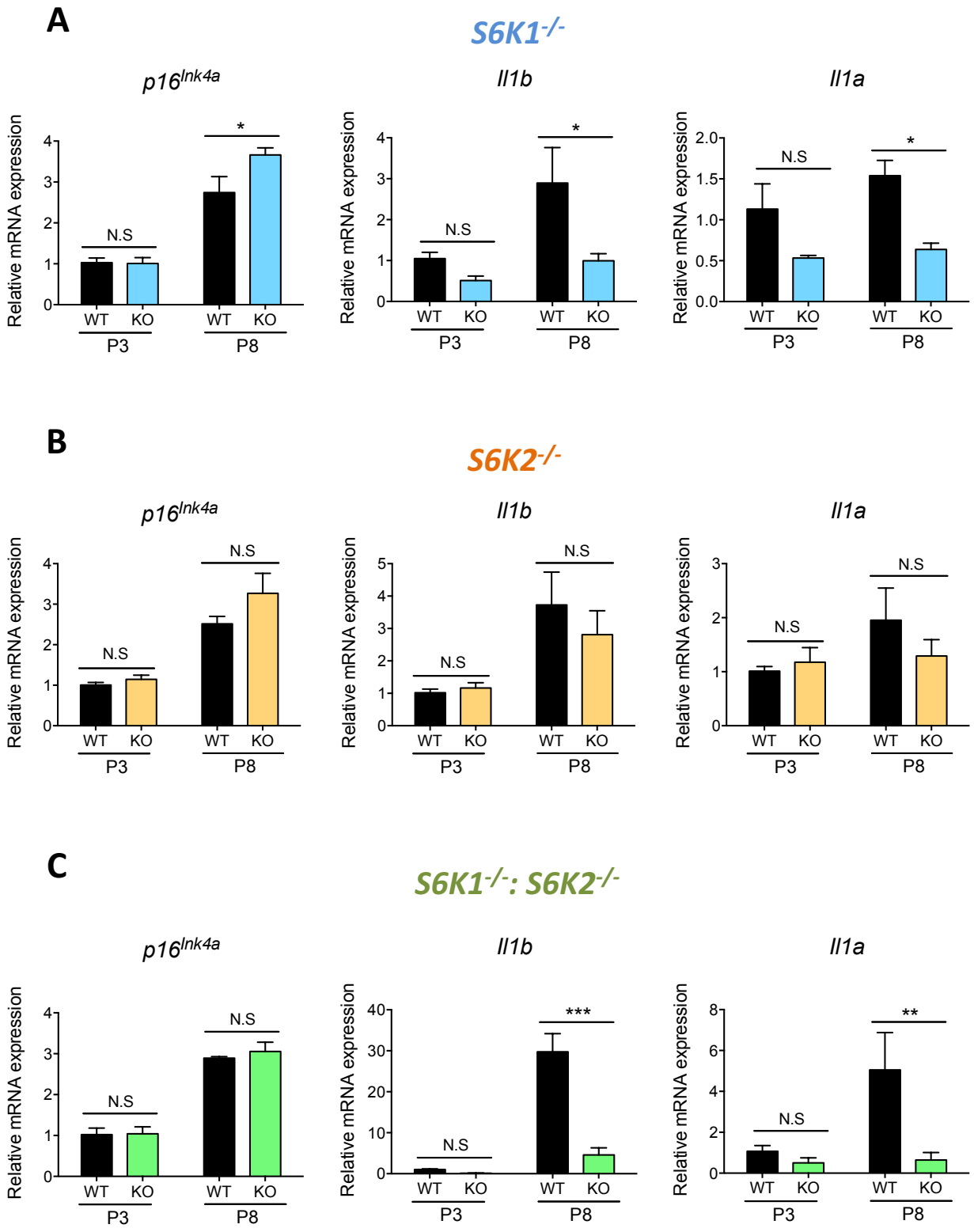

Figure 4.5. Deletion of S6K1 and/or S6K2 blunts *Il1b* and *Il1a* expression in replicative senescence.
Relative mRNA expression for *p16*^{Ink4a}, *Il1b* and *Il1a* assessed by RT-qPCR from passage 3 (P3) and P8 MEFs. mRNA expression was normalized to *Rps14* housekeeping gene. **A.** *S6K1* wild type (WT) and knockout (KO) MEFs. **B.** *S6K2* WT and KO MEFs. **C.** *S6K1: S6K2* WT and double knockout MEFs. Data are expressed as mean ± SD. MEFs isolated from 3-5 independent pairs of embryos from at least 3 different mothers were used. Statistical significance was calculated using two-way analysis of variance with Tukey's multiple comparison test (* $P < 0.01$, ** $P < 0.01$, *** $P < 0.001$). N.S: non-significant.

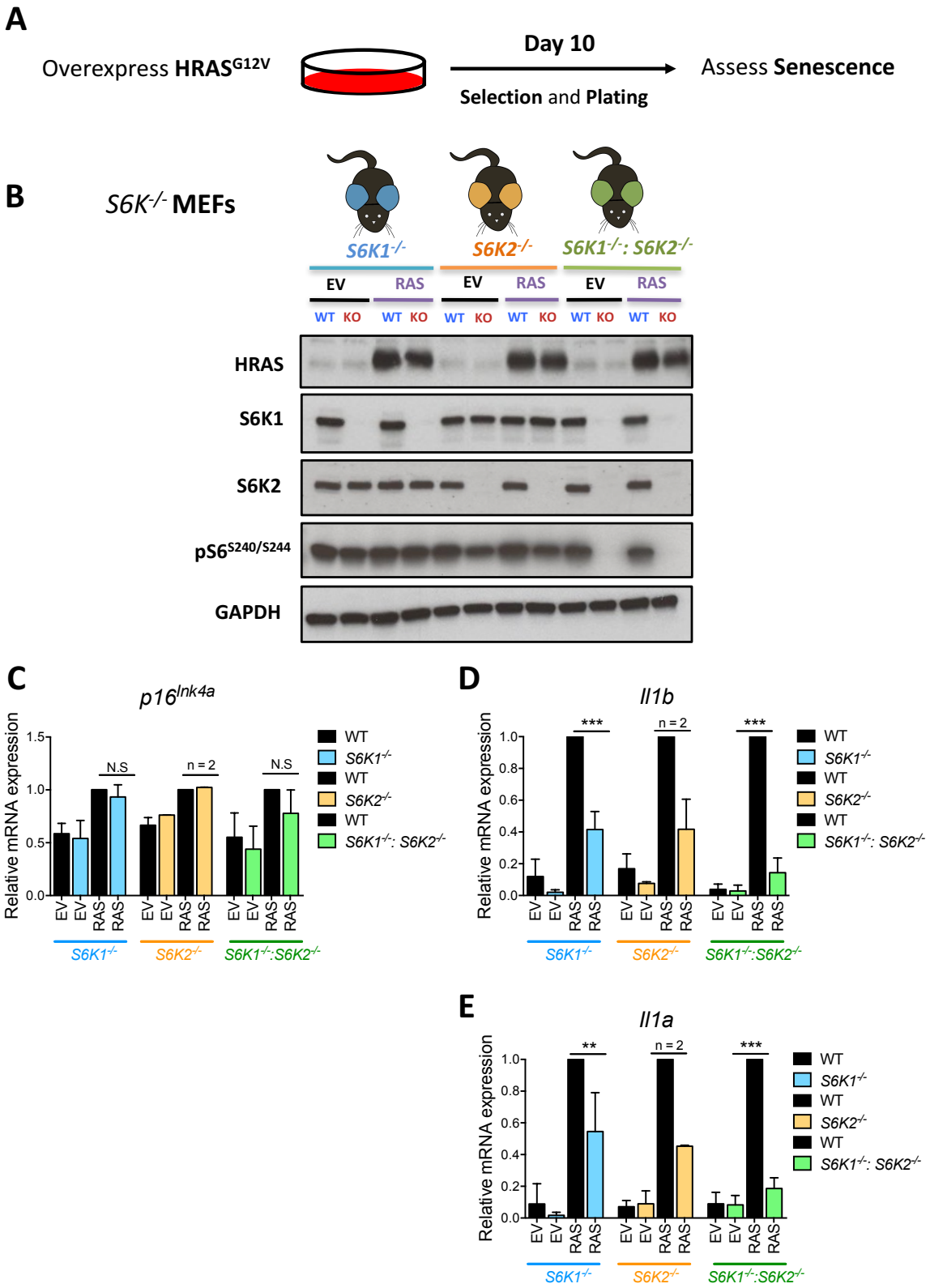

Figure 4.6. Deletion of S6K1 and/or S6K2 dampens *Il1b* and *Il1a* expression in oncogene-induced senescence (OIS).

A. Workflow of OIS experiment in MEFs. Passage 2 (P2) wild type (WT) and knockout (KO) MEFs for S6K1, S6K2 or S6K1; S6K2 were transduced with either empty vector (EV) or HRAS^{G12V} (RAS), selected and plated for SASP assessment on day 10. **B.** Western blot analysis for HRAS, S6K1, S6K2 and pS6$^{S240/S244}$ expression. GAPDH was used as the loading control. **C-E.** Relative mRNA expression for *p16^{Ink4a}*, *Il1b* and *Il1a*, respectively, assessed by RT-qPCR. mRNA expression was normalized to *Rps14* housekeeping gene. Data are expressed as mean ± SD. MEFs isolated from 3 independent pairs of embryos from at least 3 different mothers were used. S6K2 MEF experiment was only performed with 2 independent pairs of embryos. Statistical significance was calculated using two-way analysis of variance with Tukey's multiple comparison test (* $P < 0.05$, ** $P < 0.01$, *** $P < 0.001$). N.S: non-significant.

4.4. S6K depletion in IMR90 primary human fibroblasts blunts the proinflammatory SASP.

Upon confirming that S6 kinases regulate mRNA expression of proinflammatory factors in both the ageing liver and in different cellular senescence models in mouse embryonic fibroblasts, we then investigated whether S6 kinases also regulate the senescence secretome in human cells. To do this, we utilised the well-established IMR90 ER: RAS (chimaeric fusion protein consisting of oestrogen receptor bound to $HRAS^{G12V}$) inducible model of OIS (Figure 4.7A). In this system, primary IMR-90 human lung fibroblasts were first stably infected with the pLNC-ER: RAS retroviral vector. RAS activation by treatment with 4-hydroxytamoxifen (4OHT - 125 nM) induced the characteristic senescence phenotype (Figure 4.7 and 4.8). Specifically, the cells underwent a morphological change (flattened and enlarged) and a potent growth arrest as observed by colony formation assays and BrdU incorporation (Figure 4.7 B and C). Moreover, RAS activation also induced other prototypic senescence features such as activation of the cell cycle inhibitors ($p16^{INK4A}$, $p21^{CIP1}$) and p53, as well as a DNA damage response (DDR - γ-H2AX) and expression of the SASP (Figure 4.7 C and D and Figure 4.8). These senescence effectors were monitored using quantitative immunofluorescence (IF) by high-throughput microscopy and high-content analysis (InCell Analyzer 2000).

Next, we aimed to determine whether S6K1 or S6K2 is required for regulation of the SASP in human fibroblasts. To this end, we depleted S6K1 and S6K2 in isolation or in combination using two independent siRNAs (small interfering RNAs) targeting each kinase. Knockdown was confirmed by both RT-qPCR and western blotting (Figure 4.9 A and B). Phosphorylation of ribosomal protein S6 (S240/S244) was only noticeably reduced when depleting S6K1 and S6K2 in combination (Figure 4.9 C and D). We then confirmed that depleting S6 kinases does not affect the senescence growth arrest in human fibroblasts by assessing BrdU incorporation and expression of various senescence effectors and markers ($p16^{INK4A}$, $p21^{CIP1}$, p53 and γ-H2AX) (Figure 4.10 A). Knockdown of $p16^{INK4A}$ or p53 and C/EBPβ was used as positive controls for senescence bypass and SASP ablation, respectively. Interestingly, knocking down either S6K1 or S6K2 significantly diminished the induction of the proinflammatory components of the SASP at both mRNA (IL1A, IL1B, IL6, IL8 and CCL20) and protein (IL-1β and IL-8) level. This effect was stronger upon combined knockdown of S6K1 and S6K2 (Figure 4.9 B and 4.10 B). These data indicate that S6 kinases regulate the proinflammatory arm of the SASP without affecting the senescence growth arrest.

To complement these results, we assessed the effects of chemical inhibition (LY2584702 – a specific inhibitor of S6K) of S6 kinases on regulation of the SASP, as this would be the most likely approach for any future therapeutic intervention (Figure 4.11 A). A dose response (0.2 – 2 μM) was first done using phosphorylation of RPS6 (S240/S244) as a readout of S6K activity. We observed that 2 μM of LY2584702 significantly reduced RPS6 (S240/S244) phosphorylation

without significantly affecting phosphorylation of another mTOR target 4EBP1 (T37/T46) (Figure 4.11 B-D). Of note, it is likely that 2 μM of LY2584702 inhibits the activity of both S6K1 and S6K2 since the S240/S244 residue is phosphorylated by both the S6 kinases (Pende et al., 2004). The dual mTORC1/mTORC2 inhibitor Torin1 was used as a control since Torin1 was previously reported to abolish SASP induction (Herranz et al., 2015). In line with genetic deletion of S6 kinases, chemical inhibition of S6 kinases did not affect the senescence growth arrest or significantly reduce SA-β-Gal activity in cells undergoing OIS (Figure 4.12 A and B). S6K inhibition, however, blunted the induction of two SASP components (IL-1α and IL-1β) at both mRNA and protein level (Figure 4.12 C-E). Importantly, LY2584702 did not affect IL1B and IL1A mRNA induction to the same extent as combined deletion of both S6K1 and S6K2.

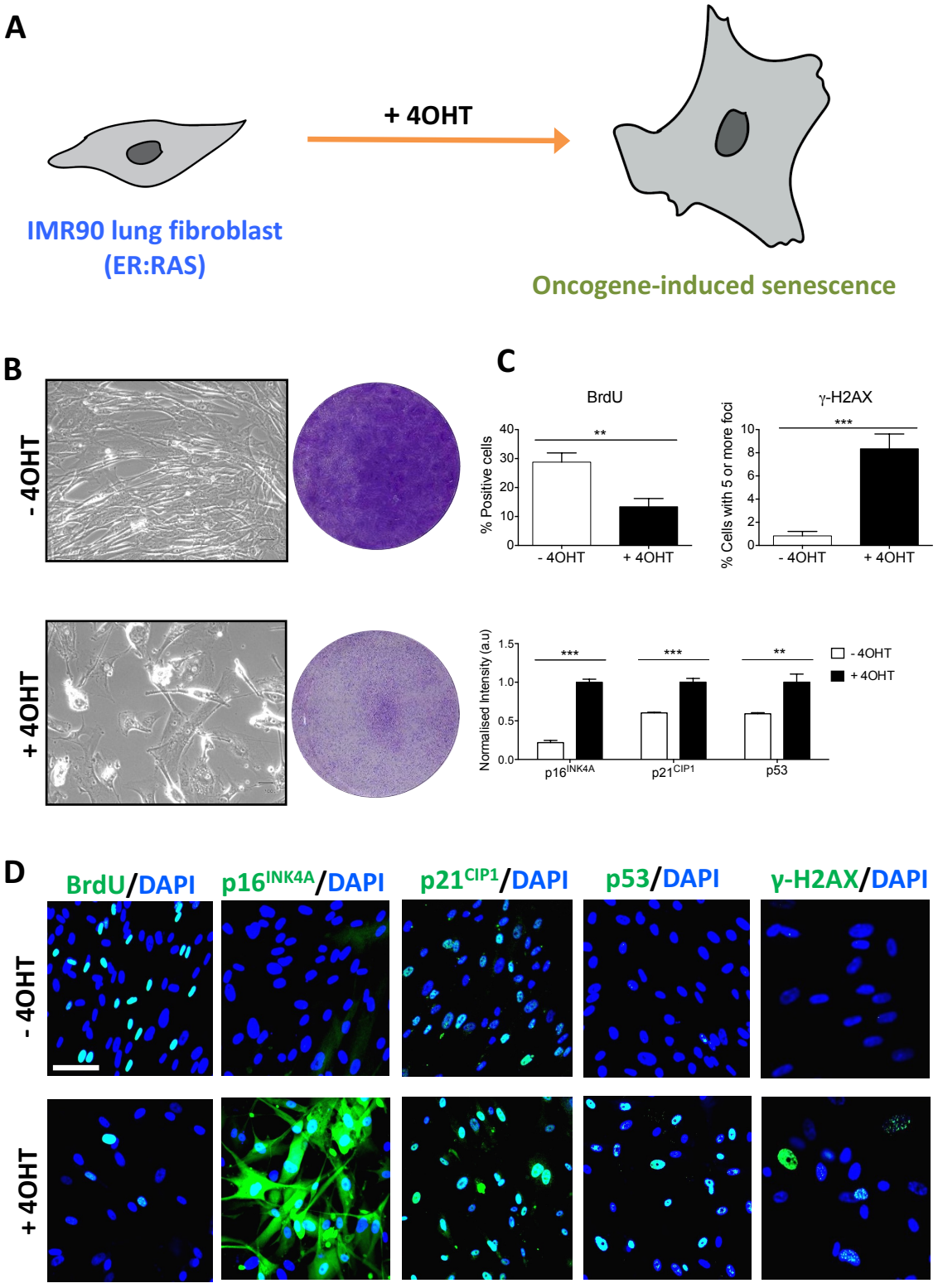

Figure 4.7. IMR90 ER: RAS system of oncogene-induced senescence (OIS).
A. Workflow of OIS experiments performed in IMR90 human lung fibroblasts. IMR90 fibroblasts were stably transduced with the pLNC-ER: RAS retroviral vector and treated with 4-hydroxytamoxifen (4OHT – 125 nM) for 4-14 days for senescence induction. **B. Left:** microphotographs displaying the effects on cell morphology of IMR-90 cells upon oncogenic RAS activation. **Right:** cell proliferation assessed by crystal violet staining following 13 days in culture. **C.** Percentage positive cells for BrdU incorporation, γH2AX, $p16^{INK4A}$, $p21^{CIP1}$ and p53 upon RAS activation following 7 days of 4OHT treatment. Quantified using high-throughput microscopy and high-content analysis. **D.** Representative immunofluorescence (IF) staining of the indicated markers. Data are expressed as means ± SD performed in triplicate wells of a single experiment. Statistical significance was calculated using unpaired student's t-test (** $P < 0.01$ and *** $P < 0.001$). Scale bar, 100 μm.

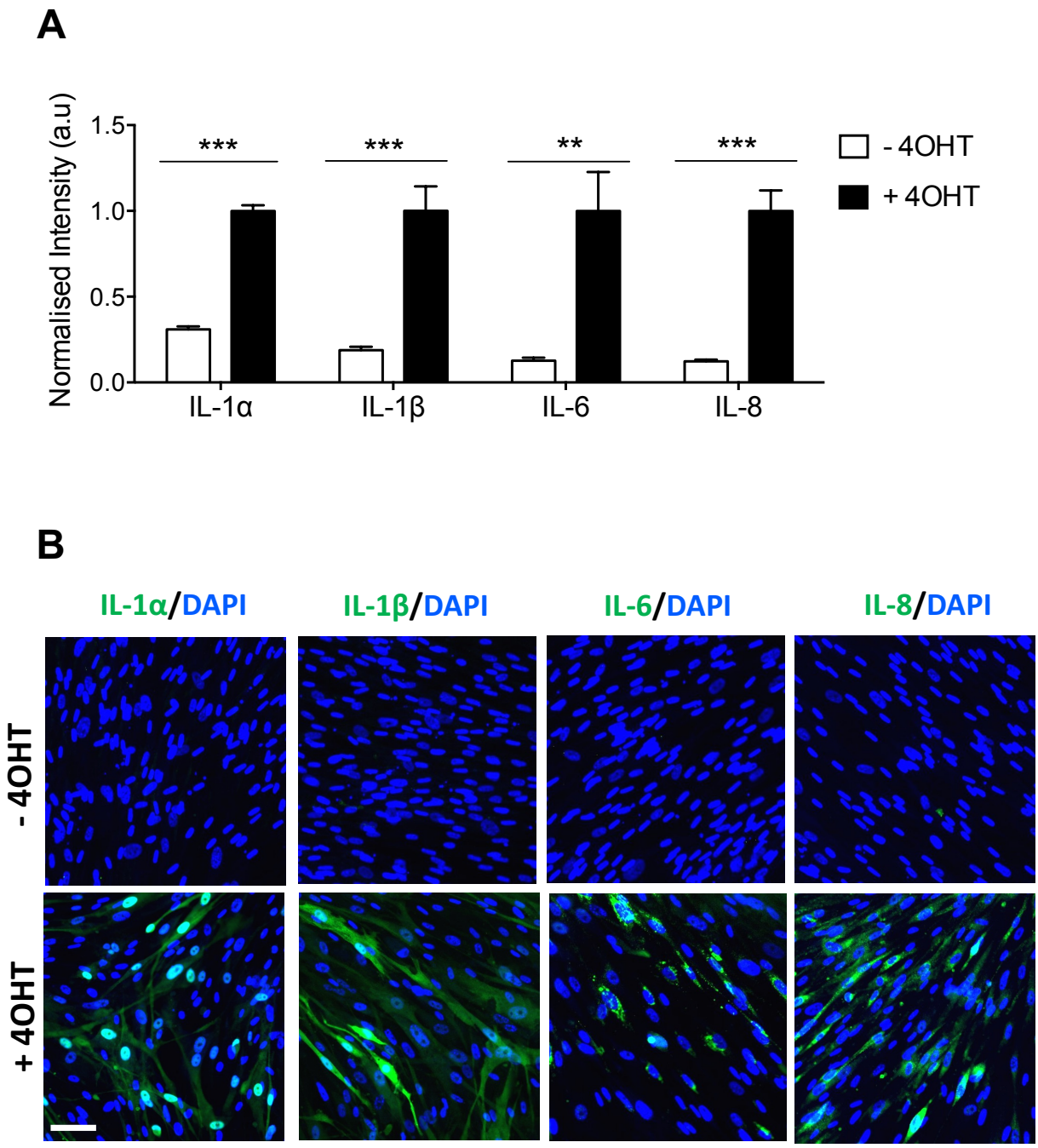

Figure 4.8. Senescence-associated secretory phenotype (SASP) following RAS activation in IMR90 fibroblasts.
IMR90 human lung fibroblasts were stably transduced with the pLNC-ER: RAS retroviral vector and treated with 4-hydroxytamoxifen (4OHT – 125 nM) for 8 days for SASP induction. **A.** Percentage positive cells for IL-1α, IL-1β, IL-6 and IL-8 quantified by high-throughput microscopy and high-content analysis. **C.** Representative immunofluorescence (IF) staining of the indicated markers. Data are expressed as means ± SD performed in triplicate wells of a single experiment. Scale bar, 100 μm.

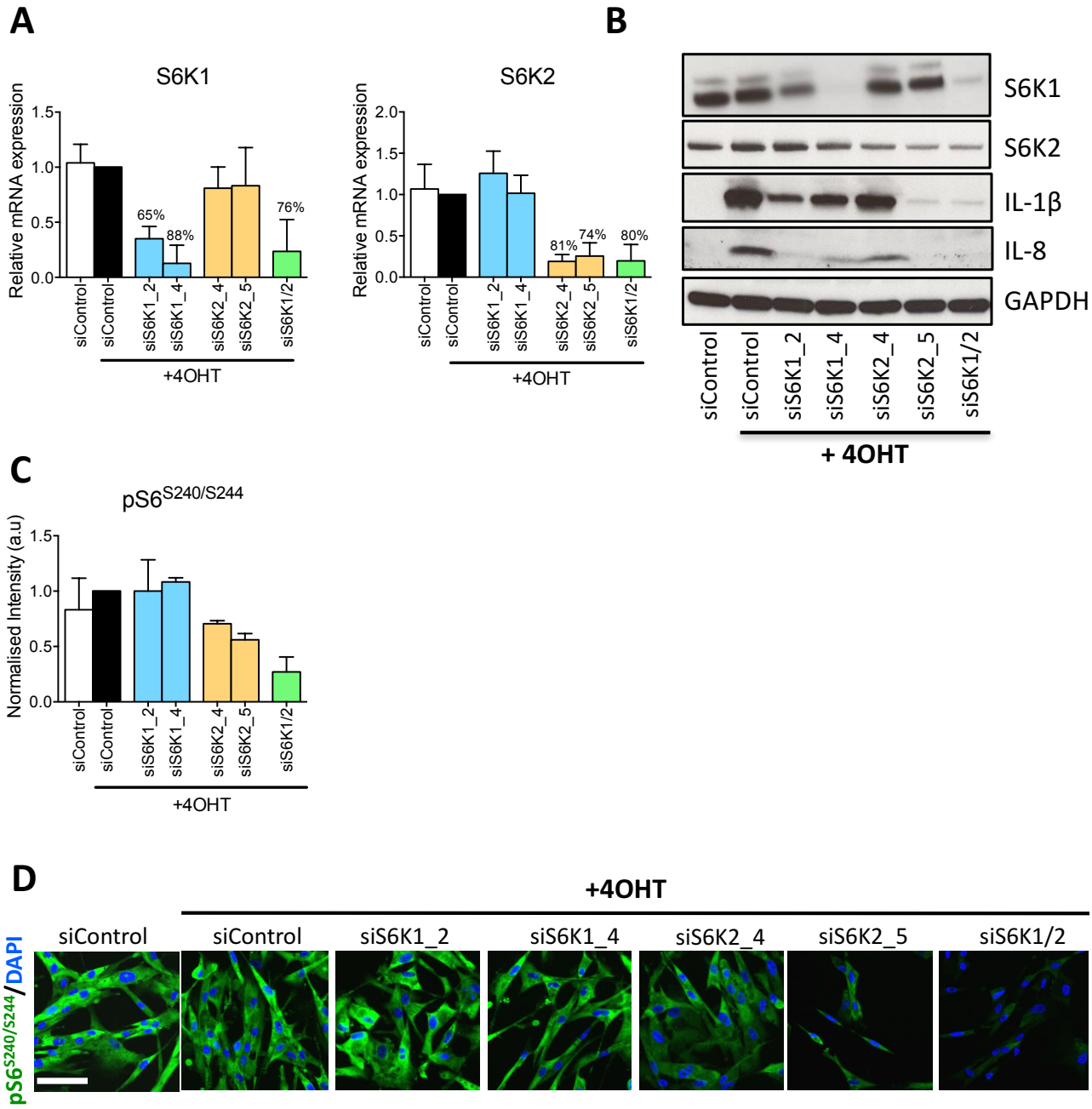

Figure 4.9. S6K1 and S6K2 depletion in human fibroblasts.
IMR-90 ER: RAS cells were reverse transfected with either Allstars (scrambled sequence - siControl) or siRNAs targeting S6K1 and/or S6K2. Cells were induced with 4-hydroxytamoxifen (4OHT – 125 nM) on the following day. **A.** Knockdown of S6K1 or S6K2 assessed by qRT-PCR 4 days following 4OHT treatment. **B.** Total protein levels of S6K1, S6K2, IL-1β and IL-8 assessed by immunoblot following 7 days of 4OHT treatment. GAPDH was used as the loading control **C.** Quantification of immunofluorescence (IF) staining for phosphorylated ribosomal protein S6 (S240/S244) following 5 days of 4OHT treatment. **D.** Representative IF images for ribosomal protein S6 (S240/S244). Data are expressed as means ± SD; n = 4 independent experiments. Scale bar, 100 μm.

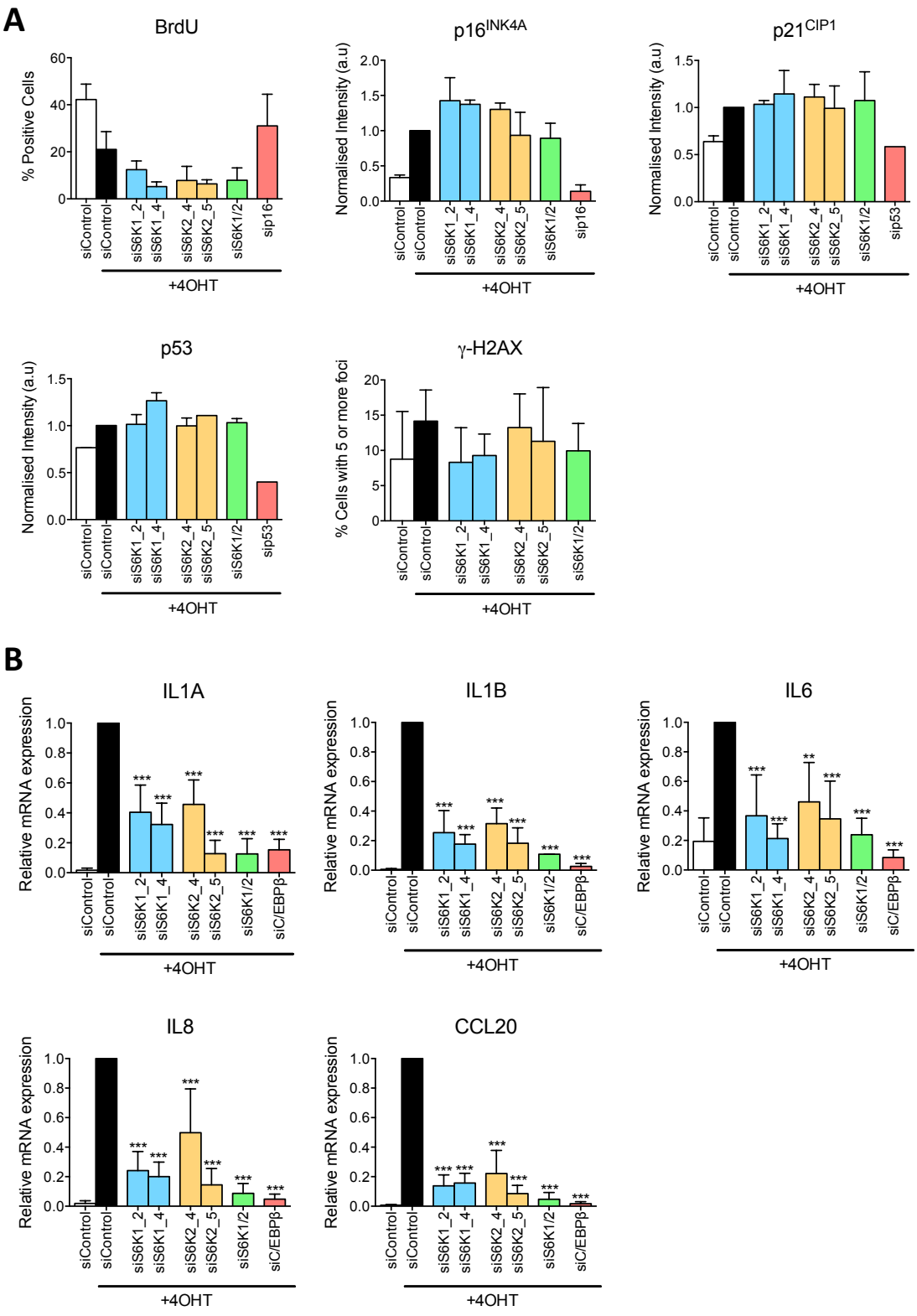

Figure 4.10. S6K1 and S6K2 depletion in human fibroblasts attenuates the senescence-associated secretory phenotype (SASP) without affecting senescence.
IMR-90 ER: RAS cells were reverse transfected with either Allstars (scrambled sequence - siControl) or the indicated siRNAs. Cells were induced with 4-hydroxytamoxifen (4OHT – 125 nM) on the following day. **A.** Quantification of immunofluorescence (IF) staining for BrdU incorporation, $p16^{INK4A}$, $p21^{CIP1}$, p53 and γ-H2AX following 5 days of 4OHT treatment. Quantification by high-throughput microscopy and high-content analysis. **B.** Relative mRNA expression by RT-qPCR of proinflammatory SASP components (IL1A, IL1B, IL6, IL8 and CCL20) following 4 days of 4OHT treatment. Data are expressed as means ± SD; n = 2 and n = 4 independent experiments for A and B, respectively. Statistical significance was calculated using one-way analysis of variance with Dunnett's multiple comparison test (** P < 0.01, *** P < 0.001).

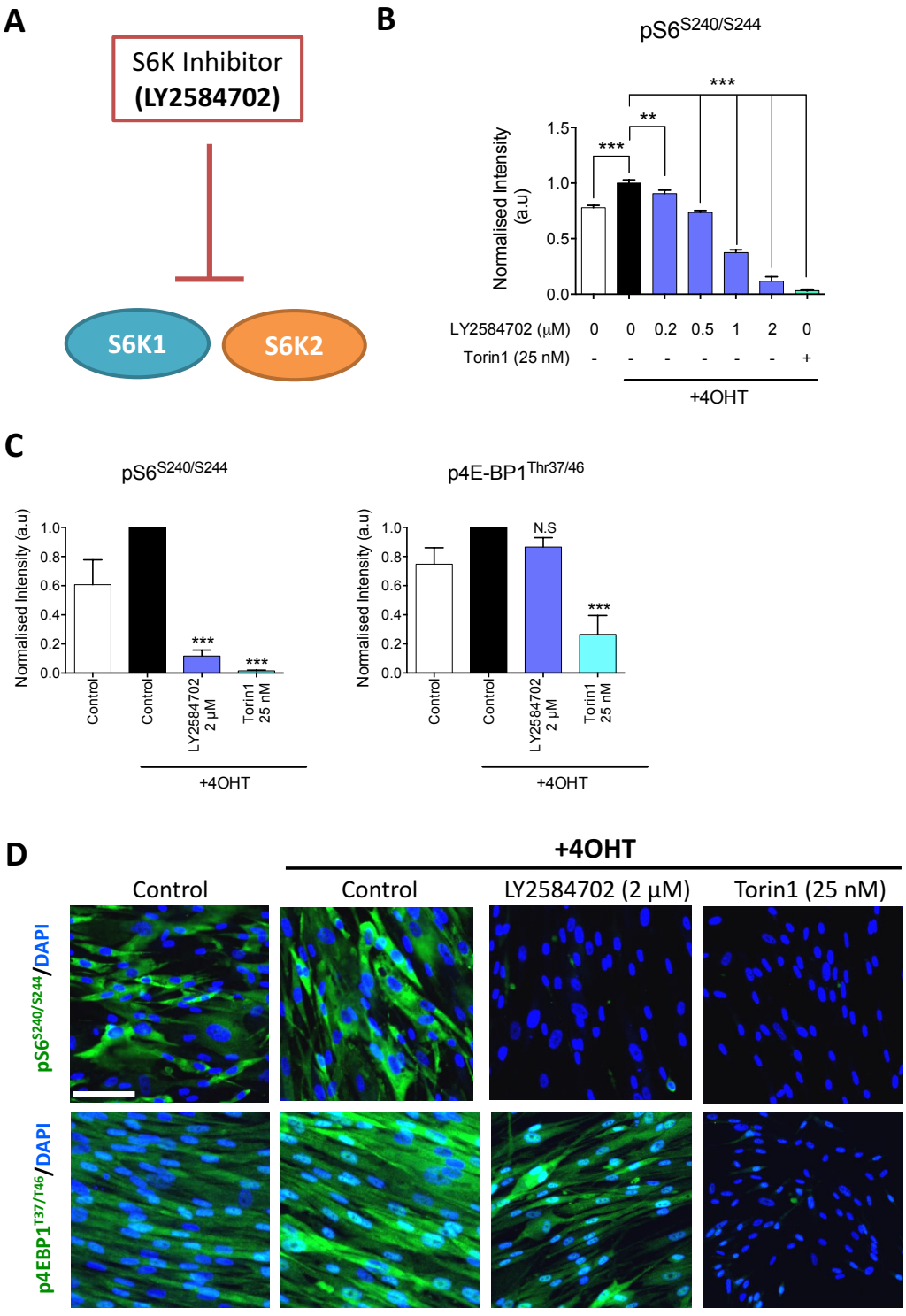

Figure 4.11. Chemical inhibition of S6 kinases in human fibroblasts.
IMR-90 ER: RAS cells were treated simultaneously with 4-hydroxytamoxifen (4OHT – 125 nM) and either the S6K1/2 inhibitor LY2584702 or Torin1 for 7 days. LY2584702 and Torin1 were replaced every 2 days. **A.** Schematic depicting LY2584702 inhibiting S6K1 and S6K2. **B.** Quantification of immunofluorescence (IF) staining for phosphorylated ribosomal protein S6 (RPS6 - S240/S244) with the indicated doses (0.2 - 2 μM) of LY2584702 or 25 nM of Torin1. Quantification shown following 7 days of 4OHT treatment. **C.** Quantification of IF staining for phosphorylated RPS6 (S240/S244) and phosphorylated eukaryotic translation initiation factor 4E binding protein 1 (4EBP1 - T37/T46) following treatment with LY2584702 (2 μM) or Torin1 (25 nM). Quantification shown following 7 days of 4OHT treatment. **D.** Representative IF images for phosphorylated RPS6 (S240/S244) and 4EBP1 (T37/T46). Data are expressed as means ± SD; n = 1 independent experiment performed in triplicate wells for B and n = 3 independent experiments for C and D. Statistical significance was calculated using one-way analysis of variance with Dunnett's multiple comparison test (** P < 0.01, *** P < 0.001). N.S: non-significant. Scale bar, 100 μm.

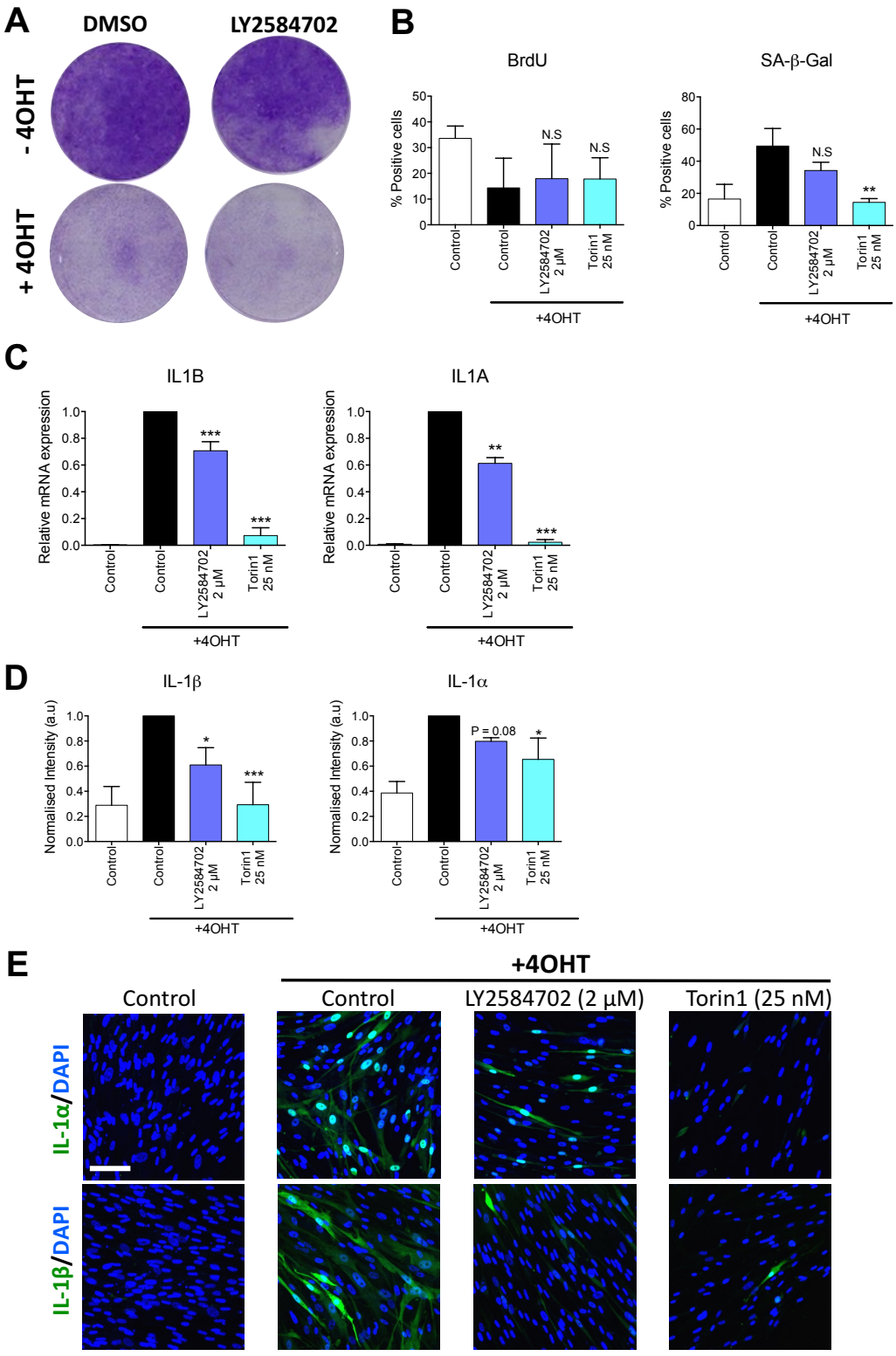

Figure 4.12. Chemical inhibition of S6 kinases attenuates IL1B and IL1A expression affecting senescence.
IMR-90 ER: RAS cells were treated simultaneously with 4-hydroxytamoxifen (4OHT – 125 nM) and either the S6K1/2 inhibitor LY2584702 or Torin1 for 7-13 days. LY2584702 and Torin1 were replaced every 2 days. **A.** Cell proliferation assessed by colony formation assay (crystal violet staining) following 13 days in culture. **B.** Quantification of immunofluorescence (IF) staining for BrdU incorporation and SA-β-Gal activity on day 7 of 4OHT treatment. **C.** Relative mRNA expression by RT-qPCR of IL1B and IL1A following 6 days of 4OHT treatment. **D.** Quantification of IF staining for IL-1β and IL-1α following 8 days of 4OHT treatment. **E.** Representative IF images for IL-1β and IL-1α. Data are expressed as means ± SD; n = 3 independent experiments. Statistical significance was calculated using one-way analysis of variance with Dunnett's multiple comparison test (* P < 0.01, ** P < 0.01, *** P < 0.001). N.S: non-significant. Scale bar, 100 μm.

4.5. Focussed screen of S6K targets to identify potential mediators of SASP regulation.

To identify potential downstream targets of S6 kinases mediating SASP regulation, we performed a focussed screen of known S6K targets that could regulate the SASP during OIS in IMR90 ER: RAS fibroblasts (Figure 4.13). We depleted these targets using either 4 siRNAs (transient knockdown) or a pool of 4 shRNAs (short hairpin RNAs – stable knockdown) targeting each gene and assessed the SASP using either high throughput microscopy or by RT-qPCR.

We first confirmed that RAS activation induced prototypic SASP factors including IL-1β and IL-8, and this induction was abolished with siRNA targeting known SASP regulators such as mTOR and c/EBPβ (Figure 4.14). As expected, siRNAs against S6K1 or S6K2 also reduced the number of IL-1β and IL-8 positive cells but to a lesser extent than depleting mTOR (Figure 4.14 B and C). Depleting the selected S6 kinase targets with siRNA or shRNA, however, did not robustly affect the SASP as expected for a mediator of S6K effects (Figure 4.14 B and C and Figures 4.15-16). Although the siRNAs targeting some of the genes such as CREM, RORC or YY1 reduced the SASP, this effect could not be confirmed with shRNA depletion of these candidate genes (Figure 4.16 and 4.17). shRNAs targeting either mTOR or interleukin-1 receptor (IL-1R) were used as positive controls for the SASP. This discrepancy could be due to differences in siRNA vs shRNA depletion (acute vs chronic) or because the effects we observe with S6K deletion is a consequence of the cumulative effects of many targets. In addition, shRNA depletion of these potential targets did not bypass the senescence growth arrest (Figure 4.17). Finally, senescence and SASP was also assessed in MEFs isolated from knockin mice for RPS6 where all the phosphorylation sites have been mutated, thus preventing RPS6 phosphorylation by S6K1/S6K2 and other kinases (Ruvinsky et al., 2005). MEFs isolated from RPS6 knockin mice, however, did not prevent replicative senescence and did not affect the SASP. *Characterisation of RPS6 knockin MEFs was done with Dr. Silvia MA Pedroni in Prof. Withers' group.*

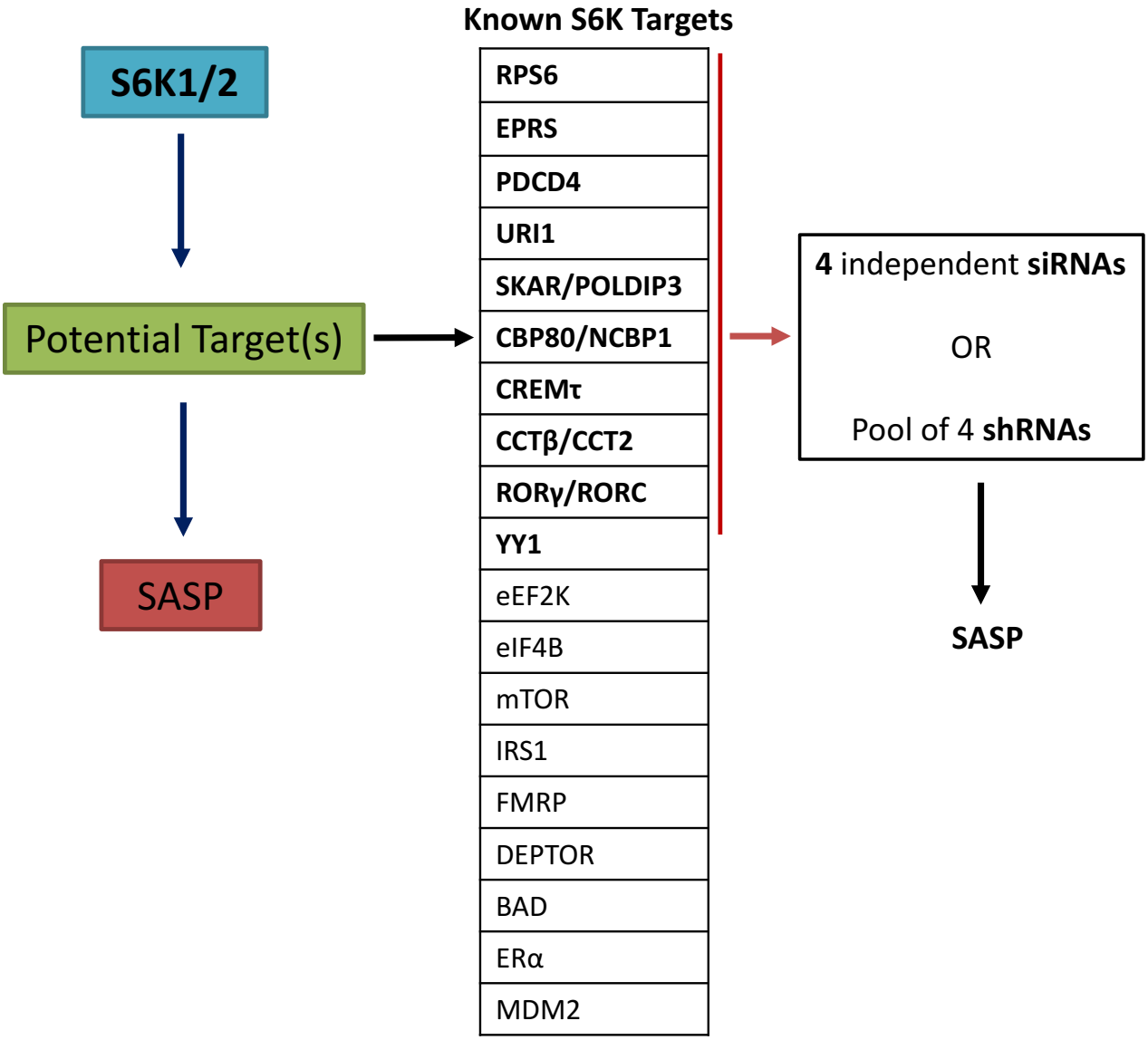

Figure 4.13. Schematic depicting the workflow for the focussed S6K target screen.
S6 kinases regulate the SASP via potential downstream targets. Several known S6K targets from the literature were depleted using either 4 independent siRNAs (small interfering RNAs) or a pool of 4 shRNAs (short hairpin RNAs) targeting each gene. The senescence-associated secretory phenotype (SASP) was then assessed by high through microscopy coupled to high content analysis (InCell Analyzer 2000) or by RT-qPCR.

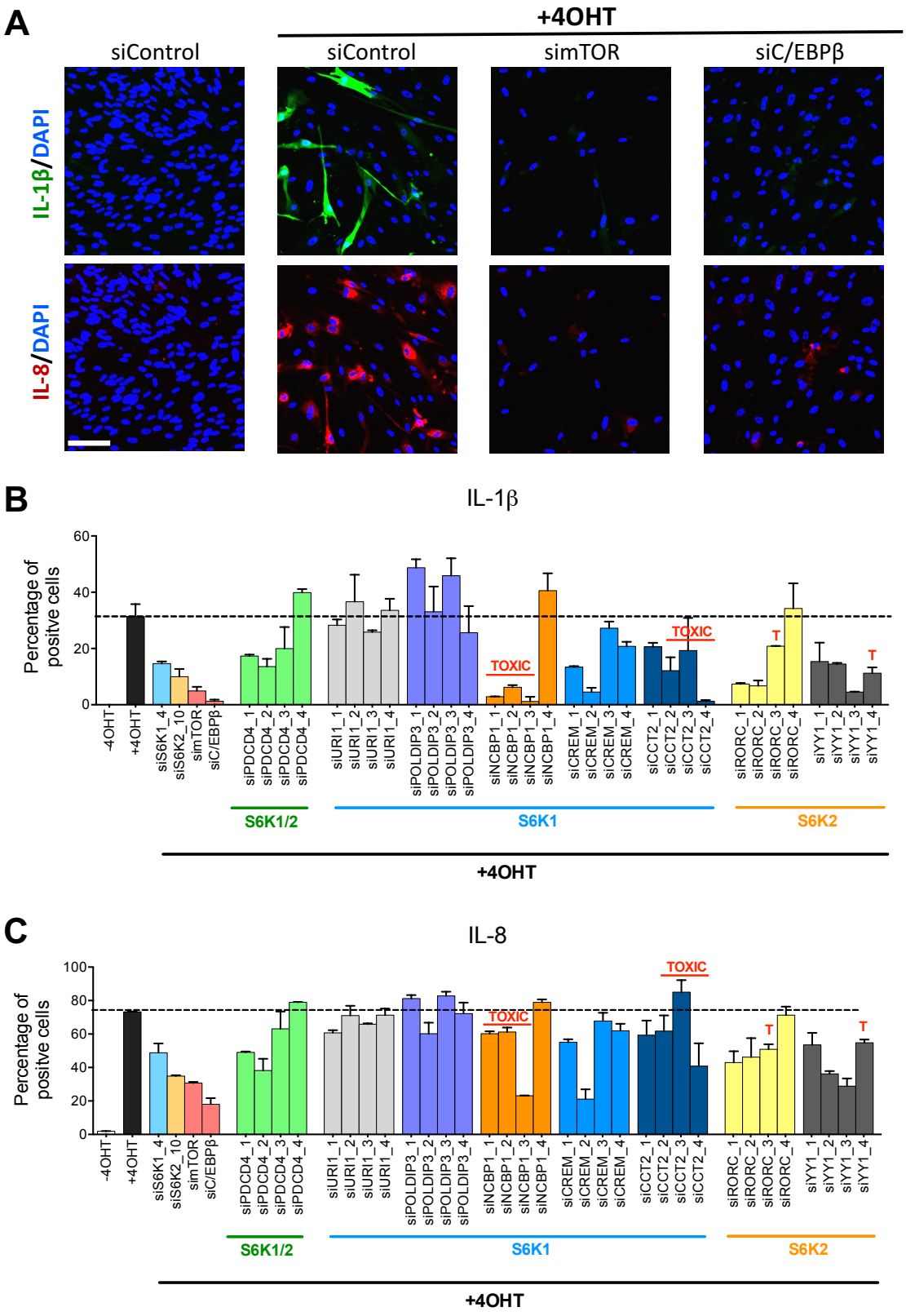

Figure 4.14. Effect of depleting S6K targets on the senescence-associated secretory phenotype (SASP).
IMR-90 ER: RAS cells were reverse transfected with either Allstars (scrambled sequence - siControl) or the indicated siRNAs. Cells were induced with 4-hydroxytamoxifen (4OHT – 125 nM) on the following day and the SASP was assessed on day 8. **A.** Representative immunofluorescence (IF) images for IL-1β and IL-8 upon RAS activation and when depleting mTOR or C/EBPβ. **B.** Quantification of IF staining for IL-1β and IL-8 following 8 days of 4OHT treatment. Quantification by high-throughput microscopy and high-content analysis. Data are expressed as means ± SD performed in duplicate wells of a single experiment. Representative of 2 independent experiments. T: toxic. Scale bar, 100 μm.

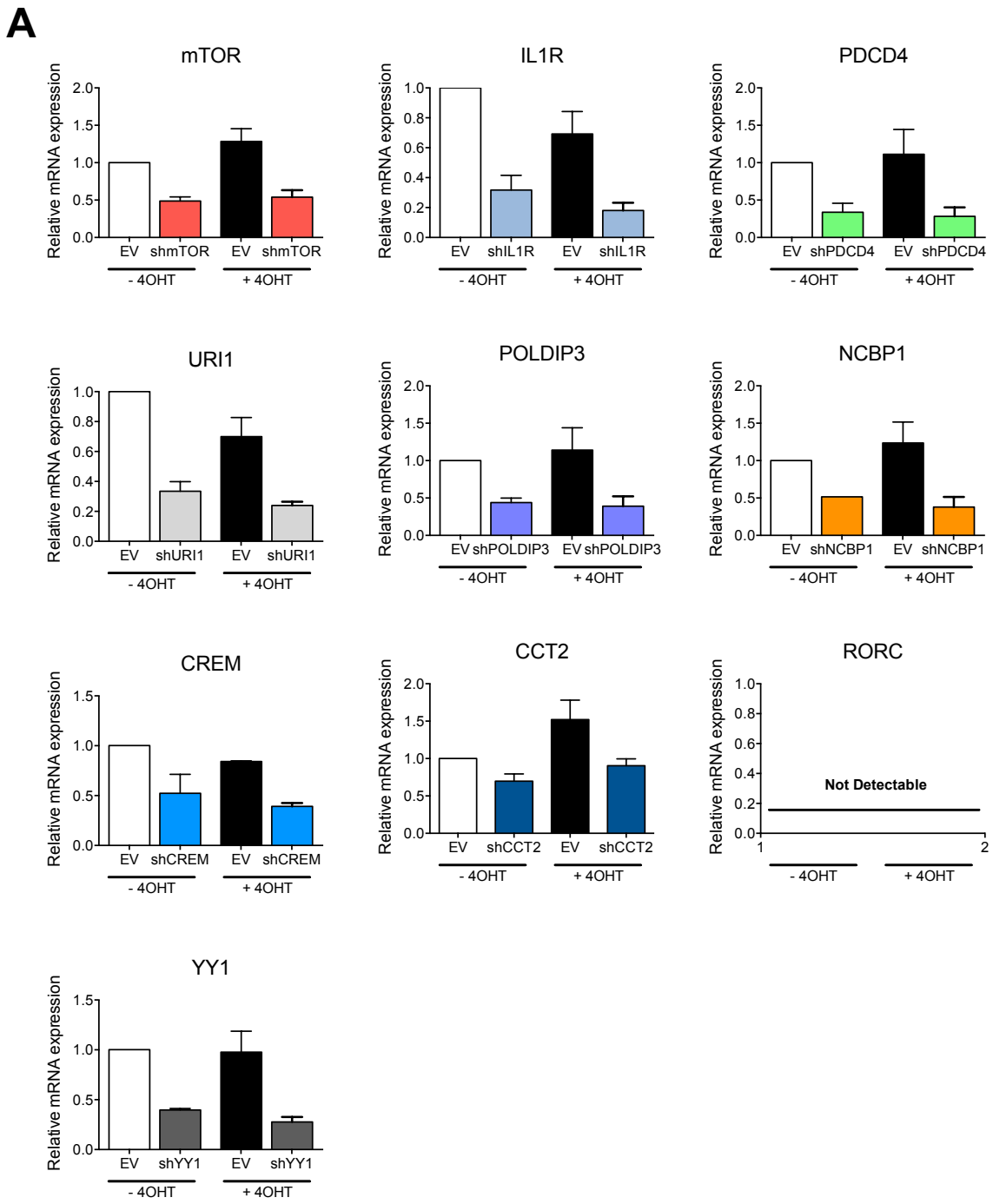

Figure 4.15. Confirmation of knockdown of S6K targets.
IMR90 ER: RAS fibroblasts were transduced with either empty vector (EV) or a pool of 4 shRNAs (short hairpin RNAs) targeting each gene. **A.** Relative mRNA expression by RT-qPCR of mTOR, IL1R, PDCD4, URI1, POLDIP3, NCBP1. CREM, CCT2, RORC and YY1 following treatment with or without 4-hydroxytamoxifen (4OHT – 125 nM) for 6 days. Data are expressed as mean ± SD; n = 2 independent experiments.

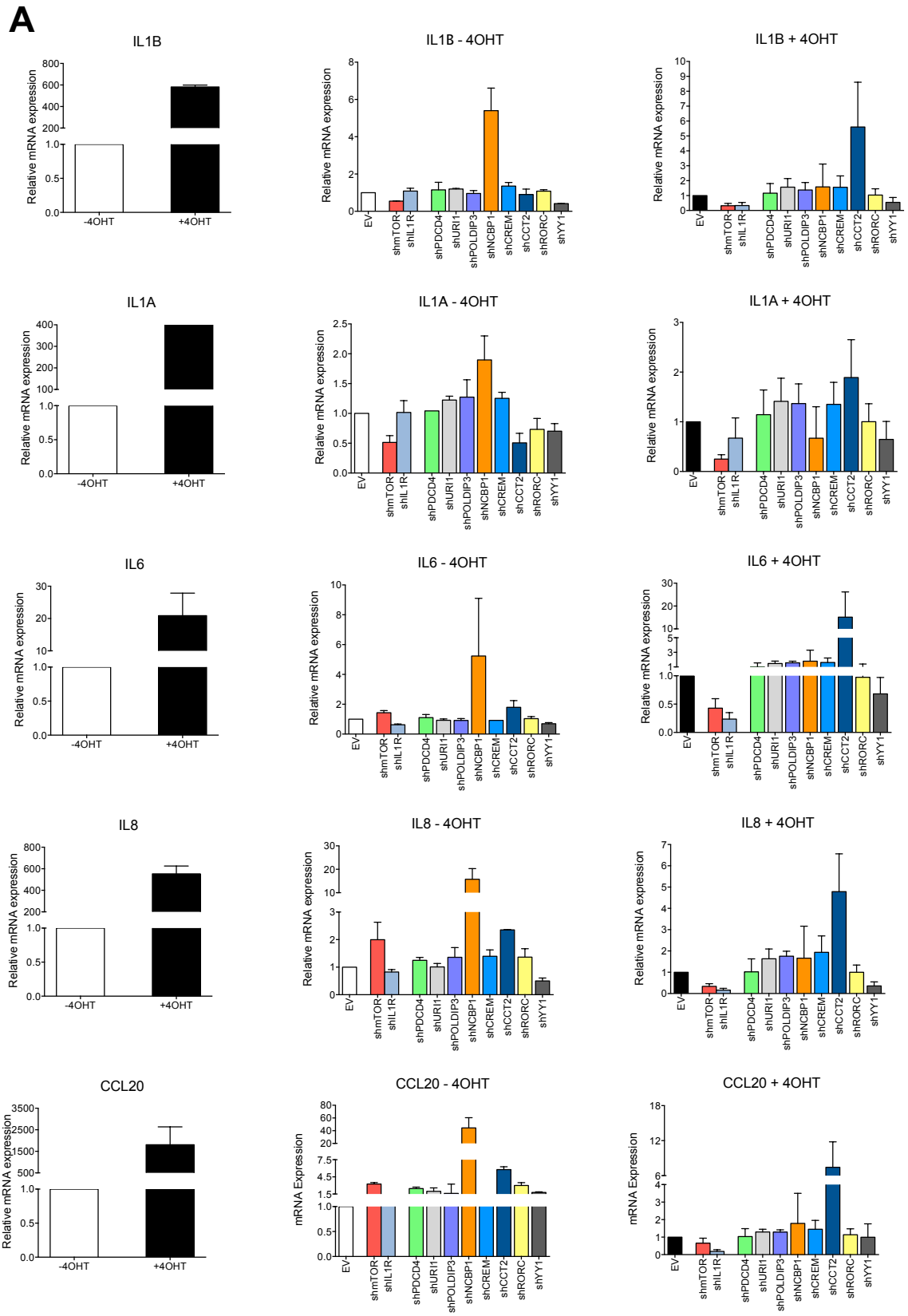

Figure 4.16. Knockdown of S6K targets does not attenuate the senescence secretome. IMR90 ER: RAS fibroblasts were transduced with either empty vector (EV) or a pool of 4 shRNAs (short hairpin RNAs) targeting the indicated genes. **A.** Relative mRNA expression by RT-qPCR of IL1B, IL1A, IL6, IL8 and CCL20 following treatment with or without 4-hydroxytamoxifen (4OHT – 125 nM) for 6 days. **Left:** induction of senescence-associated secretory phenotype (SASP) following treatment with 4OHT. **Middle:** Effect of depleting S6K targets on the SASP in IMR90 ER: RAS fibroblasts without 4OHT treatment (growing cells). **Right:** Effect of depleting S6K targets on the SASP in IMR90 ER: RAS fibroblasts with 4OHT treatment (senescence). Data are expressed as mean ± SD; n = 2 independent experiments.

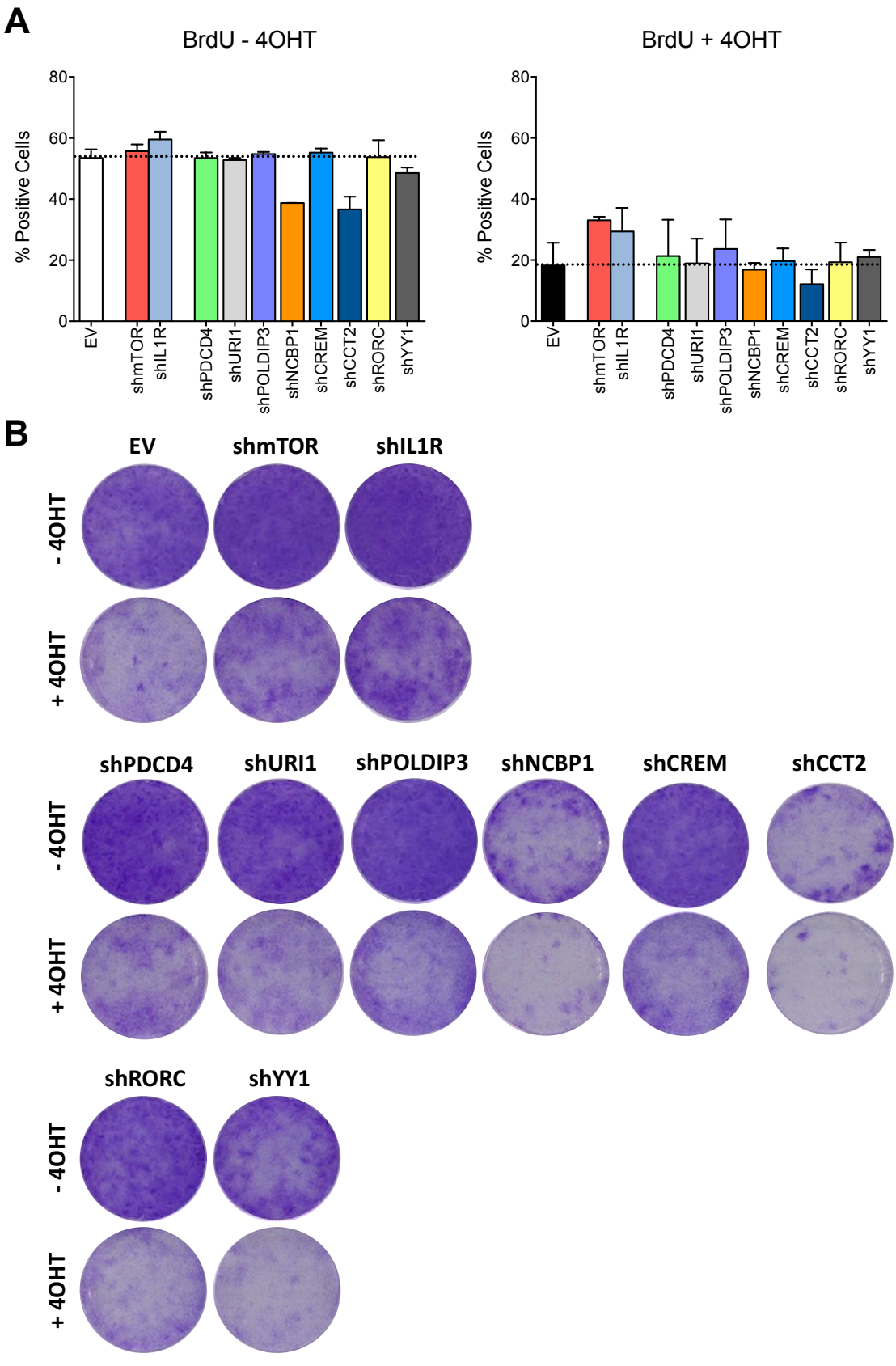

Figure 4.17. Knockdown of S6K targets does not bypass senescence.
IMR90 ER: RAS fibroblasts were transduced with either empty vector (EV) or a pool of 4 shRNAs (short hairpin RNAs) targeting the indicated genes. **A.** Quantification of immunofluorescence (IF) staining for BrdU incorporation following 6 days of treatment with or without 4-hydroxytamoxifen (4OHT – 125 nM). Quantification by high-throughput microscopy and high-content analysis. **B.** Cell proliferation assessed by colony formation assay (crystal violet staining) following 13 days in culture with or without 4-hydroxytamoxifen (4OHT – 125 nM). Data are expressed as mean ± SD; n = 2 independent experiments.

4.6. Knockdown of EPRS (glutamyl-prolyl-tRNA synthetase) induced senescence and the SASP.

The recently identified S6K1 target EPRS has been implicated in regulating mammalian lifespan and adiposity (Arif et al., 2017). Importantly, the authors showed that S6K1 regulates a non-canonical function of EPRS by phosphorylating the S999 residue, which in adipocytes causes EPRS to bind FATP1 (fatty acid transport protein 1 – also called SLC27A1) and regulate fatty acid uptake (Figure 4.18). Thus, EPRS S999A phospho-deficient mice have lower body weight similar to *S6K1*$^{-/-}$ mice (Arif et al., 2017; Selman et al., 2009). What was surprising, however, was that EPRS S999A homozygous mice did not show any differences in systemic inflammation considering the other non-canonical role of EPRS in the GAIT (IFN-γ-activated inhibitor of translation) complex (Arif et al., 2017). Nevertheless, we investigated whether EPRS regulates cellular senescence and the SASP considering it is the only known downstream target of S6K1 that regulates lifespan and healthspan.

Knockdown of EPRS was first confirmed using 4 independent shRNAs (Figure 4.19 A). Interestingly, EPRS knockdown induced mRNA expression of IL6 and IL8 in IMR90 ER: RAS fibroblasts even without stimulating senescence with 4OHT or in other words in growing cells (Figure 4.19 B). In addition, EPRS depletion further increased mRNA expression of IL6 and IL8 as well as IL1A and IL1B in cells undergoing OIS (Figure 4.19 B). Furthermore, EPRS knockdown also induced a striking growth arrest as observed by colony formation assay, cell count and BrdU incorporation (Figure 4.20). Importantly, the growth arrest was markedly stronger than depletion of mTOR (Figure 4.20).

It is imperative to note that EPRS is part of the tRNA synthetase complex; it is therefore feasible that knocking down EPRS induces such a striking growth arrest. It is equally important to mention that EPRS primarily regulated IL6 and IL8 expression, suggesting that there is still some specificity in its regulation. In fact the GAIT complex primarily regulates translation of inflammatory mRNAs containing a GAIT element within their 3' untranslated region (Mukhopadhyay et al., 2009). Given the feedback loops associated with the SASP, it is also not surprising that we observed a striking effect on the mRNA level of IL6 and IL8 when depleting EPRS. Nevertheless, it is unlikely that the reduction in inflammation observed in *S6K1*$^{-/-}$ mice or MEFs is due to loss of EPRS phosphorylation given the directionality of the effects we have observed with EPRS knockdown and that the EPRS S999A mice do not have a reduction in inflammation in ageing. Although we cannot completely rule out any involvement of EPRS considering we have taken a knockdown approach as opposed to using an EPRS S999A phosphomutant, it is likely that S6K1/2 also regulate these proinflamamtory factors in a phosphorylation-independent manner since we observed a stronger effect with *S6K1*$^{-/-}$*: S6K2*$^{-/-}$ MEFs compared to S6K1/2 inhibition with LY2584702, but this would require follow-up experiments to confirm.

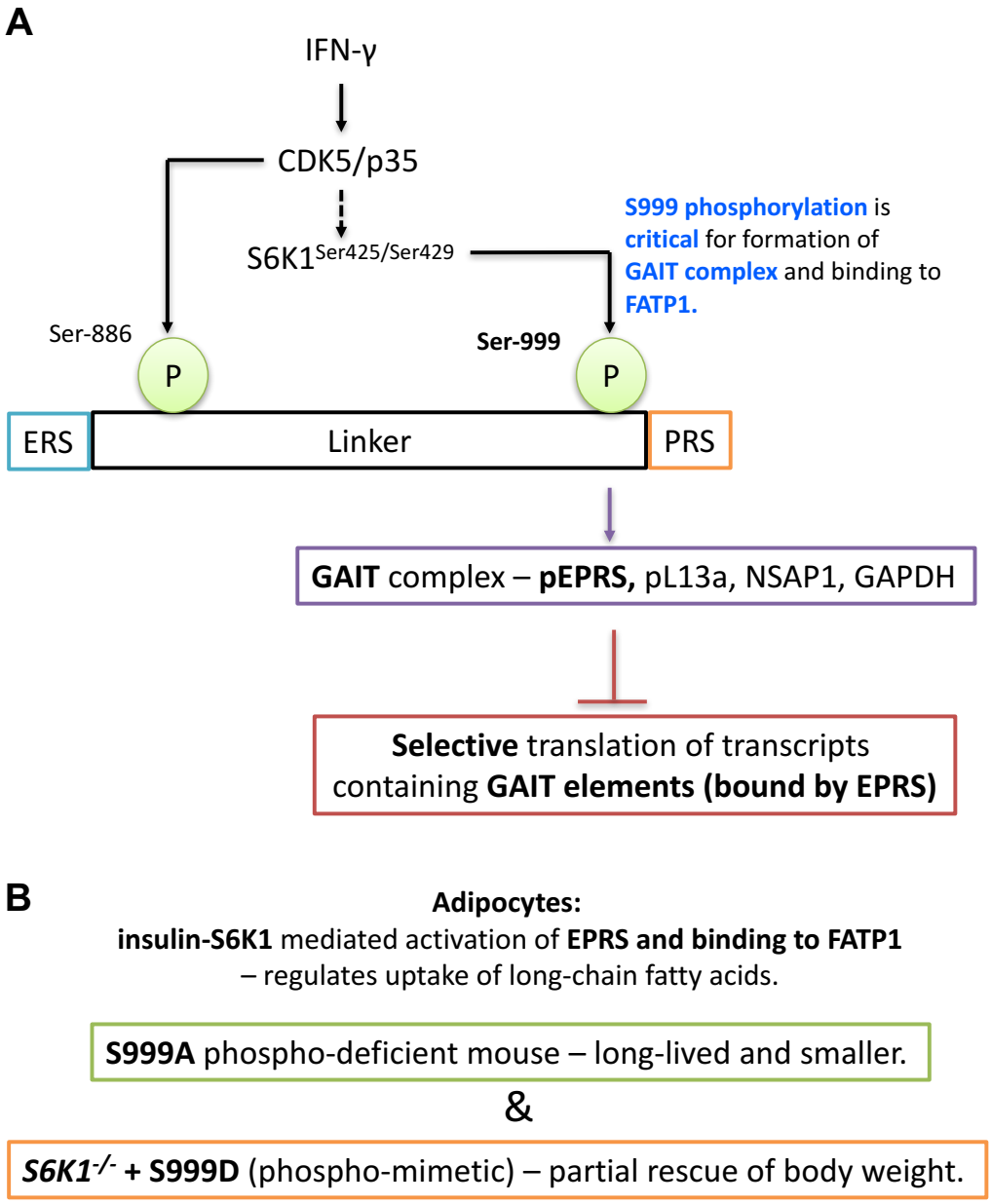

Figure 4.18. Schematic depicting the activation of EPRS.
A. Interferon-γ (IFN-γ) induces phosphorylation and activation of EPRS (glutamyl-prolyl-tRNA synthetase) through CDK5/p35 kinase and S6K1 in peripheral blood monocytes. S6K1 phosphorylates EPRS at S999 residue, which releases EPRS from the tRNA synthetase complex and allows execution of non-canonical functions including formation of the GAIT (IFN-γ-activated inhibitor of translation) complex. The GAIT complex comprises of EPRS, ribosomal protein L13a (L13a), NS1-associated protein (NSAP1) and glyceraldehyde 3-phosphate dehydrogenase (GAPDH). The GAIT complex selectively inhibits translation of transcripts containing a GAIT element including VEGF-A (vascular endothelial growth factor A) and CCL22 (C-C motif chemokine ligand 22). **B.** In adipocytes, insulin-S6K1 mediated activation of EPRS allows binding to FATP1 (fatty acid transporter protein 1) and regulation of long-chain fatty acid uptake. EPRS S999A phospho-deficient mice are long-lived and are smaller. Crossing *S6K1*$^{-/-}$ mice with EPRS S999D phospho-mimetic mice partially rescues body weight. Adapted from (Arif et al., 2017; Selman and Withers, 2017).

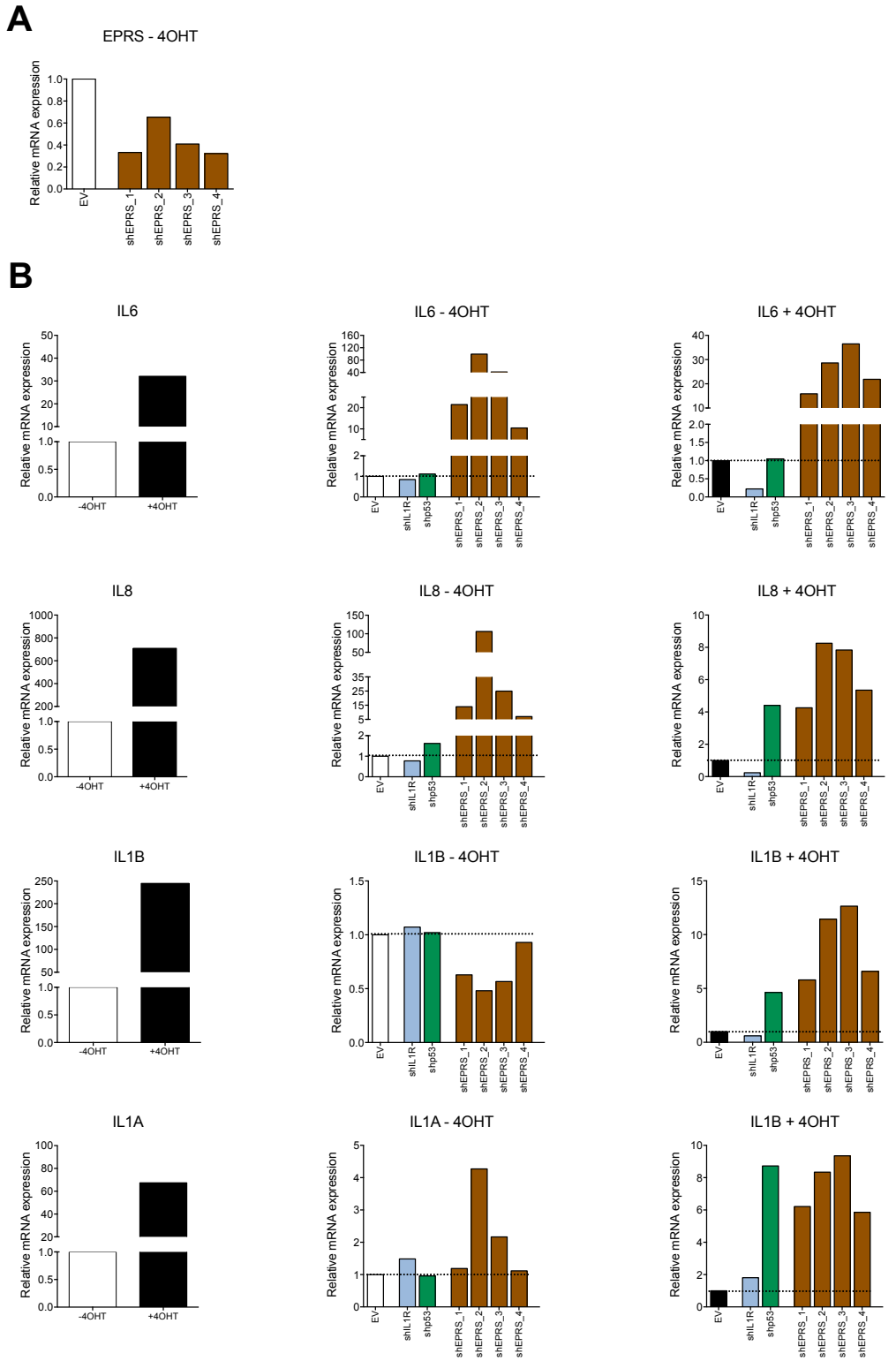

Figure 4.19. shRNA mediated depletion of EPRS robustly induces IL6 and IL8 mRNA expression.
IMR90 ER: RAS fibroblasts were transduced with empty vector (EV) or shRNAs against EPRS. shRNAs against interleukin-1 receptor (IL-1R) or p53 were used as positive controls. Cells were induced with or without 4-hydroxytamoxifen (4OHT – 125 nM) and the SASP was assessed on day 6. **A.** Confirmation of EPRS knockdown in growing (- 4OHT) cells using RT-qPCR. **B.** Relative mRNA expression by RT-qPCR of IL6, IL8, IL1A and IL1B on day 6 following cell seeding. **Left:** induction of senescence-associated secretory phenotype (SASP) following treatment with 4OHT. **Middle:** effect of depleting EPRS on the SASP in IMR90 ER: RAS fibroblasts without 4OHT treatment (growing cells). **Right:** Effect of depleting EPRS on the SASP in IMR90 ER: RAS fibroblasts with 4OHT treatment (senescence). Data are expressed as mean ± SD; n = 1 independent experiment performed with 4 independent shRNAs against EPRS. shRNA: short hairpin RNA.

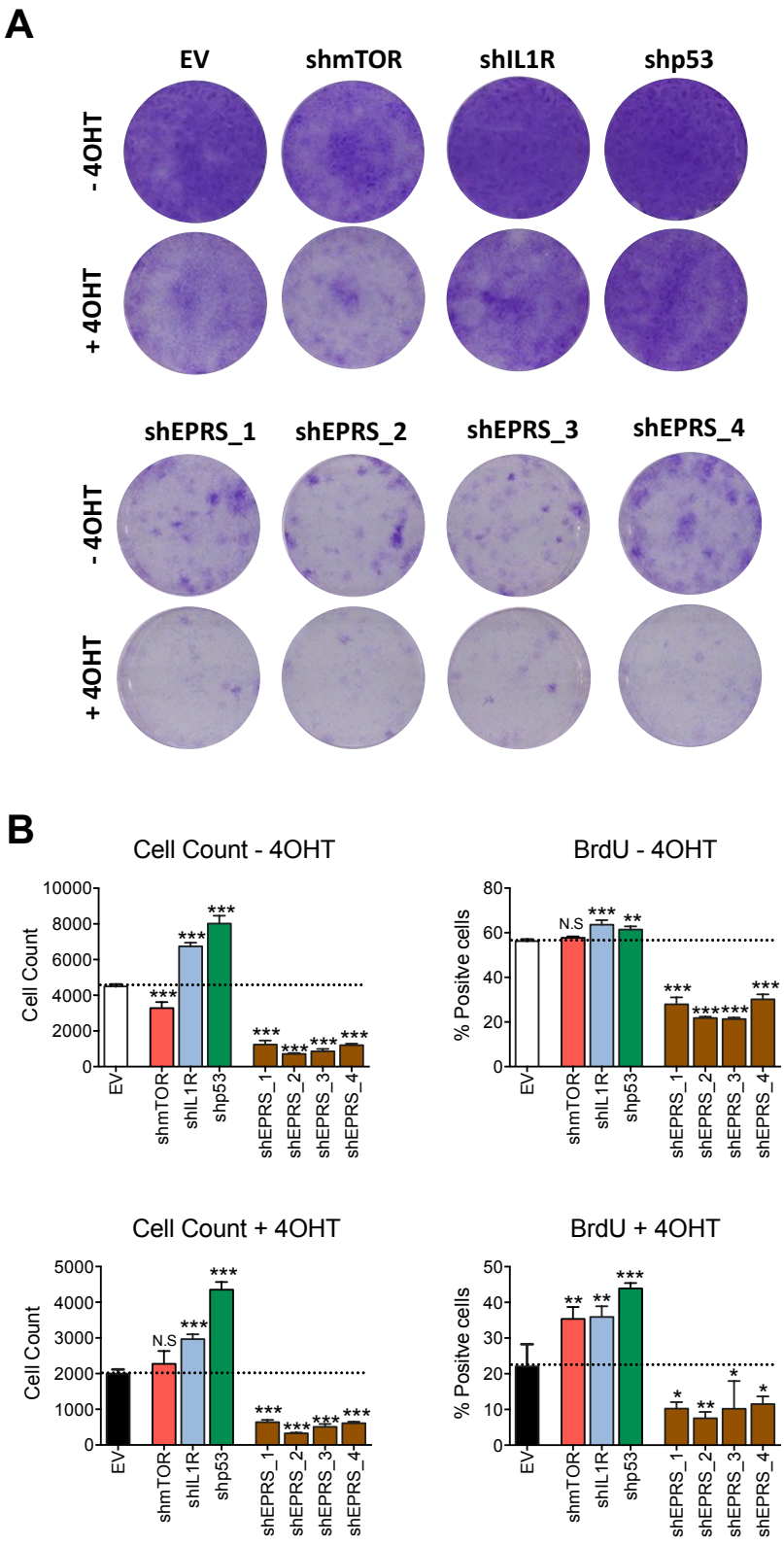

Figure 4.20. shRNA mediated depletion of EPRS induces a striking growth arrest.
IMR90 ER: RAS fibroblasts were transduced with empty vector (EV) or shRNAs against EPRS. shRNAs against mTOR, interleukin-1 receptor (IL-1R) or p53 were used as positive controls. Cells were induced with or without 4-hydroxytamoxifen (4OHT – 125 nM) for 6-13 days. **A.** Cell proliferation assessed by colony formation assay (crystal violet staining) following 13 days in culture with or without 4-hydroxytamoxifen (4OHT – 125 nM). Depletion of IL-1R or p53 were used as controls of senescence bypass. **B.** Quantification of immunofluorescence (IF) staining for DAPI (cell count) and BrdU incorporation following 6 days of treatment with or without 4OHT. Quantification by high-throughput microscopy and high-content analysis. Data are expressed as mean ± SD; n = 1 independent experiment performed in triplicates with 4 independent shRNAs against EPRS.

4.7. Summary.

S6K1 and/or S6K2 deletion in MEFs did not prevent replicative senescence but attenuated induction of *Il1b* and *Il1a* expression. This was confirmed in cells undergoing oncogene-induced senescence in both MEFs and in primary human fibroblasts with either siRNA depletion or chemical inhibition of S6 kinases, suggesting that this is a conserved effect of S6 kinases in multiple forms of senescence. A focused screen of S6K targets did not identify any potential candidates that could mediate the effects of S6 kinases in regulation of the SASP. Furthermore, knockdown of EPRS, a recently identified downstream target of S6K1, rather induced a striking growth arrest and increased expression of IL6 and IL8. Nonetheless, we have taken a knockdown approach for EPRS whereas S6K1 specifically regulates translocation of EPRS from the tRNA synthetase complex to the GAIT complex. Therefore, an alternative approach would be to overexpress the EPRS S999A phosphomutant that cannot be phosphorylated by S6K1 and thus preventing EPRS translocation to the GAIT complex and then to determine whether this impacts SASP expression.

Importantly, we have only looked at how S6 kinases regulate a specific subset of proinflammatory factors, but to understand the extent of SASP regulation by S6 kinases, global approaches utilising either an antibody array or mass spectrometry analysis of the conditioned medium of senescent cells and cells depleted of S6 kinases can be carried out. The SASP promotes paracrine senescence in normal cells or proliferation and invasion in tumoural cells. Therefore, to understand whether the SASP regulated by S6 kinases has a functional consequence, we can test the conditioned medium from senescent cells depleted of S6 kinases in their ability to promote paracrine senescence or tumorigenesis.

We have yet to elucidate the mechanisms by which S6 kinases regulate the SASP. Although difficult to compare directly, deletion of S6K1 and S6K2 in MEFs had a stronger effect on the SASP than chemical inhibition of S6 kinases, suggesting a non-catalytic activity to be important for SASP regulation. Breeding colonies of S6K1 kinase dead mice are now established in Professor Withers' laboratory. Therefore, we aim to isolate MEFs from these mice and determine whether they regulate senescence and the SASP. This will allow us to dissect whether the catalytic domain of S6K1 plays an essential role in SASP regulation.

Several global approaches can be carried out to identify potential downstream targets of S6 kinases mediating SASP expression. Since S6K1 is a kinase and that we still cannot rule out involvement of the kinase activity, global phosphoproteomics of MEFs isolated from *S6K1*$^{-/-}$, *S6K2*$^{-/-}$ and *S6K1*$^{-/-}$*: S6K2*$^{-/-}$ mice undergoing senescence can be done. Alternatively, S6K1 and/or S6K2 can be overexpressed in cells undergoing senescence followed by immunoprecipitation of S6 kinases and mass spectrometry to identify any potential interactors that could be mediating the

effects of S6 kinase on the SASP. Otherwise, S6K1 and/or S6K2 could be overexpressed in an S6K1 or S6K2 null background and RNA-sequencing performed at early time points (30 minutes to 6 hours) to identify pathways or transcription factors that are upregulated, as these could be potential mechanisms of SASP regulation by S6 kinases.

Chapter 5: Liver-specific deletion of S6K1 and S6K2 induces a sexually dimorphic response in a model of non-alcoholic steatohepatitis (NASH).

5.1. Introduction.

The prevalence of non-alcoholic fatty liver disease (NAFLD) and the more severe NASH are rising due to increased numbers of obesity, type-2 diabetes and an ageing population (Hardy et al., 2016). NASH is a risk factor for the development of hepatocellular carcinoma (HCC), which is the most common malignancy of the liver and a leading cause of cancer-related deaths (El-Serag and Kanwal, 2014). Nevertheless, the underlying mechanisms of NASH and NASH-driven HCC are still not completely understood. In addition, there is no approved treatment for end-stage liver cancer in the United Kingdom, thus there is a need for the identification of novel treatments for this debilitating disease (Wong et al., 2016). It has been previously shown that the ribosomal protein S6 kinases (S6K1 and S6K2) are critical regulators of cell growth, proliferation and metabolism (Magnuson et al., 2012). Furthermore, abrogation of S6K1 alone, in combination with S6K2 globally (mixed background) or liver-specific depletion of S6K1 and S6K2 by adeno-associated viruses (AAVs) protects against metabolic dysfunction in response to a high-fat diet (HFD) (Bae et al., 2012; Castañeda et al., 2012; Hee Um et al., 2004). It is not yet known, however, whether S6 kinases are important for regulation of diet-induced liver fibrosis and cancer. Therefore, given the close link between obesity, hepatic steatosis and cancer, we aimed to assess the effect of specifically deleting S6K1 and S6K2 in the liver in a diet-induced model of NASH and HCC.

5.2. Characterisation of mice with liver specific deletion of S6K1 and S6K2.

To functionally investigate the role of S6 kinases in NASH and NASH-driven HCC, we generated mice with liver-specific deletion of S6K1 and S6K2 (Figure 5.1 A). Breeding colonies of mice with homozygosity for the floxed allele of S6K1 and S6K2 were already established in Professor Withers' laboratory, and from here on these mice will be referred to as either "control" or *S6K1$^{fl/fl}$: S6K2$^{fl/fl}$* mice. Importantly, *S6K1$^{fl/fl}$: S6K2$^{fl/fl}$* mice were phenotypically indistinguishable from C57BL/6 WT mice. *S6K1$^{fl/fl}$: S6K2$^{fl/fl}$* mice were subsequently bred with mice expressing cre-recombinase driven by the albumin promoter to specifically delete S6K1 and S6K2 in the liver, namely in hepatocytes and cholangiocytes. Specific deletion of S6K1 and S6K2 in the liver was confirmed by genotyping and immunoblotting, and from here on these mice will be referred to as *S6K1$^{-/-}$: S6K2$^{-/-}$* mice (Figure 5.2 B and C). Importantly, phosphorylation of RPS6 (S240/S244) was drastically reduced in the whole liver with S6K1 and S6K2 deletion, thus providing a functional readout of the deletion (Figure 5.2 B and C). This was not a complete ablation since S6K1 and S6K2 were not deleted from all liver cells such as the hepatic stellate cells and in any infiltrated immune cells, but for simplicity, this will be referred to as liver-specific deletion of S6K1 and S6K2.

Global S6K1 and S6K2 deletion in a C57BL/6 background is embryonic lethal after 13.5 days, and given the importance of the liver in glucose homeostasis and other processes, we first aimed to confirm that liver-specific deletion of S6K1 and S6K2 does not yield undesirable metabolic phenotypes prior to feeding the mice with an HFD. *S6K1*$^{-/-}$*: S6K2*$^{-/-}$ mice, however, did not show any significant differences in their body weight, fat/lean mass ratio (EchoMRI), glucose or insulin tolerance or in their fed (only mildly in females) or fasted glucose levels in either sex compared to age-matched littermate *S6K1*$^{fl/fl}$*: S6K2*$^{fl/fl}$ controls (Figure 5.2 and 5.3). Overall, liver-specific deletion of S6K1 and S6K2 are metabolically indistinguishable from their littermate controls when fed a chow diet.

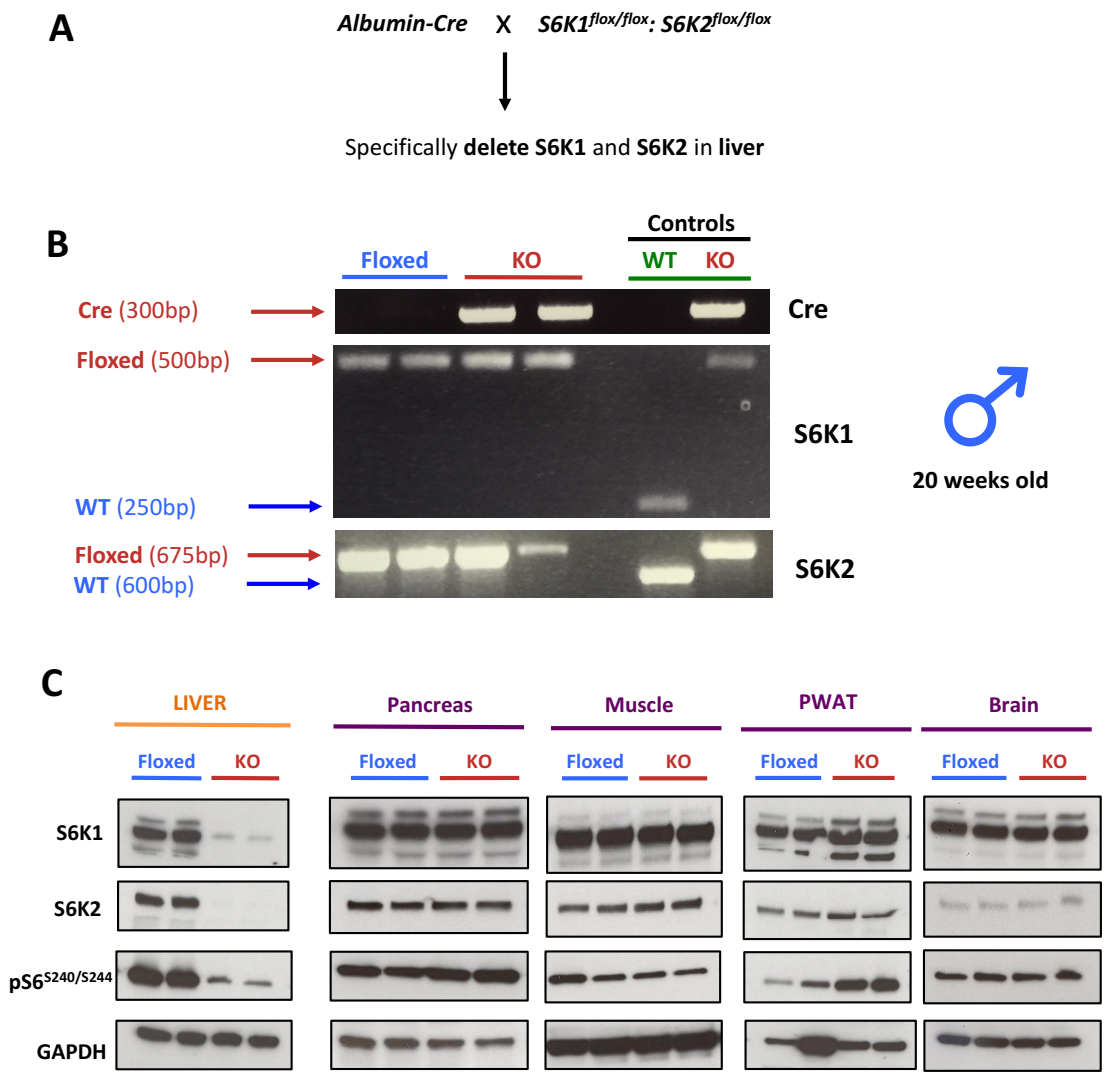

Figure 5.1. Generation of mice with liver-specific deletion of S6K1 and S6K2.
A. Schematic illustrating generation of mice with liver-specific deletion of S6K1 and S6K2 by breeding *S6K1*$^{fl/fl}$*: S6K2*$^{fl/fl}$ mice with mice expressing cre-recombinase driven by the albumin promoter. **B.** Representative PCR analysis from a tail tip for cre-recombinase as well as S6K1 and S6K2 floxed (top) and WT (bottom) alleles in 20-week-old male mice. **C.** Representative immunoblot analysis of S6K1, S6K2, pS6$^{S240/S2440}$ and GAPDH expression in whole lysates from liver, pancreas, muscle, perigonadal white adipose tissue (PWAT) and brain from S6K1 and S6K2 floxed and knockout mice. n = 2 mice per genotype.

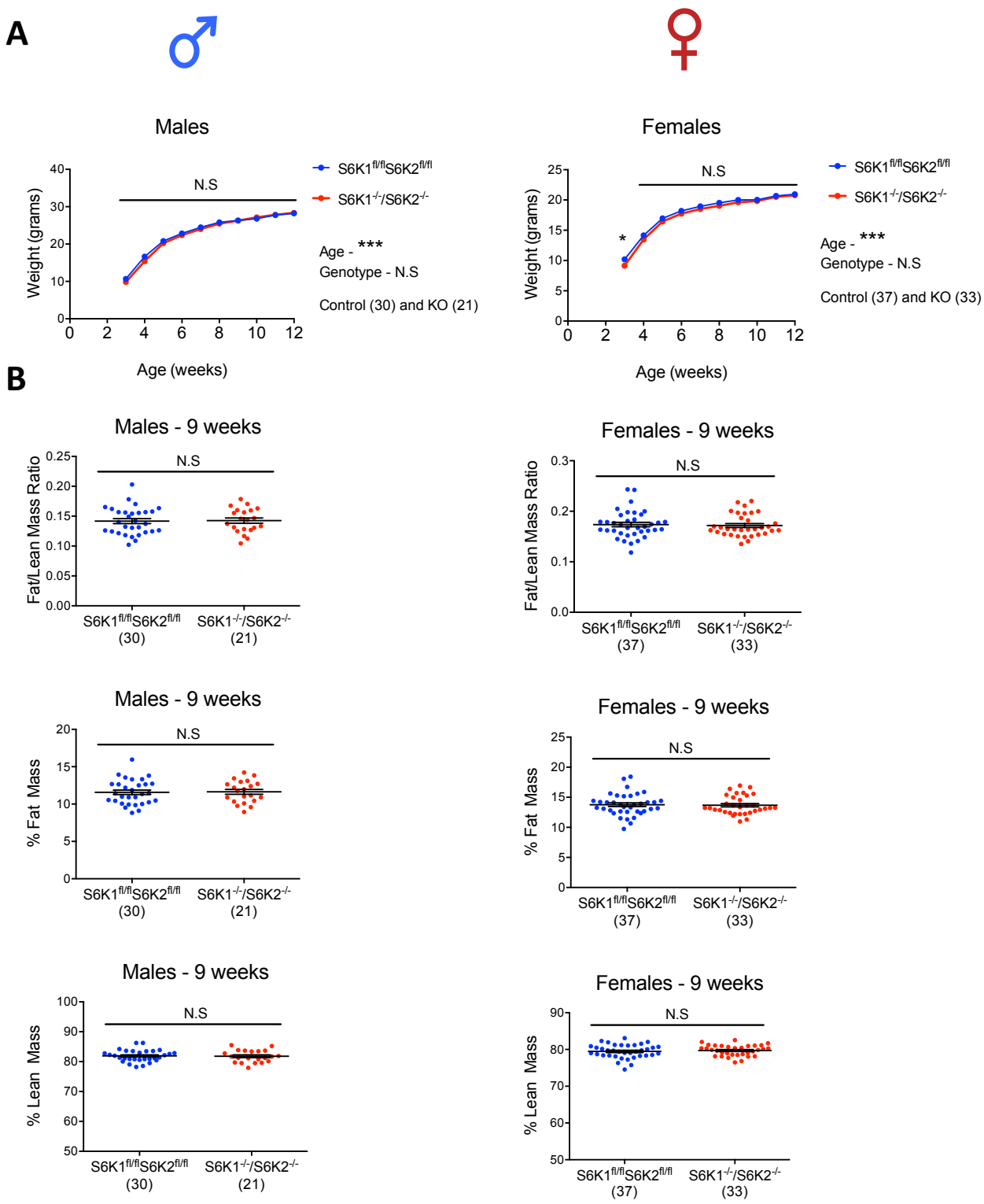

Figure 5.2. Liver-specific S6K1 and S6K2 deletion does not affect body weight or fat mass in male and female chow-fed mice.
A. Bodyweight curves from 3-12 weeks of male (left) and female (right) S6K1 and S6K2 floxed and knockout mice. **B.** EchoMRI analysis of male (left) and female (right) S6K1 and S6K2 floxed and knockout mice at 9 weeks of age. Fat/lean mass ratio (top), % fat mass (middle) and % lean mass (bottom). Data are expressed as mean ± SEM and number of mice used is indicated directly on all graphs. Statistical significance was calculated using either repeated two-way repeated-measures analysis of variance with Sidak's multiple comparison test (A) or unpaired student's t-test (B) (* $P < 0.05$, ** $P < 0.01$, *** $P < 0.001$). N.S: non-significant.

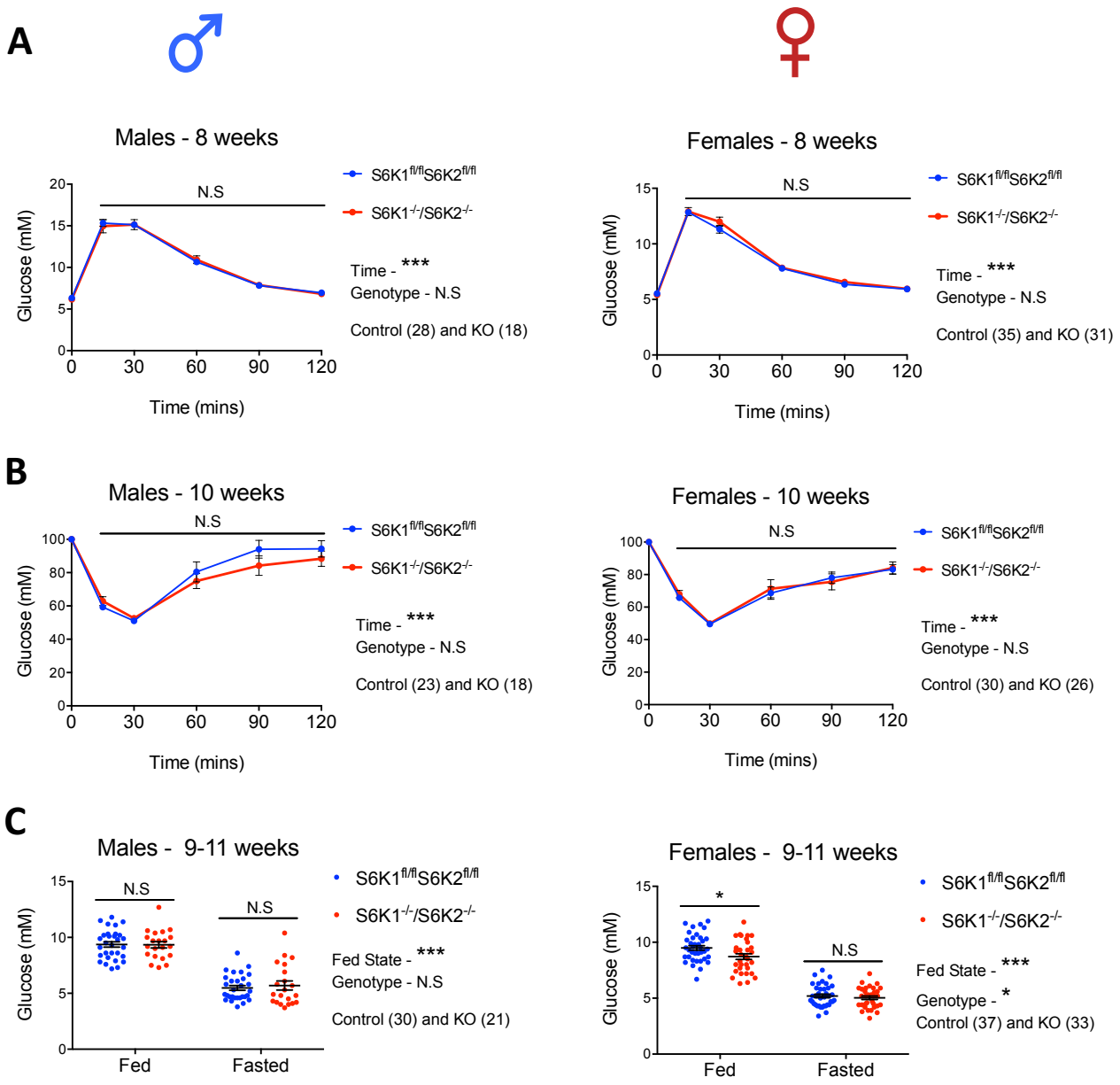

Figure 5.3. Liver-specific S6K1 and S6K2 deletion does not affect glucose homeostasis in male and female chow-fed mice.
A. Glucose-tolerance tests in male (left) and female (right) S6K1 and S6K2 floxed and knockout mice at 8 weeks of age. **B.** Insulin-tolerance tests in male (left) and female (right) S6K1 and S6K2 floxed and knockout mice at 10 weeks of age. **C.** Fed and fasted blood glucose levels (mM) in male (left) and female (right) S6K1 and S6K2 floxed and knockout mice at 9-11 weeks of age. Data are expressed as mean ± SEM and number of mice used is indicated directly on all graphs. Statistical significance was calculated using either two-way repeated-measures analysis of variance with Sidak's multiple comparison test (A and B) or two-way analysis of variance with Tukey's multiple comparison test (C) (* $P < 0.05$, *** $P < 0.001$). N.S: non-significant.

5.3. A diet rich in transaturated fat, fructose and cholesterol (HTF – high trans-fat) to induce NASH.

There is currently no murine model of NASH that fully resembles the human disease, but several genetic and diet-induced models exist that partially recapitulates some aspects of the pathology (Hardy et al., 2016). We were interested in using a diet-induced model of NASH that induces liver fibrosis because fibrosis is not only present in 80-90% of patients with HCC but is also considered one of the major risk factors for development of HCC (Hardy et al., 2016; Hashimoto et al., 2009). A common diet-induced model of NASH is the methionine-choline deficient (MCD) diet because of its short time-span and the severity of fibrosis induction, but this is far from perfect since the mice generally become severely ill with rapid loss of weight and do not become insulin resistant (Hardy et al., 2016). A diet utilising a combination of transaturated fat (40% fat – mostly primex), fructose (20%) and cholesterol (2%), however, robustly induced many characteristics of NASH including obesity, inflammation and fibrosis, as well as hepatic steatosis and ballooning degeneration when given to mice for 30 weeks (Clapper et al., 2013). The diet has been independently validated by three recent studies to induce many aspects of human NASH according to the now widely recognised clinical-histological derived classification system developed by Kleiner *et al* (Honda et al., 2017; Kleiner et al., 2005; Kristiansen et al., 2016; McCommis et al., 2017). This diet is termed the AMLN/HTF-C diet or in this study will be referred to as the high trans-fat (HTF) diet.

Once metabolic characterisation of the mice on a chow diet was done, both the control and knockout mice from 16 weeks of age were fed either the chow or HTF diet for 30 weeks (Figure 5.4). Importantly, the mice were 16 weeks of age when the treatment began, thus we were studying adult onset obesity and hepatic dysfunction. Equally, both sexes were used for the study given some of the known sexual differences in the global S6K1 knockout mice. The mice were metabolically phenotyped after 20 weeks of the diet. Following 10 further weeks on the specific diet (30 weeks in total), the mice were culled and assessed for liver functional tests, as well as liver damage, fibrosis and inflammation.

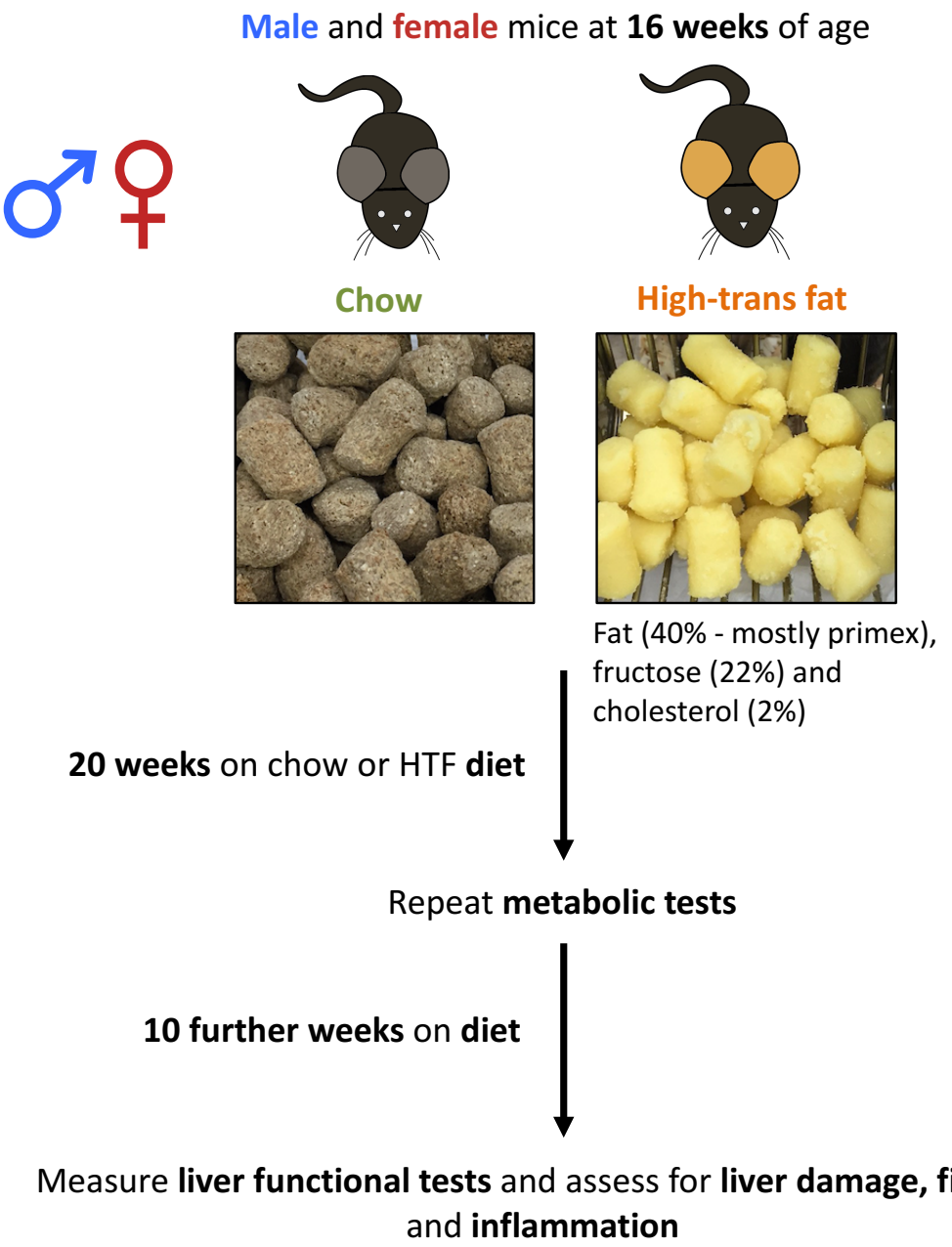

Figure 5.4. A diet rich in transaturated fat, fructose and cholesterol (HTF) to induce non-alcoholic steatohepatitis (NASH).
Schematic illustrating the experimental workflow for the NASH experiment. S6K1 and S6K2 floxed and knockout mice of both sexes were put on either chow or HTF diet at 16-weeks of age. Following 20 weeks on the diet, the mice were metabolically phenotyped. 10 weeks following this, mice were sacrificed 10 weeks later (30 weeks of diet in total) and assessed for liver function, damage, fibrosis and inflammation.

5.4. Liver-specific deletion of S6K1 and S6K2 partially protects against HTF-induced metabolic dysfunction in male mice.

The effects of the HTF diet on male mice will be discussed first followed by females later. This is due to observing a sexually dimorphic phenotype with both the diet and upon deleting S6K1 and S6K2. Thus, for clarity the two sexes will be discussed separately. Furthermore, the prevalence of NASH and HCC are higher in men, and this is also depicted in our cohorts.

Following 20 weeks of either chow or HTF feeding, mice were subjected once again to metabolic phenotyping. In line with previous observations, there were no alterations in glucose or insulin tolerance tests or in the fat/lean mass ratio between the two genotypes of male mice when kept under a chow diet at 36-38 weeks of age (Figure 5.5). *S6K1*$^{-/-}$*: S6K2*$^{-/-}$ male mice, however, showed a mild improvement in their glucose tolerance and insulin sensitivity, as well as a significant attenuation in the increase in fat/lean mass ratio and body weight gain when given an HTF diet (Figure 5.5 and 5.6). There were no significant differences in the fed or fasted glucose levels with either diet or genotype (Figure 5.6 B). This suggests that the liver is one of but not the sole contributor to the metabolic protection observed in the global S6K1 and S6K2 knockout mice (mixed background) in response to feeding a high-fat diet (Castañeda et al., 2012).

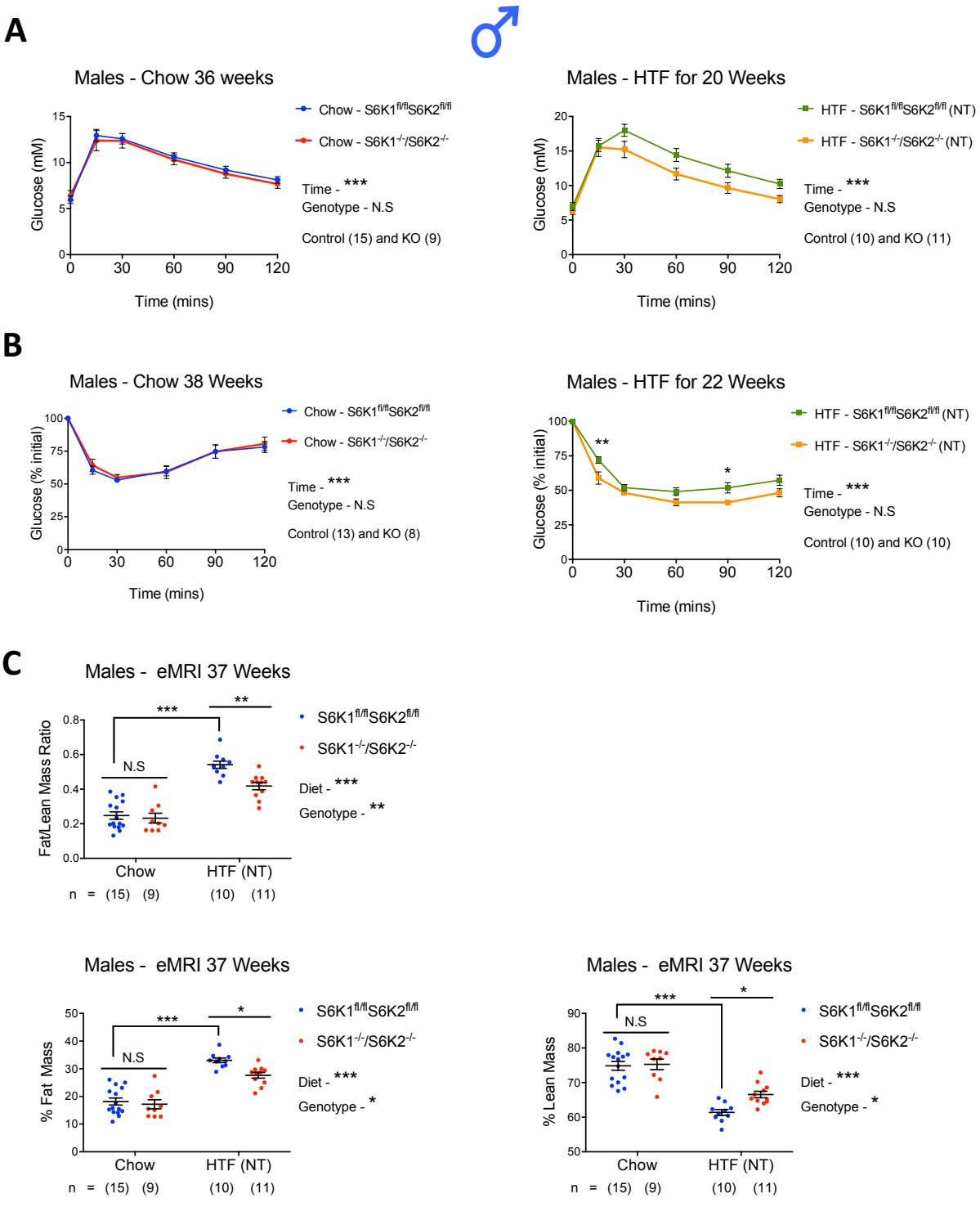

Figure 5.5. Liver-specific S6K1 and S6K2 deletion partially protects against HTF-induced metabolic dysfunction in male mice.
A. Glucose-tolerance tests in male S6K1 and S6K2 floxed and knockout mice either fed a chow (left) or an HTF diet (right). Both chow-fed and HTF-fed mice were 36 weeks of age. HTF diet was given for 20 weeks. **B.** Insulin-tolerance tests in male S6K1 and S6K2 floxed and knockout mice either fed a chow (left) or an HTF diet (right). Both chow-fed and HTF-fed mice were 38 weeks of age. HTF diet was given for 22 weeks. **C.** EchoMRI analysis of male S6K1 and S6K2 floxed and knockout mice fed either a chow or an HTF diet at 37 weeks of age. HTF diet was given for 21 weeks. Fat/lean mass ratio (top), % fat mass (bottom left) and % lean mass (bottom right). Data are expressed as mean ± SEM and number of mice used is indicated directly on all graphs. Statistical significance was calculated using either two-way repeated-measures analysis of variance with Sidak's multiple comparison test (A and B) or two-way analysis of variance with Tukey's multiple comparison test (C) (* $P < 0.05$, ** $P < 0.01$, *** $P < 0.001$). N.S: non-significant.

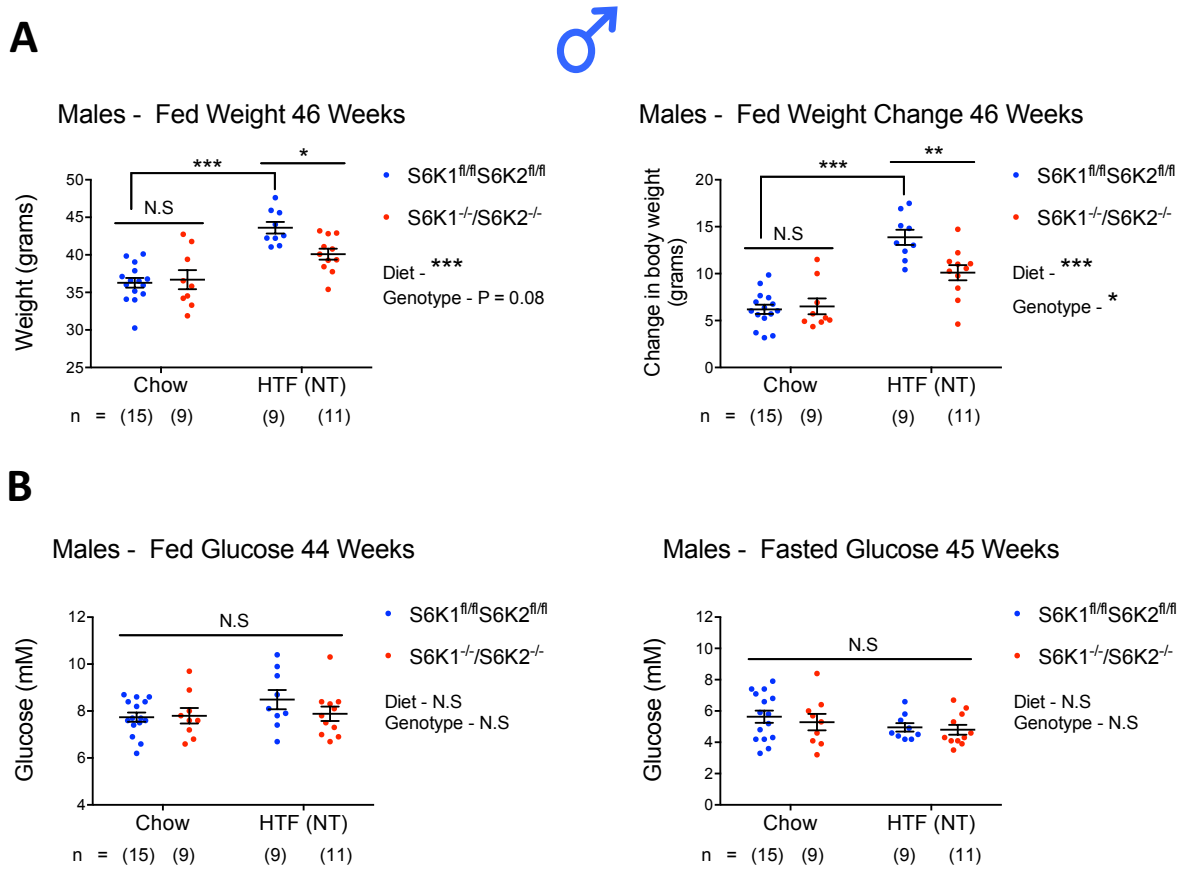

Figure 5.6. Liver-specific S6K1 and S6K2 deletion attenuates HTF-induced weight again without altering glucose levels in male mice.
A. Bodyweight (left) and change in body weight (right) in male S6K1 and S6K2 floxed and knockout mice either fed a chow or an HTF diet. **B.** Fed (left) and fasted (right) blood glucose levels (mM) in male S6K1 and S6K2 floxed and knockout mice fed either a chow (left) or an HTF diet (right). Data are expressed as mean ± SEM and number of mice used is indicated directly on all graphs. Statistical significance was calculated using two-way analysis of variance with Tukey's multiple comparison test (* $P < 0.05$, ** $P < 0.01$, *** $P < 0.001$). N.S: non-significant.

5.5. Male mice displayed two distinct phenotypes when fed an HTF diet.

The mice were sacrificed 10 weeks following metabolic phenotyping (30 weeks of diet in total). At this point, various liver functional tests were performed and the tissues were assessed for liver damage and fibrosis. We observed that male control (*S6K1*$^{fl/fl}$*: S6K2*$^{fl/fl}$) mice showed two distinct macroscopic liver phenotypes at the time of cull. As expected, control mice on the HTF diet showed clear hepatomegaly (enlargement of the liver) and discolouration (lipid accumulation) (Figure 5.7 A). Several control mice on the HTF diet developed multiple outgrowths of the liver, suggestive of HCC (Figure 5.7 A). In retrospect, when classifying the control mice on the HTF diet to either non-tumours (NT) or tumours (T), they showed clear differences in metabolic parameters. For example, all the HTF (NT) control mice gained significant weight and were glucose and insulin intolerant compared to chow controls (Figure 5.7 B and C). The HTF (T) mice, however, did not gain any weight and showed normal response to glucose and insulin (Figure 5.7 B and C).

Male control mice displayed various grades of hepatic steatosis and liver fibrosis in response to the HTF diet (Figure 5.8). This degree of heterogeneity is expected when feeding wild type C57BL/6 mice with a high-fat diet (Burcelin et al., 2002). All male mice fed the HTF diet had some degree of hepatic steatosis and liver fibrosis, but what was noticeable was that mice with more advanced fibrosis had reduced steatosis (Figure 5.8). Importantly, control mice with tumours (HTF – T) displayed a robust activation of the stromal component (hepatic stellate cells and/or cholangiocytes) by haematoxylin and eosin (H&E) staining, as well as severe fibrosis with the typical “chicken-wire fibrosis’ pattern that is present in human NASH (Figure 5.8). Liver fibrosis was assessed by staining liver sections with picrosirius red for collagen deposition and visualised by circularly polarised light. Images (original magnification X40) were stitched in ImageJ software to produce a complete liver section image and the collagen (orange) was quantified as a percentage of total liver section area.

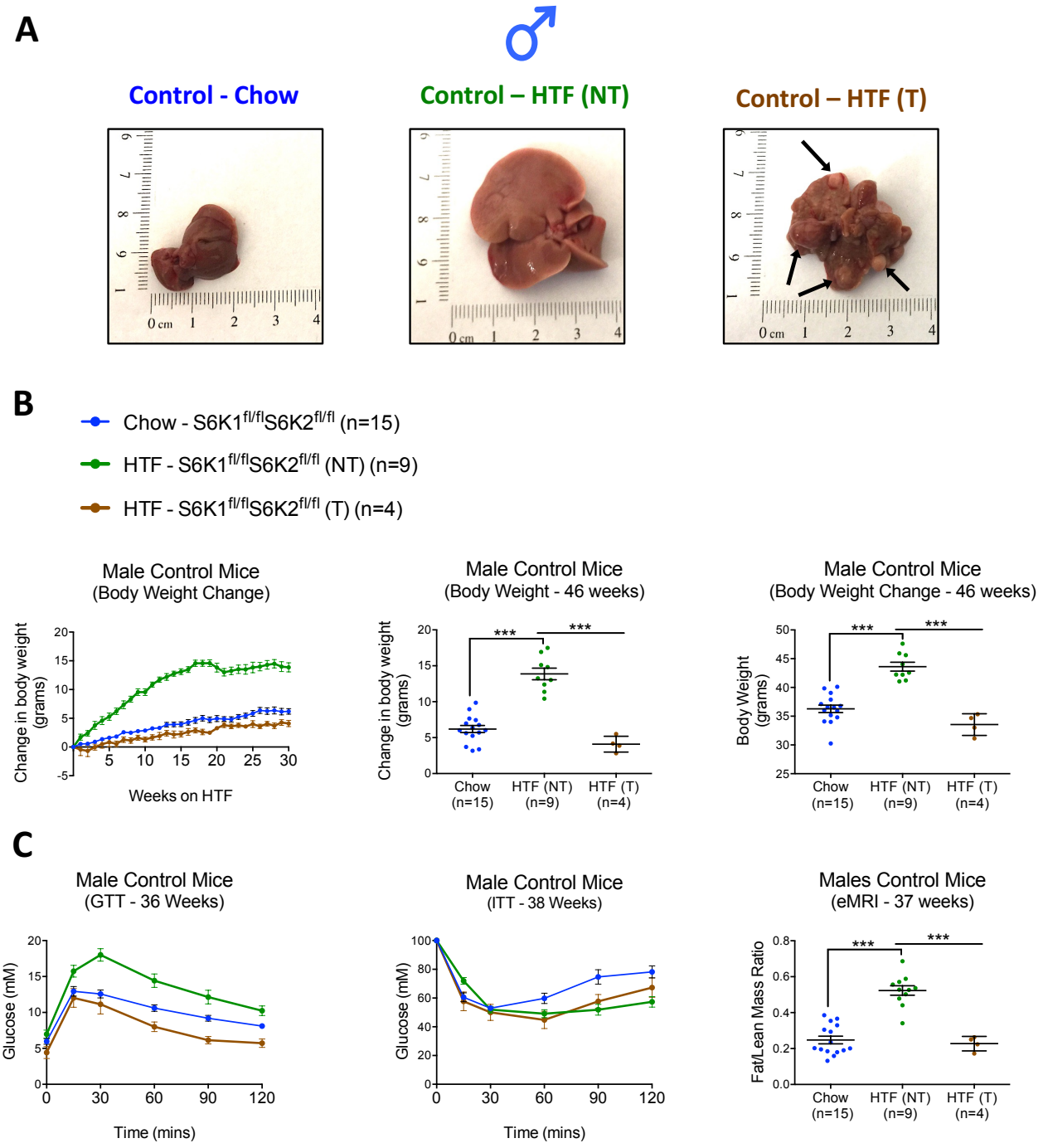

Figure 5.7. Control male mice displayed two distinct phenotypes when fed an HTF diet. **A.** Representative photographs of livers from male mice fed a chow diet (left) or an HTF diet (middle and right) following 30 weeks of the respective diet. HTF-fed mice showed hepatomegaly without overt tumours (middle) or with tumours (right). **B.** Change in body weight represented as either a curve (left) or at the final time point (46 weeks of age - middle) in male mice fed either a chow or an HTF diet. Bodyweight (grams) is shown on the right. **C.** Glucose-tolerance test (left), insulin-tolerance test (middle) and echoMRI analysis of fat/lean mass ratio (right) in male S6K1 and S6K2 floxed and knockout mice either fed a chow diet or an HTF diet. Data are expressed as mean ± SEM and number of mice used is indicated directly on all graphs. Statistical significance was calculated using one-way analysis of variance with Tukey's multiple comparison test (bodyweight) (* $P < 0.05$, ** $P < 0.01$, *** $P < 0.001$). N.S: non-significant.

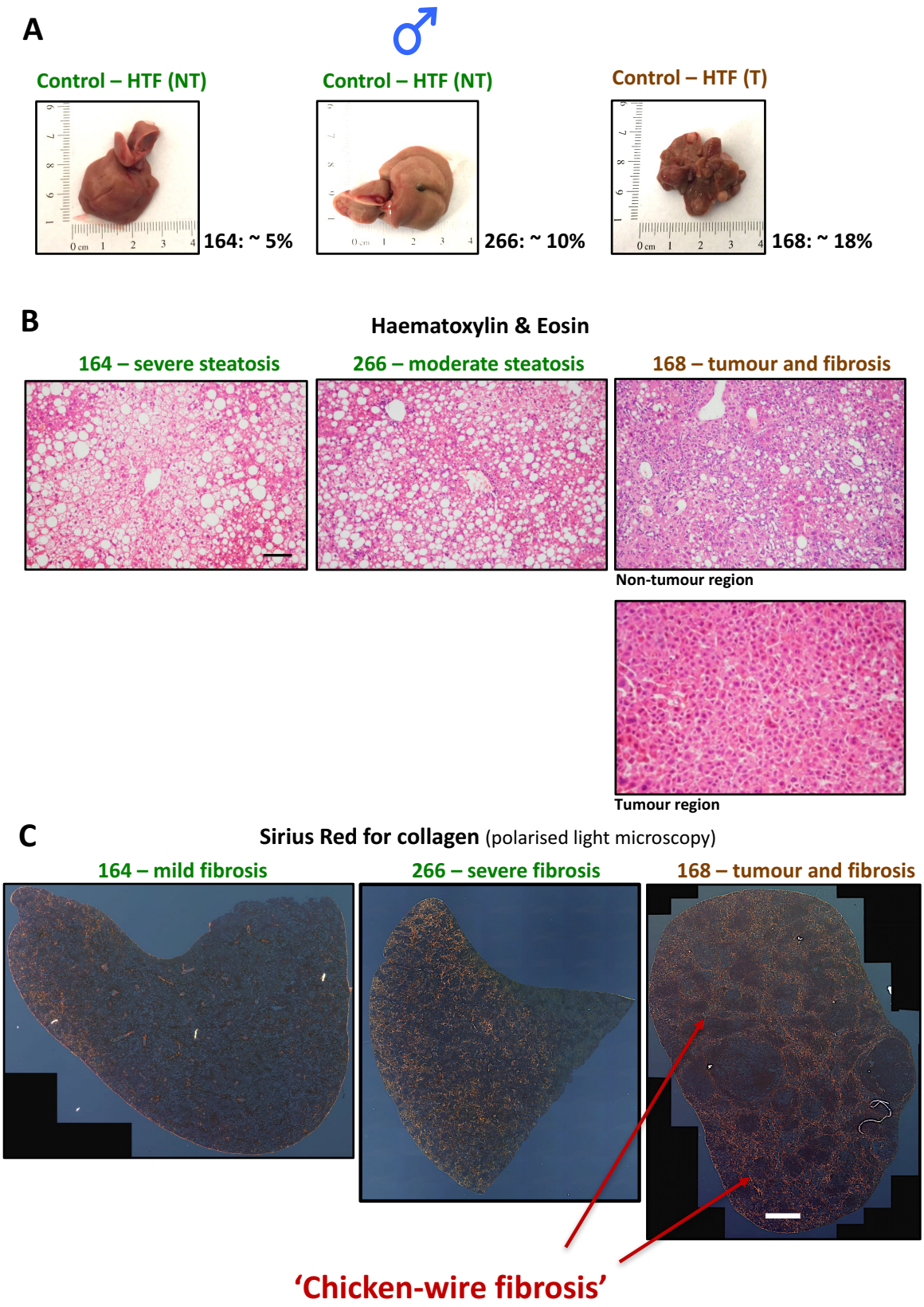

Figure 5.8. Control male mice displayed various grades of fibrosis when fed an HTF diet. **A.** Representative photographs of livers from male mice fed an HTF diet for 30 weeks with varying degrees of fibrosis (5%, 10%, and 18%). HTF-fed mice showed hepatomegaly without overt tumours (middle) or with tumours (right). **B.** Representative microphotographs of hematoxylin and eosin staining of the liver of the indicated mice. Both the non-tumour (top) and tumour (bottom) region are shown for the representative mouse that developed liver tumours. **C.** Liver sections stained with picrosirius red for collagen deposition and visualised by circularly polarised light. Images (and original magnification X40) were stitched in ImageJ software to produce a complete liver section image and the collagen (orange) was quantified as a percentage of total liver section area. Scale bar, 100 μm (top) and 1 mm (bottom).

5.6. Liver-specific deletion of S6K1 and S6K2 in male mice attenuated HTF-induced liver damage, fibrosis and incidence of hepatocellular carcinoma (HCC).

At the time of sacrifice (30 weeks of the diet), biochemical analysis of key metabolic parameters in whole blood was done using the VetScan VS2 with the liver diagnostic profile to assess liver functionality (Figure 5.9). As expected, there was a significant increase in serum cholesterol, as well as various liver damage markers such as alanine aminotransferase (ALT), alkaline phosphatase (ALP) and bile acids in control mice fed an HTF diet (HTF – NT) compared to chow controls (Figure 5.9). Importantly, the increase in serum ALT levels was significantly diminished in male *S6K1*$^{-/-}$*: S6K2*$^{-/-}$ mice fed an HTF diet, suggestive of attenuated hepatocyte damage (Figure 5.9). In addition, there was also lower levels of serum cholesterol in male *S6K1*$^{-/-}$*: S6K2*$^{-/-}$ mice fed an HTF diet with near significance (P = 0.06, two-way ANOVA with Tukey's post-hoc). There was, however, no alterations in biliary damage markers (ALP or bile acids) upon deleting S6K1 and S6K2 in male mice (Figure 5.9) or no alterations between the genotypes in serum albumin, total bilirubin or blood urea nitrogen was observed when feeding the HTF diet between the genotypes (Figure 5.9).

Control mice with tumours (HTF – T) showed higher levels of serum ALP and bile acids and lower levels of ALT and cholesterol compared to control mice without overt tumours (HTF – NT) (Figure 5.9). Importantly, serum ALP and bile acids showed a significant positive correlation with fibrosis (considering all HTF mice – both control and knockout), whereas serum ALT levels did not significantly correlate with fibrosis (Figure 5.10 A-C). Serum ALT levels, however, showed a positive correlation with serum cholesterol levels; although this was not statistically significant (Figure 5.10 B). This suggests that serum ALP and bile acids are better indicators of liver fibrosis than ALT when feeding this HTF diet. Importantly, others have shown that ALT levels increase at the time of lipid accumulation (late stage) rather than during the initial immune cell infiltration (early stage), and given that control mice with tumours (HTF – T) showed less steatosis compared to control mice without overt tumours on the HTF diet, our data is consistent with what has been published by other groups (Gomes et al., 2016; Tummala et al., 2014).

We then assessed the effects of deleting S6K1 and S6K2 on liver pathology. As expected, control mice fed an HTF diet (HTF- NT) displayed a significant increase in liver weight even when correcting for the body weight, but this was not significantly reduced in male *S6K1*$^{-/-}$*: S6K2*$^{-/-}$ mice (Figure 5.11 A and B). Unexpectedly, 30.7% (4/13) of the control mice fed an HTF diet developed overt liver outgrowths, suggestive of HCC, and in contrast this was seen only in 8.3% (1/12) of the male *S6K1*$^{-/-}$*: S6K2*$^{-/-}$ mice, indicating that deleting S6K1 and S6K2 specifically in the liver partially protects these mice from development of NASH-driven HCC. Importantly, the incidence of tumours in control mice is comparable to other NASH diets that recapitulate both the metabolic and pathological aspects of human NASH. Specifically, 25% of the wild type mice fed a choline-

deficient high-fat diet (CD-HFD) also developed HCC following 12 months of feeding (Wolf et al., 2014). The CD-HFD characterised by the Heikenwälder group also recapitulates many aspects of human NASH including obesity and glucose intolerance, as well as pathological manifestations including Mallory-Denk body (MDB) formation, steatosis, hepatocyte ballooning, satellitosis (immune infiltrates surrounding liver cells) but show only mild fibrosis; thus the CD-HFD is a better model of steatohepatitis, whereas the HTF/AMLN diet better recapitulates NASH driven by fibrosis (Clapper et al., 2013; Wolf et al., 2014).

We next investigated whether deleting S6 kinases protect against hepatic steatosis and fibrosis. H&E staining clearly depicted macrosteatosis in control mice fed an HTF diet (HTF – NT), and this steatosis was reduced to an extent (size and number of lipid droplets) in male *S6K1*$^{-/-}$*: S6K2*$^{-/-}$ mice (Figure 5.12 A and B). Control mice with overt tumours (HTF – T) did not show much steatosis but did display a pronounced expansion of the stromal (hepatic stellate cells and/or cholangiocytes) in the non-tumour regions, whereas the knockout mouse that developed HCC still showed hepatic steatosis. Oil Red O staining must be done to conclusively show this, but it has already been demonstrated that liver-specific depletion of S6K1 and S6K2 by AAVs partially protect from HFD-induced hepatic steatosis (Bae et al., 2012). Similarly, there was a significant increase in fibrosis (polarised light microscopy quantification of picrosirius red staining) in control mice fed an HTF diet (both NT and T combined), and there was a trend towards an attenuation in male *S6K1*$^{-/-}$*: S6K2*$^{-/-}$ mice ($P = 0.08$, two-way ANOVA with Tukey's post-hoc) (Figure 5.13). There was considerable heterogeneity in the fibrotic response even within control mice (HTF NT and T), thus when classifying the mice according to different degrees of fibrosis (< 5%, 5-10% and > 10%), it was evident that 38.5% of control mice (HTF NT and T) displayed > 10% fibrosis, whereas this was only found in 16.7% of male *S6K1*$^{-/-}$*: S6K2*$^{-/-}$ mice (Figure 5.13B). Importantly, all mice that developed HCC (both control and knockout) developed severe fibrosis with the typical "chicken-wire fibrosis" pattern (Figure 5.14). Overall, the data indicate that deletion of S6K1 and S6K2 in male mice reduces HTF-induced liver damage and protects, at least partially, from advanced fibrosis and development of HCC.

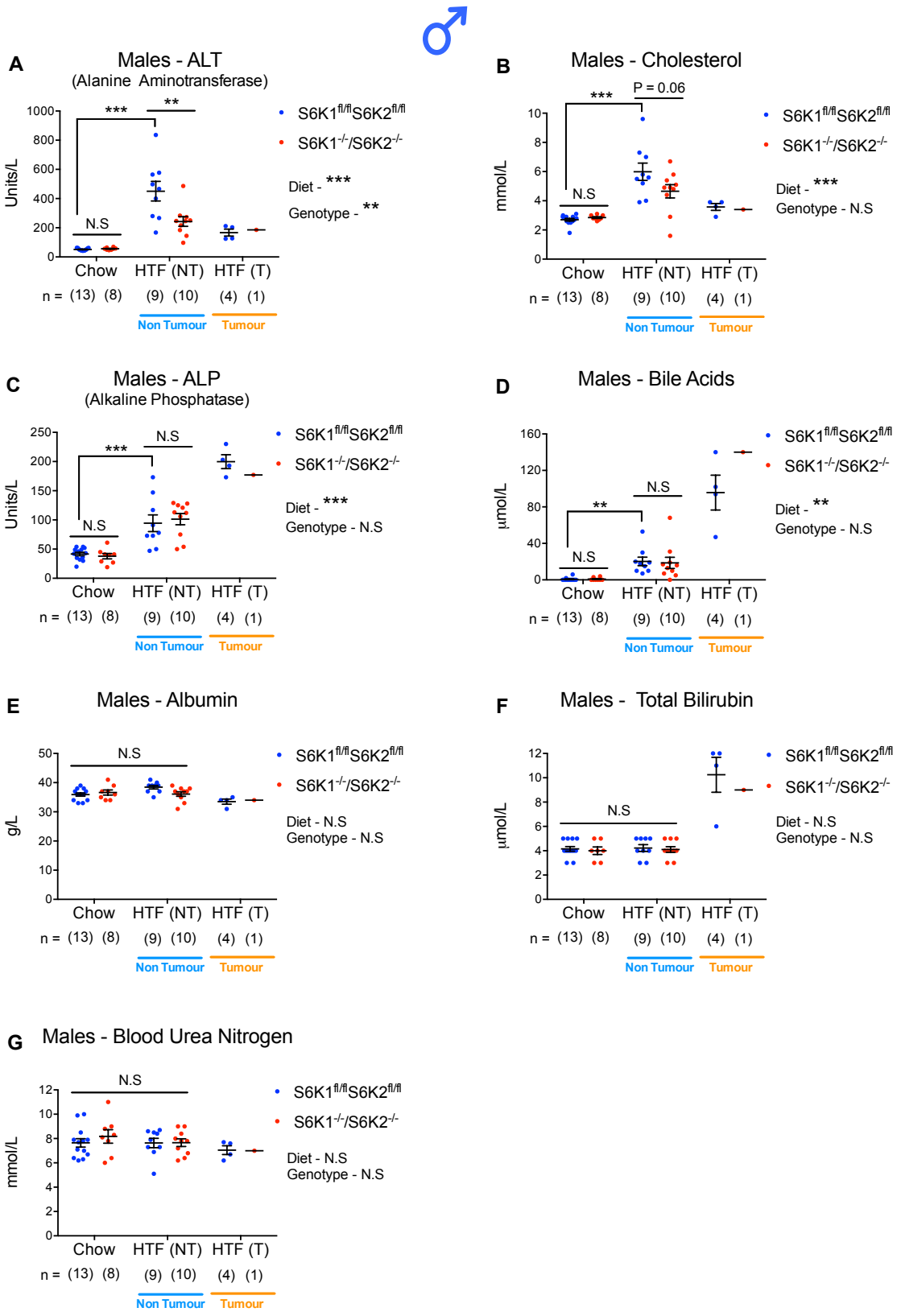

Figure 5.9. Analysis of blood parameters in chow-fed and HTF-fed male mice.
Whole blood was used to analyse the concentration of various blood parameters in S6K1 and S6K2 floxed and knockout chow-fed or HTF-fed male mice following 30 weeks of the respective diet. **A.** Alanine aminotransferase (Units/L). **B.** Cholesterol (mmol/L). **C.** Alkaline phosphatase (Units/L). **D.** Bile acids (µmol/L). **E.** Albumin (g/L). **F**. Total bilirubin (µmol/L). **G.** Blood urea nitrogen (mmol/L). Data are expressed as mean ± SEM and number of mice used is indicated directly on all graphs. Statistical significance was calculated using two-way analysis of variance with Tukey's multiple comparison test (* $P < 0.05$, ** $P < 0.01$, *** $P < 0.001$). N.S: non-significant.

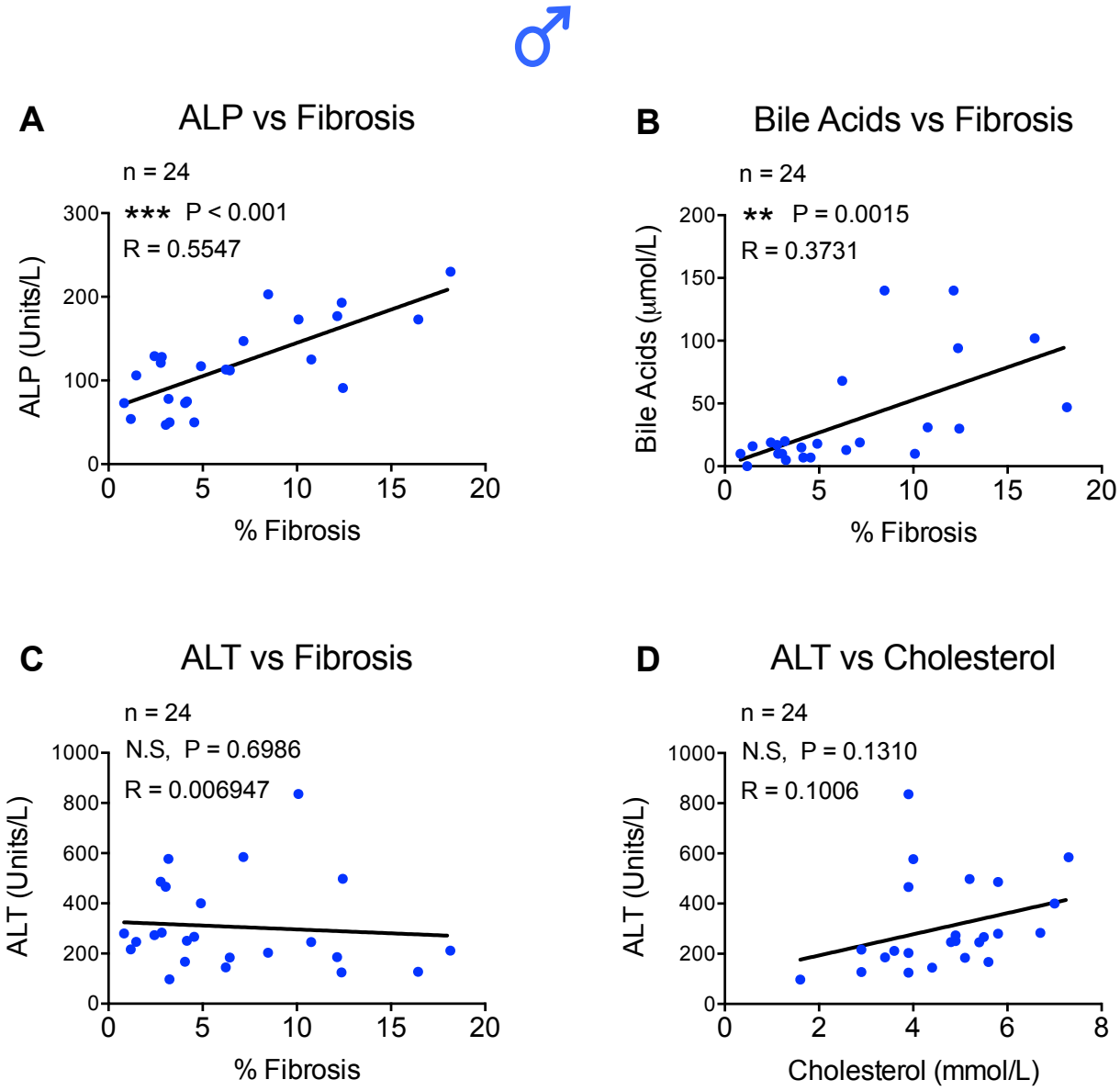

Figure 5.10. Correlation between liver damage markers and fibrosis in HTF-fed male mice. All HTF-fed S6K1 and S6K2 floxed and knockout male mice were used to investigate correlation between liver fibrosis and markers of liver damage. **A.** Correlation between alkaline phosphatase (ALP) levels (Units/L) and percentage liver fibrosis. **B.** Correlation between bile acids (µmol/L) and percentage liver fibrosis. **C.** Correlation between alanine aminotransferase (ALT) levels (Units/L) and percentage liver fibrosis. **D.** Correlation between ALT (Units/L) and cholesterol (mmol/L) levels. Statistical significance was calculated using linear regression (* P < 0.05, ** P < 0.01, *** P < 0.001). N.S: non-significant.

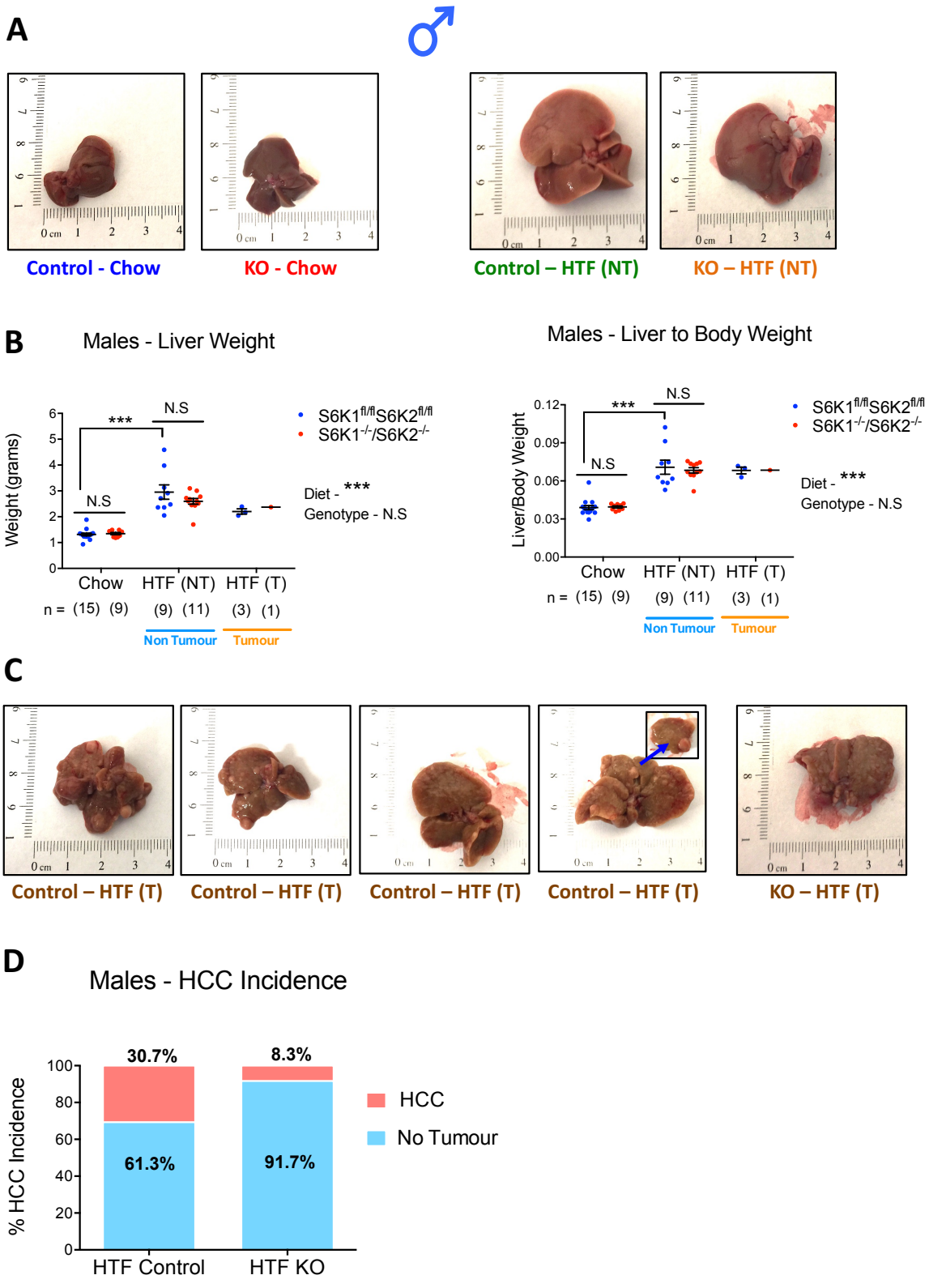

Figure 5.11. Liver-specific S6K1 and S6K2 deletion attenuates HTF-induced liver damage and incidence of hepatocellular carcinoma (HCC) in male mice.
A. Representative photographs of livers from S6K1 and S6K2 floxed and knockout male mice fed either a chow or an HTF diet following 30 weeks of the respective diet. **B.** Left: liver weight (grams). Right: liver weight corrected for the bodyweight. HTF-fed mice showed hepatomegaly without overt tumours (middle) or with tumours (right). **C.** Representative photographs of livers from S6K1 and S6K2 floxed and knockout male mice that developed tumours when fed an HTF-diet for 30 weeks. **D.** Percentage of mice described in (C) bearing liver tumours. Data are expressed as mean ± SEM and number of mice used is indicated directly on all graphs. Statistical significance was calculated using two-way analysis of variance with Tukey's multiple comparison test (*** $P < 0.001$). N.S: non-significant.

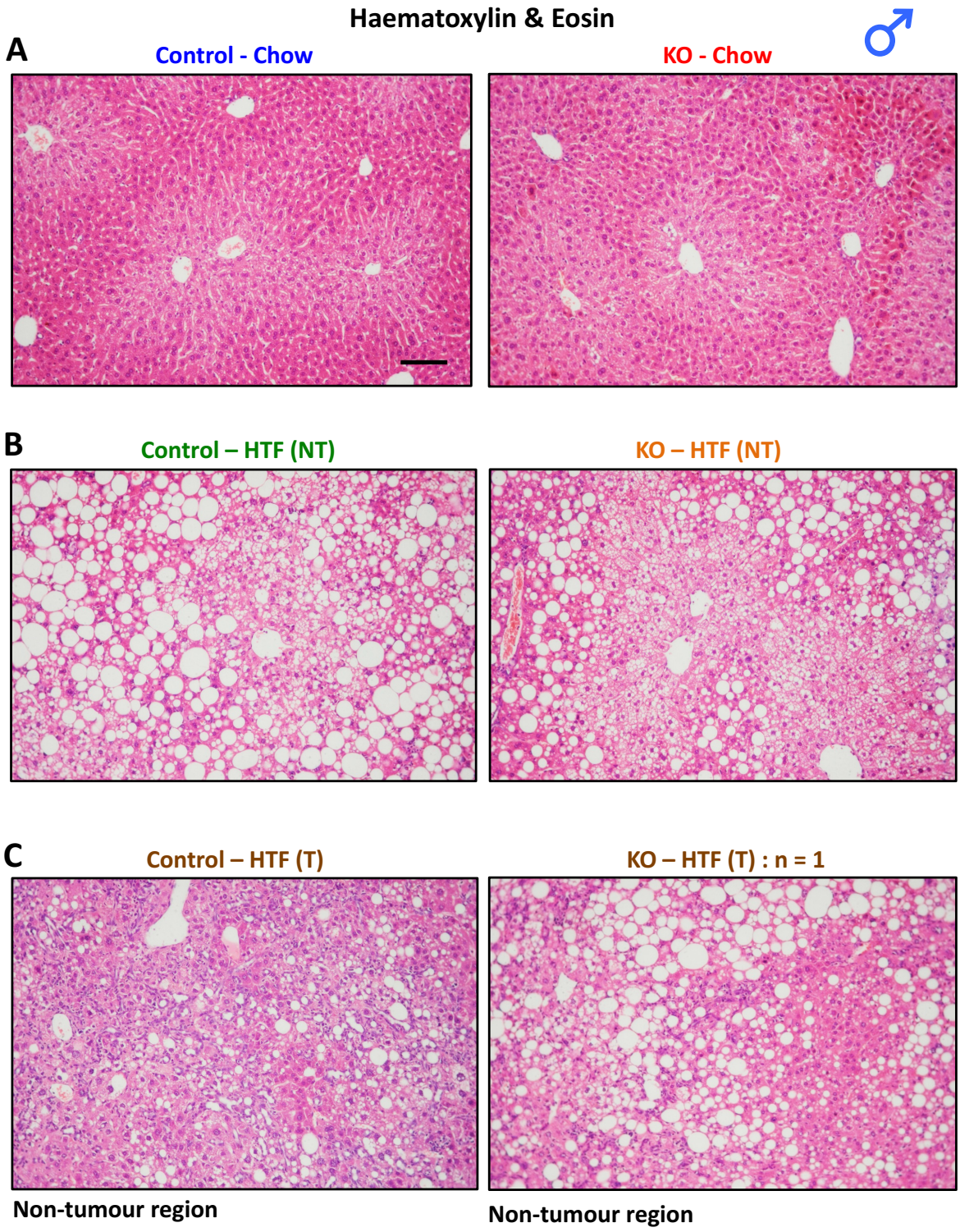

Figure 5.12. Haematoxylin and eosin staining of livers in male S6K1 and S6K2 floxed and knockout mice.
Representative microphotographs of hematoxylin and eosin staining of the liver from the indicated mice. **A.** 46-week-old male S6K1 and S6K2 floxed and knockout mice fed a chow diet. **B.** Male S6K1 and S6K2 floxed and knockout mice without tumours fed an HTF diet for 30 weeks. **C.** Non-tumour region of the liver from male S6K1 and S6K2 floxed and knockout mice that developed tumours following HTF feeding for 30 weeks. Only one S6K1 and S6K2 knockout mouse developed tumours. Scale bar, 100 μm.

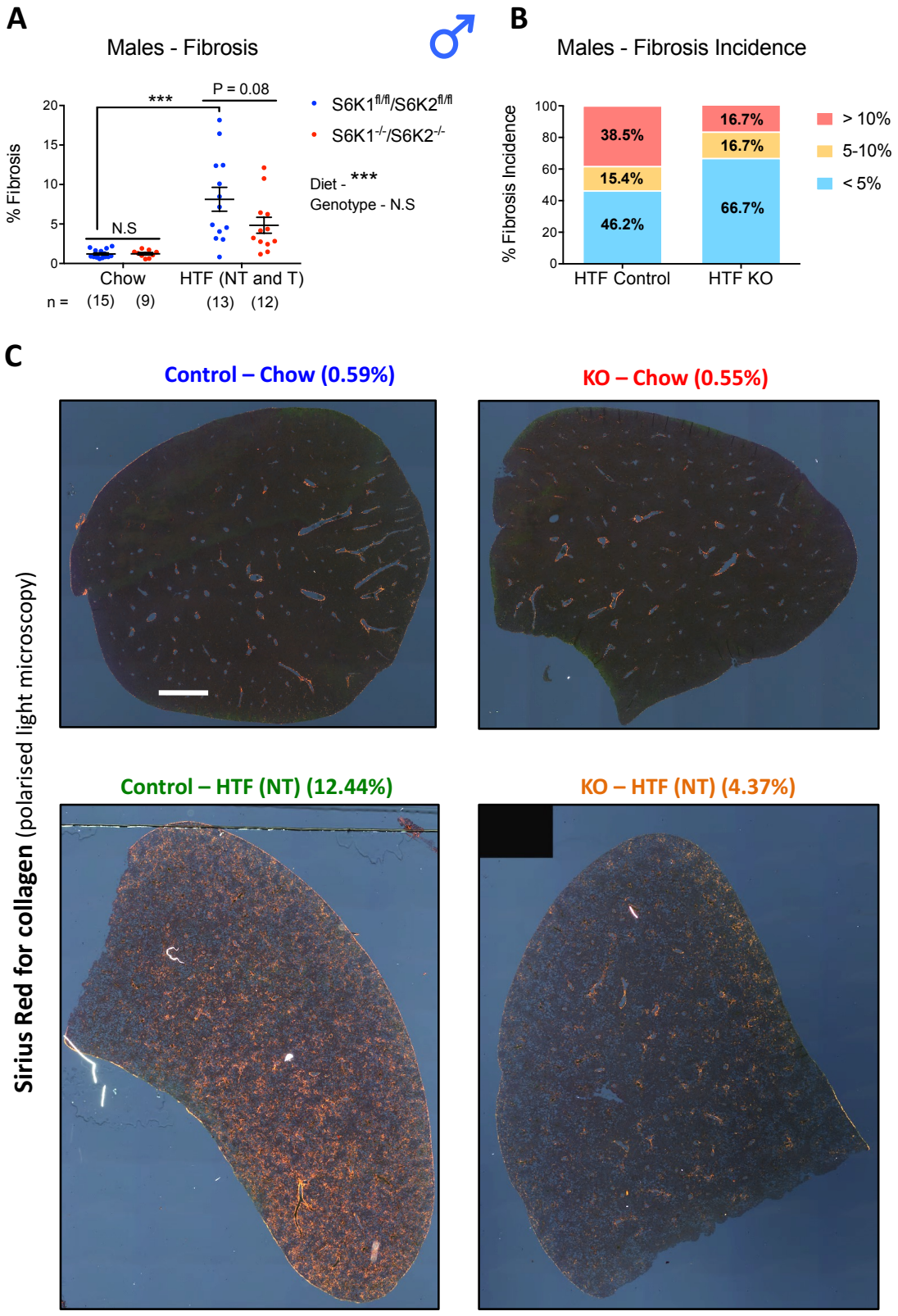

Figure 5.13. Liver-specific S6K1 and S6K2 deletion attenuates HTF-induced liver fibrosis in male mice.

A. Quantification of picrosirius red staining of collagen fibres in liver sections of S6K1 and S6K2 floxed and knockout male mice fed either a chow or an HTF diet for 30 weeks. **B.** Percentage of HTF-fed mice described in (A) categorised into severity of fibrosis. **C.** Representative liver sections from (A) stained with picrosirius red for collagen deposition and visualised by circularly polarised light. Images (original magnification X40) were stitched in ImageJ software to produce a complete liver section image and the collagen (orange) was quantified as a percentage of total liver section area. Data are expressed as mean ± SEM and number of mice used is indicated directly on all graphs. Statistical significance was calculated using two-way analysis of variance with Tukey's multiple comparison test (*** $P < 0.001$). N.S: non-significant. Scale bar, 1 mm.

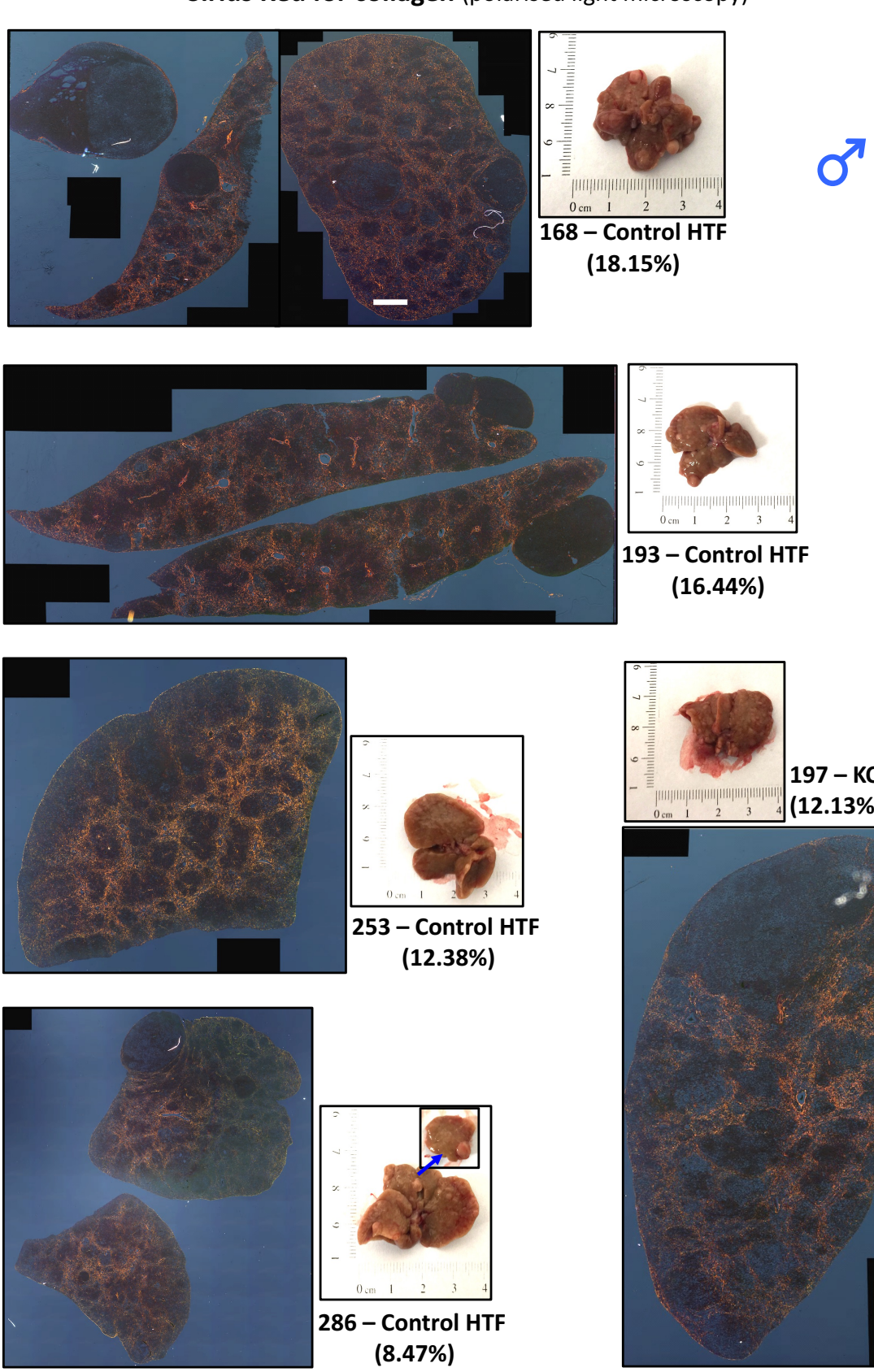

Figure 5.14. All male mice with HCC show marked liver fibrosis.
Liver sections from male mice that developed HCC following HTF feeding stained with picrosirius red for collagen deposition and visualised by circularly polarised light. Livers from the representative mice and the quantification of fibrosis is shown. Images (original magnification X40) were stitched in ImageJ software to produce a complete liver section image and the collagen (orange) was quantified as a percentage of total liver section area. Scale bar, 1 mm.

5.7. Liver-specific deletion of S6K1 and S6K2 in male mice does not affect inflammatory gene expression or proliferation.

In addition to fibrosis, inflammation and immune infiltration are hallmarks of NASH (Hardy et al., 2016). We therefore investigated whether inflammatory markers are also activated in our HTF model of NASH and the impact of liver-specific S6K deletion on this process. As anticipated, there was a significant increase in the mRNA expression of several inflammatory genes (*Ccl2, Ccl5 and Cxcl5*) and a marker of macrophages (*Cd68*) in control mice fed an HTF diet (NT and T combined) compared to chow controls, but the expression of these markers was not significantly altered in the *S6K1*$^{-/-}$*: S6K2*$^{-/-}$ mice (Figure 5.15). This was validated using a global approach (RNA-sequencing) that will be discussed in length later.

Hepatocyte damage, apoptosis and subsequent proliferation are some of the underlying mechanisms driving malignant transformation and development of HCC (Bataller et al., 2005; Llovet et al., 2016). In addition, S6K1 regulates mouse liver proliferation following partial hepatectomy (Espeillac et al., 2011). We therefore sought to elucidate whether S6 kinases also regulate NASH-driven proliferation in the liver. There was a significant increase in the number of positive cells for the proliferation marker Ki67 when analysing all liver cells in control mice fed an HTF diet (HTF - NT) compared to chow controls, and there was a further increase in Ki67 positive cells in control mice that developed tumours (HTF – T) even within the non-tumour region (Figure 5.16). Deletion of S6K1 and S6K2, however, did not significantly alter the number of Ki67 positive cells in either the chow or HTF (NT) group compared to their respective male controls (Figure 5.16). Nevertheless, the single knockout mouse that developed HCC showed a marked reduction in Ki67 positive cells compared to the HTF (T) controls, but more mice are required to understand whether S6K1 affects proliferation in NASH to HCC transition, as the data would suggest (Figure 5.16).

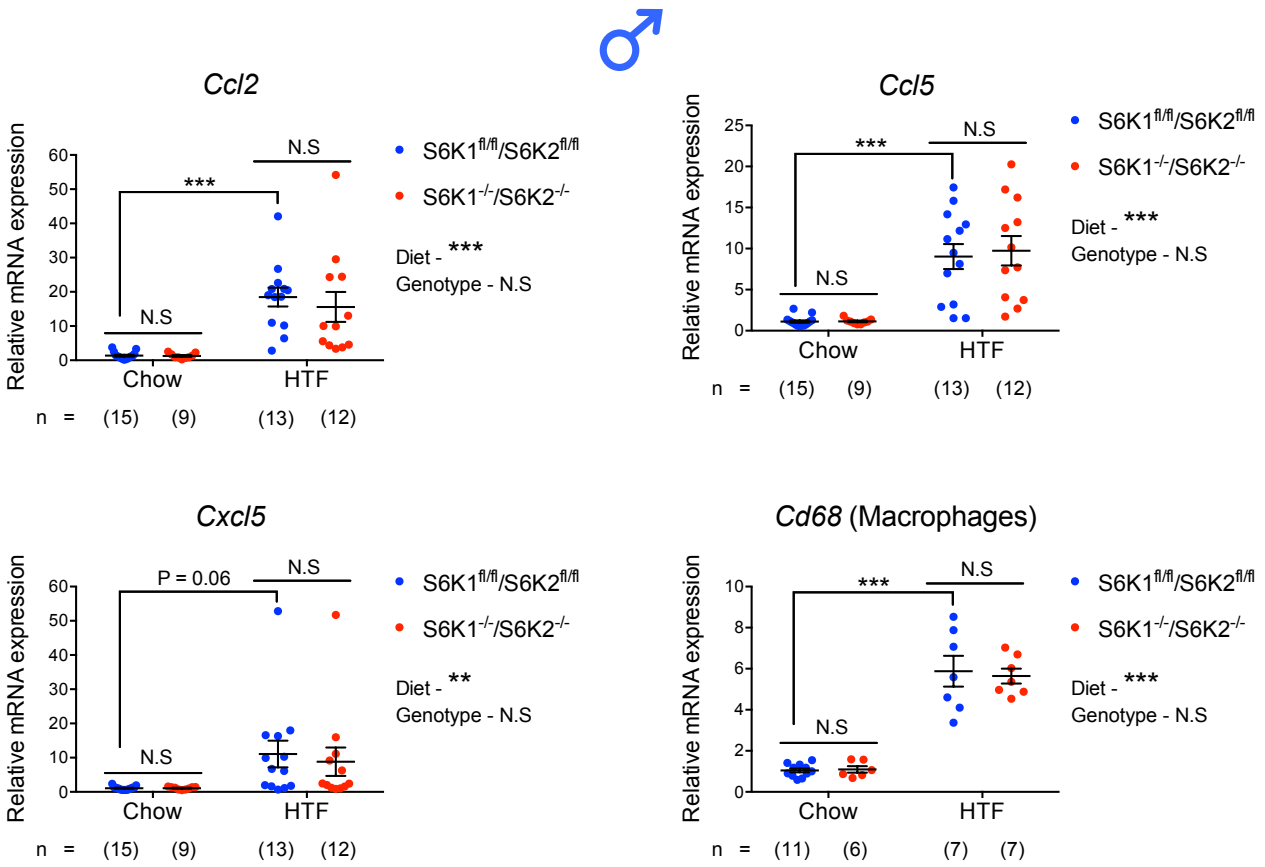

Figure 5.15. Liver-specific S6K1 and S6K2 deletion does not affect inflammatory gene expression in male mice.
Relative mRNA expression of *Ccl2, Ccl5, Cxcl5* and *Cd68* assessed by RT-qPCR from liver lysates in S6K1 and S6K2 floxed and knockout male mice fed either a chow or an HTF diet for 30 weeks. mRNA expression was normalized to *Rps14* housekeeping gene. Data are expressed as mean ± SEM and number of mice used is indicated directly on all graphs. Statistical significance was calculated using two-way analysis of variance with Tukey's multiple comparison test (*** P < 0.001). N.S: non-significant.

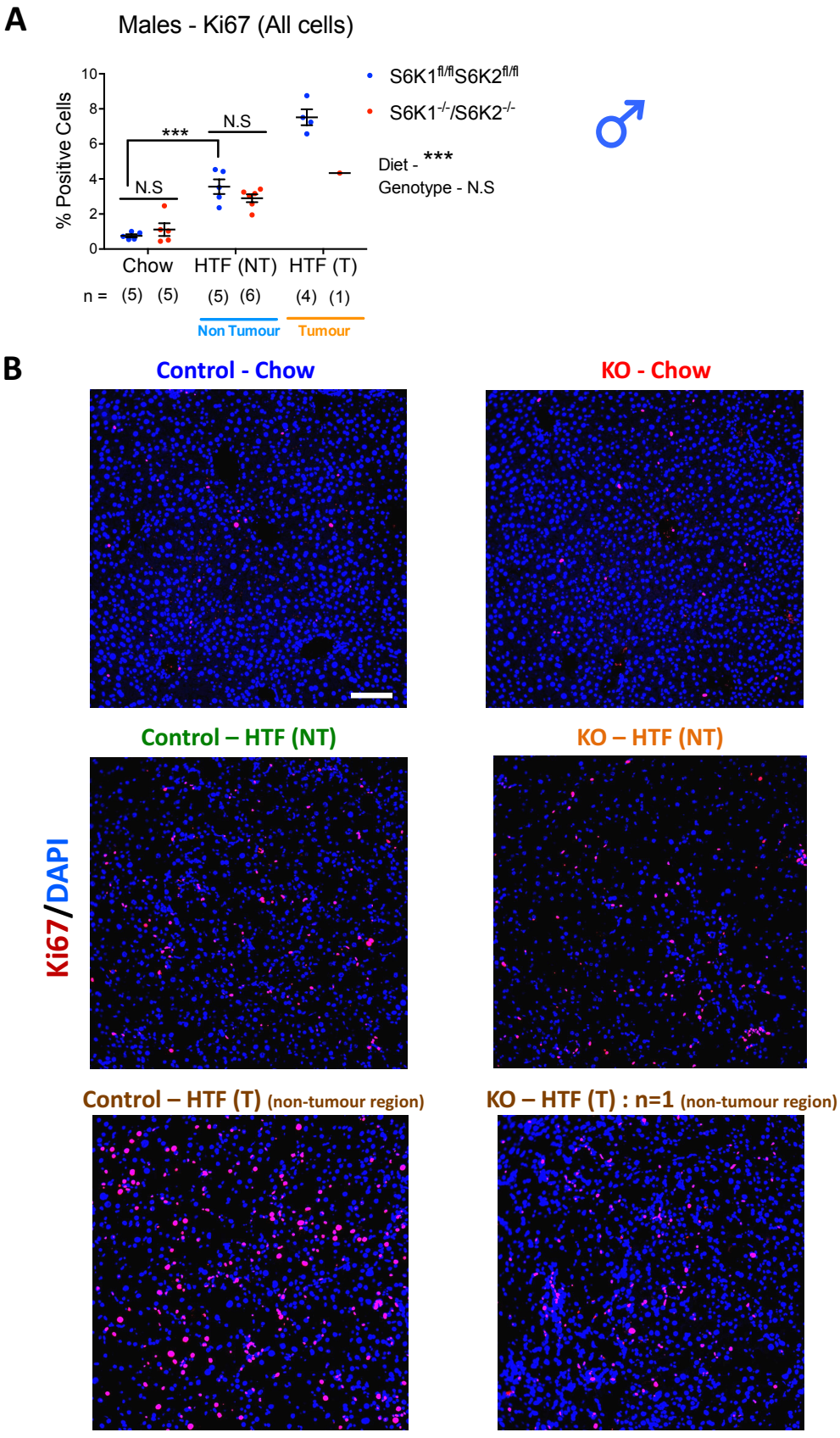

Figure 5.16. Liver-specific S6K1 and S6K2 deletion does not affect liver proliferation in male mice.

A. Percentage of Ki67 positive cells in S6K1 and S6K2 floxed and knockout male mice fed either a chow or an HTF diet for 30 weeks quantified by high-throughput microscopy. **B.** Representative microphotographs for Ki67 staining. Data are expressed as mean ± SEM and number of mice used is indicated directly on all graphs. Statistical significance was calculated using two-way analysis of variance with Tukey's multiple comparison test (*** $P < 0.001$). N.S: non-significant. Scale bar, 100 µm.

5.8. HTF feeding in female mice failed to induce metabolic dysfunction.

Although the data so far has focused on male mice, both genders were used for the study given the known sexual differences in liver pathogenesis and in the global S6K1 knockout mice. It is important to mention, however, that other studies have not given this diet to female mice, thus making any comparison to the literature difficult. The female mice were subjected to the same tests as the males, thus 20 weeks following chow or HTF feeding from 16 weeks of age, the mice underwent metabolic phenotyping. Surprisingly, even 20 weeks of HTF feeding failed to induce glucose or insulin (only at 120 minutes) intolerance or an increase in the fat/lean mass ratio (echoMRI) in female control mice compared to the chow controls, suggesting that female mice in our cohorts are inherently more resistant to HTF-induced metabolic dysfunction (Figure 5.17). In addition, there were no significant differences in glucose tolerance or in the fat/lean mass between the genotypes under chow or HTF feeding (Figure. 5.17). Female *S6K1*$^{-/-}$*: S6K2*$^{-/-}$ mice, however, showed a mild delay in glucose recovery (time = 90 minutes) during the insulin tolerance test, suggesting a possible impairment in hepatic glucose production (Figure 5.17 B). Furthermore, HTF feeding failed to increase fed or fasted body weight or serum glucose levels (Figure 5.18).

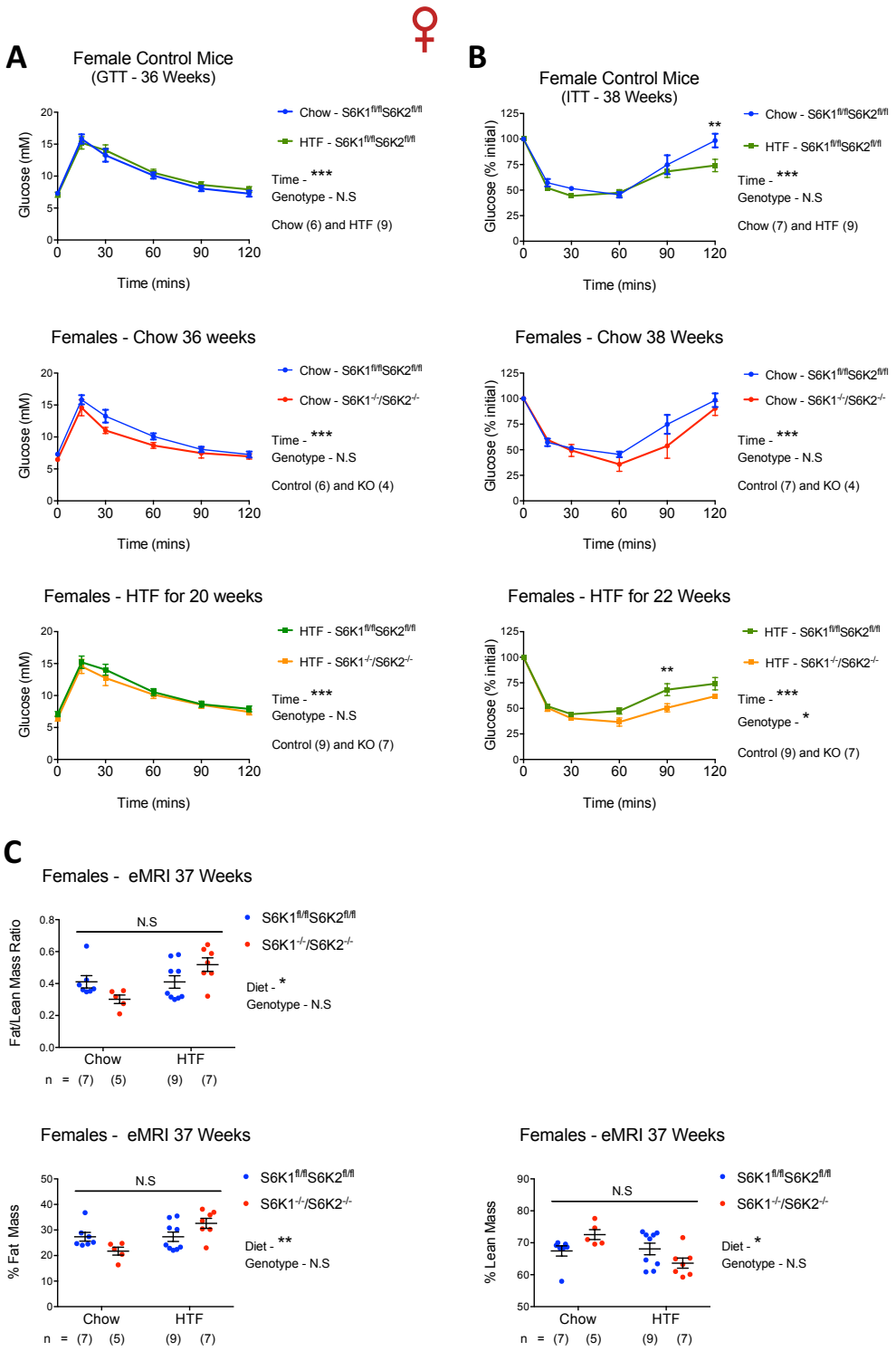

Figure 5.17. HTF-feeding in female mice failed to induce metabolic dysfunction.
A. Glucose-tolerance tests in female S6K1 and S6K2 floxed and knockout mice. Top: Chow vs HTF control mice. Middle: Chow-fed S6K1 and S6K2 floxed vs knockout mice. Bottom: HTF-fed S6K1 and S6K2 floxed vs knockout mice. Both chow-fed and HTF-fed mice were 36 weeks of age. HTF diet was given for 20 weeks. **B** Insulin-tolerance tests in S6K1 and S6K2 floxed and knockout mice. Top: Chow vs HTF control mice. Middle: Chow-fed S6K1 and S6K2 floxed vs knockout mice. Bottom: HTF-fed S6K1 and S6K2 floxed vs knockout mice. Both chow-fed and HTF-fed mice were 38 weeks of age. HTF diet was given for 22 weeks. **C.** EchoMRI analysis of female S6K1 and S6K2 floxed and knockout mice fed either a chow or an HTF diet at 37 weeks of age. HTF diet was given for 21 weeks. Fat/lean mass ratio (top), % fat mass (bottom left) and % lean mass (bottom right). Data are expressed as mean ± SEM and number of mice used is indicated directly on all graphs. Statistical significance was calculated using either two-way repeated-measures analysis of variance with Sidak's multiple comparison test (A and B) or two-way analysis of variance with Tukey's multiple comparison test (C) (* $P < 0.05$, ** $P < 0.01$, *** $P < 0.001$). N.S: non-significant.

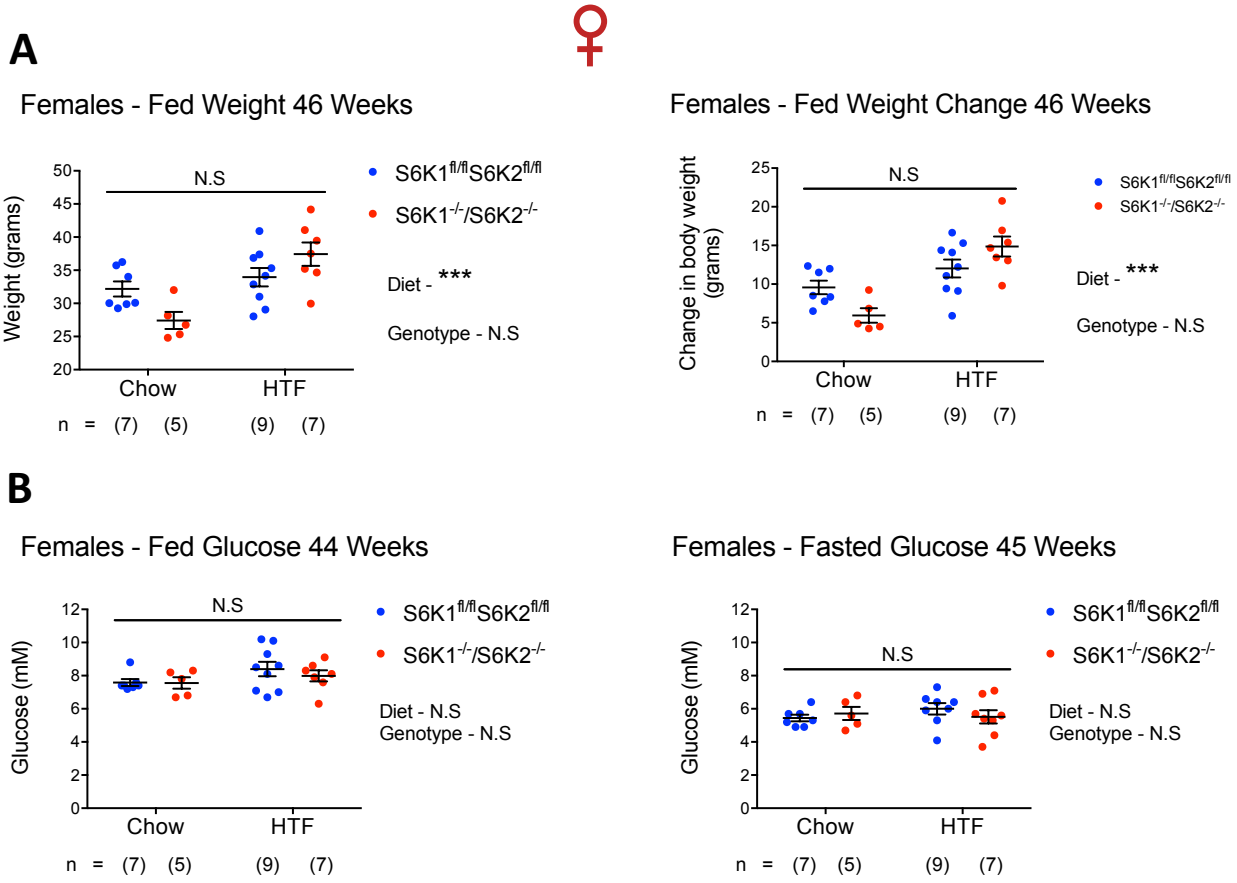

Figure 5.18. HTF-feeding in female mice failed to increase bodyweight or glucose levels. **A.** Bodyweight (left) and change in body weight (right) in female S6K1 and S6K2 floxed and knockout mice either fed a chow or an HTF diet. **B.** Fed (left) and fasted (right) blood glucose levels (mM) in female S6K1 and S6K2 floxed and knockout mice fed either a chow (left) or an HTF diet (right). Data are expressed as mean ± SEM and number of mice used is indicated directly on all graphs. Statistical significance was calculated using two-way analysis of variance with Tukey's multiple comparison test (*** $P < 0.001$). N.S: non-significant.

5.9. Liver-specific deletion of S6K1 and S6K2 in female mice exacerbated HTF-induced hepatomegaly, liver damage, fibrosis and inflammation.

Female mice were also subjected to biochemical analysis of key blood parameters utilising either specific liver functional tests or the VetScan VS2 with the liver diagnostic profile (Figure 5.19). Serum aspartate aminotransferase (AST) levels, which is a marker of liver damage, was measured following 20 weeks of HTF treatment, and a significant increase was observed with HTF feeding in control mice, and surprisingly AST levels further increased in female *S6K1*$^{-/-}$*: S6K2*$^{-/-}$ mice fed an HTF diet (Figure 5.19 A). In line, complete liver functional tests at the time of sacrifice (30 weeks of diet in total) also showed a significant increase in serum cholesterol levels, as well as significant increases in serum ALP and bile acids (markers of biliary damage) in female *S6K1*$^{-/-}$*: S6K2*$^{-/-}$ mice given an HTF diet compared to the respective controls (Figure 5.19 B). Interestingly, serum ALT levels (marker of hepatocyte damage) were unchanged between the two genotypes fed an HTF diet, suggesting that deletion of S6K1 and S6K2 in female mice specifically exacerbates biliary damage after 30 weeks of HTF feeding (Figure 5.19 B).

Macroscopic liver abnormalities in females was then assessed. Once again, female control mice fed an HTF diet developed hepatomegaly and this was even greater in female *S6K1*$^{-/-}$*: S6K2*$^{-/-}$ mice (Figure 5.20 A and B). We then aimed to understand whether this happens at earlier time points, so we sacrificed the other female cohorts at either 18 or 23 weeks following HTF feeding. Interestingly, exacerbated hepatomegaly in female *S6K1*$^{-/-}$*: S6K2*$^{-/-}$ mice was already evident at 18 weeks following HTF feeding, and there were more female *S6K1*$^{-/-}$*: S6K2*$^{-/-}$ mice with overt/macroscopic fibrosis (18.8% in KOs vs 5.26% in WTs) at all the time points (Figure 5.20 C-E).

Next, we focussed on the impact of S6K1 and S6K2 deletion in females on hepatic steatosis and fibrosis. Female *S6K1*$^{-/-}$*: S6K2*$^{-/-}$ mice showed a greater tendency towards hepatic steatosis with immune infiltration compared to HTF control mice (Figure 5.21). In accordance with greater biliary damage (elevated serum ALP and bile acids) in female *S6K1*$^{-/-}$*: S6K2*$^{-/-}$ mice fed an HTF diet, these mice also showed more fibrosis assessed by immunohistochemistry (picrosirius red staining quantified by polarised light microscopy) and relative mRNA expression for various fibrosis markers (*Col1a1, Col4a1, Timp1, Tgfb1, Pdgfa, Acta2/Sma*) compared to respective controls (Figure 5.22). Importantly, however, fibrosis was induced to a lower degree in female control mice fed an HTF diet compared to their male counterparts (mean % fibrosis – 8.13% males vs 1.64% in females). Although female *S6K1*$^{-/-}$*: S6K2*$^{-/-}$ mice fed an HTF diet had greater fibrosis compared to sex-matched controls, it was still lower than male *S6K1*$^{-/-}$*: S6K2*$^{-/-}$ mice fed the same diet (mean % fibrosis – 4.83% males vs 2.56% females).

In addition, female *S6K1*$^{-/-}$*: S6K2*$^{-/-}$ mice displayed elevated mRNA expression for various inflammatory (*Ccl2, Ccl5, Cxcl5, Il6, Il1a and Il1b*) and immune cell (*Cd68, Ncf2, Cd3e, Ptprc, Klrd1*) markers (Figure 5.23). There were, however, no significant differences in mRNA expression for several markers of lipogenesis (*Pck1, Fasn and Dgat2*) but there was a tendency towards elevated lipolysis (*Pnpla2* and *Fabp4*) between female mice fed an HTF diet (Figure 5.24). The increase in fatty acid binding protein 4 (*Fabp4*) may be due to increased macrophages found in the female *S6K1*$^{-/-}$*: S6K2*$^{-/-}$ mice given that *Fabp4* is also expressed in these cells. It is also important to note that the mice were overnight fasted (>16 hours) prior to culling, hence this may have masked any differences between either diet or genotype when looking at lipogenesis/lipolysis. Nevertheless, overnight fasting was crucial because feeding strongly impacts mTOR signalling, thus fasting allows us to understand the underlying mechanisms driving the phenotype at a basal state. Overall, the data indicate that deletion of S6K1 and S6K2 in female mice exacerbates HTF-induced biliary damage and fibrosis and increases markers of inflammation.

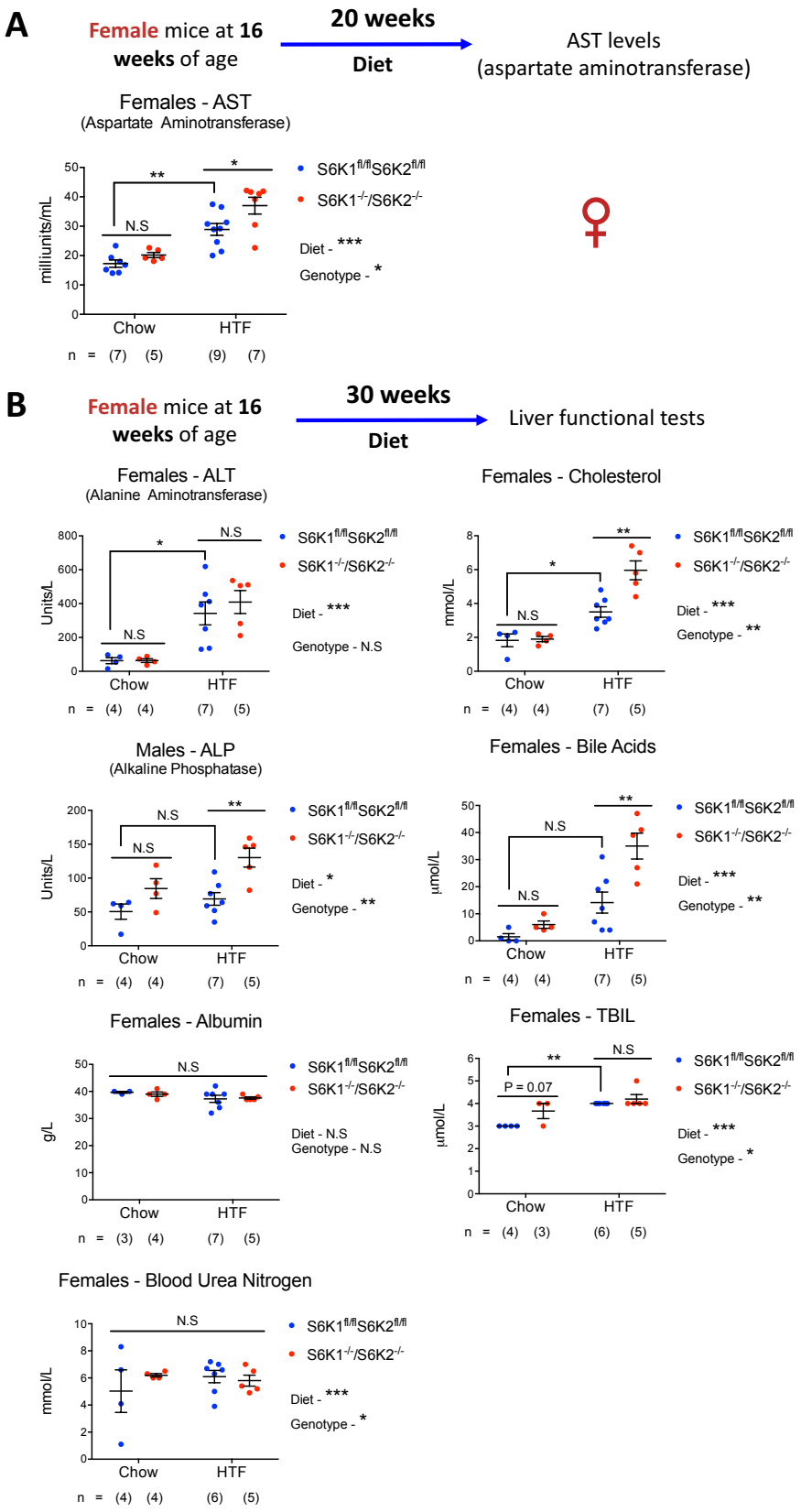

Figure 5.19. Analysis of blood parameters in chow-fed and HTF-fed female mice.
Serum or whole blood was used to analyse the concentration of various blood parameters in S6K1 and S6K2 floxed and knockout chow-fed or HTF-fed female mice following 20 or 30 weeks of the respective diet. **A.** Aspartate aminotransferase (milliunits/mL). **B.** Alanine aminotransferase (Units/L). Cholesterol (mmol/L). Alkaline phosphatase (Units/L). Bile acids (µmol/L). Albumin (g/L). Total bilirubin (µmol/L). Blood urea nitrogen (mmol/L). Data are expressed as mean ± SEM and number of mice used is indicated directly on all graphs. Statistical significance was calculated using two-way analysis of variance with Tukey's multiple comparison test (* $P < 0.05$, ** $P < 0.01$, *** $P < 0.001$). N.S: non-significant.

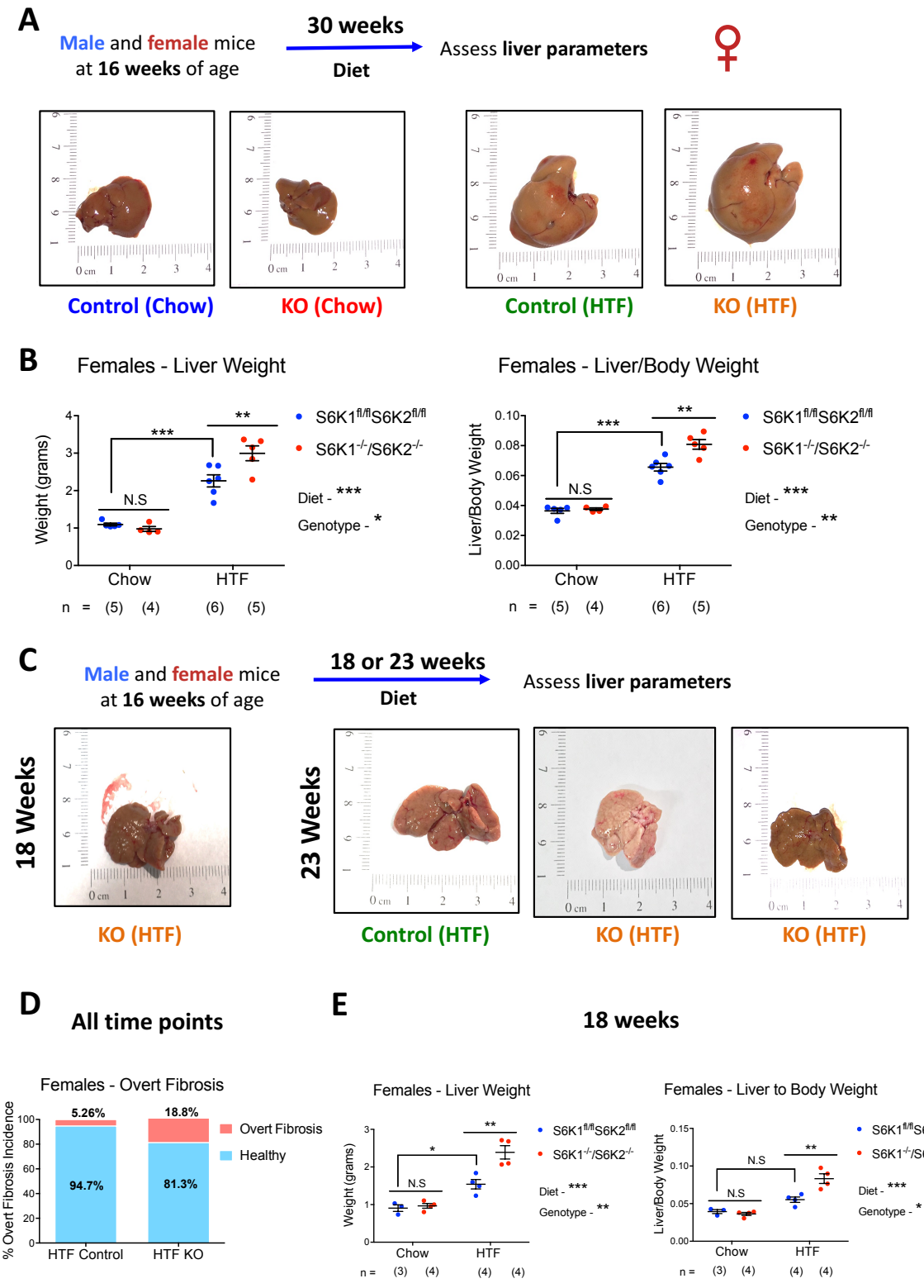

Figure 5.20. Liver-specific S6K1 and S6K2 deletion exacerbates hepatomegaly and overt fibrosis in female mice.

A. Representative photographs of livers from S6K1 and S6K2 floxed and knockout female mice fed either a chow or an HTF diet following 30 weeks of the respective diet. **B.** Left: liver weight (grams). Right: liver weight corrected for the bodyweight. Female mice were fed with the respective diet for 30 weeks. **C.** Representative photographs of livers from S6K1 and S6K2 floxed and knockout female mice with macroscopic liver abnormalities when fed an HTF-diet for 18 or 23 weeks. **D.** Percentage of mice described in (C) bearing liver abnormalities/overt fibrosis. **E.** Left: liver weight (grams). Right: liver weight corrected for the bodyweight. Female mice were fed with the respective diet for 18 weeks. Data are expressed as mean ± SEM and number of mice used is indicated directly on all graphs. Statistical significance was calculated using two-way analysis of variance with Tukey's multiple comparison test (*** $P < 0.001$). N.S: non-significant.

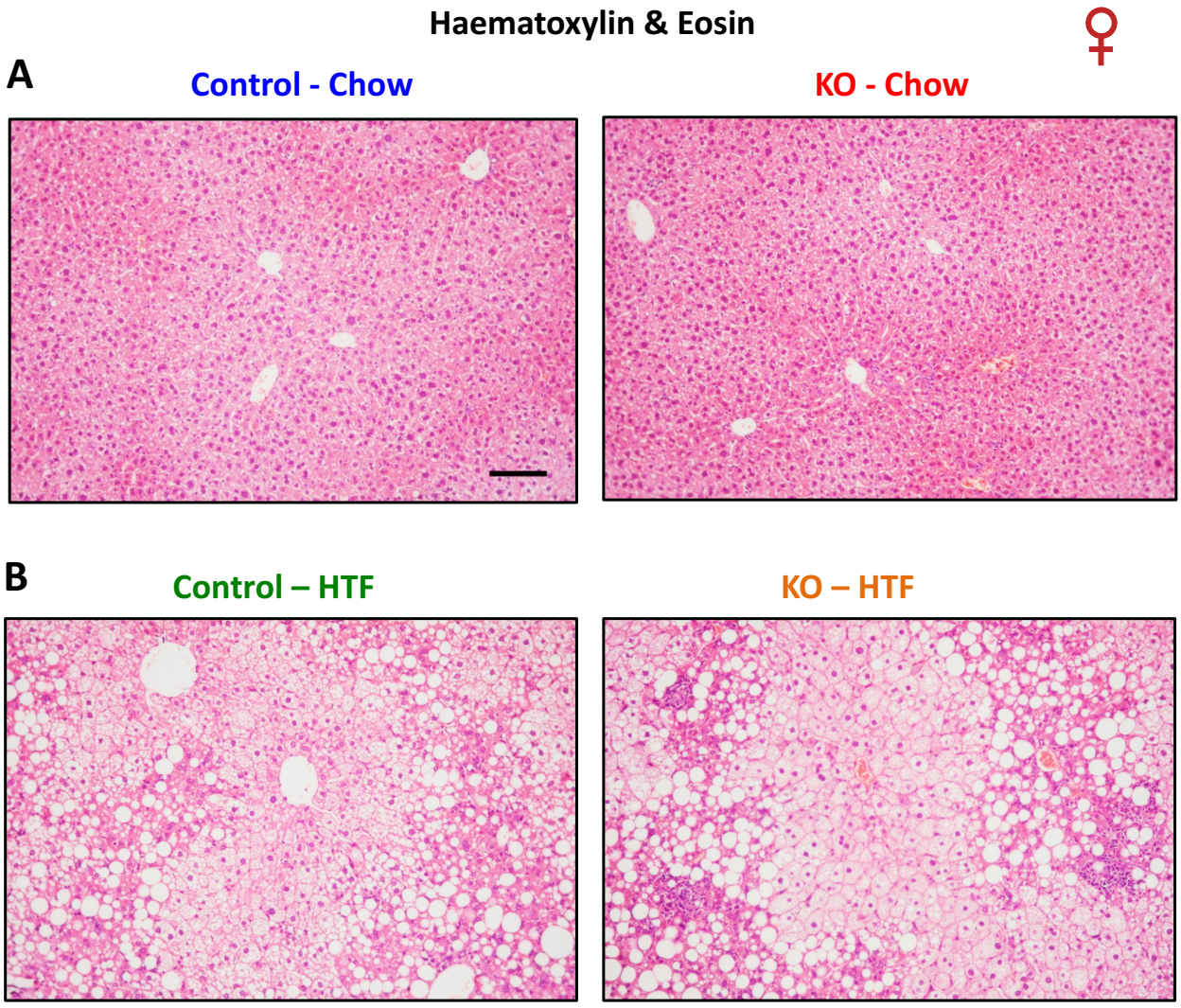

Figure 5.21. Haematoxylin and eosin staining of livers in female S6K1 and S6K2 floxed and knockout mice.
Representative microphotographs of hematoxylin and eosin staining of the liver from the indicated mice. **A.** 46-week-old female S6K1 and S6K2 floxed and knockout mice fed a chow diet. **B.** Female S6K1 and S6K2 floxed and knockout mice fed an HTF diet for 30 weeks. Scale bar, 100 μm.

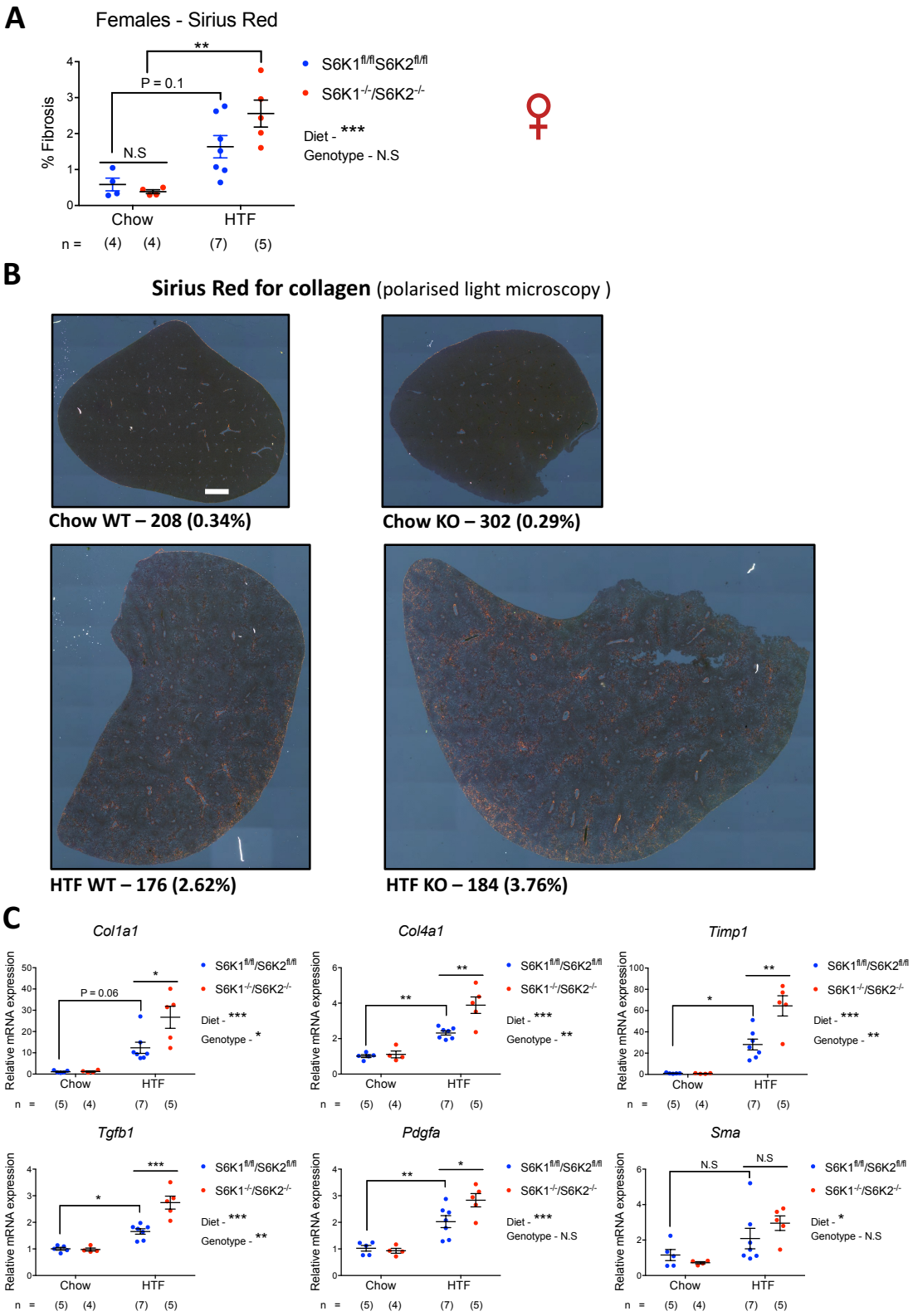

Figure 5.22. Liver-specific S6K1 and S6K2 deletion exacerbates liver fibrosis in female mice. **A.** Quantification of picrosirius red staining of collagen fibres in liver sections of S6K1 and S6K2 floxed and knockout female mice fed either a chow or an HTF diet for 30 weeks. **B.** Representative liver sections from (A) stained with picrosirius red for collagen deposition and visualised by circularly polarised light. Images (original magnification X40) were stitched in ImageJ software to produce a complete liver section image and the collagen (orange) was quantified. **C.** Relative mRNA expression of *Col1a1, Col4a1, Timp1, Tgfb1, Pdgfa* and *Sma* assessed by RT-qPCR from liver lysates in S6K1 and S6K2 floxed and knockout female mice fed either a chow or an HTF diet for 30 weeks. mRNA expression was normalized to *Rps14* housekeeping gene. Data are expressed as mean ± SEM and number of mice used is indicated directly on all graphs. Statistical significance was calculated using two-way analysis of variance with Tukey's multiple comparison test (* P < 0.05, ** P < 0.01, *** P < 0.001). N.S: non-significant. Scale bar, 1 mm.

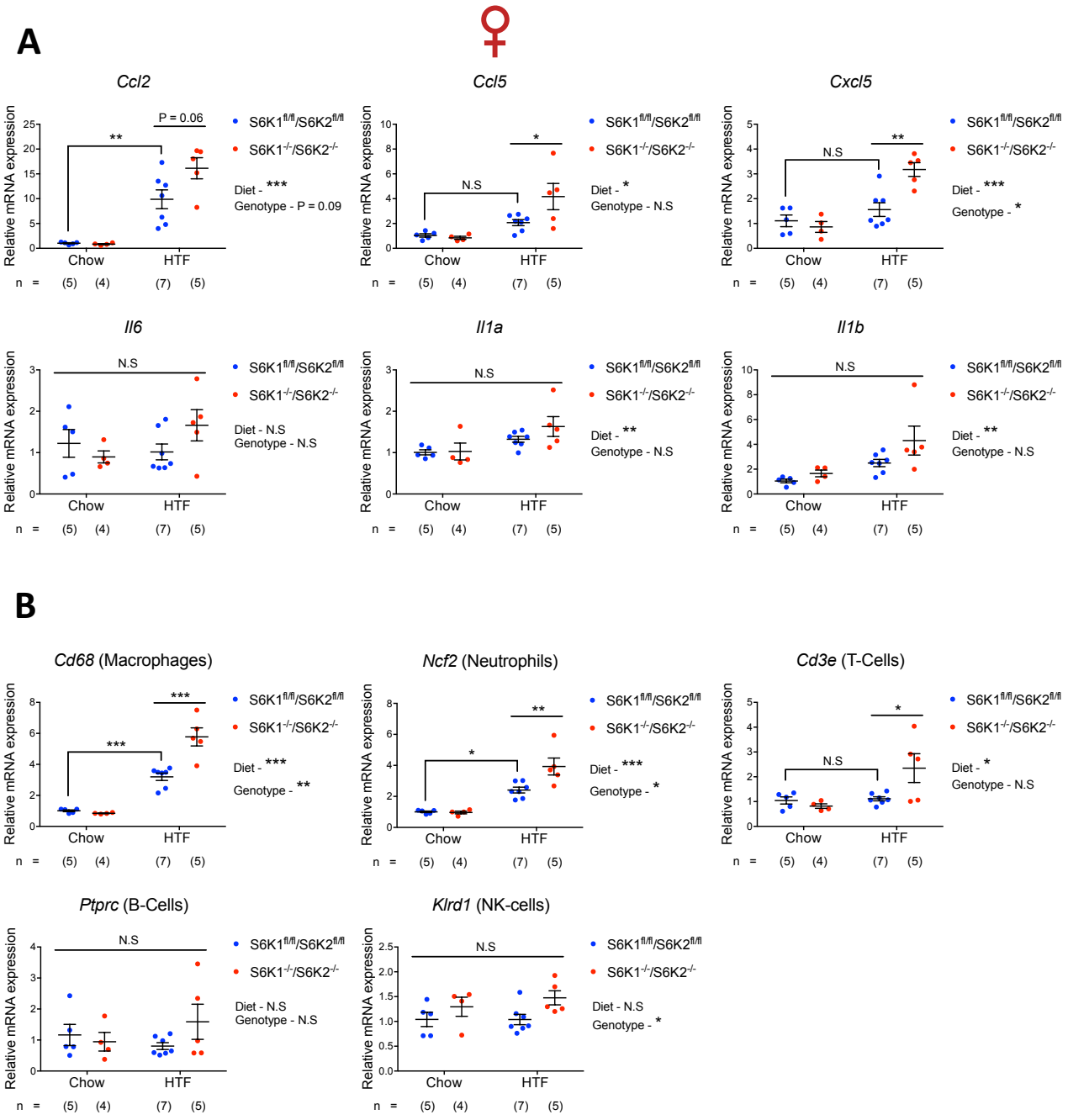

Figure 5.23. Liver-specific S6K1 and S6K2 deletion increases inflammatory gene expression in female mice.
Relative mRNA expression of the indicated genes for inflammation (*Ccl2, Ccl5, Cxcl5, Il6, Il1a* and *Il1b*) and markers of immune infiltration (*Cd68, Ncf2, Cd3e, Ptprc* and *Klrd1*) assessed by RT-qPCR from liver lysates in S6K1 and S6K2 floxed and knockout female mice fed either a chow or an HTF diet for 30 weeks. mRNA expression was normalized to *Rps14* housekeeping gene. Data are expressed as mean ± SEM and number of mice used is indicated directly on all graphs. Statistical significance was calculated using two-way analysis of variance with Tukey's multiple comparison test (* P < 0.05, ** P < 0.01, *** P < 0.001). N.S: non-significant.

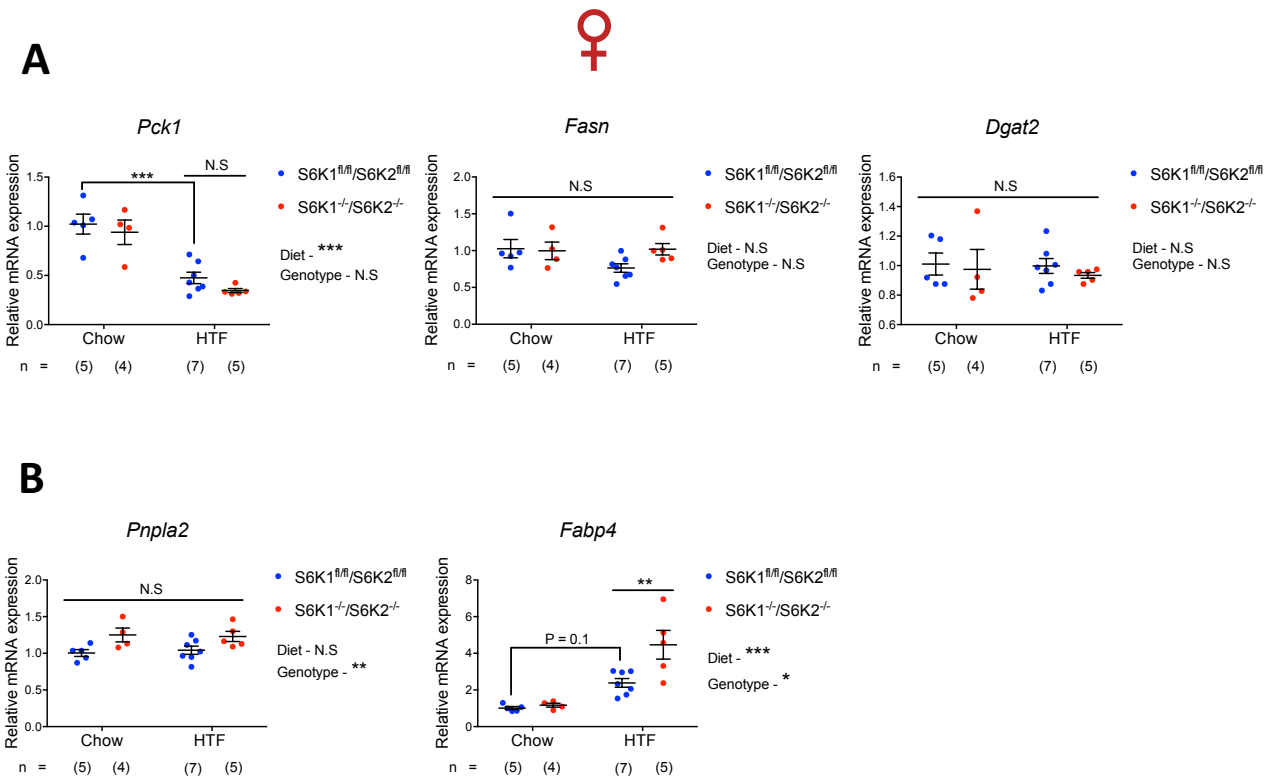

Figure 5.24. Expression of lipogenesis and lipolysis markers in female mice.
Relative mRNA expression of lipogenesis (*Pck1, Fasn* and *Dgat2*) and lipolysis *(Pnpla2* and *Fabp4)* markers assessed by RT-qPCR from liver lysates in S6K1 and S6K2 floxed and knockout female mice fed either a chow or an HTF diet for 30 weeks. mRNA expression was normalized to *Rps14* housekeeping gene. Data are expressed as mean ± SEM and number of mice used is indicated directly on all graphs. Statistical significance was calculated using two-way analysis of variance with Tukey's multiple comparison test (** P < 0.01, *** P < 0.001). N.S: non-significant.

5.10. mTOR signalling in liver and adipose tissue upon deletion of S6K1 and S6K2 in male and female mice.

As we found a sexually dimorphic response with liver-specific deletion of S6K1 and S6K2 in response to an HTF diet, we investigated whether there were any underlying alterations in mTOR signalling between sexes with this diet.

Before elucidating mTOR signalling, however, we first validated the picrosirius red staining by immunoblotting for collagen. Immunoblotting showed a marked increase in collagen type 1 (COL1A1) in the liver of male control mice without tumours upon HTF-feeding (HTF-NT) and this induction was noticeably less in male *S6K1*$^{-/-}$*: S6K2*$^{-/-}$ mice coinciding with reduced fibrosis (Figure 5.25). As expected, all male mice that developed tumours regardless of genotype showed high levels of COL1A1 in the liver (Figure 5.26).

We then examined mTOR signalling in the liver. HTF-feeding of mice resulted in an increase in RPS6 phosphorylation (S240/244 and S235/236), and this was significantly reduced in male S6K1$^{-/-}$; S6K2$^{-/-}$ mice (Figure 5.25). An increase in p4EBP1 (T37/46) and pAkt (S473) was also observed upon HTF-feeding in male control mice, but this was not altered in male *S6K1*$^{-/-}$*: S6K2*$^{-/-}$ mice (Figure 5.26). Female mice also showed a similar increase in mTOR signalling in the liver with HTF-feeding but to a lesser extent than in male mice (Figures 25 and 26).

S6K1 can also be phosphorylated and activated in perigonadal white adipose tissue (PWAT) by HFD feeding, and S6K1 plays a critical role in early adipocyte differentiation (Bae et al., 2012; Carnevalli et al., 2010). Therefore, we investigated whether there were any alterations in mTOR signalling in PWAT between genotypes of male mice upon HTF feeding because there could be a compensatory increase in RPS6 phosphorylation when deleting S6K1 and S6K2 in the liver. Nevertheless, no noticeable differences in phosphorylation of RPS6 (S240/S244 and S235/S236), p4EBP1 (T37/T46) or pAkt (S473) was noticed in male mice between genotypes with HTF-feeding (Figure 5.27). It is important to reiterate that mice were overnight fasted, thus any differences upon diet may be masked since we are looking at basal states in mTOR signalling, and this is especially important for PWAT.

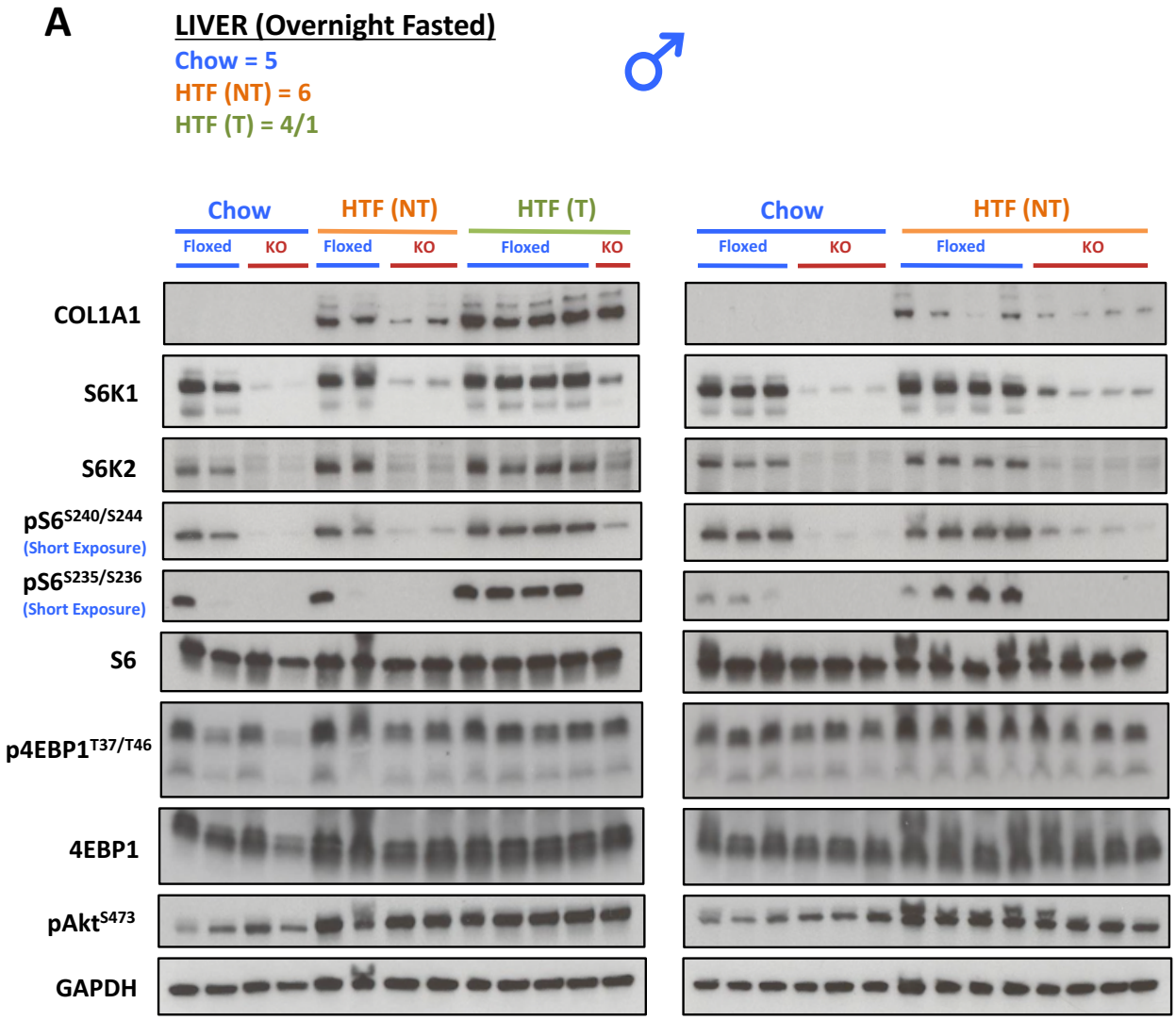

Figure 5.25. mTOR signalling in liver upon deletion of S6K1 and S6K2 in male mice. Immunoblot analysis of COL1A1, S6K1, S6K2, pS6$^{S240/S2440}$, pS6$^{S235/S236}$, S6, p4EBP1$^{T37/T46}$, 4EBP1, pAkt^{S473} and GAPDH expression in whole liver lysates of S6K1 and S6K2 floxed and knockout male mice fed either a chow or an HTF diet for 30 weeks. Mice were overnight fasted prior to tissue harvest. The number of mice used is indicated on the graph.

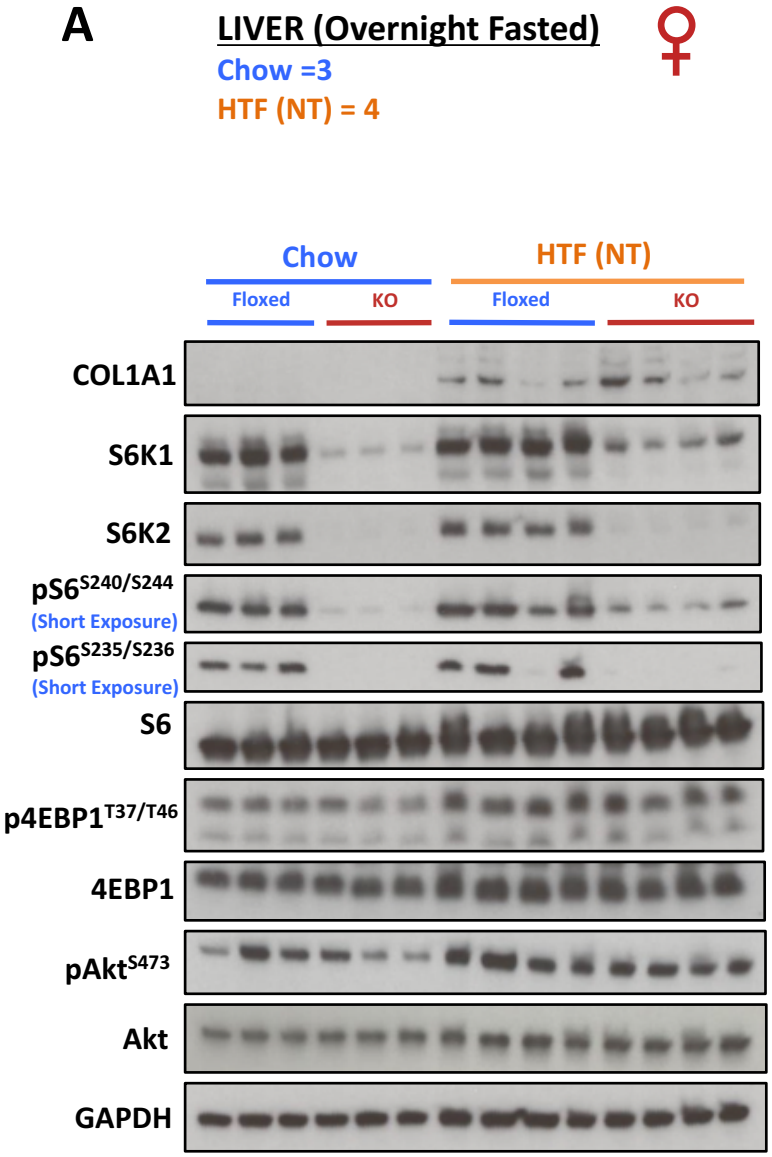

Figure 5.26. mTOR signalling in liver upon deletion of S6K1 and S6K2 in female mice. Immunoblot analysis of COL1A1, S6K1, S6K2, pS6$^{S240/S2440}$, pS6$^{S235/S236}$, S6, p4EBP1$^{T37/T46}$, 4EBP1, pAkt^{S473}, Akt and GAPDH expression in whole liver lysates of S6K1 and S6K2 floxed and knockout female mice fed either a chow or an HTF diet for 30 weeks. Mice were overnight fasted prior to tissue harvest. The number of mice used is indicated on the graph.

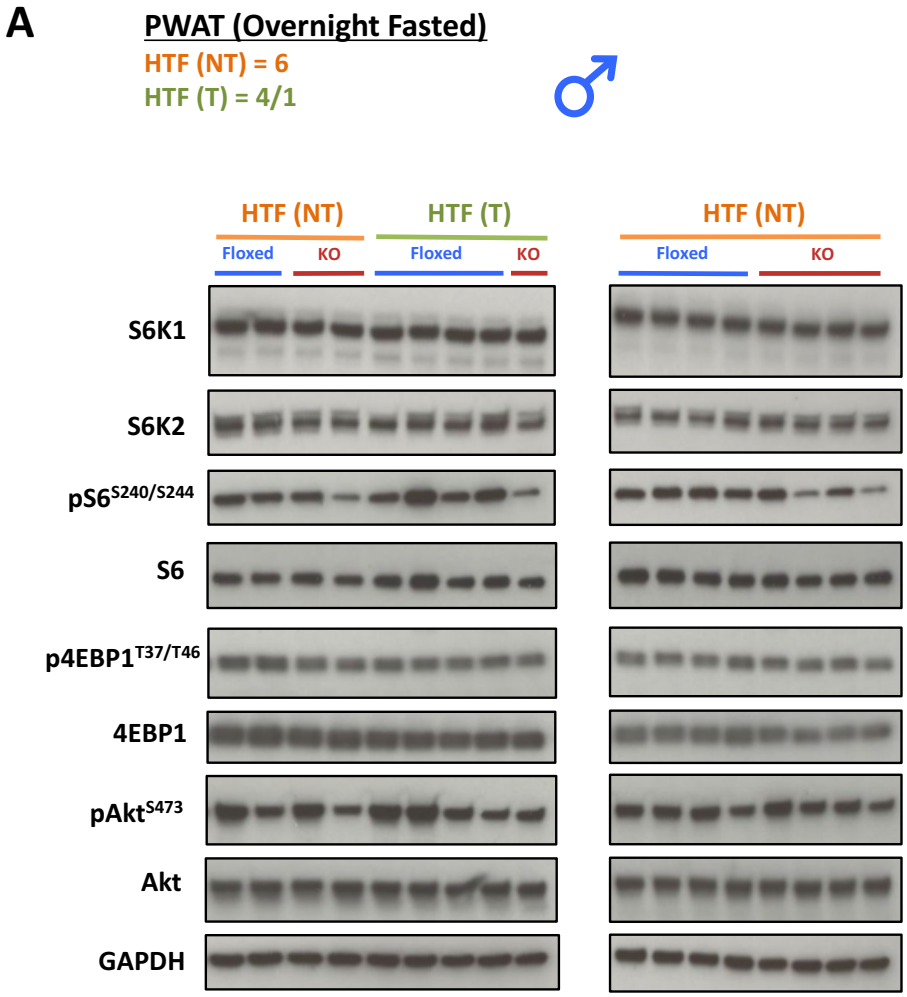

Figure 5.27. mTOR signalling in perigonadal white adipose tissue (PWAT) upon deletion of S6K1 and S6K2 in male mice.
Immunoblot analysis of COL1A1, S6K1, S6K2, pS6$^{S240/S2440}$, S6, p4EBP1$^{T37/T46}$, 4EBP1, pAkt^{S473,} Akt and GAPDH expression in whole liver lysates of S6K1 and S6K2 floxed and knockout male mice fed either a chow or an HTF diet for 30 weeks. Mice were overnight fasted prior to tissue harvest. The number of mice used is indicated on the graph.

5.11. RNA-sequencing analysis validated sexually dimorphic response and revealed dysregulated fatty acid metabolism in HTF-fed mice.

To understand the possible mechanisms driving the differences in liver damage, fibrosis and inflammation between genotypes and sexes, we performed RNA-sequencing in liver homogenates from all groups (chow, HTF-NT and HTF-T) and genotypes (control and knockout) for both sexes (Figure 5.28 A). *The MRC LMS Core Facility prepared and sequenced the cDNA library. The bioinformatics analysis was carried out primarily by Mr. Gopuraja Dharmalingam.* Principal component analysis illustrated that the largest difference was caused by the diet/different groups (chow, HTF-NT and HTF-T), which accounted for 53.73% of the variation followed by gender (28.35% of the variation) (Figure 5.28 B). Clustering analysis also showed that chow-fed male and female mice cluster separately and male mice that developed tumours cluster separately to HTF-fed mice without overt tumours (Figure 5.28 C).

When looking at male mice separately, principal component analysis once again showed that the largest difference was caused by group (chow, HTF-NT and HTF-T), which accounted for 83.64% of the variation (Figure 5.29 A). When comparing just HTF-fed control and knockout male mice, principal component analysis showed 57.52% variation between the two groups (Figure 5.29 B). Gene ontology (GO) analysis showed that inflammation, leukocyte activation, extracellular matrix organisation and apoptosis were amongst the most highly upregulated processes in HTF-fed non-tumour control mice when compared to chow control mice (Figure 5.29 C and D). In contrast, fatty acid metabolism and mitochondrion were amongst the most down regulated processes in HTF-fed non-tumour control mice when compared to chow control mice (Figure 5.29 C and D). Interestingly, HTF-fed *S6K1*$^{-/-}$*: S6K2*$^{-/-}$ male mice showed an enrichment for fatty acid metabolism and mitochondrion while downregulation for extracellular matrix, ERK1/2 signalling and response to growth factors when compared to HTF-fed control mice without overt tumours (Figure 5.29 E and F). Inflammation, however, was not altered in *S6K1*$^{-/-}$*: S6K2*$^{-/-}$ male mice. In addition, GSEA illustrated that many of the most highly enriched gene sets with HTF-feeding correspond to HCC pathways and these were already significantly enriched in HTF-fed control mice without overt tumours and were significantly downregulated in *S6K1*$^{-/-}$*: S6K2*$^{-/-}$ male mice (Figure 5.30 A).

Hepatocyte nuclear factor 4A (HNF4A) and the downstream HNF1A are transcription factors that have been causally implicated in suppressing liver tumorigenesis in both hepatocellular carcinoma and intrahepatic cholangiocarcinoma (Patitucci et al., 2017; Saha et al., 2014). In line, GSEA revealed that HNF4A and HNF1A signatures are significantly downregulated/suppressed in HTF-fed control male mice compared to chow controls, whereas male *S6K1*$^{-/-}$*: S6K2*$^{-/-}$ mice show a significant enrichment for these signatures (Figure 5.30 B). In fact, an enrichment for HNF4A was the most significant gene set in *S6K1*$^{-/-}$*: S6K2*$^{-/-}$ male mice with a normalised enrichment score (NES) of 3.115 and an FDR $q < 0.000$. Importantly, the HNF4A gene set was generated by taking

the top downregulated genes in liver-samples in mice with a liver-specific deletion of HNF4A, thus making this is a robust, specific gene set for assessing HNF4A targets (Ohguchi et al., 2008).

As expected, GSEA revealed a significant downregulation for ribosome biogenesis in male *S6K1*$^{-/-}$*: S6K2*$^{-/-}$ mice, as well as a significant enrichment in IRS-1/IRS-2 signalling due to loss of the negative feedback loop (Figure 5.30 C).

The transcriptome of female mice showed a greater degree of variability. Even so, principal component analysis showed a 32.75% and 47.59% difference between the two genotypes in chow-fed and HTF-fed mice, respectively (Figure 5.31 A and B). GO analysis of female mice showed similar findings to males when comparing HTF-fed control mice to chow-fed control mice such as upregulation of inflammation, extracellular matrix and apoptosis as well as downregulation of fatty acid metabolism (Figure 5.31 C and D). GSEA of HTF-fed *S6K1*$^{-/-}$*: S6K2*$^{-/-}$ female mice compared to HTF-fed control mice in general showed an exacerbated response with further enrichment for liver cancer pathways, liver development and stem cells and downregulation of peroxisome, fatty acid metabolism and HNF4A, suggesting possible progression to tumorigenesis (Figure 5.31 E). Nevertheless, differences observed between HTF-fed females of the two genotypes were not as striking as in male mice since the female knockouts also develop the pathology akin to control mice but just to a greater degree. Whereas, male knockout mice are protected from NASH-HCC, thus cluster closer to chow-fed mice, which is in the opposite direction to that of HTF-fed control mice that develop the full NASH pathology.

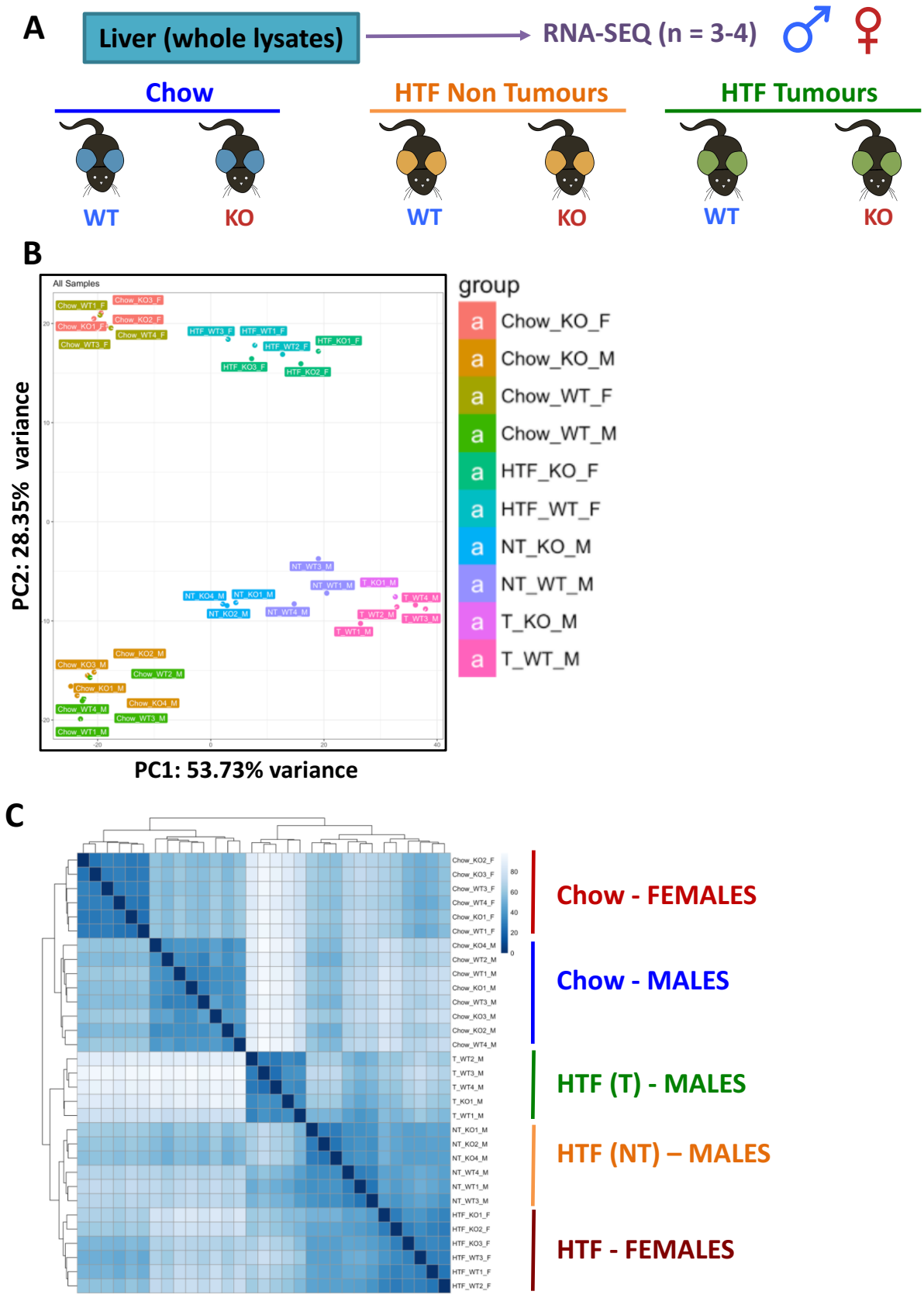

Figure 5.28. RNA-sequencing of liver from male and female mice in the HTF experiment. **A.** Schematic illustrating the workflow for the RNA sequencing. **B.** Principal component analysis of the top 1000 most variable genes between male and female S6K1 and S6K2 floxed and knockout mice fed either a chow or an HTF diet. **C.** Clustering analysis by gene expression between male and female S6K1 and S6K2 floxed and knockout mice fed either a chow or an HTF diet. 3-4 mice per genotype per group were used for the RNA sequencing and analysis.

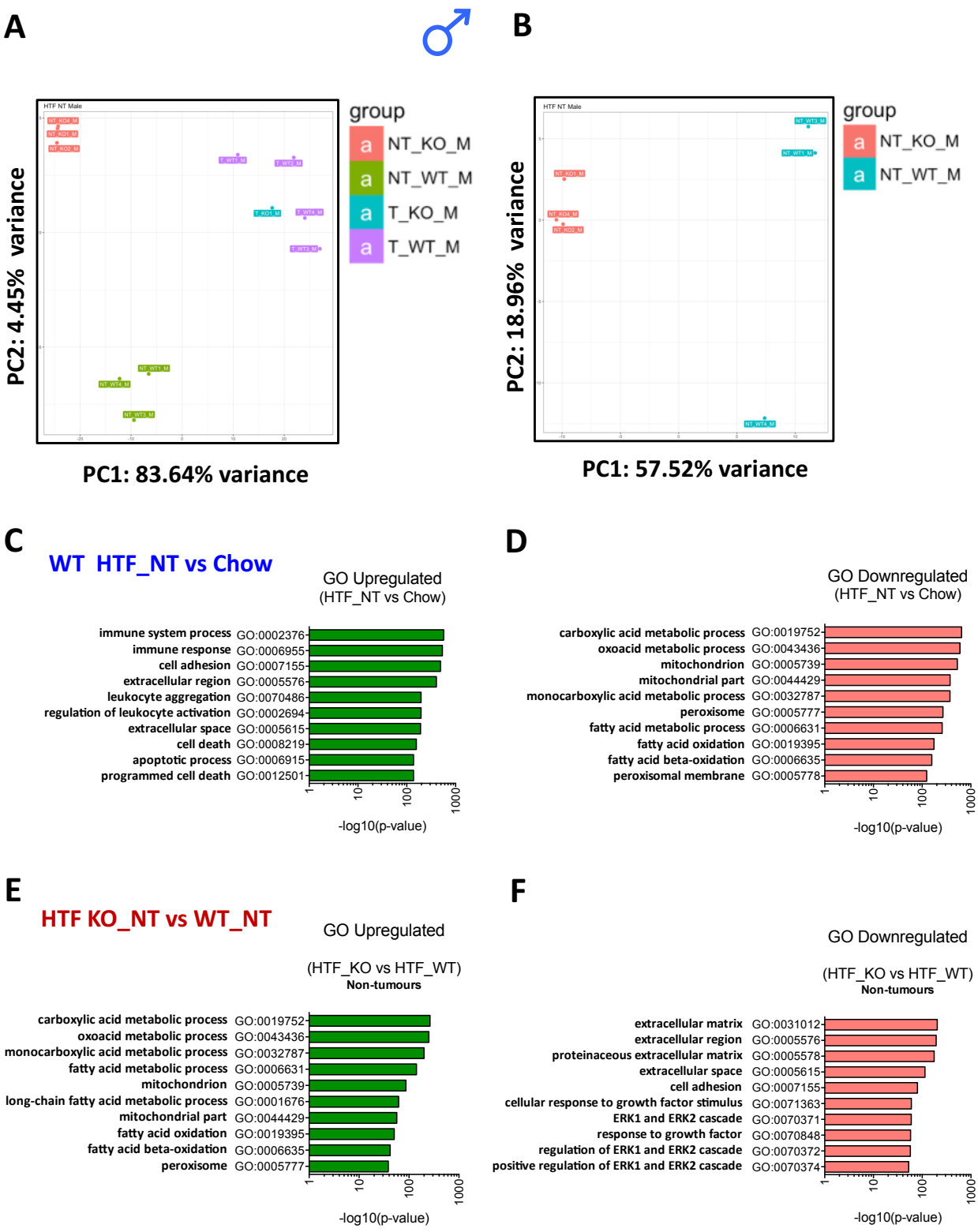

Figure 5.29. RNA-sequencing of liver from male mice in the HTF experiment.
A. Principal component analysis of the top 1000 most variable genes in male S6K1 and S6K2 floxed and knockout mice with and without tumours fed an HTF diet. **B.** Principal component analysis of the top 1000 most variable genes in male S6K1 and S6K2 floxed and knockout mice without tumours fed an HTF diet. **C.** Gene ontology analysis of top upregulated processes with $p < 0.05$ in HTF-fed control mice compared to chow-fed mice. **D.** Gene ontology analysis of top downregulated processes with $p < 0.05$ in HTF-fed control mice compared to chow-fed mice. **E.** Gene ontology analysis of top upregulated processes with $p < 0.05$ in HTF-fed knockout mice compared to control mice. **F.** Gene ontology analysis of top downregulated processes with $p < 0.05$ in HTF-fed knockout mice compared to control mice. 3-4 mice per genotype per group were used for the RNA sequencing and analysis.

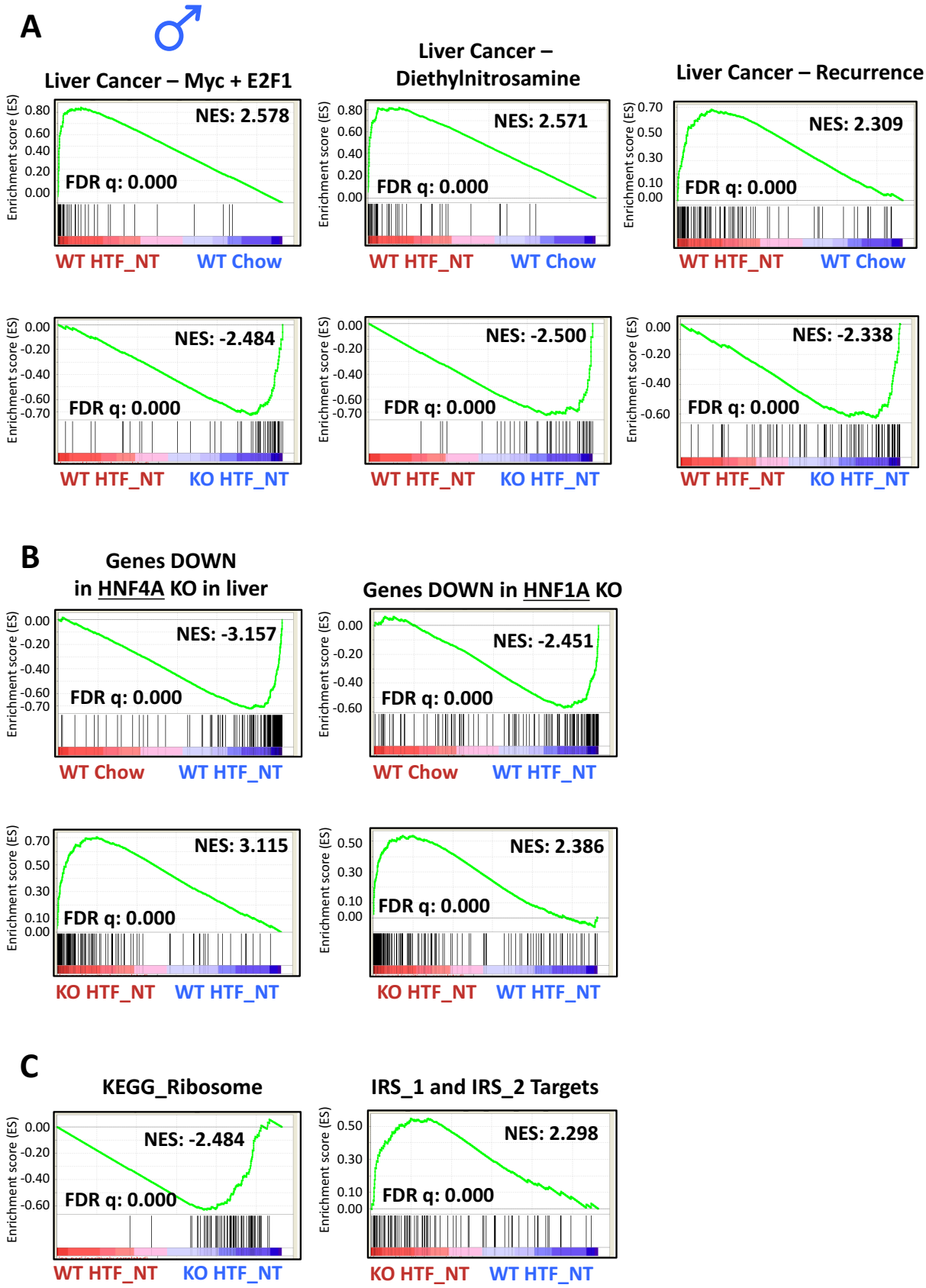

Figure 5.30. Gene-set enrichment analysis (GSEA) of male mice upon HTF-feeding.
A. GSEA depicting the indicated hepatocellular carcinoma signatures that increases with HTF-feeding in control mice and decline in liver of S6K1 and S6K2 knockout mice. **B.** GSEA depicting the HNF4A and HNF1A signatures that decreased with HTF-feeding in control mice and increase in liver of S6K1 and S6K2 knockout mice. **C.** GSEA depicting the KEGG_Ribosome and IRS_1 and IRS_2 signatures that decrease and increase, respectively in HTF-fed S6K1 and S6K2 knockout mice. 3-4 mice per genotype per group were used for the RNA sequencing and analysis.

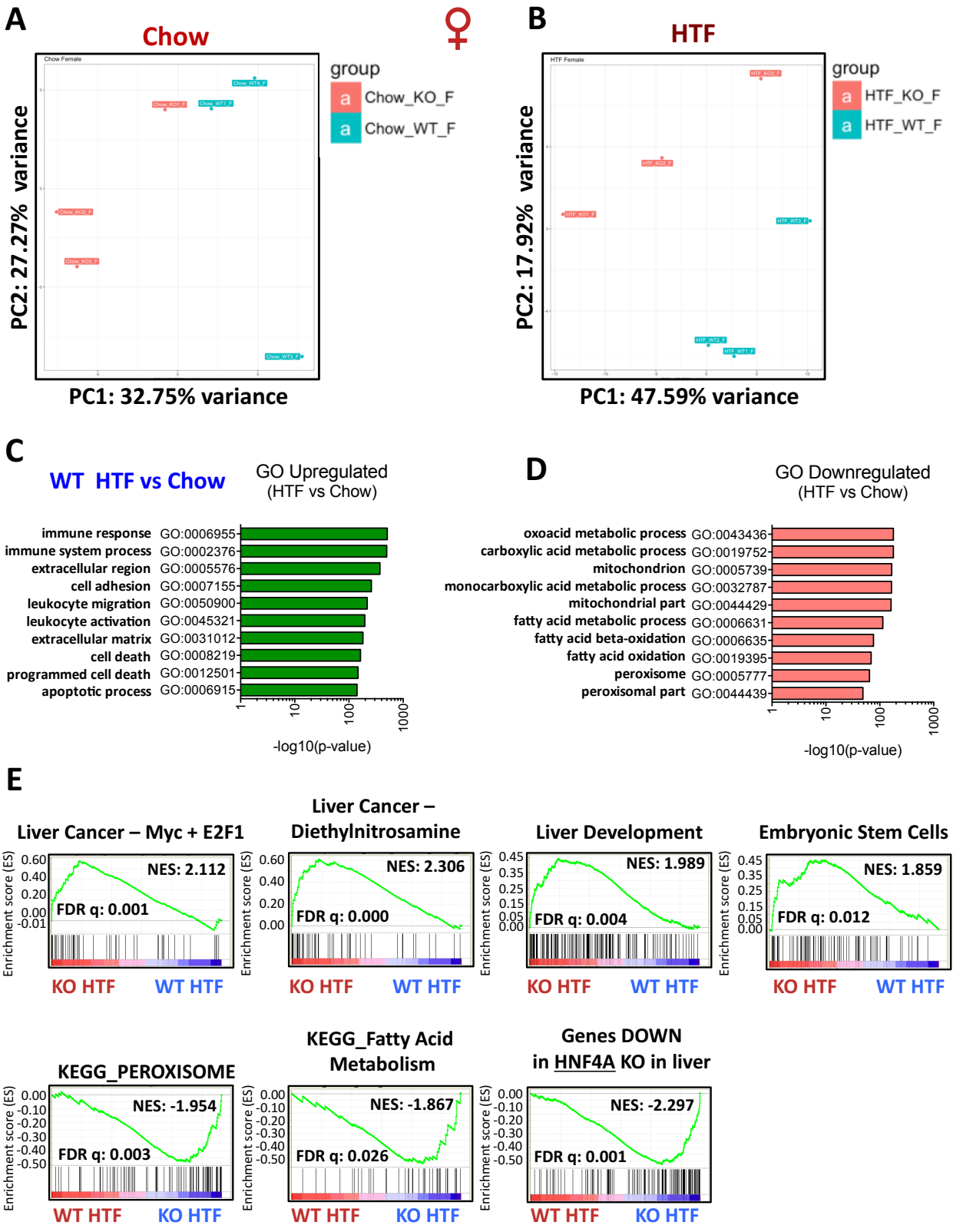

Figure 5.31. RNA-sequencing of liver from female mice in the HTF experiment.
A and B. Principal component analysis of the top 1000 most variable genes in female S6K1 and S6K2 floxed and knockout mice fed either a chow or an HTF diet, respectively. **C.** Gene ontology analysis of top upregulated processes with $p < 0.05$ in HTF-fed control female mice compared to chow-fed mice. **D.** Gene ontology analysis of top downregulated processes with $p < 0.05$ in HTF-fed control female mice compared to chow-fed mice. **E.** GSEA depicting the indicated gene sets that either increase or decrease in liver of S6K1 and S6K2 knockout mice fed an HTF diet compared to HTF-fed control mice. 3 mice per genotype per group were used for the RNA sequencing and analysis.

5.12. Summary

Altogether, we have observed a sexually dimorphic phenotype upon liver-specific deletion of S6K1 and S6K2 when feeding mice with an HTF diet, and the key findings are summarised in Figure 5.32. Deletion of S6K1 and S6K2 in liver does not affect body weight or metabolic function in chow-fed mice in either sex. Male *S6K1*$^{-/-}$*: S6K2*$^{-/-}$ mice fed an HTF diet, however, displayed a partial improvement in metabolic parameters and attenuation of liver damage and fibrosis as well as decreased incidence of HCC. In contrast, female *S6K1*$^{-/-}$*: S6K2*$^{-/-}$ mice fed an HTF diet showed a worsened outcome with an exacerbated NASH response with greater hepatomegaly, biliary damage, fibrosis and inflammation compared to respective controls.

There are several follow-up experiments that remain to be done to elucidate the potential mechanisms by which S6 kinases impact fatty liver disease. These are once again discussed in length in the main Discussion chapter, thus will be alluded to briefly here. First, however, all slides will be sent to a fully certified pathologist to understand whether the HTF diet robustly induced NASH characteristics such as hepatic steatosis, ballooning and Mallory-Denk body formation. In addition, it is also important to understand whether what we have observed is a carcinoma (invasive) or an adenoma (benign). A full pathological examination will allow us to stratify the mice according to different stages of fatty liver disease. We then aim to compare our mice RNA-sequencing data to human data (Prof. Quentin Anstee – see main Discussion) to determine whether commonalities exist between the two species in NASH pathology. In addition, we aim to understand whether pathways shown to be regulated by S6 kinases such as HNF4A are also implicated in human fatty liver disease, as this could yield potential therapeutic targets.

It is still not clear the exact reasons underlying the sexual dimorphism in *S6K1*$^{-/-}$*: S6K2*$^{-/-}$ mice in response to the HTF diet. We therefore aim to understand this by initially comparing the RNA-sequencing data between the two sexes. It is also likely that hormonal changes will play a role in this. Therefore, this could be pursued by either carrying out castrations in male mice or ovariectomies in female mice and examining the outcomes in NASH.

Hepatocellular carcinoma is not only a highly heterogeneous disease with multiple pathways regulating progression but has a strong immunological component. Accordingly, we observed a robust increase in inflammatory gene expression, particularly in male mice, with the HTF diet. Therefore, it is important to carry out a full immunohistochemistry analysis of infiltration of various immune cells, including macrophages (F4/80), T-cells (CD3e) and B-cells (B220) to determine which immune cells are important for driving the NASH pathology and to determine whether deletion of S6K1/S6K2 has an impact on this.

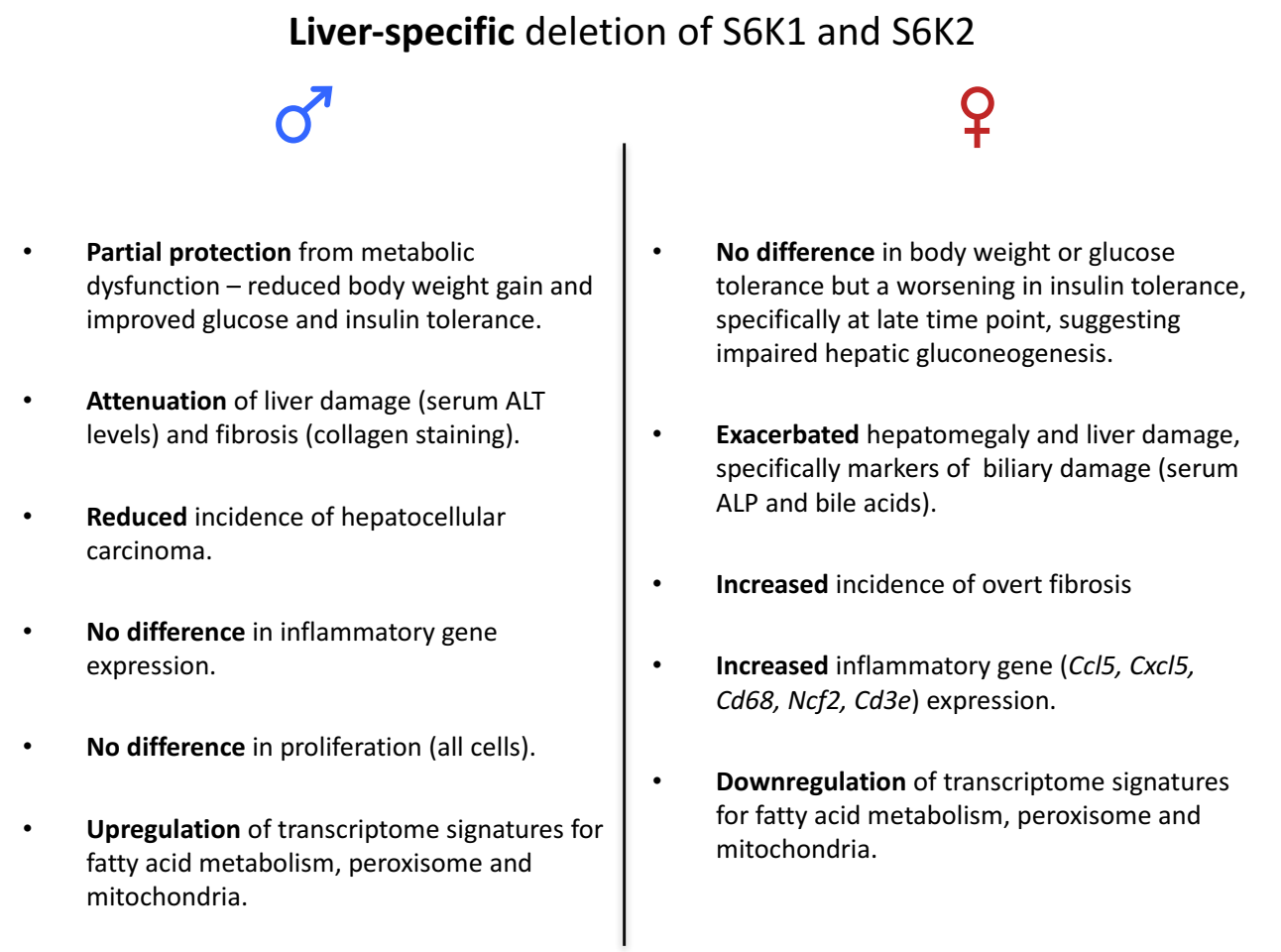

Figure 5.32. Summary of the phenotypic outcomes during NASH in male and female S6K1 and S6K2 knockout mice.

Chapter 6: Discussion.

There has been a steady increase in human lifespan since the middle of the 19th century due to the likes of improved sanitation, science, technology and medicine (Oeppen and Vaupel, 2002). This now means that at least in the Western world, extreme poverty, undernutrition and death by infectious diseases that were once a bane in human history are now things of the past (Oeppen and Vaupel, 2002). This is attributed primarily to a reduction in early-life mortality and to a lesser extent to a decline in late-life mortality. Whilst lifespan continues to increase in some countries, there has been a stagnation in others; and large regional variations exist in lifespan and social inequality even within the U.K (Marmot, 2005; Marmot and Bell, 2012; Marmot et al., 1991). Recent evidence based on analysis of global demographic data postulates a "natural limit" to human lifespan, as the authors argue that although there are mythical stories of Methuselah (969 years old) and others who have lived extraordinarily long lives, our bodies are subjected to natural constraints (Dong et al., 2016). For example, the maximal recorded human lifespan (Jeanne Calment, 122 years) has not increased since the 1990s and that upon reaching 100 years of age there is a tendency towards a decline in improvements to survival (Dong et al., 2016). In the 1990s, Olshansky and colleagues also proposed that there are upper limits to human longevity (Olshansky et al., 1990). Nevertheless, there is still much debate amongst epidemiologists regarding whether there really is an upper limit to human lifespan (Olshansky, 2016; Rozing et al., 2017). Regardless of which party is correct, the emphasis should be placed on improving healthspan, as this is what would yield the greatest benefit to society.

Ageing is the single largest risk factor for a panoply of diseases including neurodegeneration, cardiovascular disease and cancer (López-Otín et al., 2013). Ageing may also be characterised by years of disability and frailty; therefore, targeting ageing will not only improve the quality of life of the elderly but also help reduce the ongoing burden on health services (Campisi, 2013). Accordingly, the discovery that manipulating individual genes can alter lifespan and healthspan has invigorated our hopes of targeting the ageing process as a whole (Gems and Partridge, 2013). It has been a remarkable advancement from the initial discovery by Michael Klass in 1983 utilising *C. elegans* to the present moment where various dietary, genetic and pharmacological approaches exist for extension of lifespan (Klass, 1983; López-Otín et al., 2013). In line, the Withers' group and others have reported that deletion of S6K1, a downstream effector of mTOR, in mice prolongs lifespan and improves insulin sensitivity, motor function, immune function and bone density (Arif et al., 2017; Selman et al., 2009). Potential therapeutic avenues, however, would require a thorough understanding of the molecular basis to ensure the safety of such interventions, especially since they could be long-term. There is now increasing evidence that cellular senescence and inflammation drive age-related pathology (López-Otín et al., 2013). mTOR signalling has recently also been implicated in senescence and SASP regulation, thus raising possible questions as to whether these two crucial biological processes (nutrient sensing and

cellular senescence) are linked. Therefore, we first aimed to investigate how S6K1 affect senescence and inflammation during ageing (Chapter 3 and 4). Given the close link between ageing, obesity and cancer, we also aimed to understand whether S6 kinases (S6K1 and S6K2) play a causal role in non-alcoholic steatohepatitis and its progression to hepatocellular carcinoma (Chapter 5). Showing a causal role for S6 kinases in an age-associated pathology such as fatty liver disease was of importance considering that natural ageing is a slow process that is difficult to study.

6.1. S6 kinases in mammalian ageing and cellular senescence.

We initially investigated whether senescence was affected in the ageing liver because senescence has shown to play a key role in hepatic steatosis, fibrosis and HCC (Kang et al., 2011; Krizhanovsky et al., 2008; Ogrodnik et al., 2017). In addition, a recent study by the Kaeberlein group illustrated that whole body or conditional deletion of S6K1 in liver increase lifespan and improves neurological defects in mice with a deficiency in mitochondrial complex 1 (*Ndufs4*$^{-/-}$*),* thus providing evidence for S6K1 regulating mammalian lifespan in a non-cell autonomous fashion and specifically that loss of liver S6K1 signalling may have systemic beneficial effects (Ito et al., 2017).

600-day-old *S6K1*$^{-/-}$ mice, did not show a significant reduction in senescence markers ($p16^{INK4A}$ or $p19^{ARF}$ mRNA levels) compared to age-matched controls, suggesting that S6K1 does not regulate senescence. Furthermore, preliminary SA-β-Gal staining of the liver actually showed a greater number of positive cells in otherwise healthy *S6K1*$^{-/-}$ mice compared to healthy WT counterparts, suggesting diminished senescence clearance in ageing. It is important to highlight that there are caveats since it is technically difficult to detect senescent cells in tissues such as by SA-β-Gal staining, thus this need to be repeated. Nonetheless, the observed reduction in inflammation in *S6K1*$^{-/-}$ mice could be down to either an attenuation of the SASP and as a result decreased immune infiltration or a systemic defect in development and activation of immune cells. The latter seems unlikely since *S6K1*$^{-/-}$ mice did not show any significant alterations in the absolute number of immune cells in peripheral blood, and previous reports have demonstrated that the haematopoietic stem cell function is preserved in these mice with age (Ghosh et al., 2016; Selman et al., 2016). Still, we observed a significant reduction in age-related induction of macrophage markers in the liver of old *S6K1*$^{-/-}$ mice compared to WT counterparts. Therefore, we investigated whether macrophage activation was affected instead by preparing BMDMs from 10-week-old WT and *S6K1*$^{-/-}$ mice. S6K1 deletion, however, did not blunt the proinflammatory response to LPS stimulation. BMDMs were also generated, with the aid of Dr. Silvia Pedroni, and stimulated with either LPS (M1) or IL4 (M2) in 600-day-old WT and *S6K1*$^{-/-}$ mice to assess whether there is an age-dependent effect on macrophage activation (currently been processed). All this led us to hypothesise that perhaps the SASP response is blunted in the liver of old *S6K1*$^{-/-}$ mice, and this is the cause for the decreased immune cell infiltration. In agreement, *S6K1*$^{-/-}$ mice displayed a

significant reduction in age-related induction of interleukins and chemokines, immune cell markers, particularly of macrophages, as well as downregulation of several inflammatory pathways and age-related secreted factors. Altogether, given that inflammation drives many age-related pathologies, it is likely that at least some of the benefits observed in *S6K1*$^{-/-}$ mice are due to reduced tissue inflammation.

Our data linking S6K1 to inflammation is consistent with previous literature connecting mTOR signalling and inflammation. As reviewed by Powell and colleagues, mTOR has been implicated in regulating the activity of a range of immune cells including T and B cells, NK cells, neutrophils and macrophages (Powell et al., 2012). The complex link between inflammation and mTOR is beginning to be unravelled, but it is still difficult to derive a conclusive result as the data can be contradictory in nature due to differences in deletion (e.g., adipose tissue or liver), type and duration of obesogenic diet and the complexity of the mTOR signalling network (Laplante and Sabatini, 2012; Saxton et al., 2017; Zoncu et al., 2011). Several studies suggest that mTOR signalling regulates inflammation during ageing and obesity. For example, we and others have previously reported that rapamycin treatment in old mice reduced inflammatory gene expression in liver (Correia-Melo et al., 2016; Herranz et al., 2015). In addition, specific deletion of RAPTOR, which is essential for mTORC1 assembly and function, in macrophages improved insulin sensitivity and reduced inflammation in liver and adipose tissue when fed a high-fat diet (Jiang et al., 2014).

An important question that still remains to be answered is what is underpinning the reduction in immune cell markers and inflammation in *S6K1*$^{-/-}$ mice? This is primarily because senescence and inflammation were assessed in whole liver lysates, thus making it difficult to conclude whether the senescent cells in *S6K1*$^{-/-}$ mice have reduced SASP expression or whether the reduction in inflammation is simply due to a decrease in immune cell infiltration. It is likely that the reduction in inflammation observed in *S6K1*$^{-/-}$ mice is due to a combination of these two factors. Nevertheless, clarifying this is of importance for future therapeutic approaches targeting senescence or S6 kinases, particularly because many SASP factors are expressed by immune cells, including Kupffer cells.

To answer this, we are carrying out single-cell RNA sequencing of perfused liver from young and old wild type and *S6K1*$^{-/-}$ mice utilising the recently described 10X platform (Zheng et al., 2017). This is being carried out in collaboration with Dr. Tom Bird, Dr. Kristina Kirschner and Dr. Tamir Chandra (University of Glasgow and University of Edinburgh, U.K), and the bioinformatics analysis is currently ongoing. In addition, we have fractionated separate cell populations from the liver of young and old mice for the two genotypes by performing liver perfusions followed by Percoll gradients to isolate hepatocytes as well as MACS (magnetic-activated cell sorting) separation to isolate CD45+ immune cells or the remaining stromal

component (Figure 6.1). Fractionations were done with the aid of Dr. Santiago Vernia (MRC LMS) and Dr. Silvia Pedroni. By combining single-cell RNA sequencing with cell fractionation, we aim to not only elucidate whether senescent cells in old *S6K1*$^{-/-}$ mice express less SASP components but also to identify exactly which cell type(s) is undergoing senescence, the percentage of senescence and the composition of the SASP in senescent cells in the ageing liver. In addition to ageing, the role of S6 kinases in SASP regulation *in vivo* can be studied in the model of oncogenic NRAS^{G12V} induced senescence in hepatocytes to further strengthen the argument. Following senescence induction, GFP+ (green fluorescent protein) senescent hepatocytes can be isolated by combining liver perfusions with FACS (fluorescence-activated cell sorting) and then assessing SASP components by RT-qPCR. Senescent hepatocytes are usually cleared by the adaptive immune system; thus, one would expect the senescent hepatocytes to persist in either the *S6K1*$^{-/-}$ mice or in the *Alb-Cre X S6K1*$^{fl/fl}$ mice due to decreased SASP expression. This is indeed what occurred with rapamycin treatment (Herranz et al., 2015).

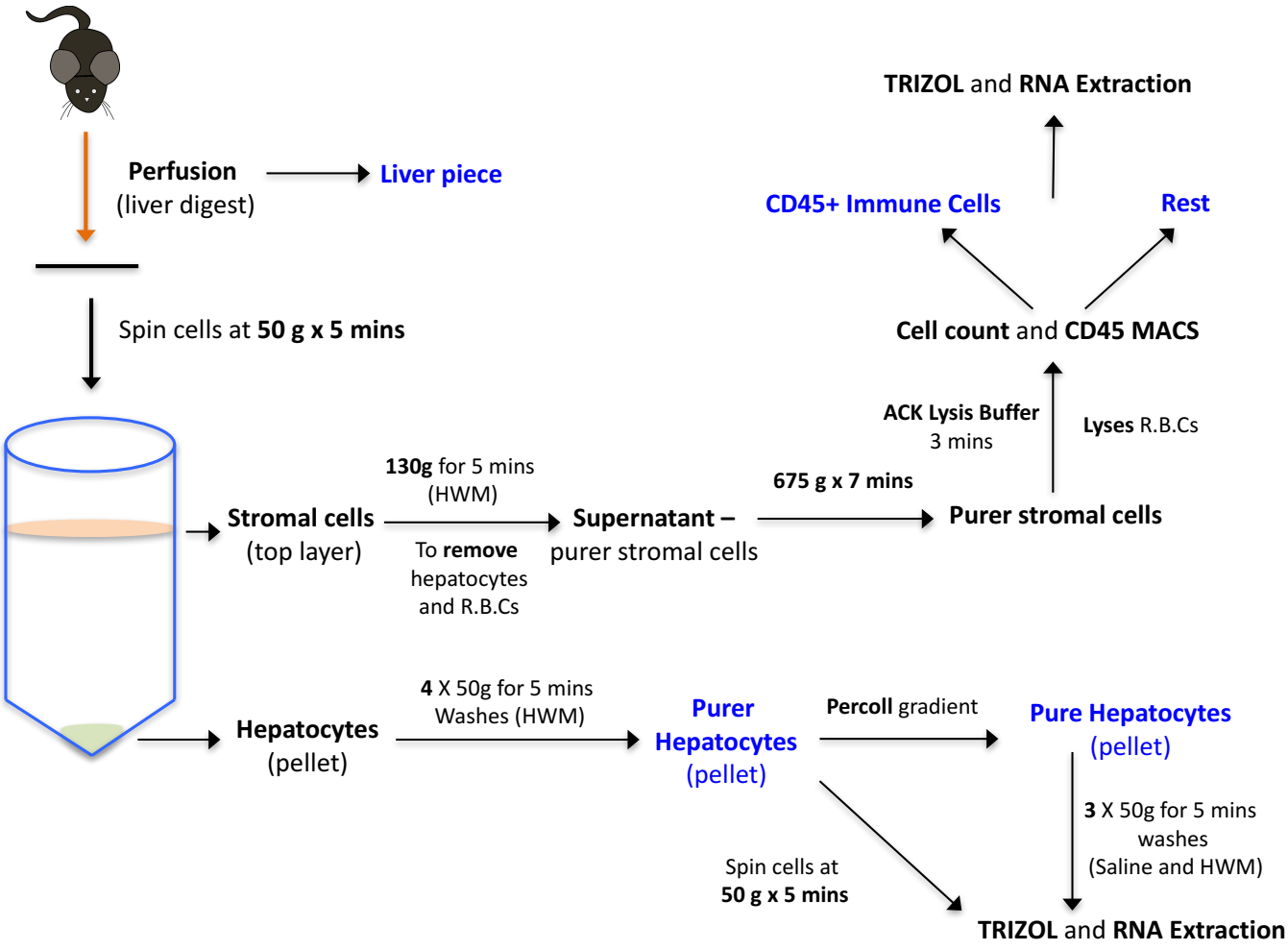

Figure 6.1. Isolation of hepatic cell fractions to assess senescence.

Livers of young (90 days) and old (600 days) WT and *S6K1*$^{-/-}$ mice were perfused with collagenase, disaggregated, and spun down to separate the stromal and hepatocyte fractions. Hepatocytes were purified with a Percoll gradient. Stromal fraction was depleted of red blood cells and then CD45+ immune cells and the remaining stromal cells were isolated by MACS (magnetic-activated cell sorting) separation. A liver piece was taken before liver disaggregation to assess senescence in the whole liver. HWM: hepatocyte wash medium. R.B.Cs – red blood cells.

Given that S6K1 also regulates obesity and the close link between obesity and inflammation, one may question whether the reduction in age-related inflammation observed in *S6K1*$^{-/-}$ mice is merely due to the fact that these mice are protected from age-related fat gain? It is likely that this will contribute to some degree, but it is also unlikely that this is the sole reason. We observed a reduction in inflammation not only in the liver but also in the brain and kidney, which suggest that S6K1 regulates age-related inflammation in multiple organs, but this could still be a systemic effect of decreased fat. In addition, MEFs isolated from S6K1 and/or S6K2 knockout mice display a reduction in *Il1a* and *Il1b* mRNA expression in both replicative senescence and OIS. Depletion or chemical inhibition of S6 kinases also diminishes expression of inflammatory factors in human IMR90 fibroblasts undergoing RAS-induced senescence. Therefore, S6 kinases regulate the SASP in established models of senescence *in vitro*, suggesting that this is not merely an indirect effect of many processes occurring in the ageing liver.

It is nonetheless important to highlight that no causal relationship between the SASP and age-related pathologies exist as of yet. This remains one of the most difficult but crucial avenues for future senescence research. This is primarily due to the difficulty in manipulating senescent cells *in vivo*. There are, however, several ways to tackle this problem such as by generating a specific mouse strain that would allow selective inhibition of the SASP in senescent cells. Such a mouse is indeed being established in the Withers/Gil labs by a combined approach. First, a mouse was generated where the p16^{INK4A} promoter drives expression of CRE-ERT2 (cre-recombinase activated by tamoxifen) and Antares (a dual bioluminescent reporter and cyan-excitable orange fluorescent protein). These mice were then bred with a mouse harbouring a constitutively active mutant of ZFP36L1 that is induced upon cre-mediated excision of a floxed stop codon. Thus, if the final mouse strain works as intended, the mutant ZFP36L1 will be expressed specifically in p16+ cells and selectively degrade SASP components. This mouse could then be used to assess the effect of the SASP in age-related pathologies such as kidney glomerulosclerosis or atherosclerosis, where there the SASP is suspected to play an important role (Baker et al., 2016; Childs et al., 2016).

The specific regulation of the SASP without affecting senescence (*i.e.,* attenuation of the SASP with an intact senescence growth arrest) has not been demonstrated in mammalian ageing thus far. Our data suggest that this may indeed be the case in long-lived *S6K1*$^{-/-}$ mice since we observed normal levels of senescent cells in the ageing liver but with lower expression of proinflammatory factors in *S6K1*$^{-/-}$ mice. In addition, deletion of S6K1 in isolation or together with S6K2 did not prevent replicative senescence but blunted the induction of *Il1a* and *Il1b* in MEFs. We observed a similar pattern in human IMR90 fibroblasts undergoing OIS with either chemical inhibition or siRNA-mediated depletion of S6 kinases. Therefore, S6K deletion/depletion/inhibition results in attenuation of the proinflammatory SASP without affecting the senescence growth arrest.

Importantly, this seems to be distinct from mTOR inhibition since rapamycin (and other mTOR inhibitors) treatment bypassed replicative senescence in fibroblasts (Kolesnichenko et al., 2012; Walters et al., 2016). In addition, mTOR inhibition in cells undergoing OIS showed a significant reduction in many senescent markers such as $p16^{INK4A}$, $p21^{CIP1}$, p53 and SA-β-Gal activity, suggesting the cells were no longer senescent; but they remained arrested due to inhibition of cyclin D1 and D3 (Herranz et al., 2015; Laberge et al., 2015). Alternatively, depletion of S6 kinases did not affect SA-β-Gal activity or any other senescent markers, suggesting that the cells remained senescent but with a blunted SASP response. A similar phenotype has recently been shown in senescent fibroblasts where the chromatin reader BRD4 specifically regulated transcription of SASP genes by associating with super enhancers without regulating the growth arrest (Tasdemir et al., 2016).

Following on from the *in vivo* work, we utilised the *in vitro* systems to also study the potentials mechanisms of how S6 kinases regulate the SASP, as this is difficult to do *in vivo.* S6 kinases seem to most robustly regulate IL1B and IL1A expression and to a lesser extent other inflammatory factors in fibroblasts, suggesting selective SASP regulation. In addition, MEFs isolated from *S6K1*$^{-/-}$*: S6K2*$^{-/-}$ mice seem to display a stronger inhibition of the SASP induction than chemical inhibition of S6 kinases, suggesting a non-catalytic activity of S6 kinases may be important for mediating some aspect of SASP regulation. This, however, needs to be explored further by for example isolating MEFs from the S6K1 kinase dead mutant mice that is now established in Withers' laboratory. In line, S6K1 has recently been identified as an interacting partner with the signalling adaptor STING (stimulator of interferon genes) during host anti-viral responses (Wang et al., 2016). Importantly, STING lies downstream of cGAS (cyclic GMP-AMP synthase), which is a cytosolic sensor of double stranded DNA that upon activation synthesises cGAMP and thereby promote STING-mediated expression of inflammatory cytokines; and cGAS-STING has also recently been implicated in senescence and SASP regulation (Glück et al., 2017; Yang et al., 2017). Therefore, S6 kinases may possibly regulate the SASP via interaction with the cGAS-STING pathway, although this is yet to be studied. It is still unclear how S6 kinases regulate the SASP. This is especially so because none of the S6K targets that we tested seem to robustly regulate the SASP. This could be because many S6K targets act in concert or opposing directions, thus what we observed with S6K deletion is a cumulative effect of many potential targets. S6 kinases are also involved in many feedback loops, thus further complicating identifying the exact mechanism of SASP regulation. Importantly, it is very likely that the recently identified S6K1 target EPRS is not responsible for the reduction in inflammation observed in old *S6K1*$^{-/-}$ mice. This is because not only the directionality of SASP regulation by EPRS was different to S6 kinases but also because long-lived loss of function *EPRS*^{S999A} mutants did not show any significant alterations in systemic inflammation (Arif et al., 2017).

mTOR acts primarily through either the S6 kinases or the 4EBPs (Saxton et al., 2017). Thus, one may ask whether the attenuation of inflammation in the ageing liver is due to excessive activation of S6K2 or further downregulation of 4EBPs as a result of increased phosphorylation of these targets by mTOR due to S6K1 absence. Although this is difficult to completely rule out, it is unlikely that at least the regulation of the SASP is due to increased S6K2 in cells lacking S6K1 since deletion of S6K2 also showed a reduced SASP and the effect was stronger with combined S6K1 and S6K2 deletion, suggesting an additive rather than opposing effect of the two kinases. In addition, it is also unlikely that inhibition of 4EBPs result in reduced SASP since we have previously demonstrated that it is over activation of 4EBP1 that blunts the SASP by utilising a 4EBP1 dominant negative mutant that cannot be phosphorylated by mTOR (Herranz et al., 2015).

One may also ask whether the reduction in SASP is linked to cell size since S6K1 regulates cell size in certain cell types such as pancreatic beta cells (Pende et al., 2000). We did not observe any noticeable change in cell size with S6K1/2 deletion in MEFs as opposed to mTOR depletion/inhibition, so this is unlikely to be the case. For example, depletion of EPRS results in strikingly smaller cells but they have increased mRNA and protein expression of proinflammatory cytokines such as IL6 and IL8, thus suggesting that it is not a straight forward linear relationship between cell size and SASP expression.

Finally, it is important to highlight that it is extremely difficult to dissect and recapitulate the complexity of a global knockout model during mammalian ageing in fibroblasts since many processes would likely contribute to the reduction in inflammation that we have observed. Nevertheless, the *in vitro* data support the argument that S6 kinases indeed regulate the SASP and what we have observed is not merely an indirect effect of many processes occurring simultaneously in an ageing context. Therefore, it is likely that S6K1 regulation of the SASP contributes at least to some degree the effects on age-related inflammation.

6.2. S6 kinases regulate NASH and HCC.

Ageing and metabolic dysfunction are tightly linked. Thus, it is unsurprising that in addition to regulation of mammalian lifespan, S6 kinases also play a critical role in regulation of obesity and hepatic steatosis (Bae et al., 2012; Hee Um et al., 2004). Furthermore, obesity and hepatic steatosis are major risk factors for the development of NASH and HCC; for which there is currently no available treatments for end-stage disease. We therefore generated mice with liver-specific deletion of S6K1 and S6K2 and investigated whether these mice are protected from NASH and HCC.

We did not observe significant alterations in body weight or metabolic phenotypes upon liver-specific deletion of S6K1 and S6K2 in chow-fed mice for either sex. It was also recently

shown that liver-specific deletion of S6K1 alone does not affect body weight (Ito et al., 2017). Feeding mice with the HTF diet, resulted in a heterogeneous response even amongst control mice. Female control mice showed a less pronounced NASH response compared to male mice, which could be explained by oestrogen being protective against liver fibrosis (Xu et al., 2002). Male control mice showed distinct macroscopic phenotypes whereby some not only developed NASH but also progressed to HCC. This was further complicated by the sexual dimorphic response observed with liver-specific deletion of S6K1 and S6K2.

As hypothesised, male *S6K1*$^{-/-}$*: S6K2*$^{-/-}$ mice (liver-specific deletion) showed partial protection from metabolic dysfunction, liver damage, fibrosis and HCC incidence. Both global deletion of S6K1 and S6K2 (mixed background) and liver-specific depletion of S6K1 and S6K2 by AAVs also showed metabolic protection and reduction in hepatic steatosis in male mice when fed an HFD (Bae et al., 2012; Castañeda et al., 2012). Global deletion of S6K1 or S6K2, however, did not protect mice from HCC development driven by PTEN loss, suggesting underlying differences in stimulus and diet may confer phenotypic alterations (Nemazanyy et al., 2013). Importantly, a full pathology of NASH (*e.g.,* hepatic steatosis, ballooning and Mallory-Denk body formation) and HCC is required to understand whether the HTF diet induced most features of NASH as predicted and the effects of S6K1/2 deletion on NASH. Therefore, all histology slides will be sent to a histopathologist to be assessed. In addition to the NASH characteristics, it is of particular importance to also understand whether what we have observed is truly a hepatocellular carcinoma (invasion and malignancy) or a hepatic adenoma (benign tumour). Given that multiple lesions or outgrowths were observed, it is likely to be a carcinoma, but this will require confirmation by a certified pathologist.

Given the prominent role of S6 kinases in cell growth, proliferation and metabolism, it was to be expected that male *S6K1*$^{-/-}$*: S6K2*$^{-/-}$ mice would show a protection from NASH induced HCC development. When looking at publically available databases including the TCGA (The Cancer Genome Atlas) database, it was evident that both S6K1 (*RPS6KB1*) and S6K2 (*RPS6KB2*) are often amplified and sometimes mutated in many cancers including liver cancer (9.6%) with a tendency towards co-occurrence (Figure 6.2) (cbioportal.org) (Cerami et al., 2012; Gao et al., 2013). Importantly, however, the mTOR-S6K axis is more often found to be functionally activated (RPS6 S240/S244 or S235/S236 phosphorylation) rather than amplified/mutated in liver cancer (Guichard et al., 2012; Sieghart et al., 2007; Villanueva et al., 2008).

A

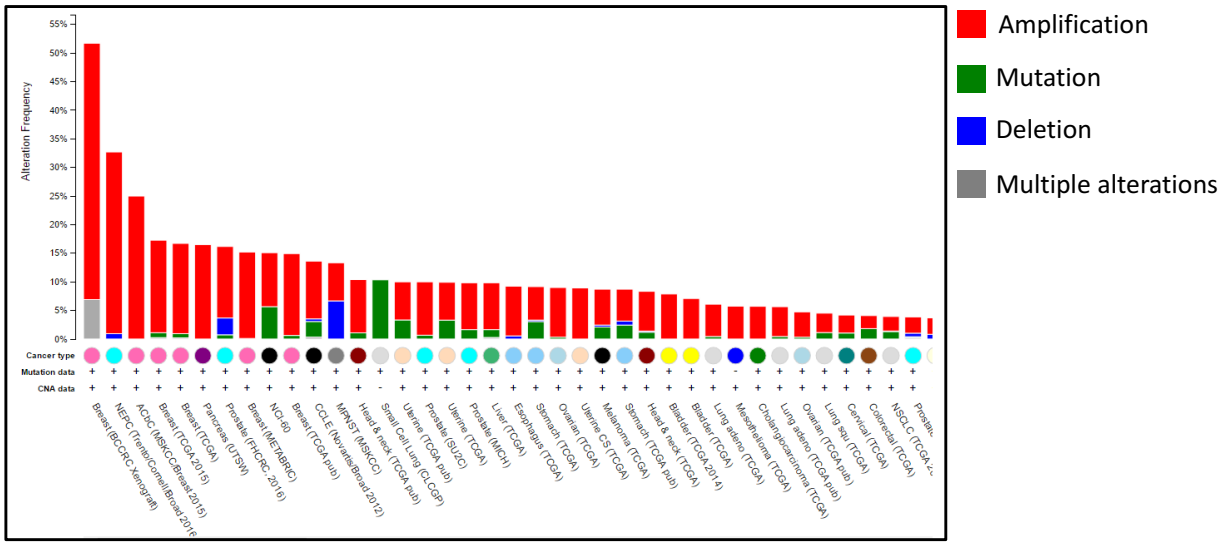

B

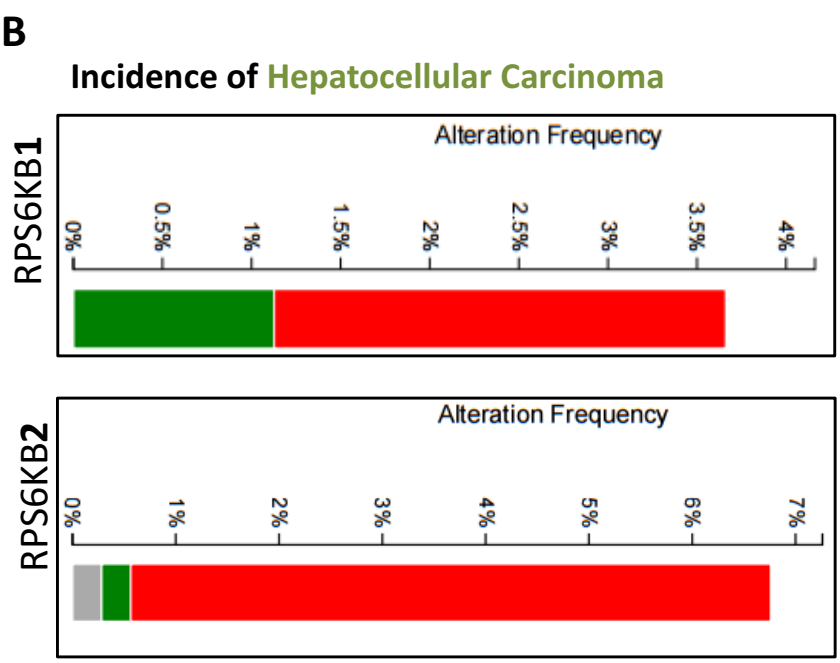

C

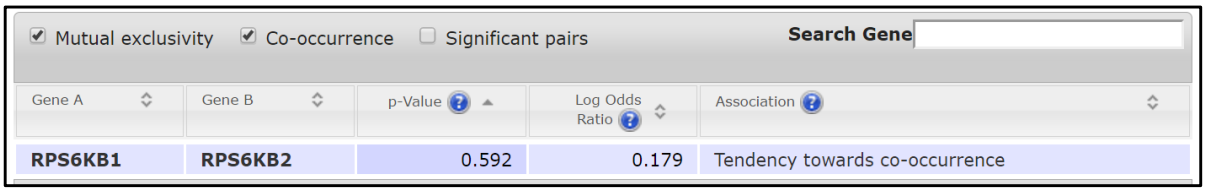

Figure 6.2. Amplification and/or mutations of RPS6KB1 (S6K1) and RPS6KB2 (S6K2) in many human cancers including hepatocellular carcinoma.
A and B. Amplifications (red) and/or mutations (green) of RPS6KB1 (S6K1) and RPS6KB2 (S6K2) have been identified in several human cancers including hepatocellular carcinoma. **C.** Tendency towards co-occurrence for RPS6KB1 (S6K1) and RPS6KB2 (S6K2) gene alterations in cancer. Data derived from cbioportal.org (Cerami et al., 2012; Gao et al., 2013).

We did not observe any differences in mRNA expression for inflammatory and immune cell markers between male control and *S6K1*$^{-/-}$*: S6K2*$^{-/-}$ mice, suggesting that the protection may not be due to a difference in inflammation. The fact that we did not observe differences in inflammation may not be surprising given that S6K1 and S6K2 were not deleted in immune cells, such as Kupffer cells but rather specifically in hepatocytes and cholangiocytes. We, however, have not looked specifically at infiltration of different immune subtypes into the liver by immunohistochemistry, so we still cannot completely rule this out. Therefore, a full characterisation of immune infiltration will be done in collaboration with Prof. Mathias Heikenwälder (DKFZ-Heidelberg, Germany). Although S6K1 has been implicated in regulating hepatic proliferation following partial hepatectomy, there was, however, no significant differences in proliferation during NASH between genotypes (Espeillac et al., 2011). S6K1 also regulates hepatic apoptosis, and apoptosis is thought to contribute to NASH progression by activating hepatic stellate cells and Kupffer cells (Bataller and Brenner, 2005; González-Rodriguez et al., 2009). RNA-sequencing did not reveal apoptosis to be significantly altered between the two genotypes, but this needs to be assessed in detail by immunohistochemistry staining for cleaved-caspase 3 or other markers of apoptosis.

On the other hand, RNA-sequencing analysis showed a significant upregulation of fatty acid metabolism, peroxisome and mitochondria signatures in male *S6K1*$^{-/-}$*: S6K2*$^{-/-}$ mice fed an HTF-diet compared to controls, suggesting that deletion of S6 kinases ameliorates the dysregulation of fatty acid metabolism during NASH. This observation is in line with previous studies where the CD-HFD model of NASH also showed dysregulation of fatty acid metabolism and this was partly rescued in *Rag*$^{-/-}$ mice lacking T-cells, B-cells and NK-cells (Wolf et al., 2014). Moreover, dysregulation of fatty acid metabolism has also been observed in NASH patients independent of obesity (Walle et al., 2016). Fatty acid oxidation in hepatocytes occurs primarily in mitochondria and peroxisomes where they are eventually broken down into acetyl coenzyme A in the cytoplasm and used in the tricarboxylic acid (TCA) cycle (Hardy et al., 2016). It has been previously highlighted that S6K1 plays an important role in the regulation of fatty acid metabolism and gluconeogenesis (Lustig et al., 2011). In brief, activated S6 kinases phosphorylate PGC-1α (peroxisome proliferator-activated receptor gamma, coactivator 1 alpha), which interfered with its ability to bind HNF4A but not other transcription factors such as PPARα, thus allowing separation of gluconeogenesis and fatty acid metabolism (Lustig et al., 2011). In addition, global *S6K1*$^{-/-}$ mice during ageing also displayed upregulation of fatty acid metabolism and peroxisome signatures in the liver, thus indicating that although the stimulus (ageing vs NASH) may differ, the underlying protective pathways may be similar.

In particular, we could hypothesise that S6K deletion is accompanied by an upregulation of HNF4A activity. This increase in HNF4A was indeed observed in male *S6K1*$^{-/-}$*: S6K2*$^{-/-}$ mice by

RNA sequencing, as there was an enrichment for both HNF4A and its downstream target HNF1A. Importantly, both HNF4A and HNF1A have been shown to suppress liver tumorigenesis (Patitucci et al., 2017; Saha et al., 2014). Further experiments will be needed, however, to show that S6 kinases drive NASH-HCC through downregulation of HNF4A activity. If the argument holds, there would be more nuclear staining of HNF4A in livers of male *S6K1*$^{-/-}$*: S6K2*$^{-/-}$ mice. In addition, tail-vein injection of AAVs carrying shRNAs targeting HNF4A in male *S6K1*$^{-/-}$*: S6K2*$^{-/-}$ mice fed an HTF-diet would confer loss of HCC protection. Importantly, male mice did not show a complete protection, and it is likely that S6 kinases in other tissues including immune cells and adipose tissue will also play an important role in NASH pathology. It would also be of interest to study the consequence of pharmacological inhibition of S6 kinases in NASH and HCC, particularly for prospective therapy, but unfortunately current inhibitors such as LY2584702 have so far shown to be toxic (Hollebecque et al., 2014; Tolcher et al., 2014).

Female *S6K1*$^{-/-}$*: S6K2*$^{-/-}$ mice fed an HTF diet showed a worsened outcome with greater hepatomegaly, biliary damage, fibrosis and inflammation. There was, however, no significant alterations in metabolic parameters such as glucose or insulin tolerance or in the body weight between genotypes, suggesting that the deleterious phenotype is pathological in nature. It is important to mention that we have a limited number of mice for each of the time points for the female data since we culled the second and third female cohorts at different time points during the experiment in order to dissect the pathogenesis of the disease with relation to S6K deletion. The worsened outcome in female knockouts was rather surprising given that female *S6K1*$^{-/-}$ (global) mice show a better response. This is most likely due to complex interactions between this specific HTF diet that induces biliary damage and hormonal alterations. Pursuing such sexual dimorphisms at a mechanistic level is both extremely time-consuming and expensive. Although it is beyond the scope of the thesis, castration of male *S6K1*$^{-/-}$*: S6K2*$^{-/-}$ mice or ovariectomy of female *S6K1*$^{-/-}$*: S6K2*$^{-/-}$ mice could be done to test whether sex hormones play an important role in this process. Alternatively, oestrogen pulses could be given to male *S6K1*$^{-/-}$*: S6K2*$^{-/-}$ mice to determine whether it would result in a worsened outcome. It is likely that oestrogen and activation of oestrogen receptors (ERs), in particular ERα, play a crucial role in the observed sexual dimorphism uncovered in this thesis considering the high level of expression of ERs in liver and the fact that ERα is an S6K1 target (Della Torre and Maggi, 2017).

Understanding this sexual dimorphism is further complicated by the fact that, to our knowledge, no study utilising the HTF diet has used females, thus making it impossible to compare our data with the literature. In addition, most of the reported literature have only given the HTF diet to mice for only 16-20 weeks instead of 30 weeks as done in the original study, hence not much is known about end-stage fibrosis or tumour incidence (Clapper et al., 2013; Honda et al., 2017; Kristiansen et al., 2016; McCommis et al., 2017). Nevertheless, to understand possible mechanisms

underpinning this sexual dimorphism, we are now in the process of comparing the RNA-sequencing data between sexes, as so far, we have only analysed the sexes separately. Therefore, the differentially expressed genes between female mice of the two genotypes will be compared to the differentially expressed genes between male knockouts verses controls. This will allow us to potentially identify pathways or processes that differ not only between sexes (*i.e.,* processes that confer greater protection to NASH in females) but also to understand the sexual dimorphism amongst the knockouts. We are also in the process of comparing the RNA-sequencing data of mice with liver-specific deletion of S6K1 and S6K2 to non-phosphorylatable RPS6 knock-in mice (Dr. Silvia Pedroni has characterised these mice) since ribosomal protein S6 is one of the most well-known targets of S6 kinases and these RPS6 knock-in mice should, in theory at least, recapitulate what is occurring in *S6K1*$^{-/-}$*: S6K2*$^{-/-}$ mice. We will also compare our RNA-sequencing analysis in HTF-fed mice to transcriptome analysis from patient liver samples at different stages of fatty liver disease in collaboration with Prof. Quentin Anstee (Newcastle University, U.K), who holds this data as part of a European consortium for elucidating pathways of steatohepatitis. This will enable us to determine whether any of the potential pathways we have identified such as HNF4A downregulation also occur in humans. This can be followed up by carrying out immunohistochemistry on human tissues.

6.3. Conclusions.

The ageing population is increasing at a rapid pace and ageing remains the largest risk factor for a number of pathologies, including neurodegeneration, cancer and cardiovascular disease. In addition, the prevalence of obesity is also on the rise, and this is associated with a growing body of pathologies including fatty liver disease. There is also a close link between ageing and obesity. Therefore, there is a great need to better understand the underlying mechanisms driving these complex processes, as doing so may yield new insights not only into ageing and obesity but numerous other diseases as well with the ultimate aim of improving the health and well-being of the population.

The mTOR signalling network, including the downstream S6 kinases, have been implicated in both ageing and obesity but the exact mechanisms underpinning this connection are still unclear. Therefore, we aimed to characterise the effects of deleting S6K1 or combined deletion of S6K1 and S6K2 in the liver in mammalian ageing or in fatty liver disease, respectively. In summary, we found that global *S6K1*$^{-/-}$ mice show an attenuated SASP and inflammatory response in the liver during mammalian ageing, which may in part be responsible for the improved healthspan and lifespan observed in these mice. On the other hand, we observed that liver-specific deletion of S6K1 and S6K2 induces a sexually dimorphic response in a model of NASH and HCC with males showing a beneficial response whilst the females showing a worsened outcome, suggesting that gender disparity is an important factor for metabolic and cancer therapy.

There are many questions that remain to be answered in the field of ageing. The most important is perhaps deciding which of the potential pathways to target for ageing therapy whether it is mTOR signalling or cellular senescence; but these processes may in fact be tightly interlinked as demonstrated here. In addition, what would be the age at which these therapies be initiated or whether they should be given in a chronic or intermittent fashion? Equally, would lifespan extending drugs still leave a period of frailty and morbidity, which would continue to burden the society at large? Nonetheless, it is vital to not blame the elderly, as it would be unjust and unfair to further guilt a population that has already contributed a lifetime to society and to caste them aside at the time they require our greatest empathy and support. Therefore, it is the responsibility of the society to adjust to an increasingly ageing population by first changing our attitudes and perceptions regarding the elderly and how we move to tackle this issue and also by providing the necessary infrastructure required for their care. This is of particular importance considering that ageing is characterised by years of disability, frailty and loss of independence. Therefore, it is this period of frailty and disability that we as biomedical scientists must strive to conquer. This requires our immediate attention as if we do not act soon, we may not only see a dramatic reduction in the quality of life but may also witness a lasting impact on health services that fail to cope with the increased demand. We may still be a long way off until we manage to therapeutically target the ageing process, but given the rapid advances that are undergoing in the field of ageing, what was once just a pipe-dream may soon be a reality.

Final thoughts.

A far wiser person than I once said, “listen to everything but do not believe in everything”. I believe this holds true today as it did more than two and a half thousand years ago. This is equally important not only for our daily lives but especially so in science, because “the data are the data, it is only in our misinterpretations that we reach false conclusions”.

I truly believe that science is one of the finest examples to portray the transitory nature of all conditioned phenomena, thus illustrating the futility of grasping to what can only cause suffering. It has been said since time immemorial that all things must come to an end whether good or bad. Accordingly, I have felt a great sense of nostalgia and melancholy this past year knowing that one of the greatest experiences of my life thus far will come to an end. This struck me slowly but deeper as the inevitability reached closer. Seeing the departure of many colleagues who have made a profound impact on my experience, also came the difficult realisation that it is finally time for me to move on from somewhere I have and will always call home - Imperial College London. You have been my comfort and support and guided me from when I first entered as a naïve but ever hopeful eighteen-year-old to finally emerging as a moulded soldier but with still much to learn about both life and science. It is through you that I have met some of the finest people I will ever meet and became the man that I am today. I truly believe that I am now ready to embark on this next chapter of my life with a new sense of apprehension but also of excitement of the uncertainty of what is yet to come. Only time will tell.

To all my friends, family and teachers, as Barack Obama put it so well, “you all will have a lifelong appreciation of a grateful friend and scientist. Thank you for believing all the way, through every hill, through every valley, you lifted me up the whole way, and I will always be grateful for all that you have done”.

References.

Abe, Y., Yoon, S.O., Kubota, K., Mendoza, M.C., Gygi, S.P., and Blenis, J. (2009). p90 ribosomal S6 kinase and p70 ribosomal S6 kinase link phosphorylation of the eukaryotic chaperonin containing TCP-1 to growth factor, insulin, and nutrient signaling. J. Biol. Chem. *284*, 14939–14948.

Acosta, J.C., O'Loghlen, A., Banito, A., Guijarro, M. V, Augert, A., Raguz, S., Fumagalli, M., Da Costa, M., Brown, C., Popov, N., et al. (2008). Chemokine Signaling via the CXCR2 Receptor Reinforces Senescence. Cell *133*, 1006–1018.

Acosta, J.C., Banito, A., Wuestefeld, T., Georgilis, A., Janich, P., Morton, J.P., Athineos, D., Kang, T.-W., Lasitschka, F., Andrulis, M., et al. (2013). A complex secretory program orchestrated by the inflammasome controls paracrine senescence. Nat. Cell Biol. *15*, 978–990.

Alessi, D.R., Kozlowski, M.T., Weng, Q.-P., Morrice, N., and Avruch, J. (1998). 3-Phosphoinositide-dependent protein kinase 1 (PDK1) phosphorylates and activates the p70 S6 kinase in vivo and in vitro. Curr. Biol. *8*, 69–81.

Alspach, E., Flanagan, K.C., Luo, X., Ruhland, M.K., Huang, H., Pazolli, E., Donlin, M.J., Marsh, T., Piwnica-Worms, D., Monahan, J., et al. (2014). p38MAPK plays a crucial role in stromal-mediated tumorigenesis. Cancer Discov. *4*, 716–729.

Andersen, J.B., Spee, B., Blechacz, B.R., Avital, I., Komuta, M., Barbour, A., Conner, E.A., Gillen, M.C., Roskams, T., Roberts, L.R., et al. (2012). Genomic and genetic characterization of cholangiocarcinoma identifies therapeutic targets for tyrosine kinase inhibitors. Gastroenterology *142*, 1021–1031.e15.

Arif, A., Terenzi, F., Potdar, A.A., Jia, J., Sacks, J., China, A., Halawani, D., Vasu, K., Li, X., Brown, J.M., et al. (2017). EPRS is a critical mTORC1–S6K1 effector that influences adiposity in mice. Nature *542*, 361.

Baar, M.P., Brandt, R.M.C., Putavet, D.A., Klein, J.D.D., Derks, K.W.J., Bourgeois, B.R.M., Stryeck, S., Rijksen, Y., van Willigenburg, H., Feijtel, D.A., et al. (2017). Targeted Apoptosis of Senescent Cells Restores Tissue Homeostasis in Response to Chemotoxicity and Aging. Cell *169*, 132–147.

Baba, H.A., Wohlschlaeger, J., Cicinnati, V.R., Hilgard, P., Lang, H., Sotiropoulos, G.C., Takeda, A., Beckebaum, S., and Schmitz, K.J. (2009). Phosphorylation of p70S6 kinase predicts overall survival in patients with clear margin-resected hepatocellular carcinoma. Liver Int. *29*, 399–405.

Bae, E.J., Xu, J., Oh, D.Y., Bandyopadhyay, G., Lagakos, W.S., Keshwani, M., and Olefsky, J.M. (2012). Liver-specific p70 S6 kinase depletion protects against hepatic steatosis and systemic insulin resistance. J. Biol. Chem. *287*, 18769–18780.

Baker, D., Weaver, R., and VanDeursen, J. (2013a). p21 Both Attenuates and Drives Senescence and Aging in BubR1 Progeroid Mice. Cell Rep. *3*, 1164–1174.

Baker, D.J., Jeganathan, K.B., Cameron, J.D., Thompson, M., Juneja, S., Kopecka, A., Kumar, R.,

Jenkins, R.B., de Groen, P.C., Roche, P., et al. (2004). BubR1 insufficiency causes early onset of aging-associated phenotypes and infertility in mice. Nat. Genet. *36*, 744–749.
Baker, D.J., Perez-Terzic, C., Jin, F., Pitel, K.S., Pitel, K., Niederländer, N.J., Jeganathan, K., Yamada, S., Reyes, S., Rowe, L., et al. (2008). Opposing roles for p16Ink4a and p19Arf in senescence and ageing caused by BubR1 insufficiency. Nat. Cell Biol. *10*, 825–836.
Baker, D.J., Wijshake, T., Tchkonia, T., LeBrasseur, N.K., Childs, B.G., van de Sluis, B., Kirkland, J.L., and van Deursen, J.M. (2011). Clearance of p16Ink4a-positive senescent cells delays ageing-associated disorders. Nature *479*, 232–236.
Baker, D.J., Dawlaty, M.M., Wijshake, T., Jeganathan, K.B., Malureanu, L., van Ree, J.H., Crespo-Diaz, R., Reyes, S., Seaburg, L., Shapiro, V., et al. (2013b). Increased expression of BubR1 protects against aneuploidy and cancer and extends healthy lifespan. Nat. Cell Biol. *15*, 96–102.
Baker, D.J., Childs, B.G., Durik, M., Wijers, M.E., Sieben, C.J., Zhong, J., Saltness, R.A., Jeganathan, K.B., Verzosa, G.C., Pezeshki, A., et al. (2016). Naturally occurring p16(Ink4a)-positive cells shorten healthy lifespan. Nature *530*, 184–189.
Banerjee, P., Ahmad, M.F., Grove, J.R., Kozlosky, C., Price, D.J., and Avruch, J. (1990). Molecular structure of a major insulin/mitogen-activated 70-kDa S6 protein kinase. Proc. Natl. Acad. Sci. U. S. A. *87*, 8550–8554.
Banito, A., and Lowe, S.W. (2013). A new development in senescence. Cell *155*, 977–978.
Barilari, M., Bonfils, G., Treins, C., Koka, V., De Villeneuve, D., Fabrega, S., and Pende, M. (2017). ZRF1 is a novel S6 kinase substrate that drives the senescence programme. EMBO J. *36*, 736–750.
Baron, J.A., Cole, B.F., Sandler, R.S., Haile, R.W., Ahnen, D., Bresalier, R., McKeown-Eyssen, G., Summers, R.W., Rothstein, R., Burke, C.A., et al. (2003a). A Randomized Trial of Aspirin to Prevent Colorectal Adenomas. N. Engl. J. Med. *348*, 891–899.
Baron, J.A., Cole, B.F., Sandler, R.S., Haile, R.W., Ahnen, D., Bresalier, R., McKeown-Eyssen, G., Summers, R.W., Rothstein, R., Burke, C.A., et al. (2003b). A Randomized Trial of Aspirin to Prevent Colorectal Adenomas. N. Engl. J. Med. *348*, 891–899.
Bataller, R., and Brenner, D. (2005). Liver fibrosis. J. Clin. Invest. *115*, 209–218.
Bataller, R., Brenner, D.A., Hughes, N., O'Brien, P., and Rodes, J. (2005). Liver fibrosis. J. Clin. Invest. *115*, 209–218.
Bavik, C., Coleman, I., Dean, J.P., Knudsen, B., Plymate, S., and Nelson, P.S. (2006). The Gene Expression Program of Prostate Fibroblast Senescence Modulates Neoplastic Epithelial Cell Proliferation through Paracrine Mechanisms. Cancer Res *66*, 794–802.
Beauséjour, C.M., Krtolica, A., Galimi, F., Narita, M., Lowe, S.W., Yaswen, P., and Campisi, J. (2003). Reversal of human cellular senescence: Roles of the p53 and p16 pathways. EMBO J. *22*, 4212–4222.
Benatar, T., Yang, W., Amemiya, Y., Evdokimova, V., Kahn, H., Holloway, C., and Seth, A. (2012). IGFBP7 reduces breast tumor growth by induction of senescence and apoptosis pathways. Breast

Cancer Res. Treat. *133*, 563–573.
Bhaumik, D., Scott, G.K., Schokrpur, S., Patil, C.K., Orjalo, A. V, Rodier, F., Lithgow, G.J., and Campisi, J. (2009). MicroRNAs miR-146a/b negatively modulate the senescence-associated inflammatory mediators IL-6 and IL-8. Aging (Albany. NY). *1*, 402–411.
Bitto, A., Ito, T.K., Pineda, V. V, Letexier, N.J., Huang, H.Z., Sutlief, E., Tung, H., Vizzini, N., Chen, B., Smith, K., et al. (2016). Transient rapamycin treatment can increase lifespan and healthspan in middle-aged mice. Elife *5*.
Blommaart, E.F.C., Luiken, J.J.F.P., Blommaart, P.J.E., Van Woerkom, G.M., and Meijer, A.J. (1995). Phosphorylation of ribosomal protein S6 is inhibitory for autophagy in isolated rat hepatocytes. J. Biol. Chem. *270*, 2320–2326.
Braig, M., Lee, S., Loddenkemper, C., Rudolph, C., Peters, A.H.F.M., Schlegelberger, B., Stein, H., Dörken, B., Jenuwein, T., and Schmitt, C.A. (2005). Oncogene-induced senescence as an initial barrier in lymphoma development. Nature *436*, 660–665.
Brown, A.J., Sun, L., Feramisco, J.D., Brown, M.S., and Goldstein, J.L. (2002). Cholesterol addition to ER membranes alters conformation of SCAP, the SREBP escort protein that regulates cholesterol metabolism. Mol. Cell *10*, 237–245.
Brown, E.J., Albers, M.W., Shin, T.B., Ichikawa, K., Keith, C.T., Lane, W.S., and Schreiber, S.L. (1994). A mammalian protein targeted by G1-arresting rapamycin-receptor complex. Nature *369*, 756–758.
Brown-Borg, H.M., Borg, K.E., Meliska, C.J., and Bartke, A. (1996). Dwarf mice and the ageing process. Nature *384*, 33.
Brunn, G.J., Hudson, C.C., Sekulić, A., Williams, J.M., Hosoi, H., Houghton, P.J., Lawrence, J.C., and Abraham, R.T. (1997). Phosphorylation of the translational repressor PHAS-I by the mammalian target of rapamycin. Science (80-.). *277*, 99–101.
Burcelin, R., Crivelli, V., Dacosta, A., Roy-Tirelli, A., and Thorens, B. (2002). Heterogeneous metabolic adaptation of C57BL/6J mice to high-fat diet. Am. J. Physiol. Endocrinol. Metab. *282*, E834–E842.
Burd, C.E., Sorrentino, J.A., Clark, K.S., Darr, D.B., Krishnamurthy, J., Deal, A.M., Bardeesy, N., Castrillon, D.H., Beach, D.H., and Sharpless, N.E. (2013). Monitoring tumorigenesis and senescence in vivo with a p16 INK4a-luciferase model. Cell *152*, 340–351.
Burnett, P.E., Barrow, R.K., Cohen, N.A., Snyder, S.H., and Sabatini, D.M. (1998). RAFT1 phosphorylation of the translational regulators p70 S6 kinase and 4E-BP1. Proc. Natl. Acad. Sci. U. S. A. *95*, 1432–1437.
Bursuker, I., Rhodes, J.M., and Coldman, R. (1982). Beta-Galactosidase - An Indicator of the Maturational Stage of Mouse and Human Mononuclear Phagocytes. J. Cell. Physiol. *112*, 385–390.
Calvisi, D.F., Wang, C., Ho, C., Ladu, S., Lee, S.A., Mattu, S., Destefanis, G., Delogu, S., Zimmermann, A., Ericsson, J., et al. (2011). Increased lipogenesis, induced by AKT-mTORC1-

RPS6 signaling, promotes development of human hepatocellular carcinoma. Gastroenterology *140*, 1071–1083.
Campisi, J. (2013). Aging, Cellular Senescence, and Cancer. Annu. Rev. Physiol. *75*, 685–705.
Campisi, J., and d'Adda di Fagagna, F. (2007). Cellular senescence: when bad things happen to good cells. Nat. Rev. Mol. Cell Biol. *8*, 729–740.
Carnevalli, L.S., Masuda, K., Frigerio, F., Le Bacquer, O., Um, S.H., Gandin, V., Topisirovic, I., Sonenberg, N., Thomas, G., and Kozma, S.C. (2010). S6K1 plays a critical role in early adipocyte differentiation. Dev. Cell *18*, 763–774.
Castañeda, T.R., Abplanalp, W., Um, S.H., Pfluger, P.T., Schrott, B., Brown, K., Grant, E., Carnevalli, L., Benoit, S.C., Morgan, D.A., et al. (2012). Metabolic control by S6 kinases depends on dietary lipids. PLoS One *7*, e32631.
Cerami, E., Gao, J., Dogrusoz, U., Gross, B.E., Sumer, S.O., Aksoy, B.A., Jacobsen, A., Byrne, C.J., Heuer, M.L., Larsson, E., et al. (2012). The cBio Cancer Genomics Portal: An open platform for exploring multidimensional cancer genomics data. Cancer Discov. *2*, 401–404.
Chang, J., Wang, Y., Shao, L., Laberge, R.-M., Demaria, M., Campisi, J., Janakiraman, K., Sharpless, N.E., Ding, S., Feng, W., et al. (2016). Clearance of senescent cells by ABT263 rejuvenates aged hematopoietic stem cells in mice. Nat Med *22*, 78–83.
Chantranupong, L., Wolfson, R.L., and Sabatini, D.M. (2015). Nutrient-sensing mechanisms across evolution. Cell *161*, 67–83.
Chauvin, C., Koka, V., Nouschi, A., Mieulet, V., Hoareau-Aveilla, C., Dreazen, A., Cagnard, N., Carpentier, W., Kiss, T., Meyuhas, O., et al. (2014). Ribosomal protein S6 kinase activity controls the ribosome biogenesis transcriptional program. Oncogene *33*, 474–483.
Chen, C., Liu, Y., Liu, Y., and Zheng, P. (2009). mTOR Regulation and Therapeutic Rejuvenation of Aging Hematopoietic Stem Cells. Sci. Signal. *2*, ra75-ra75.
Chen, H., Ruiz, P.D., McKimpson, W.M., Novikov, L., Kitsis, R.N., and Gamble, M.J. (2015). MacroH2A1 and ATM Play Opposing Roles in Paracrine Senescence and the Senescence-Associated Secretory Phenotype. Mol. Cell *59*, 719–731.
Chen, Z., Trotman, L.C., Shaffer, D., Lin, H.-K., Dotan, Z.A., Niki, M., Koutcher, J.A., Scher, H.I., Ludwig, T., Gerald, W., et al. (2005). Crucial role of p53-dependent cellular senescence in suppression of Pten-deficient tumorigenesis. Nature *436*, 725–730.
Chien, Y., Scuoppo, C., Wang, X., Fang, X., Balgley, B., Bolden, J.E., Premsrirut, P., Luo, W., Chicas, A., Lee, C.S., et al. (2011). Control of the senescence-associated secretory phenotype by NF-kB promotes senescence and enhances chemosensitivity. Genes Dev. *25*, 2125–2136.
Childs, B.G., Baker, D.J., Kirkland, J.L., Campisi, J., and van Deursen, J.M. (2014). Senescence and apoptosis: dueling or complementary cell fates? EMBO Rep. *15*, 1139–1153.
Childs, B.G., Durik, M., Baker, D.J., and van Deursen, J.M. (2015). Cellular senescence in aging and age-related disease: from mechanisms to therapy. Nat. Med. *21*, 1424–1435.
Childs, B.G., Baker, D.J., Wijshake, T., Conover, C.A., Campisi, J., and van Deursen, J.M. (2016).

Senescent intimal foam cells are deleterious at all stages of atherosclerosis. Science (80-.). *354*, 472–477.
Chung, J., Kuo, C.J., Crabtree, G.R., and Blenis, J. (1992). Rapamycin-FKBP specifically blocks growth-dependent activation of and signaling by the 70 kd S6 protein kinases. Cell *69*, 1227–1236.
Clapper, J.R., Hendricks, M.D., Gu, G., Wittmer, C., Dolman, C.S., Herich, J., Athanacio, J., Villescaz, C., Ghosh, S.S., Heilig, J.S., et al. (2013). Diet-induced mouse model of fatty liver disease and nonalcoholic steatohepatitis reflecting clinical disease progression and methods of assessment. Am J Physiol Gastrointest Liver Physiol *305*, G483-95.
Cleary, S.P., Jeck, W.R., Zhao, X., Chen, K., Selitsky, S.R., Savich, G.L., Tan, T.X., Wu, M.C., Getz, G., Lawrence, M.S., et al. (2013). Identification of driver genes in hepatocellular carcinoma by exome sequencing. Hepatology *58*, 1693–1702.
Collado, M., Gil, J., Efeyan, A., Guerra, C., Schuhmacher, A.J., Barradas, M., Benguría, A., Zaballos, A., Flores, J.M., Barbacid, M., et al. (2005). Tumour biology: senescence in premalignant tumours. Nature *436*, 642.
Conboy, I.M., Conboy, M.J., Wagers, A.J., Girma, E.R., Weissman, I.L., and Rando, T. a (2005). Rejuvenation of aged progenitor cells by exposure to a young systemic environment. Nature *433*, 760–764.
Coppé, J.-P., Kauser, K., Campisi, J., and Beauséjour, C.M. (2006). Secretion of vascular endothelial growth factor by primary human fibroblasts at senescence. J. Biol. Chem. *281*, 29568–29574.
Coppé, J.-P., Patil, C.K., Rodier, F., Sun, Y., Muñoz, D.P., Goldstein, J., Nelson, P.S., Desprez, P.-Y., and Campisi, J. (2008). Senescence-associated secretory phenotypes reveal cell-nonautonomous functions of oncogenic RAS and the p53 tumor suppressor. PLoS Biol. *6*, 2853–2868.
Coppé, J.-P., Desprez, P.-Y., Krtolica, A., and Campisi, J. (2010a). The Senescence-Associated Secretory Phenotype: The Dark Side of Tumor Suppression. Annu. Rev. Pathol. Mech. Dis. *5*, 99–118.
Coppé, J.-P., Patil, C.K., Rodier, F., Krtolica, A., Beauséjour, C.M., Parrinello, S., Hodgson, J.G., Chin, K., Desprez, P.-Y., and Campisi, J. (2010b). A human-like senescence-associated secretory phenotype is conserved in mouse cells dependent on physiological oxygen. PLoS One *5*, e9188.
Coppé, J.-P., Rodier, F., Patil, C.K., Freund, A., Desprez, P.-Y., and Campisi, J. (2011). Tumor suppressor and aging biomarker p16(INK4a) induces cellular senescence without the associated inflammatory secretory phenotype. J. Biol. Chem. *286*, 36396–36403.
Correia-Melo, C., Marques, F.D., Anderson, R., Hewitt, G., Hewitt, R., Cole, J., Carroll, B.M., Miwa, S., Birch, J., Merz, A., et al. (2016). Mitochondria are required for pro-ageing features of the senescent phenotype. EMBO J. *35*, 724–742.
Dam-Larsen, S., Becker, U., Franzmann, M.-B., Larsen, K., Christoffersen, P., and Bendtsen, F. (2009). Final results of a long-term, clinical follow-up in fatty liver patients. Scand. J. Gastroenterol.

44, 1236–1243.
Damsky, W., Micevic, G., Meeth, K., Muthusamy, V., Curley, D.P., Santhanakrishnan, M., Erdelyi, I., Platt, J.T., Huang, L., Theodosakis, N., et al. (2015). mTORC1 Activation Blocks BrafV600E-Induced Growth Arrest but Is Insufficient for Melanoma Formation. Cancer Cell *27*, 41–56.
Davalos, A.R., Kawahara, M., Malhotra, G.K., Schaum, N., Huang, J., Ved, U., Beausejour, C.M., Coppe, J.P., Rodoer, F., and Campisi, J. (2013). p53-dependent release of Alarmin HMGB1 is a central mediator of senescent phenotypes. J. Cell Biol. *201*, 613–629.
Demaria, M., Ohtani, N., Youssef, S.A., Rodier, F., Toussaint, W., Mitchell, J.R., Laberge, R.M., Vijg, J., VanSteeg, H., Doll??, M.E.T., et al. (2014). An essential role for senescent cells in optimal wound healing through secretion of PDGF-AA. Dev. Cell *31*, 722–733.
Demaria, M., O'Leary, M.N., Chang, J., Shao, L., Liu, S., Alimirah, F., Koenig, K., Le, C., Mitin, N., Deal, A.M., et al. (2017). Cellular Senescence Promotes Adverse Effects of Chemotherapy and Cancer Relapse. Cancer Discov. *7*, 165–176.
Demidenko, Z.N., Zubova, S.G., Bukreeva, E.I., Pospelov, V.A., Pospelova, T. V., and Blagosklonny, M. V. (2009). Rapamycin decelerates cellular senescence. Cell Cycle *8*, 1888–1895.
van Deursen, J.M. (2014). The role of senescent cells in ageing. Nature *509*, 439–446.
Dong, X., Milholland, B., and Vijg, J. (2016). Evidence for a limit to human lifespan. Nature *538*, 257–259.
Dörr, J.R., Yu, Y., Milanovic, M., Beuster, G., Zasada, C., Däbritz, J.H.M., Lisec, J., Lenze, D., Gerhardt, A., Schleicher, K., et al. (2013). Synthetic lethal metabolic targeting of cellular senescence in cancer therapy. Nature *501*, 421–425.
Dorrello, N.V., Peschiaroli, A., Guardavaccaro, D., Colburn, N.H., Sherman, N.E., and Pagano, M. (2006). S6K1- and TRCP-Mediated Degradation of PDCD4 Promotes Protein Translation and Cell Growth. Science (80-.). *314*, 467–471.
Easton, J.B., and Houghton, P.J. (2006). mTOR and cancer therapy. Oncogene *25*, 6436–6446.
Efeyan, A., Comb, W.C., and Sabatini, D.M. (2015). Nutrient-sensing mechanisms and pathways. Nature *517*, 302–310.
Eggert, T., Wolter, K., Ji, J., Ma, C., Yevsa, T., Klotz, S., Medina-Echeverz, J., Longerich, T., Forgues, M., Reisinger, F., et al. (2016). Distinct Functions of Senescence-Associated Immune Responses in Liver Tumor Surveillance and Tumor Progression. Cancer Cell *30*, 533–547.
Ekstedt, M., Franzén, L.E., Mathiesen, U.L., Thorelius, L., Holmqvist, M., Bodemar, G., and Kechagias, S. (2006). Long-term follow-up of patients with NAFLD and elevated liver enzymes. Hepatology *44*, 865–873.
El-Serag, H.B. (2011). Hepatocellular Carcinoma. N. Engl. J. Med. *365*, 1118–1127.
El-Serag, H.B., and Kanwal, F. (2014). Epidemiology of hepatocellular carcinoma in the United States: Where are we? Where do we go? Hepatology *60*, 1767–1775.
Engelman, J.A., Chen, L., Tan, X., Crosby, K., Guimaraes, A.R., Upadhyay, R., Maira, M.,

McNamara, K., Perera, S.A., Song, Y., et al. (2008). Effective use of PI3K and MEK inhibitors to treat mutant Kras G12D and PIK3CA H1047R murine lung cancers. Nat. Med. *14*, 1351–1356.
Espeillac, C., Mitchell, C., Celton-Morizur, S., Chauvin, C., Koka, V., Gillet, C., Albrecht, J.H., Desdouets, C., and Pende, M. (2011). S6 kinase 1 is required for rapamycin-sensitive liver proliferation after mouse hepatectomy. J. Clin. Invest. *121*, 2821–2832.
Fagagna, F. d'Adda di, Reaper, P.M., Clay-Farrace, L., Fiegler, H., Carr, P., von Zglinicki, T., Saretzki, G., Carter, N.P., and Jackson, S.P. (2003). A DNA damage checkpoint response in telomere-initiated senescence. Nature *426*, 194–198.
Faivre, S., Kroemer, G., and Raymond, E. (2006). Current development of mTOR inhibitors as anticancer agents. Nat. Rev. Drug Discov. *5*, 671–688.
Fenton, T.R., and Gout, I.T. (2011). Functions and regulation of the 70 kDa ribosomal S6 kinases. Int. J. Biochem. Cell Biol. *43*, 47–59.
Ferrari, S., Regina Bandi, H., Hofsteenge, J., Russian, B.M., and Thomas, G. (1991). Mitogen-activated 70K S6 kinase: Identification of in vitro 40 S ribosomal S6 phosphorylation sites. J. Biol. Chem. *266*, 22770–22773.
Ferrucci, L., Harris, T.B., Guralnik, J.M., Tracy, R.P., Corti, M.C., Cohen, H.J., Penninx, B., Pahor, M., Wallace, R., and Havlik, R.J. (1999). Serum IL-6 level and the development of disability in older persons. J. Am. Geriatr. Soc. *47*, 639–646.
Filonenko, V. V, Tytarenko, R., Azatjan, S.K., Savinska, L.O., Gaydar, Y. a, Gout, I.T., Usenko, V.S., and Lyzogubov, V. V (2004). Immunohistochemical analysis of S6K1 and S6K2 localization in human breast tumors. Exp. Oncol. *26*, 294–299.
Finn, R.S., and Slamon, D.J. (2015). The cyclin-dependent kinase 4/6 inhibitor palbociclib in combination with letrozole versus letrozole alone as first-line treatment of oestrogen receptor-positive, HER2-negative, advanced breast cancer (PALOMA-1/TRIO-18): a randomised phase 2 study. Lancet Oncol. *16*, 25–35.
Finn, R.S., Dering, J., Conklin, D., Kalous, O., Cohen, D.J., Desai, A.J., Ginther, C., Atefi, M., Chen, I., Fowst, C., et al. (2009). PD 0332991, a selective cyclin D kinase 4/6 inhibitor, preferentially inhibits proliferation of luminal estrogen receptor-positive human breast cancer cell lines in vitro. Breast Cancer Res. *11*, R77.
Finn, R.S., Martin, M., Rugo, H.S., Jones, S., Im, S.-A., Gelmon, K., Harbeck, N., Lipatov, O.N., Walshe, J.M., Moulder, S., et al. (2016). Palbociclib and Letrozole in Advanced Breast Cancer. N. Engl. J. Med. *375*, 1925–1936.
Flynn, J.M., O'Leary, M.N., Zambataro, C.A., Academia, E.C., Presley, M.P., Garrett, B.J., Zykovich, A., Mooney, S.D., Strong, R., Rosen, C.J., et al. (2013). Late-life rapamycin treatment reverses age-related heart dysfunction. Aging Cell *12*, 851–862.
Fontana, L., Partridge, L., Longo, V.D., and Longo4, V.D. (2010). Extending Healthy Life Span—From Yeast to Humans. Science (80-.). *328*, 321–326.
Ford, D.E., Erlinger, T.P., N, R., M, C., CH, H., and H, N. (2004). Depression and C-Reactive

Protein in US Adults. Arch. Intern. Med. *164*, 1010.
Franceschi, C., Bonafè, M., Valensin, S., Olivieri, F., De Luca, M., Ottaviani, E., and De Benedictis, G. (2000). Inflamm-aging. An evolutionary perspective on immunosenescence. Ann. N. Y. Acad. Sci. *908*, 244–254.
Franceschi, C., Capri, M., Monti, D., Giunta, S., Olivieri, F., Sevini, F., Panourgia, M.P., Invidia, L., Celani, L., Scurti, M., et al. (2007). Inflammaging and anti-inflammaging: A systemic perspective on aging and longevity emerged from studies in humans. Mech. Ageing Dev. *128*, 92–105.
Freund, A., Orjalo, A. V., Desprez, P.-Y., and Campisi, J. (2010). Inflammatory networks during cellular senescence: causes and consequences. Trends Mol. Med. *16*, 238–246.
Freund, A., Patil, C.K., and Campisi, J. (2011). p38MAPK is a novel DNA damage response-independent regulator of the senescence-associated secretory phenotype. EMBO J. *30*, 1536–1548.
Fried, L.P., Xue, Q.-L., Cappola, A.R., Ferrucci, L., Chaves, P., Varadhan, R., Guralnik, J.M., Leng, S.X., Semba, R.D., Walston, J.D., et al. (2009). Nonlinear multisystem physiological dysregulation associated with frailty in older women: implications for etiology and treatment. J. Gerontol. A. Biol. Sci. Med. Sci. *64*, 1049–1057.
Friedman, S.L. (2008). Mechanisms of Hepatic Fibrogenesis. Gastroenterology *134*, 1655–1669.
Gao, J., Aksoy, B., Dogrusoz, U., and Dresdner, G. (2013). Integrative analysis of complex cancer genomics and clinical profiles using the cBioPortal. Sci. Signal. *6*, 1–20.
García-Prat, L., Martínez-Vicente, M., Perdiguero, E., Ortet, L., Rodríguez-Ubreva, J., Rebollo, E., Ruiz-Bonilla, V., Gutarra, S., Ballestar, E., Serrano, A.L., et al. (2016). Autophagy maintains stemness by preventing senescence. Nature *529*, 37–42.
Geiger, H., de Haan, G., and Florian, M.C. (2013). The ageing haematopoietic stem cell compartment. Nat. Rev. Immunol. *13*, 376–389.
Gems, D., and Partridge, L. (2013). Genetics of Longevity in Model Organisms: Debates and Paradigm Shifts. Annu. Rev. Physiol *75*, 621–644.
Ghosh, J., Kobayashi, M., Ramdas, B., Chatterjee, A., Ma, P., Mali, R.S., Carlesso, N., Liu, Y., Plas, D.R., Chan, R.J., et al. (2016). S6K1 regulates hematopoietic stem cell self-renewal and leukemia maintenance. J. Clin. Invest. *126*, 2621–2625.
Gil, J., and Peters, G. (2006). Regulation of the INK4b-ARF-INK4a tumour suppressor locus: all for one or one for all. Nat. Rev. Mol. Cell Biol. *7*, 667–677.
Gil, J., and Withers, D.J. (2016). Ageing: Out with the old. Nature *530*, 164–165.
Glück, S., Guey, B., Gulen, M.F., Wolter, K., Kang, T.-W., Schmacke, N.A., Bridgeman, A., Rehwinkel, J., Zender, L., and Ablasser, A. (2017). Innate immune sensing of cytosolic chromatin fragments through cGAS promotes senescence. Nat. Cell Biol. *19*, 1061–1070.
Goel, S., DeCristo, M.J., Watt, april C., BrinJones, H., Sceneay, J., Li, B.B., Khan, N., Ubellacker, J.M., Xie, S., Metzger-Filho, O., et al. (2017). CDK4/6 inhibition triggers anti-tumour immunity. Nature *548*.

Gomes, A.L., Teijeiro, A., Burén, S., Tummala, K.S., Yilmaz, M., Waisman, A., Theurillat, J.P., Perna, C., and Djouder, N. (2016). Metabolic Inflammation-Associated IL-17A Causes Non-alcoholic Steatohepatitis and Hepatocellular Carcinoma. Cancer Cell *30*, 161–175.
González-Rodriguez, Á., Alba, J., Zimmerman, V., Kozma, S.C., and Valverde, Á.M. (2009). S6K1 deficiency protects against apoptosis in hepatocytes. Hepatology *50*, 216–229.
Gorgoulis, V.G., and Halazonetis, T.D. (2010). Oncogene-induced senescence: the bright and dark side of the response. Curr. Opin. Cell Biol. *22*, 816–827.
Gout, I., Minami, T., Hara, K., Tsujishita, Y., Filonenko, V., Waterfield, M.D., and Yonezawa, K. (1998). Molecular cloning and characterization of a novel p70 S6 kinase, p70 S6 kinase beta containing a proline-rich region. J. Biol. Chem. *273*, 30061–30064.
Granville, C.A., Memmott, R.M., Gills, J.J., and Dennis, P.A. (2006). Handicapping the race to develop inhibitors of the phosphoinositide 3-kinase/Akt/mammalian target of rapamycin pathway. Clin. Cancer Res. *12*, 679–689.
de Groot, R.P., Ballou, L.M., and Sassone-Corsi, P. (1994). Positive regulation of the cAMP-responsive activator CREM by the p70 S6 kinase: An alternative route to mitogen-induced gene expression. Cell *79*, 81–91.
Grove, J.R., Banerjee, P., Balasubramanyam, A., Coffer, P.J., Price, D.J., Avruch, J., and Woodgett, J.R. (1991). Cloning and expression of two human p70 S6 kinase polypeptides differing only at their amino termini. Mol. Cell. Biol. *11*, 5541–5550.
Guan, X., LaPak, K.M., Hennessey, R.C., Yu, C.Y., Shakya, R., Zhang, J., and Burd, C.E. (2017). Stromal Senescence By Prolonged CDK4/6 Inhibition Potentiates Tumor Growth. Mol. Cancer Res. *15*, 237–249.
Guertin, D.A., and Sabatini, D.M. (2007). Defining the Role of mTOR in Cancer. Cancer Cell *12*, 9–22.
Guichard, C., Amaddeo, G., Imbeaud, S., Ladeiro, Y., Pelletier, L., Maad, I. Ben, Calderaro, J., Bioulac-Sage, P., Letexier, M., Degos, F., et al. (2012). Integrated analysis of somatic mutations and focal copy-number changes identifies key genes and pathways in hepatocellular carcinoma. Nat. Genet. *44*, 694–698.
Haghighat, A., Mader, S., Pause1, A., and Sonenberg2, N. (1995). Repression of cap-dependent translation by 4E-binding protein 1: competition with p220 for binding to eukaryotic initiation factor-4E. EMBO J. *14*, 5701–5709.
Hannan, K.M., Brandenburger, Y., Jenkins, A., Sharkey, K., Cavanaugh, A., Rothblum, L., Moss, T., Poortinga, G., McArthur, G.A., Pearson, R.B., et al. (2003). mTOR-Dependent Regulation of Ribosomal Gene Transcription Requires S6K1 and Is Mediated by Phosphorylation of the Carboxy-Terminal Activation Domain of the Nucleolar Transcription Factor UBF. Mol. Cell. Biol. *23*, 8862–8877.
Hansen, M., and Kennedy, B.K. (2016). Does Longer Lifespan Mean Longer Healthspan? Trends Cell Biol. *26*, 565–568.

Hara, K., Yonezawa, K., Weng, Q.P., Kozlowski, M.T., Belham, C., and Avruch, J. (1998). Amino acid sufficiency and mTOR regulate p70 S6 kinase and eIF-4E BP1 through a common effector mechanism. J. Biol. Chem. *273*, 14484–14494.
Hara, K., Maruki, Y., Long, X., Yoshino, K. ichi, Oshiro, N., Hidayat, S., Tokunaga, C., Avruch, J., and Yonezawa, K. (2002). Raptor, a binding partner of target of rapamycin (TOR), mediates TOR action. Cell *110*, 177–189.
Hardie, D.G., Ross, F. a., and Hawley, S. a. (2012). AMPK: a nutrient and energy sensor that maintains energy homeostasis. Nat. Rev. Mol. Cell Biol. *13*, 251–262.
Hardy, T., Oakley, F., Anstee, Q.M., and Day, C.P. (2016). Nonalcoholic Fatty Liver Disease: Pathogenesis and Disease Spectrum. Annu. Rev. Pathol. Mech. Dis. *11*, 451–496.
Harley, C.B., Futcher, A.B., and Greider, C.W. (1990). Telomeres shorten during ageing of human fibroblasts. Nature *345*, 458–460.
Hashimoto, E., Yatsuji, S., Tobari, M., Taniai, M., Torii, N., Tokushige, K., and Shiratori, K. (2009). Hepatocellular carcinoma in patients with nonalcoholic steatohepatitis. J. Gastroenterol. *44*, 89–95.
Hay, N., and Sonenberg, N. (2004). Upstream and downstream of mTOR. Genes Dev. *18*, 1926–1945.
Hayakawa, T., Iwai, M., Aoki, S., Takimoto, K., Maruyama, M., Maruyama, W., and Motoyama, N. (2015). SIRT1 suppresses the senescence-associated secretory phenotype through epigenetic gene regulation. PLoS One *10*, e0116480.
Hayflick, L. (1965). The limited in vitro lifetime of human diploid cell strains. Exp. Cell Res. *37*, 614–636.
Hayflick, L., and Moorhead, P.S. (1961). The serial cultivation of human diploid cell strains. Exp. Cell Res. *25*, 585–621.
He, S., Nakada, D., and Morrison, S.J. (2009). Mechanisms of stem cell self-renewal. Annu. Rev. Cell Dev. Biol. *25*, 377–406.
Hee Um, S., Frigerio, F., Watanabe, M., Picard, F., Joaquin, M., Sticker, M., Fumagalli, S., Allegrini, P.R., Kozma, S.C., Auwerx, J., et al. (2004). Absence of S6K1 protects against age- and diet-induced obesity while enhancing insulin sensitivity. Nature *431*, 485–485.
Helman, A., Klochendler, A., Azazmeh, N., Gabai, Y., Horwitz, E., Anzi, S., Swisa, A., Condiotti, R., Granit, R.Z., Nevo, Y., et al. (2016). p16(Ink4a)-induced senescence of pancreatic beta cells enhances insulin secretion. Nat. Med. *22*, 412–420.
Herbig, U., Jobling, W.A., Chen, B.P.., Chen, D.J., and Sedivy, J.M. (2004). Telomere Shortening Triggers Senescence of Human Cells through a Pathway Involving ATM, p53, and p21CIP1, but Not p16INK4a. Mol. Cell *14*, 501–513.
Herranz, N., Gallage, S., Mellone, M., Wuestefeld, T., Klotz, S., Hanley, C.J., Raguz, S., Acosta, J.C., Innes, A.J., Banito, A., et al. (2015). mTOR regulates MAPKAPK2 translation to control the senescence-associated secretory phenotype. Nat. Cell Biol. *17*, 1205–1217.
Hirasawa, A., Tsumaya, K., Awaji, T., Katsuma, S., Adachi, T., Yamada, M., Sugimoto, Y.,

Miyazaki, S., and Tsujimoto, G. (2005). Free fatty acids regulate gut incretin glucagon-like peptide-1 secretion through GPR120. Nat Med *11*, 90–94.
Hoare, M., Ito, Y., Kang, T.-W., Weekes, M.P., Matheson, N.J., Patten, D.A., Shetty, S., Parry, A.J., Menon, S., Salama, R., et al. (2016). NOTCH1 mediates a switch between two distinct secretomes during senescence. Nat. Cell Biol. *18*, 979–992.
Hofmann, J.W., Zhao, X., De Cecco, M., Peterson, A.L., Pagliaroli, L., Manivannan, J., Hubbard, G.B., Ikeno, Y., Zhang, Y., Feng, B., et al. (2015). Reduced expression of MYC increases longevity and enhances healthspan. Cell *160*, 477–488.
Hollebecque, A., Houédé, N., Cohen, E.E.W., Massard, C., Italiano, A., Westwood, P., Bumgardner, W., Miller, J., Brail, L.H., Benhadji, K.A., et al. (2014). A phase Ib trial of LY2584702 tosylate, a p70 S6 inhibitor, in combination with erlotinib or everolimus in patients with solid tumours. Eur. J. Cancer *50*, 876–884.
Honda, Y., Kessoku, T., Ogawa, Y., Tomeno, W., Imajo, K., Fujita, K., Yoneda, M., Takizawa, T., Saito, S., Nagashima, Y., et al. (2017). Pemafibrate, a novel selective peroxisome proliferator-activated receptor alpha modulator, improves the pathogenesis in a rodent model of nonalcoholic steatohepatitis. Sci. Rep. *7*, 42477.
Hsieh, A.C., Costa, M., Zollo, O., Davis, C., Feldman, M.E., Testa, J.R., Meyuhas, O., Shokat, K.M., and Ruggero, D. (2010). Genetic Dissection of the Oncogenic mTOR Pathway Reveals Druggable Addiction to Translational Control via 4EBP-eIF4E. Cancer Cell *17*, 249–261.
Hsu, P.P., Kang, S.A., Rameseder, J., Zhang, Y., Ottina, K.A., Lim, D., Peterson, T.R., Choi, Y., Gray, N.S., Yaffe, M.B., et al. (2011). The mTOR-Regulated Phosphoproteome Reveals a Mechanism of mTORC1-Mediated Inhibition of Growth Factor Signaling. Science (80-.). *332*, 1317–1322.
Hubackova, S., Krejcikova, K., Bartek, J., and Hodny, Z. (2012). IL1- and TGFβ-Nox4 signaling, oxidative stress and DNA damage response are shared features of replicative, oncogene-induced, and drug-induced paracrine “bystander senescence”. Aging (Albany. NY). *4*, 932–951.
Iannello, A., Thompson, T.W., Ardolino, M., Lowe, S.W., and Raulet, D.H. (2013). p53-dependent chemokine production by senescent tumor cells supports NKG2D-dependent tumor elimination by natural killer cells. J. Exp. Med. *210*, 2057–2069.
Iglesias-Bartolome, R., Patel, V., Cotrim, A., Leelahavanichkul, K., Molinolo, A.A., Mitchell, J.B., and Gutkind, J.S. (2012). mTOR inhibition prevents epithelial stem cell senescence and protects from radiation-induced mucositis. Cell Stem Cell *11*, 401–414.
Ito, T.K., Lu, C., Khan, J., Nguyen, Q., Huang, H.Z., Kim, D., Phillips, J., Tan, J., Lee, Y., Nguyen, T., et al. (2017). Hepatic S6K1 Partially Regulates Lifespan of Mice with Mitochondrial Complex I Deficiency. Front. Genet. *8*, 113.
Itoh, Y., Kawamata, Y., Harada, M., Kobayashi, M., Fujii, R., Fukusumi, S., Ogi, K., Hosoya, M., Tanaka, Y., Uejima, H., et al. (2003). Free fatty acids regulate insulin secretion from pancreatic β cells through GPR40. Nature *422*, 173–176.

Janzen, V., Forkert, R., Fleming, H.E., Saito, Y., Waring, M.T., Dombkowski, D.M., Cheng, T., DePinho, R.A., Sharpless, N.E., and Scadden, D.T. (2006). Stem-cell ageing modified by the cyclin-dependent kinase inhibitor p16INK4a. Nature *443*, 421–426.
Jeck, W.R., Siebold, A.P., and Sharpless, N.E. (2012). Review: a meta-analysis of GWAS and age-associated diseases. Aging Cell *11*, 727–731.
Jeon, O.H., Kim, C., Laberge, R.-M., Demaria, M., Rathod, S., Vasserot, A.P., Chung, J.W., Kim, D.H., Poon, Y., David, N., et al. (2017). Local clearance of senescent cells attenuates the development of post-traumatic osteoarthritis and creates a pro-regenerative environment. Nat. Med. *23*, 775–781.
Jiang, H., Westerterp, M., Wang, C., Zhu, Y., and Ai, D. (2014). Macrophage mTORC1 disruption reduces inflammation and insulin resistance in obese mice. Diabetologia *57*, 2393–2404.
Johnson, S.C., and Kaeberlein, M. (2016). Rapamycin in aging and disease: maximizing efficacy while minimizing side effects. Oncotarget *7*.
Johnson, S.C., Rabinovitch, P.S., and Kaeberlein, M. (2013). mTOR is a key modulator of ageing and age-related disease. Nature *493*, 338–345.
Jun, J.-I., and Lau, L.F. (2010). The matricellular protein CCN1 induces fibroblast senescence and restricts fibrosis in cutaneous wound healing. Nat. Cell Biol. *12*, 676–685.
Kan, Z., Zheng, H., Liu, X., Li, S., Barber, T.D., Gong, Z., Gao, H., Hao, K., Willard, M.D., Xu, J., et al. (2013). Whole-genome sequencing identifies recurrent mutations in hepatocellular carcinoma. Genome Res. *23*, 1422–1433.
Kang, C., Xu, Q., Martin, T.D., Li, M.Z., Demaria, M., Aron, L., Lu, T., Yankner, B.A., Campisi, J., and Elledge, S.J. (2015). The DNA damage response induces inflammation and senescence by inhibiting autophagy of GATA4. Science *349*, aaa5612.
Kang, T.-W., Yevsa, T., Woller, N., Hoenicke, L., Wuestefeld, T., Dauch, D., Hohmeyer, A., Gereke, M., Rudalska, R., Potapova, A., et al. (2011). Senescence surveillance of pre-malignant hepatocytes limits liver cancer development. Nature *479*, 547–551.
Karni, R., de Stanchina, E., Lowe, S.W., Sinha, R., Mu, D., and Krainer, A.R. (2007). The gene encoding the splicing factor SF2/ASF is a proto-oncogene. Nat. Struct. Mol. Biol. *14*, 185–193.
de Keizer, P.L.J., and al., et (2017). The Fountain of Youth by Targeting Senescent Cells? Trends Mol. Med. *23*, 6–17.
Kim, D., Akcakanat, A., Singh, G., Sharma, C., and Meric-Bernstam, F. (2009). Regulation and localization of ribosomal protein S6 kinase 1 isoforms. Growth Factors *27*, 12–21.
Kim, S.Y., Baik, K.-H., Baek, K.-H., Chah, K.-H., Kim, K.A., Moon, G., Jung, E., Kim, S.-T., Shim, J.-H., Greenblatt, M.B., et al. (2014). S6K1 negatively regulates TAK1 activity in the toll-like receptor signaling pathway. Mol. Cell. Biol. *34*, 510–521.
Klass, M.R. (1983). A method for the isolation of longevity mutants in the nematode Caenorhabditis elegans and initial results. Mech. Ageing Dev. *22*, 279–286.
Kleiner, D.E., Brunt, E.M., Van Natta, M., Behling, C., Contos, M.J., Cummings, O.W., Ferrell, L.D.,

Liu, Y.C., Torbenson, M.S., Unalp-Arida, A., et al. (2005). Design and validation of a histological scoring system for nonalcoholic fatty liver disease. Hepatology *41*, 1313–1321.
Koh, H., Jee, K., Lee, B., Kim, J., Kim, D., Yun, Y.H., Kim, J.W., Choi, H.S., and Chung, J. (1999). Cloning and characterization of a nuclear S6 kinase, S6 kinase-related kinase (SRK); a novel nuclear target of Akt. Oncogene *18*, 5115–5119.
Kojima, S.I., Watanabe, N., Numata, M., Ogawa, T., and Matsuzaki, S. (2003). Increase in the prevalence of fatty liver in Japan over the past 12 years: analysis of clinical background. J. Gastroenterol. *38*, 954–961.
Kolesnichenko, M., Hong, L., Liao, R., Vogt, P.K., and Sun, P. (2012). Attenuation of TORC1 signaling delays replicative and oncogenic RAS-induced senescence. Cell Cycle *11*, 2391–2401.
Kozma, S.C., Ferrari, S., Bassand, P., Siegmann, M., Totty, N., and Thomas, G. (1990). Cloning of the mitogen-activated S6 kinase from rat liver reveals an enzyme of the second messenger subfamily. Proc. Natl. Acad. Sci. U. S. A. *87*, 7365–7369.
Krishnamurthy, J., Torrice, C., Ramsey, M.R., Kovalev, G.I., Al-Regaiey, K., Su, L., and Sharpless, N.E. (2004). Ink4a/Arf expression is a biomarker of aging. J. Clin. Invest. *114*, 1299–1307.
Kristiansen, M.N.B., Veidal, S.S., Rigbolt, K.T.G., Tølbøl, K.S., Roth, J.D., Jelsing, J., Vrang, N., and Feigh, M. (2016). Obese diet-induced mouse models of nonalcoholic steatohepatitis-tracking disease by liver biopsy. World J. Hepatol. *8*, 673–684.
Krizhanovsky, V., Yon, M., Dickins, R.A., Hearn, S., Simon, J., Miething, C., Yee, H., Zender, L., and Lowe, S.W. (2008). Senescence of Activated Stellate Cells Limits Liver Fibrosis. Cell *134*, 657–667.
Krtolica, A., Parrinello, S., Lockett, S., Desprez, P.Y., and Campisi, J. (2001). Senescent fibroblasts promote epithelial cell growth and tumorigenesis: a link between cancer and aging. Proc. Natl. Acad. Sci. U. S. A. *98*, 12072–12077.
Kuilman, T., and Peeper, D.S. (2009). Senescence-messaging secretome: SMS-ing cellular stress. Nat. Rev. Cancer *9*, 81–94.
Kuilman, T., Michaloglou, C., Vredeveld, L.C.W., Douma, S., van Doorn, R., Desmet, C.J., Aarden, L.A., Mooi, W.J., and Peeper, D.S. (2008). Oncogene-induced senescence relayed by an interleukin-dependent inflammatory network. Cell *133*, 1019–1031.
Kuilman, T., Michaloglou, C., Mooi, W.J., and Peeper, D.S. (2010). The essence of senescence. Genes Dev. *24*, 2463–2479.
Kuo, C.J., Chung, J., Fiorentino, D.F., Flanagan, W.M., Blenis, J., and Crabtree, G.R. (1992). Rapamycin selectively inhibits interleukin-2 activation of p70 S6 kinase. Nature *358*, 70–73.
Kurebayashi, Y., Nagai, S., Ikejiri, A., Ohtani, M., Ichiyama, K., Baba, Y., Yamada, T., Egami, S., Hoshii, T., Hirao, A., et al. (2012). PI3K-Akt-mTORC1-S6K1/2 Axis Controls Th17 Differentiation by Regulating Gfi1 Expression and Nuclear Translocation of RORγ. Cell Rep. *1*, 360–373.
Laberge, R.-M., Awad, P., Campisi, J., and Desprez, P.-Y. (2012). Epithelial-mesenchymal transition induced by senescent fibroblasts. Cancer Microenviron. *5*, 39–44.

Laberge, R.-M., Sun, Y., Orjalo, A. V, Patil, C.K., Freund, A., Zhou, L., Curran, S.C., Davalos, A.R., Wilson-Edell, K.A., Liu, S., et al. (2015). MTOR regulates the pro-tumorigenic senescence-associated secretory phenotype by promoting IL1A translation. Nat. Cell Biol. *17*, 1049–1061.
Lai, K.P., Leong, W.F., Chau, J.F.L., Jia, D., Zeng, L., Liu, H., He, L., Hao, A., Zhang, H., Meek, D., et al. (2010). S6K1 is a multifaceted regulator of Mdm2 that connects nutrient status and DNA damage response. EMBO J. *29*, 2994–3006.
Lamming, D.W., Ye, L., Katajisto, P., Goncalves, M.D., Saitoh, M., Stevens, D.M., Davis, J.G., Salmon, A.B., Richardson, A., Ahima, R.S., et al. (2012). Rapamycin-Induced Insulin Resistance Is Mediated by mTORC2 Loss and Uncoupled from Longevity. Science (80-.). *335*, 1638–1643.
Lamming, D.W., Ye, L., Sabatini, D.M., and Baur, J.A. (2013). Rapalogs and mTOR inhibitors as anti-aging therapeutics. J. Clin. Invest. *123*, 980–989.
Lamming, D.W., Mihaylova, M.M., Katajisto, P., Baar, E.L., Yilmaz, O.H., Hutchins, A., Gultekin, Y., Gaither, R., and Sabatini, D.M. (2014). Depletion of Rictor, an essential protein component of mTORC2, decreases male lifespan. Aging Cell *13*, 911–917.
Lanquillon, S., Krieg, J.-C., Bening-Abu-Shach, U., and Vedder, H. (2000). Cytokine Production and Treatment Response in Major Depressive Disorder. Neuropsychopharmacology *22*, 370–379.
Laplante, M., and Sabatini, D.M. (2012). mTOR Signaling in Growth Control and Disease. Cell *149*, 274–293.
Lazzerini Denchi, E., Attwooll, C., Pasini, D., and Helin, K. (2005). Deregulated E2F activity induces hyperplasia and senescence-like features in the mouse pituitary gland. Mol. Cell. Biol. *25*, 2660–2672.
Lee-Fruman, K.K., Kuo, C.J., Lippincott, J., Terada, N., and Blenis, J. (1999). Characterization of S6K2, a novel kinase homologous to S6K1. Oncogene *18*, 5108–5114.
Leng, S., Chaves, P., Koenig, K., and Walston, J. (2002). Serum interleukin-6 and hemoglobin as physiological correlates in the geriatric syndrome of frailty: A pilot study. J. Am. Geriatr. Soc. *50*, 1268–1271.
Liu, D., and Hornsby, P.J. (2007). Senescent Human Fibroblasts Increase the Early Growth of Xenograft Tumors via Matrix Metalloproteinase Secretion. Cancer Res *67*, 3117–3126.
Liu, Y., Sanoff, H.K., Cho, H., Burd, C.E., Torrice, C., Ibrahim, J.G., Thomas, N.E., and Sharpless, N.E. (2009). Expression of *p16* ^{INK4a} in peripheral blood T-cells is a biomarker of human aging. Aging Cell *8*, 439–448.
Llovet, J.M., Zucman-Rossi, J., Pikarsky, E., Sangro, B., Schwartz, M., Sherman, M., and Gores, G. (2016). Hepatocellular carcinoma. Nat. Rev. Dis. Prim. *2*, 16018.
Loewith, R., Jacinto, E., Wullschleger, S., Lorberg, A., Crespo, J.L., Bonenfant, D., Oppliger, W., Jenoe, P., and Hall, M.N. (2002). Two TOR complexes, only one of which is rapamycin sensitive, have distinct roles in cell growth control. Mol. Cell *10*, 457–468.
Loffredo, F.S., Steinhauser, M.L., Jay, S.M., Gannon, J., Pancoast, J.R., Yalamanchi, P., Sinha, M., Dall'Osso, C., Khong, D., Shadrach, J.L., et al. (2013). Growth differentiation factor 11 is a

circulating factor that reverses age-related cardiac hypertrophy. Cell *153*, 828–839.
López-Otín, C., Blasco, M.A., Partridge, L., Serrano, M., and Kroemer, G. (2013). The Hallmarks of Aging. Cell *153*, 1194–1217.
Lujambio, A. (2016). To clear, or not to clear (senescent cells)? That is the question. Insid. Cell *1*, 87–95.
Lujambio, A., Akkari, L., Simon, J., Grace, D., Tschaharganeh, D.F., Bolden, J.E., Zhao, Z., Thapar, V., Joyce, J.A., Krizhanovsky, V., et al. (2013). Non-Cell-Autonomous Tumor Suppression by p53. Cell *153*, 449–460.
Lustig, Y., Ruas, J.L., Estall, J.L., Lo, J.C., Devarakonda, S., Laznik, D., Choi, J.H., Ono, H., Olsen, J. V, and Spiegelman, B.M. (2011). Separation of the gluconeogenic and mitochondrial functions of pgc-1α through s6 kinase. Genes Dev. *25*, 1232–1244.
Ma, X.M., and Blenis, J. (2009). Molecular mechanisms of mTOR-mediated translational control. Nat. Rev. Mol. Cell Biol. *10*, 307–318.
Ma, X.M., Yoon, S.O., Richardson, C.J., Jülich, K., and Blenis, J. (2008). SKAR Links Pre-mRNA Splicing to mTOR/S6K1-Mediated Enhanced Translation Efficiency of Spliced mRNAs. Cell *133*, 303–313.
Magnuson, B., Ekim, B., and Fingar, D.C. (2012). Regulation and function of ribosomal protein S6 kinase (S6K) within mTOR signalling networks. Biochem. J. *441*, 1–21.
Mannick, J.B., Del Giudice, G., Lattanzi, M., Valiante, N.M., Praestgaard, J., Huang, B., Lonetto, M.A., Maecker, H.T., Kovarik, J., Carson, S., et al. (2014). mTOR inhibition improves immune function in the elderly. Sci. Transl. Med. *6*, 268ra179.
Marcotrigiano, J., Gingras, A.C., Sonenberg, N., and Burley, S.K. (1999). Cap-dependent translation initiation in eukaryotes is regulated by a molecular mimic of eIF4G. Mol. Cell *3*, 707–716.
Marmot, M. (2005). Social determinants of health inequalities. Lancet *365*, 1099–1104.
Marmot, M., and Bell, R. (2012). Fair society, healthy lives. Public Health *126*, S4–S10.
Marmot, M.G., Stansfeld, S., Patel, C., North, F., Head, J., White, I., Brunner, E., Feeney, A., Marmot, M.G., and Smith, G.D. (1991). Health inequalities among British civil servants: the Whitehall II study. Lancet *337*, 1387–1393.
Martin, N., Beach, D., and Gil, J. (2014). Ageing as developmental decay: insights from p16INK4a. Trends Mol. Med. *20*, 667–674.
Matheu, A., Maraver, A., Klatt, P., Flores, I., Garcia-Cao, I., Borras, C., Flores, J.M., Viña, J., Blasco, M.A., and Serrano, M. (2007). Delayed ageing through damage protection by the Arf/p53 pathway. Nature *448*, 375–379.
Matheu, A., Maraver, A., Collado, M., Garcia-Cao, I., Cañamero, M., Borras, C., Flores, J.M., Klatt, P., Viña, J., and Serrano, M. (2009). Anti-aging activity of the Ink4/Arf locus. Aging Cell *8*, 152–161.
Matter, M.S., Decaens, T., Andersen, J.B., and Thorgeirsson, S.S. (2014). Targeting the mTOR

pathway in hepatocellular carcinoma: Current state and future trends. J. Hepatol. *60*, 855–865.
McCommis, K.S., Hodges, W.T., Brunt, E.M., Nalbantoglu, I., McDonald, W.G., Holley, C., Fujiwara, H., Schaffer, J.E., Colca, J.R., and Finck, B.N. (2017). Targeting the mitochondrial pyruvate carrier attenuates fibrosis in a mouse model of nonalcoholic steatohepatitis. Hepatology *65*, 1543–1556.
McConnell, B.B., Starborg, M., Brookes, S., and Peters, G. (1998). Inhibitors of cyclin-dependent kinases induce features of replicative senescence in early passage human diploid fibroblasts. Curr. Biol. *8*, 351–354.
McEachern, M.J., Krauskopf, A., and Blackburn, E.H. (2000). Telomeres and Their Control. Annu. Rev. Genet. *34*, 331–358.
McKenzie, J., Fisher, B.M., Jaap, A.J., Stanley, A., Paterson, K., and Sattar, N. (2006). Effects of HRT on liver enzyme levels in women with type 2 diabetes: A randomized placebo-controlled trial. Clin. Endocrinol. (Oxf). *65*, 40–44.
Michaloglou, C., Vredeveld, L.C.W., Soengas, M.S., Denoyelle, C., Kuilman, T., van der Horst, C.M.A.M., Majoor, D.M., Shay, J.W., Mooi, W.J., and Peeper, D.S. (2005). BRAFE600-associated senescence-like cell cycle arrest of human naevi. Nature *436*, 720–724.
Michaud, K., Solomon, D.A., Oermann, E., Kim, J.S., Zhong, W.Z., Prados, M.D., Ozawa, T., James, C.D., and Waldman, T. (2010). Pharmacologic inhibition of cyclin-dependent kinases 4 and 6 arrests the growth of glioblastoma multiforme intracranial xenografts. Cancer Res. *70*, 3228–3238.
Mieulet, V., Roceri, M., Espeillac, C., Sotiropoulos, A., Ohanna, M., Oorschot, V., Klumperman, J., Sandri, M., and Pende, M. (2007). S6 kinase inactivation impairs growth and translational target phosphorylation in muscle cells maintaining proper regulation of protein turnover. Am. J. Physiol. Cell Physiol. *293*, C712–C722.
Miller, R.A., Harrison, D.E., Astle, C.M., Fernandez, E., Flurkey, K., Han, M., Javors, M.A., Li, X., Nadon, N.L., Nelson, J.F., et al. (2014). Rapamycin-mediated lifespan increase in mice is dose and sex dependent and metabolically distinct from dietary restriction. Aging Cell *13*, 468–477.
Di Mitri, D., and Alimonti, A. (2016). Non-Cell-Autonomous Regulation of Cellular Senescence in Cancer. Trends Cell Biol. *26*, 215–226.
Di Mitri, D., Toso, A., Chen, J.J., Sarti, M., Pinton, S., Jost, T.R., D'Antuono, R., Montani, E., Garcia-Escudero, R., Guccini, I., et al. (2014). Tumour-infiltrating Gr-1+ myeloid cells antagonize senescence in cancer. Nature *515*, 134–137.
Molofsky, A. V, Slutsky, S.G., Joseph, N.M., He, S., Pardal, R., Krishnamurthy, J., Sharpless, N.E., and Morrison, S.J. (2006). Increasing p16INK4a expression decreases forebrain progenitors and neurogenesis during ageing. Nature *443*, 448–452.
Mosteiro, L., Pantoja, C., Alcazar, N., Marión, R.M., Chondronasiou, D., Rovira, M., Fernández-Marcos, P., Muñoz-Martin, M., Blanco-Aparicio, C., Pastor, J., et al. (2016). Tissue damage and senescence provide critical signals for cellular reprogramming in vivo. Science (80-.). *354*.

Mukhopadhyay, R., Jia, J., Arif, A., Ray, P.S., and Fox, P.L. (2009). The GAIT system: a gatekeeper of inflammatory gene expression. Trends Biochem. Sci. *34*, 324–331.
Muñoz-Espín, D., and Serrano, M. (2014). Cellular senescence: from physiology to pathology. Nat. Rev. Mol. Cell Biol. *15*, 482–496.
Muñoz-Espín, D., Cañamero, M., Maraver, A., Gómez-López, G., Contreras, J., Murillo-Cuesta, S., Rodríguez-Baeza, A., Varela-Nieto, I., Ruberte, J., Collado, M., et al. (2013). Programmed cell senescence during mammalian embryonic development. Cell *155*, 1104–1118.
Nardella, C., Lunardi, A., Fedele, G., Clohessy, J.G., Alimonti, A., Kozma, S.C., Thomas, G., Loda, M., and Pandolfi, P.P. (2011). Differential expression of S6K2 dictates tissue-specific requirement for S6K1 in mediating aberrant mTORC1 signaling and tumorigenesis. Cancer Res. *71*, 3669–3675.
Narita, M., Young, A.R.J., Arakawa, S., Samarajiwa, S.A., Nakashima, T., Yoshida, S., Hong, S., Berry, L.S., Reichelt, S., Ferreira, M., et al. (2011). Spatial Coupling of mTOR and Autophagy Augments Secretory Phenotypes. Science (80-.). *332*, 966–970.
Nemazanyy, I., Espeillac, C., Pende, M., and Panasyuk, G. (2013). Role of PI3K, mTOR and Akt2 signalling in hepatic tumorigenesis via the control of PKM2 expression. Biochem. Soc. Trans. *41*, 917–922.
Nordenstedt, H., White, D.L., and El-Serag, H.B. (2010). The changing pattern of epidemiology in hepatocellular carcinoma. Dig. Liver Dis. *42*, 206–214.
O'Reilly, K.E., Rojo, F., She, Q.-B., Solit, D., Mills, G.B., Smith, D., Lane, H., Hofmann, F., Hicklin, D.J., Ludwig, D.L., et al. (2006). mTOR Inhibition Induces Upstream Receptor Tyrosine Kinase Signaling and Activates Akt. Cancer Res *66*, 1500–1508.
Oeppen, J., and Vaupel, J.W. (2002). Broken limits to life expectancy. Science (80-.). *296*, 1029–1031.
Ogrodnik, M., Miwa, S., Tchkonia, T., Tiniakos, D., Wilson, C.L., Lahat, A., Day, C.P., Burt, A., Palmer, A., Anstee, Q.M., et al. (2017). Cellular senescence drives age-dependent hepatic steatosis. Nat. Commun. *8*, 15691.
Ohguchi, H., Tanaka, T., Uchida, A., Magoori, K., Kudo, H., Kim, I., Daigo, K., Sakakibara, I., Okamura, M., Harigae, H., et al. (2008). Hepatocyte Nuclear Factor 4 Contributes to Thyroid Hormone Homeostasis by Cooperatively Regulating the Type 1 Iodothyronine Deiodinase Gene with GATA4 and Kruppel-Like Transcription Factor 9. Mol. Cell. Biol. *28*, 3917–3931.
Olovnikov, A.M. (1971). Principle of marginotomy in template synthesis of polynucleotides. Dokl. Akad. Nauk SSSR *201*, 1496–1499.
Olshansky, S.J. (2016). Measuring our narrow strip of life. Nature *538*, 175–176.
Olshansky, S.J., Carnes, B.A., and Cassel, C. (1990). In search of Methuselah: estimating the upper limits to human longevity. Science (80-.). *250*, 634–640.
Olshansky, S.J., Carnes, B.A., and Desesquelles, A. (2001). Demography. Prospects for human longevity. Science (80-.). *291*, 1491–1492.

Orjalo, A. V, Bhaumik, D., Gengler, B.K., Scott, G.K., and Campisi, J. (2009). Cell surface-bound IL-1alpha is an upstream regulator of the senescence-associated IL-6/IL-8 cytokine network. Proc. Natl. Acad. Sci. U. S. A. *106*, 17031–17036.

Palm, W., Park, Y., Wright, K., Pavlova, N.N., Tuveson, D.A., and Thompson, C.B. (2015). The Utilization of Extracellular Proteins as Nutrients Is Suppressed by mTORC1. Cell *162*, 259–270.

Pardo, O.E., and Seckl, M.J. (2013). S6K2: The Neglected S6 Kinase Family Member. Front. Oncol. *3*, 191.

Pardo, O.E., Arcaro, A., Salerno, G., Tetley, T.D., Valovka, T., Gout, I., and Seckl, M.J. (2001). Novel cross talk between MEK and S6K2 in FGF-2 induced proliferation of SCLC cells. Oncogene *20*, 7658–7667.

Park, E.J., Lee, J.H., Yu, G.Y., He, G., Ali, S.R., Holzer, R.G., Österreicher, C.H., Takahashi, H., and Karin, M. (2010). Dietary and Genetic Obesity Promote Liver Inflammation and Tumorigenesis by Enhancing IL-6 and TNF Expression. Cell *140*, 197–208.

Parrinello, S., Coppe, J.-P., Krtolica, A., and Campisi, J. (2005). Stromal-epithelial interactions in aging and cancer: senescent fibroblasts alter epithelial cell differentiation. J. Cell Sci. *118*, 485–496.

Patitucci, C., Couchy, G., Bagattin, A., Cañeque, T., De Reyniès, A., Scoazec, J.Y., Rodriguez, R., Pontoglio, M., Zucman-Rossi, J., Pende, M., et al. (2017). Hepatocyte nuclear factor 1α suppresses steatosisassociated liver cancer by inhibiting PPARγ transcription. J. Clin. Invest. *127*, 1873–1888.

Pause, A., and Sonenberg, N. (1992). Mutational analysis of a DEAD box RNA helicase: the mammalian translation initiation factor eIF-4A. EMBO J. *11*, 2643–2654.

Pearson, R.B., Dennis, P.B., Han, J.-W., Williamson1, N.A., Kozma, S.C., Wettenhall ', R.E.H., and Thomas2, G. (1995). The principal target of rapamycin-induced p70s6k inactivation is a novel phosphorylation site within a conserved hydrophobic domain. EMBO J. *14*, 5279–5287.

Pende, M., Kozma, S.C., Jaquet, M., Oorschot, V., Burcelin, R., Le Marchand-Brustel, Y., Klumperman, J., Thorens, B., and Thomas, G. (2000). Hypoinsulinaemia, glucose intolerance and diminished beta-cell size in S6K1-deficient mice. Nature *408*, 994–997.

Pende, M., Um, S.H., Mieulet, V., Goss, V.L., Mestan, J., Mueller, M., Fumagalli, S., Kozma, S.C., Thomas, G., and Sticker, M. (2004). S6K1-/-/S6K2-/- Mice Exibit Preinatal Lethality and Rapamycin-Sensitive 5 ' -Terminal Oligopyrimidine mRNA Translation and Reveal a Mitogen-Activated Protein Kinase-Dependent S6 Kinase Pathway. Mol. Cell. Biol. *24*, 3112–3124.

Pérez-Mancera, P.A., Young, A.R.J., and Narita, M. (2014). Inside and out: the activities of senescence in cancer. Nat. Rev. Cancer *14*, 547–558.

Powell, J.D., Pollizzi, K.N., Heikamp, E.B., and Horton, M.R. (2012). Regulation of Immune Responses by mTOR. Annu. Rev. Immunol. *30*, 39–68.

Pradhan, A.D., Manson, J.E., Rifai, N., Buring, J.E., and Ridker, P.M. (2001). C-Reactive Protein, Interleukin 6, and Risk of Developing Type 2 Diabetes Mellitus. JAMA *286*, 327.

Price, D.J., Grove, J.R., Calvo, V., Avruch, J., and Bierer, B.E. (1992). Rapamycin-Induced Inhibition of the 70-Kilodalton S6 Protein Kinase. Science (80-.). *257*, 973–977.
Pullen, N., Dennis, P.B., Andjelkovic, M., Dufner, A., Kozma, S.C., Hemmings, B.A., and Thomas, G. (1998). Phosphorylation and Activation of p70s6k by PDK1. Science (80-.). *279*, 707–710.
Qian, L.-W., Mizumoto, K., Urashima, T., Nagai, E., Maehara, N., Sato, N., Nakajima, M., and Tanaka, M. (2002). Radiation-induced Increase in Invasive Potential of Human Pancreatic Cancer Cells and Its Blockade by a Matrix Metalloproteinase Inhibitor, CGS27023. Clin. Cancer Res. *8*, 1223–1227.
Raught, B., Peiretti, F., Gingras, A.-C., Livingstone, M., Shahbazian, D., Mayeur, G.L., Polakiewicz, R.D., Sonenberg, N., and Hershey, J.W.B. (2004). Phosphorylation of eucaryotic translation initiation factor 4B Ser422 is modulated by S6 kinases. EMBO J. *23*, 1761–1769.
Rebo, J., Mehdipour, M., Gathwala, R., Causey, K., Liu, Y., Conboy, M.J., and Conboy, I.M. (2016). A single heterochronic blood exchange reveals rapid inhibition of multiple tissues by old blood. Nat. Commun. *7*, 13363.
Rebsamen, M., Pochini, L., Stasyk, T., de Araújo, M.E.G., Galluccio, M., Kandasamy, R.K., Snijder, B., Fauster, A., Rudashevskaya, E.L., Bruckner, M., et al. (2015). SLC38A9 is a component of the lysosomal amino acid sensing machinery that controls mTORC1. Nature *519*, 477–481.
Richardson, C.J., Bröenstrup, M., Fingar, D.C., Jülich, K., Ballif, B.A., Gygi, S., and Blenis, J. (2004). SKAR is a specific target of S6 kinase 1 in cell growth control. Curr. Biol. *14*, 1540–1549.
Rodier, F., Coppé, J.-P., Patil, C.K., Hoeijmakers, W.A.M., Muñoz, D.P., Raza, S.R., Freund, A., Campeau, E., Davalos, A.R., and Campisi, J. (2009). Persistent DNA damage signalling triggers senescence-associated inflammatory cytokine secretion. Nat Cell Biol *11*, 973–979.
Rodrik-Outmezguine, V.S., Okaniwa, M., Yao, Z., Novotny, C.J., Mcwhirter, C., Banaji, A., Won, H., Wong, W., Berger, M., De Stanchina, E., et al. (2016). Overcoming mTOR resistance mutations with a new-generation mTOR inhibitor. Nature *534*, 272–276.
Rozen, F., Edery, I., Meerovitch, K., Dever, T.E., Merrick, W.C., and Sonenberg, N. (1990). Bidirectional RNA helicase activity of eucaryotic translation initiation factors 4A and 4F. Mol. Cell. Biol. *10*, 1134–1144.
Rozing, M.P., Kirkwood, T.B.L., and Westendorp, R.G.J. (2017). Is there evidence for a limit to human lifespan? Nature *546*, E11–E12.
Ruvinsky, I., Sharon, N., Lerer, T., Cohen, H., Stolovich-Rain, M., Nir, T., Dor, Y., Zisman, P., and Meyuhas, O. (2005). Ribosomal protein S6 phosphorylation is a determinant of cell size and glucose homeostasis. Genes Dev. *19*, 2199–2211.
Sabatini, D.M., Erdjument-Bromage, H., Lui, M., Tempst, P., and Snyder, S.H. (1994). RAFT1: A mammalian protein that binds to FKBP12 in a rapamycin-dependent fashion and is homologous to yeast TORs. Cell *78*, 35–43.
Sabers, C.J., Martin, M.M., Brunn, G.J., Williams, J.M., Dumont, F.J., Wiederrecht, G., and

Abraham, R.T. (1995). Isolation of a protein target of the FKBP12-rapamycin complex in mammalian cells. J. Biol. Chem. *270*, 815–822.
Sager, R. (1991). Senescence As a Mode of Tumor Suppression. Environ. Health Perspect. *93*, 59–62.
Saha, S.K., Parachoniak, C.A., Ghanta, K.S., Fitamant, J., Ross, K.N., Najem, M.S., Gurumurthy, S., Akbay, E.A., Sia, D., Cornella, H., et al. (2014). Mutant IDH inhibits HNF-4α to block hepatocyte differentiation and promote biliary cancer. Nature *513*, 110–114.
Sahin, F., Kannangai, R., Adegbola, O., Wang, J., Su, G., and Torbenson, M. (2004). mTOR and P70 S6 kinase expression in primary liver neoplasms. Clin. Cancer Res. *10*, 8421–8425.
Saitoh, M., ten Dijke, P., Miyazono, K., and Ichijo, H. (1998). Cloning and Characterization of p70S6Kβ Defines a Novel Family of p70 S6 Kinases. Biochem. Biophys. Res. Commun. *253*, 470–476.
Salama, R., Sadaie, M., Hoare, M., and Narita, M. (2014). Cellular senescence and its effector programs. Genes Dev. *28*, 99–114.
Sarbassov, D.D., Ali, S.M., Kim, D.-H., Guertin, D.A., Latek, R.R., Erdjument-Bromage, H., Tempst, P., and Sabatini, D.M. (2004). Rictor, a Novel Binding Partner of mTOR, Defines a Rapamycin-Insensitive and Raptor-Independent Pathway that Regulates the Cytoskeleton. Curr. Biol. *14*, 1296–1302.
Saxton, R.A., Sabatini, D.M., Efeyan, A., Wang, S., Sancak, Y., Sabatini, D.M., Powell, J.D., Manning, B.D., Cantley, L.C., Gygi, S.P., et al. (2017). mTOR Signaling in Growth, Metabolism, and Disease. Cell *168*, 960–976.
Selman, C., and Withers, D.J. (2017). An atypical switch for metabolism and ageing. Nature *542*, 299–300.
Selman, C., Lingard, S., Choudhury, A.I., Batterham, R.L., Claret, M., Clements, M., Ramadani, F., Okkenhaug, K., Schuster, E., Blanc, E., et al. (2008). Evidence for lifespan extension and delayed age-related biomarkers in insulin receptor substrate 1 null mice. FASEB J. *22*, 807–818.
Selman, C., Tullet, J.M., Wieser, D., Irvine, E.E., Lingard, S.J., Choudhury, A.I., Claret, M., Al-Qassab, H., Carmignac, D., Ramadani, F., et al. (2009). Ribosomal protein S6 kinase 1 signaling regulates mammalian life span. Science (80-.). *326*, 140–144.
Selman, C., Sinclair, A., Pedroni, S.M.A., Irvine, E.E., Michie, A.M., Withers, D.J., Selman, C., Sinclair, A., Pedroni, S.M.A., Irvine, E.E., et al. (2016). Evidence that hematopoietic stem cell function is preserved during aging in long-lived S6K1 mutant mice. Oncotarget *7*, 29937–29943.
Serra, V., Markman, B., Scaltriti, M., Eichhorn, P.J.A., Valero, V., Guzman, M., Botero, M.L., Llonch, E., Atzori, F., Di Cosimo, S., et al. (2008). NVP-BEZ235, a dual PI3K/mTOR inhibitor, prevents PI3K signaling and inhibits the growth of cancer cells with activating PI3K mutations. Cancer Res. *68*, 8022–8030.
Serrano, M., Lin, A.W., McCurrach, M.E., Beach, D., and Lowe, S.W. (1997). Oncogenic ras Provokes Premature Cell Senescence Associated with Accumulation of p53 and p16INK4a. Cell

88, 593–602.
Sharpless, N.E., and Sherr, C.J. (2015). Forging a signature of in vivo senescence. Nat. Rev. Cancer *15*, 397–408.
Shima, H., Pende, M., Chen, Y., Fumagalli, S., Thomas, G., and Kozma, S.C. (1998). Disruption of the p70 s6k /p85 s6k gene reveals a small mouse phenotype and a new functional S6 kinase. EMBO J. *17*, 6649–6659.
Shimizu, I. (2003). Impact of oestrogens on the progression of liver disease. Liver Int. *23*, 63–69.
Sieghart, W., Fuereder, T., Schmid, K., Cejka, D., Werzowa, J., Wrba, F., Wang, X., Gruber, D., Rasoul-Rockenschaub, S., Peck-Radosavljevic, M., et al. (2007). Mammalian Target of Rapamycin Pathway Activity in Hepatocellular Carcinomas of Patients Undergoing Liver Transplantation. Transplantation *83*, 425–432.
Signer, R.A.J., Montecino-Rodriguez, E., Witte, O.N., and Dorshkind, K. (2008). Aging and cancer resistance in lymphoid progenitors are linked processes conferred by p16Ink4a and Arf. Genes Dev. *22*, 3115–3120.
Singh-Manoux, A., Dugravot, A., Brunner, E., Kumari, M., Shipley, M., Elbaz, A., and Kivimaki, M. (2014). Interleukin-6 and C-reactive protein as predictors of cognitive decline in late midlife. Neurology *83*, 486–493.
Smith, M.A., Katsouri, L., Irvine, E.E., Hankir, M.K., Pedroni, S.M.A., Voshol, P.J., Gordon, M.W., Choudhury, A.I., Woods, A., Vidal-Puig, A., et al. (2015). Ribosomal S6K1 in POMC and AgRP neurons regulates glucose homeostasis but Not feeding behavior in mice. Cell Rep. *11*, 335–343.
Souroullas, G.P., and Sharpless, N.E. (2015). mTOR Signaling in Melanoma: Oncogene-Induced Pseudo-Senescence? Cancer Cell *27*, 3–5.
Sousa-Victor, P., Gutarra, S., García-Prat, L., Rodriguez-Ubreva, J., Ortet, L., Ruiz-Bonilla, V., Jardí, M., Ballestar, E., González, S., Serrano, A.L., et al. (2014). Geriatric muscle stem cells switch reversible quiescence into senescence. Nature *506*, 316–321.
Spranger, J., Kroke, A., Mo, M., Hoffmann, K., and Bergmann, M.M. (2003). Inflammatory Cytokines and the Risk to Develop Type 2 Diabetes. Diabetes *52*, 812–817.
Storer, M., Mas, A., Robert-Moreno, A., Pecoraro, M., Ortells, M.C., Di Giacomo, V., Yosef, R., Pilpel, N., Krizhanovsky, V., Sharpe, J., et al. (2013). Senescence is a developmental mechanism that contributes to embryonic growth and patterning. Cell *155*, 1119–1130.
Tasdemir, N., Banito, A., Roe, J.-S., Alonso-Curbelo, D., Camiolo, M., Tschaharganeh, D.F., Huang, C.-H., Aksoy, O., Bolden, J.E., Chen, C.-C., et al. (2016). BRD4 Connects Enhancer Remodeling to Senescence Immune Surveillance. Cancer Discov. *6*, 612–629.
Tchkonia, T., Zhu, Y., Van Deursen, J., Campisi, J., and Kirkland, J.L. (2013). Cellular senescence and the senescent secretory phenotype: Therapeutic opportunities. J. Clin. Invest. *123*, 966–972.
Thoreen, C.C., Kang, S.A., Chang, J.W., Liu, Q., Zhang, J., Gao, Y., Reichling, L.J., Sim, T., Sabatini, D.M., and Gray, N.S. (2009). An ATP-competitive mammalian target of rapamycin inhibitor reveals rapamycin-resistant functions of mTORC1. J. Biol. Chem. *284*, 8023–8032.

Tolcher, A., Goldman, J., Patnaik, A., Papadopoulos, K.P., Westwood, P., Kelly, C.S., Bumgardner, W., Sams, L., Geeganage, S., Wang, T., et al. (2014). A phase I trial of LY2584702 tosylate, a p70 S6 kinase inhibitor, in patients with advanced solid tumours. Eur. J. Cancer *50*, 867–875.

Tominaga-Yamanaka, K., Abdelmohsen, K., Martindale, J.L., Yang, X., Taub, D.D., and Gorospe, M. (2012). NF90 coordinately represses the senescence-associated secretory phenotype. Aging (Albany. NY). *4*, 695–708.

Della Torre, S., and Maggi, A. (2017). Sex Differences: A Resultant of an Evolutionary Pressure? Cell Metab.

Tsai, K.K., Yao-Yu Chuang, E., Little, J.B., and Yuan, Z.-M. (2005). Cellular Mechanisms for Low-Dose Ionizing Radiation–Induced Perturbation of the Breast Tissue Microenvironment. Cancer Res *65*, 6734–6744.

Tummala, K.S., Gomes, A.L., Yilmaz, M., Graña, O., Bakiri, L., Ruppen, I., Ximénez-Embún, P., Sheshappanavar, V., Rodriguez-Justo, M., Pisano, D.G., et al. (2014). Inhibition of De Novo NAD+ Synthesis by Oncogenic URI Causes Liver Tumorigenesis through DNA Damage. Cancer Cell *26*, 826–839.

Turner, N.C., Ro, J., André, F., Loi, S., Verma, S., Iwata, H., Harbeck, N., Loibl, S., Huang Bartlett, C., Zhang, K., et al. (2015). Palbociclib in Hormone-Receptor–Positive Advanced Breast Cancer. N. Engl. J. Med. *373*, 209–219.

Umemura, A., Park, E.J., Taniguchi, K., Lee, J.H., Shalapour, S., Valasek, M.A., Aghajan, M., Nakagawa, H., Seki, E., Hall, M.N., et al. (2014). Liver damage, inflammation, and enhanced tumorigenesis after persistent mTORC1 inhibition. Cell Metab. *20*, 133–144.

Valovka, T., Verdier, F., Cramer, R., Zhyvoloup, A., Fenton, T., Rebholz, H., Wang, M., Gzhegotsky, M., Matsuka, G., Filonenko, V., et al. (2003). Protein Kinase C Phosphorylates Ribosomal Protein S6 Kinase β II and Regulates Its Subcellular Localization. Mollecular Cell. Biol. *23*, 852–863.

Vernon, G., Baranova, A., and Younossi, Z.M. (2011). Systematic review: the epidemiology and natural history of non-alcoholic fatty liver disease and non-alcoholic steatohepatitis in adults. Aliment. Pharmacol. Ther. *34*, 274–285.

Villanueva, A., Chiang, D.Y., Newell, P., Peix, J., Thung, S., Alsinet, C., Tovar, V., Roayaie, S., Minguez, B., Sole, M., et al. (2008). Pivotal Role of mTOR Signaling in Hepatocellular Carcinoma. Gastroenterology *135*, 1972–1983.e11.

Villeda, S.A., Luo, J., Mosher, K.I., Zou, B., Britschgi, M., Bieri, G., Stan, T.M., Fainberg, N., Ding, Z., Eggel, A., et al. (2011). The ageing systemic milieu negatively regulates neurogenesis and cognitive function. Nature *477*, 90–94.

Wajapeyee, N., Serra, R.W., Zhu, X., Mahalingam, M., and Green, M.R. (2008). Oncogenic BRAF Induces Senescence and Apoptosis through Pathways Mediated by the Secreted Protein IGFBP7. Cell *132*, 363–374.

Walle, P., Takkunen, M., Männistö, V., Vaittinen, M., Lankinen, M., Kärjä, V., Käkelä, P., Ågren, J., Tiainen, M., Schwab, U., et al. (2016). Fatty acid metabolism is altered in non-alcoholic steatohepatitis independent of obesity. Metabolism. *65*, 655–666.
Walters, H.E., Deneka-Hannemann, S., and Cox, L.S. (2016). Reversal of phenotypes of cellular senescence by pan-mTOR inhibition. Aging (Albany. NY). *8*, 231–244.
Wang, E. (1995). Senescent Human Fibroblasts Resist Programmed Cell Death, and Failure to Suppress bcl2 Is Involved. Cancer Res. *55*, 2284–2292.
Wang, F., Alain, T., Szretter, K.J., Stephenson, K., Pol, J.G., Atherton, M.J., Hoang, H.-D., Fonseca, B.D., Zakaria, C., Chen, L., et al. (2016). S6K-STING interaction regulates cytosolic DNA–mediated activation of the transcription factor IRF3. Nat. Immunol. *17*, 514–522.
Wang, S., Tsun, Z.-Y., Wolfson, R.L., Shen, K., Wyant, G.A., Plovanich, M.E., Yuan, E.D., Jones, T.D., Chantranupong, L., Comb, W., et al. (2015). Lysosomal amino acid transporter SLC38A9 signals arginine sufficiency to mTORC1. Science (80-.). *347*, 188–194.
Wang, X., Li, W., Williams, M., Terada, N., Alessi, D.R., and Proud, C.G. (2001). Regulation of elongation factor 2 kinase by p90RSK1 and p70 S6 kinase. EMBO J. *20*, 4370–4379.
Watson, J.D. (1972). Origin of Concatemeric T7DNA. Nat. New Biol. *239*, 197–201.
Wei, S., Wei, W., and Sedivy, J.M. (1999). Expression of catalytically active telomerase does not prevent premature senescence caused by overexpression of oncogenic Ha-Ras in normal human fibroblasts. Cancer Res. *59*, 1539–1543.
Wek, S.A., Zhu, S., and Wek, R.C. (1995). The histidyl-tRNA synthetase-related sequence in the eIF-2 alpha protein kinase GCN2 interacts with tRNA and is required for activation in response to starvation for different amino acids. Mol. Cell. Biol. *15*, 4497–4506.
Wiley, C.D., Velarde, M.C., Lecot, P., Liu, S., Sarnoski, E.A., Freund, A., Shirakawa, K., Lim, H.W., Davis, S.S., Ramanathan, A., et al. (2016). Mitochondrial dysfunction induces senescence with a distinct secretory phenotype. Cell Metab. *23*, 303–314.
Wilkinson, J.E., Burmeister, L., Brooks, S. V., Chan, C.C., Friedline, S., Harrison, D.E., Hejtmancik, J.F., Nadon, N., Strong, R., Wood, L.K., et al. (2012). Rapamycin slows aging in mice. Aging Cell *11*, 675–682.
Williams, G.C. (1957). Pleiotropy, Natural Selection, and the Evolution of Senescence. Evolution (N. Y). *11*, 398.
Wilson, K.F., Wu, W.J., and Cerione, R.A. (2000). Cdc42 stimulates RNA splicing via the S6 kinase and a novel S6 kinase target, the nuclear cap-binding complex. J. Biol. Chem. *275*, 37307–37310.
Wolf, M.J., Adili, A., Piotrowitz, K., Abdullah, Z., Boege, Y., Stemmer, K., Ringelhan, M., Simonavicius, N., Le Egger, M., Wohlleber, D., et al. (2014). Metabolic Activation of Intrahepatic CD8 + T Cells and NKT Cells Causes Nonalcoholic Steatohepatitis and Liver Cancer via Cross-Talk with Hepatocytes. Cancer Cell *26*, 549–564.
Wong, V.W.-S., Chitturi, S., Wong, G.L.-H., Yu, J., Chan, H.L.-Y., and Farrell, G.C. (2016).

Pathogenesis and novel treatment options for non-alcoholic steatohepatitis. Lancet Gastroenterol. Hepatol. *1*, 56–67.
Wree, A., Broderick, L., Canbay, A., Hoffman, H.M., and Feldstein, A.E. (2013). From NAFLD to NASH to cirrhosis—new insights into disease mechanisms. Nat. Rev. Gastroenterol. Hepatol. *10*, 627–636.
Wu, J.J., Liu, J., Chen, E., Wang, J., Cao, L., Narayan, N., Fergusson, M., Rovira, I., Allen, M., Springer, D., et al. (2013). Increased mammalian lifespan and a segmental and tissue-specific slowing of aging after genetic reduction of mTOR expression. Cell Rep. *4*, 913–920.
Xiong, Y., Fru, M.F., Yu, Y., Montani, J.-P., Ming, X.-F., and Yang, Z. (2014). Long term exposure to L-arginine accelerates endothelial cell senescence through arginase-II and S6K1 signaling. Aging (Albany. NY). *6*, 369–379.
Xu, J.-W., Gong, J., Chang, X.-M., Luo, J.-Y., Dong, L., Hao, Z.-M., Jia, A., and Xu, G.-P. (2002). Estrogen reduces CCL4- induced liver fibrosis in rats. World J. Gastroenterol. *8*, 883–887.
Xu, S., Cai, Y., and Wei, Y. (2014). mTOR Signaling from Cellular Senescence to Organismal Aging. Aging Dis. *5*, 263–273.
Xue, W., Zender, L., Miething, C., Dickins, R.A., Hernando, E., Krizhanovsky, V., Cordon-Cardo, C., and Lowe, S.W. (2007). Senescence and tumour clearance is triggered by p53 restoration in murine liver carcinomas. Nature *445*, 656–660.
Yamaguchi, K., Yang, L., McCall, S., Huang, J., Yu, X.X., Pandey, S.K., Bhanot, S., Monia, B.P., Li, Y.-X., and Diehl, A.M. (2007). Inhibiting triglyceride synthesis improves hepatic steatosis but exacerbates liver damage and fibrosis in obese mice with nonalcoholic steatohepatitis. Hepatology *45*, 1366–1374.
Yamnik, R.L., Digilova, A., Davis, D.C., Brodt, Z.N., Murphy, C.J., and Holz, M.K. (2009). S6 kinase 1 regulates estrogen receptor α in control of breast cancer cell proliferation. J. Biol. Chem. *284*, 6361–6369.
Yang, G., Rosen, D.G., Zhang, Z., Bast, R.C., Mills, G.B., Colacino, J.A., Mercado-Uribe, I., and Liu, J. (2006). The chemokine growth-regulated oncogene 1 (Gro-1) links RAS signaling to the senescence of stromal fibroblasts and ovarian tumorigenesis. Proc. Natl. Acad. Sci. U. S. A. *103*, 16472–16477.
Yang, H., Wang, H., Ren, J., Chen, Q., and Chen, Z.J. (2017). cGAS is essential for cellular senescence. Proc. Natl. Acad. Sci. *114*, E4612–E4620.
Yang, J.D., Abdelmalek, M.F., Pang, H., Guy, C.D., Smith, A.D., Diehl, A.M., and Suzuki, A. (2014). Gender and menopause impact severity of fibrosis among patients with nonalcoholic steatohepatitis. Hepatology *59*, 1406–1414.
Yepuri, G., Velagapudi, S., Xiong, Y., Rajapakse, A.G., Montani, J.P., Ming, X.F., and Yang, Z. (2012). Positive crosstalk between arginase-II and S6K1 in vascular endothelial inflammation and aging. Aging Cell *11*, 1005–1016.
Yi, S.A., Um, S.H., Lee, J., Yoo, J.H., Bang, S.Y., Park, E.K., Lee, M.G., Nam, K.H., Jeon, Y.J.,

Park, J.W., et al. (2016). S6K1 Phosphorylation of H2B Mediates EZH2 Trimethylation of H3: A Determinant of Early Adipogenesis. Mol. Cell *62*, 443–452.
Yilmaz, Ö.H., Katajisto, P., Lamming, D.W., Gültekin, Y., Bauer-Rowe, K.E., Sengupta, S., Birsoy, K., Dursun, A., Yilmaz, V.O., Selig, M., et al. (2012). mTORC1 in the Paneth cell niche couples intestinal stem-cell function to calorie intake. Nature *486*, 490–495.
Yosef, R., Pilpel, N., Ronit, T.-A., Biran, A., Ovadya, Y., Cohen, S., Vadai, E., Dassa, L., Shahar, E., Condiotti, R., et al. (2016). Directed elimination of senescent cells by inhibition of BCL-W and BCL-XL. Nat Commun *7*, 11190.
Yoshimoto, S., Loo, T.M., Atarashi, K., Kanda, H., Sato, S., Oyadomari, S., Iwakura, Y., Oshima, K., Morita, H., Hattori, M., et al. (2013). Obesity-induced gut microbial metabolite promotes liver cancer through senescence secretome. Nature *499*, 97–101.
Youm, Y.-H., Kanneganti, T.-D., Vandanmagsar, B., Zhu, X., Ravussin, A., Adijiang, A., Owen, J.S., Thomas, M.J., Francis, J., Parks, J.S., et al. (2012). The NLRP3 Inflammasome Promotes Age-Related Thymic Demise and Immunosenescence. Cell Rep. *1*, 56–68.
Youm, Y.-H., Grant, R.W., McCabe, L.R., Albarado, D.C., Nguyen, K.Y., Ravussin, A., Pistell, P., Newman, S., Carter, R., Laque, A., et al. (2013). Canonical Nlrp3 Inflammasome Links Systemic Low-Grade Inflammation to Functional Decline in Aging. Cell Metab. *18*, 519–532.
Young, A.R.J., Narita, M., Ferreira, M., Kirschner, K., Sadaie, M., Darot, J.F.J., Tavaré, S., Arakawa, S., Shimizu, S., Watt, F.M., et al. (2009). Autophagy mediates the mitotic senescence transition. Genes Dev. *23*, 798–803.
Zhang, Y., Kwok-Shing Ng, P., Kucherlapati, M., Chen, F., Liu, Y., Tsang, Y.H., de Velasco, G., Jeong, K.J., Akbani, R., Hadjipanayis, A., et al. (2017). A Pan-Cancer Proteogenomic Atlas of PI3K/AKT/mTOR Pathway Alterations. Cancer Cell *31*, 820–832.e3.
Zheng, G.X.Y., Terry, J.M., Belgrader, P., Ryvkin, P., Bent, Z.W., Wilson, R., Ziraldo, S.B., Wheeler, T.D., McDermott, G.P., Zhu, J., et al. (2017). Massively parallel digital transcriptional profiling of single cells. Nat. Commun. *8*, 14049.
Zhou, L., Huang, Y., Li, J., and Wang, Z. (2010). The mTOR pathway is associated with the poor prognosis of human hepatocellular carcinoma. Med. Oncol. *27*, 255–261.
Zhu, Y., Tchkonia, T., Pirtskhalava, T., Gower, A.C., Ding, H., Giorgadze, N., Palmer, A.K., Ikeno, Y., Hubbard, G.B., Lenburg, M., et al. (2015). The Achilles' heel of senescent cells: From transcriptome to senolytic drugs. Aging Cell *14*, 644–658.
Zoncu, R., Efeyan, A., and Sabatini, D.M. (2011). mTOR: from growth signal integration to cancer, diabetes and ageing. Nat. Rev. Mol. Cell Biol. *12*, 21–35.

Appendix.

Table 1. List of shRNA sequences.

shRNA (Human)	Target Sequence
shmTOR_2	AGGCCTATGGTCGAGATTT
shp53	TCTCTTCCTCTGTGCGCCG
shIL1R	ACACTCTAAGTTCTATTGA
shEPRS_1	AGGCGATTACTCAGTGTTA
shEPRS_2	CGGATCATTTTGAAACTAT
shEPRS_3	TGGAGTTCAGTGCTACAAA
shEPRS_4	CAGGTTAACTTTAAAGGGA
shPDCD4_1	CCTATATTGATAGTTACAA
shPDCD4_2	AGGAGAACTGTGTTTATGA
shPDCD4_3	TGAGAGAATTTACAATGAA
shPDCD4_4	TGGAGCGGTTTGTAGAAGA
shURI1_1	AGGATGTTGCAAGTTCAGA
shURI1_2	TGGAGATAATTCTATACCA
shURI1_3	CGGAAAGAACATGTAAGAA
shURI1_4	CTAAGAGGGTCCGAATAAA
shPOLDIP3_1	CCTTTCCTTTGTGTGTATT
shPOLDIP3_2	CGATTTCGAATCAAAGGGA
shPOLDIP3_3	GCACCAAGATGACTGTGAA
shPOLDIP3_4	CGGGAGAAGCTTTTGCAGA
shNCBP1_1	AGGATGATGACGACGATGA
shNCBP1_2	AGGAGTTGTACGAAAAGAA
shNCBP1_3	AGACTTGTGCTGCACAGTT
shNCBP1_4	AGGTTTTTTTTGATATCTT
shCREM_1	CCCAGCATGATGGAAGTAT
shCREM_2	TGCTGCAATTCGATATGAT
shCREM_3	CGCAGGAAGAAGAAAGAAT
shCREM_4	AGATTACTAGAAATATTTA
shCCT2_1	AGAGTTGACTCTACAGCAA
shCCT2_2	GGGTTCAAGATGATGAAGT
shCCT2_3	AAGACCACTTTACAAAGTT
shCCT2_4	AGGCAATTAATTTATAATT
shRORC_1	GACTCCTTGCCTCTCCCTA
shRORC_2	GAGCTCATCAGCTCCATCT
shRORC_3	CGGGAGGAAGTGACTGGCT
shRORC_4	GGGCAGAGAGAGCTTCTAT
shYY1_1	CGCTTTTCACTGGACTTCA
shYY1_2	TGCTCTATCTTGCTCTGTA
shYY1_3	TGTTGAGAGTTCAAAACTA
shYY1_4	CTCCTGATTATTCAGAATA

Table 2. List of siRNA sequences.

siRNA (Human)	Target Sequence
siC/EBPβ	CGGGCCCTGAGTAATCGCTTA
siCDKN2A ($p16^{INK4A}$)	TACCGTAAATGTCCATTTATA
siTP53	CAGAGTGCATTGTGAGGGTTA
siS6K1_2	TCGCTTTGCATCTATCAGTAA
siS6K1_4	CAGAGAGTCAATGTCATTACA
siS6K2_4	TGCCATGAAAGTCCTAAGGAA
siS6K2_5	ACCGCAGAGAACCGGAAGAAA
siEPRS_1	CAGGAGGAGACTATACAACTA
siEPRS_3	AAGGCGATTACTCAGTGTTAA

Table 3. List of RT-qPCR primers.

Human	Forward primer	Reverse primer
CCL20	GGCGAATCAGAAGCAGCAAGCAAC	ATTGGCCAGCTGCCGTGTGAA
CCT2	CACTTGTGTGCGGAACTCCT	TTTTGTCCATGCCTTTGGGTC
CREM	AACAATGAGCAAATGTGCAAGGA	GCTACCTGAGCTAAAGCAGGG
EPRS	GGAGGTGGGCTCTCATCAAG	CCTCAAGACCCAACCTGGTC
IL1A	AGTGCTGCTGAAGGAGATGCCTGA	CCCCTGCCAAGCACACCCAGTA
IL1B	TGCACGCTCCGGGACTCACA	CATGGAGAACACCACTTGTTGCTCC
IL1R	ACGTTGGGGAAGACATTGTTGAGG	ACCCAGCCAGCTGAAGCCTGA
IL6	CCAGGAGCCCAGCTATGAAC	CCCAGGGAGAAGGCAACTG
IL8	GAGTGGACCACACTGCGCCA	TCCACAACCCTCTGCACCCAGT
mTOR	TCGCTGAAGTCACACAGACC	CTTTGGCATATGCTCGGCAC
NCBP1	AAGCCGTGTATTTGGTCCGT	TACCAATCTCGTCGCACCTG
PDCD4	ACCCTGCAGATCCTGATAACT	CAGAGTCCCGGGATGAGTTT
POLDIP3	AAGTGCAGGATGCCAGAGAG	GTGGAACCTGGATGGTTTTGG
RPS14	CTGCGAGTGCTGTCAGAGG	TCACCGCCCTACACATCAAACT
RORC	AAGAAGACCCACACCTCACAA	GGATCCCAGACGACTTGTCC
S6K1	CGGGTACTTGGTAAAGGGGG	ATTGCCTTTTTAAGCACCTTCATGG
S6K2	TTCCGGCACATGAATTGGGA	TATGTGAAGCCCAGGAAGG
URI1	GTGGTCACTAACTGCCAAGAG	TGAGTCTTTCTCGAAGGGCATTA
YY1	AAGCCCTTTCAGTGCACGTT	CTCCGGTATGGATTCGCACA

Continued on next page.

Mouse	Forward primer	Reverse primer
Acta2/Sma	CTCTCTTCCAGCCATCTTTCAT	TATAGGTGGTTTCGTGGATGC
Ccl2	CATCCACGTGTTGGCTCA	GATCATCTTGCTGGTGAATGAGT
Ccl5	CTGCTGCTTTGCCTACCTCT	CGAGTGACAAACACGACTGC
Cd3e	GACTATGAGCCCATCCGCAA	AACAAGGAGTAGCAGGGTGC
Cd68	AGGACCGCTTATAGCCCAAG	GGATGGCAGGAGAGTAACGG
Col1a1	GAGAGGTGAACAAGGTCCCG	AAACCTCTCTCGCCTCTTGC
Col4a1	CTGGCACAAAAGGGACGAG	ACGTGGCCGAGAATTTCACC
Cxcl2	CCAACCACCAGGCTACAGG	GCGTCACACTCAAGCTCTG
Cxcl5	TGCGTTGTGTTTGCTTAACCG	AGCTATGACTTCCACCGTAGG
Il1a	CGCTTGAGTCGGCAAAGAAAT	TGGCAGAACTGTAGTCTTCGT
Il1b	TGCCACCTTTTGACAGTGATG	TGATGTGCTGCTGCGAGATT
Klrd1	CAGGAAGTTTCTGAATGCTGTGT	TGGATTGGGGCTGAAGAAGG
Ncf2	CTAAACTGAGCTACCGGCGT	ACCGTATGCTCACACCACAG
Ncf4	ATCAAGGACATTGCGGTGGA	CTCTCTGGAACTCACGCCTC
p16^{Ink4a}	CCCAACGCCCCGAACT	GCAGAAGAGCTGCTACGTGAA
p19^{Arf}	TGAGGCTAGAGAGGATCTTGAGA	GCAGAAGAGCTGCTACGTGAA
Pdgfa	GTGCGACCTCCAACCCTGA	GGCTCATCTCACCTCACATCT
Ptprc	TTTGTCACAGGGCAAACACC	AAGGGGTCACTTTGAGGCAG
Rps14	GACCAAGACCCCTGGACCT	CCCCTTTTCTTCGAGTGCTA
Timp1	GCAACTCGGACCTGGTCATAA	CGGCCCGTGATGAGAAACT
Tnfa	CCACCACGCTCTTCTGTCTAC	AGGGTCTGGGCCATAGAACT
Tgfb1	GGAGCAACATGTGGAACTC	CAGCAGCCGGTTACCAAG

Dgat2 - Taqman	Mm00499536_m1	
Il6 - TaqMan	Mm00446190_m1	
Pck1 - TaqMan	Mm01247058_m1	
Fasn - TaqMan	Mm00662319_m1	
Pnpla2 - TaqMan	Mm00503040_m1	
Fabp4 - TaqMan	Mm00445878_m1	

Table 4. List of antibodies and dilutions.

Target	Clone	Company	Catalogue no.	Dilution
S6K1 (WB)	49D7	Cell Signaling	#2708	1:1000
S6K2 (WB)	Polyclonal	Cell Signaling	#14130	1:500
Phospho-RPS6 (S240/S244) (WB/IF)	D68F8	Cell Signaling	#5364	1:10,000-40,000 (WB) and 1:800 (IF)
Phospho-RPS6 (S235/S235) (WB)	91B2	Cell Signaling	#4587	1:2500
RPS6 (WB)	5G10	Cell Signaling	#2217	1:2500
Phospho-4EBP1 (T37/T46) (WB/IF)	236B4	Cell Signaling	#2855	1:750 (WB/IF)
4EBP1 (WB)	53H11	Cell Signaling	#9644	1:2500
Phospho-Akt (S473) (WB)	D9E	Cell Signaling	#4060	1:2000
Akt (WB)	C67E7	Cell Signaling	#4691	1:1000
BrdU (IF)	PRB-1	Invitrogen	A21303	1:1500
$p16^{INK4A}$ (IF)	JC-8	CRUK	-	1:750
$p21^{CIP1}$ (IF)	Polyclonal	Santa Cruz	SC-471	1:200
p53 (IF)	DO1	Santa Cruz	SC-126	1:100
γ-H2AX (IF)	JBW301	Millipore	05-636	1:200
IL-1α (IF)	#4414	R&D Systems	MAB200	1:100
IL-1β (IF)	#8516	R&D Systems	MAB201	1:100
IL-1β (WB)	Polyclonal	Santa Cruz	SC-7884	1:200
IL-6	Polyclonal	R&D Systems	AF-206-NA	1:100
IL-8	Polyclonal	R&D Systems	AF-208-NA	1:100
IL-8 (WB)	6217	R&D Systems	MAB208	1:100
GAPDH (WB)	Polyclonal	Abcam	ab22555	1:2000
HRAS (WB)	Polyclonal	Santa Cruz	SC-520	1:1000
COL1A1	Polyclonal	Novus Biologicals	NBP1-30054	1:500
Ki67	SP6	Abcam	ab16667	1:500